Large Tip Clearance Flows in High Pressure Stages of Axial Compressors

RICHARD JAMES WILLIAMS

Large Tip Clearance Flows in High Pressure Stages of Axial Compressors

Richard James Williams

A Thesis presented for the degree of
Doctor of Philosophy

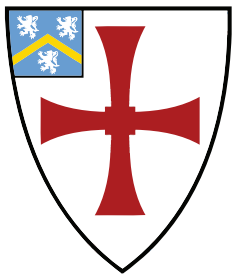

School of Engineering
University of Durham
England

September 2009

Dedicated to

Andrew, Audrey and Sarah

Large Tip Clearance Flows in High Pressure Stages of Axial Compressors

Richard James Williams

Submitted for the degree of Doctor of Philosophy
2009

Abstract

This thesis investigates over tip leakage where the tip clearance is large. In the high pressure stages of axial compressors the tip clearance can be typically 6% of span and the total blockage due to tip clearance can consume in excess of forty percent of the annulus height. Experimental and computational investigations of large tip clearance in a linear cascade have been used to investigate this phenomenon.

Two cascade builds have been used the first (Build A) consisted of a controlled diffusion aerofoil of low stagger and thirty degrees flow turning. The second cascade (Build B) consisted of an engine representative design with high stagger and around ten degrees of flow turning. The diffusion factor of both cascades was around 0.3. The major findings are that: Large tip clearances have a smaller detrimental influence on single row performance than the previous research would have suggested, for Build B the loss at 10% tip clearance was the same as the 0% tip clearance loss, though the overall flow turning was much reduced. An increase in blade loading towards the tip was observed with both builds. Both these phenomenon were attributed to the small amount of movement of the over tip leakage vortex.

An engine representative level of inlet skew was implemented using upstream injection so to assess its influence. This was found to have a remarkably small influence on the performance of a single row with the tip clearance and geometry of the blading having a much greater influence.

Finally a circumferential grooved casing treatment was applied in the linear cascade but this was found not to be an appropriate tool for such an investigation.

Declaration

The work in this thesis is based on research carried out in the School of Engineering at the University of Durham. No part of this thesis has been submitted elsewhere for any other degree or qualification and it is all my own work unless referenced to the contrary in the text.

Acknowledgements

Many thanks are owed to all the people who have helped and supported me throughout my thesis, whom only a few are mentioned here.

Firstly many thanks must go to my supervisors Dr David Gregory-Smith, Dr Grant Ingram and Prof Li He who brought support, advice, enthusiasm and vast experience to this project. David and Grant are especially thanked for seeing the project through to the end and proofreading and commenting on this thesis. The use of Li's CFD code was much appreciated and thanks must go to Li for allowing me to use it.

Thanks go to: David Sims-Williams for the advice throughout this project and in particular the use of the in-house wind-tunnel logging software; Gary Parker for his help and advice within the lab; Tony Collinson for always being willing to help and making Build-B; and Colin Wintrip for ensuring my requested parts were made promptly; Sarah and Helen are especially thanked for the laborious task of proof reading my thesis.

This project was a collaboration with Alstom Power (Switzerland). I would like to thank in particular Michael Loetzerich, for his interest in this work and ever useful comments. Without Alstom's input both financially and technically this work would not have been so engine representative.

Contents

List of Figures

List of Tables

Nomenclature and Symbols

C	Chord
C_x	Axial Chord
CFD	Computational Fluid Dynamics
C_L	Blade Force Coefficient
	$= \frac{1}{C_x}\int_0^C (Cp_{\mathrm{PS}} - Cp_{\mathrm{SS}})dx$
Cp	Pressure Coefficient
	$= \frac{P_{S,\mathrm{local}} - P_{S,\mathrm{atmospheric}}}{\frac{1}{2}\rho V^2_{\mathrm{isentropic}}} = \frac{P_{S,\mathrm{local}} - P_{S,\mathrm{atmospheric}}}{P_{T,\mathrm{upstream}} - P_{S,\mathrm{atmospheric}}}$
Cp_0	Total Pressure Loss Coefficient
	$= \frac{P_{T,\mathrm{upstream}} - P_{T,\mathrm{local}}}{\frac{1}{2}\rho V^2_{\mathrm{isentropic}}} = \frac{P_{T,\mathrm{upstream}} - P_{T,\mathrm{local}}}{P_{T,\mathrm{upstream}} - P_{\mathrm{atmospheric}}}$
DF	Diffusion Factor
	$= 1 - \frac{V_2}{V_1} + \frac{\Delta\ V_\theta}{2\sigma\ V_1}$
h	Pitch
HP or HPC	High Pressure Compressor
i	Computational Constant Tangential Plane
IGV	Inlet Guide Vain
IP or IPC	Intermediate Compressor
j	Computational Constant Axial Plane
k	Computational Constant Radial Plane
LE	Blade Leading Edge
LP or LPC	Low Pressure Compressor
$P_{atmospheric}$	Atmospheric Pressure
P_0	Stagnation Pressure
PS	Pressure Surface

P_S	Static Pressure
$P_{S,local}$	Static Pressure at Measurement Point
P_T	Total Pressure
$P_{T,local}$	Total Pressure at Measurement Point
$P_{T,upstream}$	Upstream Total Pressure
Rad	Radial
Re	Reynolds Number $= \frac{\rho\ V_1 C}{\mu}$
S	Span
SS	Suction Surface
t	Time
TE	Blade Trailing Edge
Tan	Tangential
TC	Tip Clearance
V	Velocity
V_1	Inlet Velocity
V_2	Exit Velocity
V_{isen} *or* $V_{isentropic}$	Isentropic Exit Velocity $= \sqrt{\frac{2\times(P_{T,upstream}\ -\ P_{atmospheric})}{\rho}}$
V_x	Axial Velocity
$V_{x,norm}$	Normalized Axial Velocity $= V_x\ /\ V_{isen}$
V_y *or* V_θ	Tangential Velocity
V_z	Radial Velocity
x	Axial Co-ordinate
y	Tangential Co-ordinate
z	Radial Co-ordinate

α	Yaw Angle
α_1	Inlet Yaw Angle
α_2	Exit Yaw Angle

ρ	density
σ	Solidity $=$ C/h
μ	Dynamic Viscosity

Subscripts:

1	Inlet
2	Exit

Traverse Axial Locations:

-0.5Cx	50% Axial Chord Upstream of the LE
0.0Cx	Cascade LE
0.0Cx to 1.0Cx	Axial Chord Locations Between LE and TE
1.0Cx	Cascade TE
1.2Cx	20% Axial Chord Downstream of the Cascade TE
1.5Cx	30mm 50% Axial Chord Downstream of the TE

Chapter 1

Introduction

Over tip clearance flows account for a significant percentage of the loss within compressors. These flows occur within axial compressors over the tip of non-shrouded compressor rows and they vary significantly along the length of the compressor. This work investigates clearances found within the high pressure stages of industrial axial compressors such as Alstom Power's GT26 series used for gas powered electrical generation. Within these stages, unlike within the low pressure stages, the relative clearances are high. The aim of this thesis was to further the understanding of these flows and the resultant loss to enable techniques to be developed to reduce their adverse influence on compressor performance.

Gregory-Smith [2003] reviewed end-wall flows in axial compressors for Alstom Power and found limited literature associated with large clearances in the high pressure compressor stages. Following this Walker [2004] and Walker et al. [2005] computationally investigated these flows during a final year project at Durham University. This preliminary work by Gregory-Smith and Walker lead to this thesis.

This work contributes to the vast research area surrounding clearance flows within axial compressors, specifically the area of large clearances in the region of 6% span within the high pressure axial compressor. Few authors have approached such clearance sizes, perhaps because this type of clearance is not found within aero-engines. The common design principle is to ensure the clearances are as small as possible to reduce loss and ensure maximum performance; this is indeed still the case within the high pressure industrial stages. However, because of the short blades

the clearance is relatively large as a percentage of span or chord.

The HP compressor is an integral part of some industrial axial compressors such as that found within Alstom Powers GT26 and GT24 series. Because the annulus height is small the blades are also short and this results in a relatively large clearance over the end of the blade. Also the blade span to chord ratio (blade aspect ratio) will be close to one. The clearance is required due to the relative movement between the blade casing or hub depending if it is a rotor or stator. The clearance gap required is due to the relative thermal expansion of the blade and the casing. The clearance allows for flow to pass over the tip of the blade which then forms a complex flow structure within the endwall region. Through viscosity of the air a loss occurs in the form of increased entropy and therefore decreased pressure rise. The understanding of such flow features and therefore how the loss can be reduced will allow for higher pressure ratio and lower loss compressors of the future.

This thesis presents the result of a three and half year program of research at Durham University. Collaboration with Alstom Power (Switzerland) enabled the project to use engine representative geometry and bring industrial relevance.

This thesis aimed to:

A - Investigate the influence of large clearances on compressor blade row loss and performance.

B - Investigate the influence of geometry.

C - Investigate the influence of inlet conditions and inlet boundary layer skew on clearance flows.

D - Investigate methods for reducing the loss and blockage associated within the endwall flows of such compressor rows.

To investigate this, experimental and computational studies of linear cascades were undertaken. The use of linear cascades allowed for relatively cheap and quick measurement to be carried out. The other advantage was that measurement of total pressure and flow angles can be achieved with straightforward methods. RANS computations using an in-house code allowed for further in-depth analysis.

Two linear cascades were used within this work. The first called Build-A, was an existing cascade previously used by Yang [2004]. This consisted of low stagger at 14.2° but high turning of 30° and the inlet boundary layer had a fairly high skew but low thickness. The second cascade called Build-B, was more engine representative having a higher stagger of 46.5° and lower turning of 10°. Build-B had a unique upstream tangential injection system to control the inlet boundary layer skew and thickness; two configurations were used firstly the natural cascade skew inlet which was thin and lowly skewed (called 'natural skew') and the high skew inlet which was approximately 20% of the span thick and skewed by 10° (called 'high skew'). The second cascade was later modified and circumferentially grooved casing treatment implemented (called Build-B1).

The following activities were undertaken:

- Refurbishment of the existing cascade (Build-A) for the purpose of tip leakage flow investigations.
- Design and manufacture of the second cascade (Build-B).
- Set up of both cascades to ensure quality uniform inlet flow at the required design condition.
- Modifications to Build-B for the testing of circumferential casing treatment.
- Implementation of instrumentation and software for cascade testing for both cascades.
- Extensive 5-Hole pressure probe traversing for both cascades upstream, within the passage and downstream of the case.
- Blade static pressure measurements.
- Computational validation
- Computational investigation of the effect of relative endwall motion as within a real row.
- Computational investigations of the clearance flows within both cascades.

The work within this thesis has been the subject of a number of conference and journal publications (Williams et al. [2006, 2008d, 2009]. Much of Build-B's work was also reported in a series of reports for Alstom (Williams et al. [2007a,b, 2008a,b,c]).

This thesis contains the following chapters:

1. **Introduction -**

2. **Literature Survey -** Explores the wider context of compressor over tip leakage flows, and concentrates on literature which is applicable for the high pressure stage tip clearance flows. A review of treatment methods and possible application within compressors is also undertaken.

3. **Experimental Methods and Techniques -** Describes the instrumentation and processing of the experimental data and introduces the design and flow condition of both cascades.

4. **Build-A, Results and Discussion -** The computational techniques are presented and a study of the effect of endwall motion made. The experimental and computational results are presented and discussion and conclusions drawn.

5. **Build-B, Results and Discussion -** The experimental and computational results from Build-B are presented, and discussions and conclusions made.

6. **Build-B1, Casing Treatment -** Circumferential casing treatment was implemented to Build-B, the design of which and the results are presented and discussed in this chapter.

7. **Overall Discussion -** The results from the thesis are compared and contrasted together and comparison made with the wider literature.

8. **Conclusions and Recommendations -** Concludes the thesis and recommendations for further study are made.

9. **Appendices -** supplementary data and information.

The next chapter (Literature Survey) places this work in the wider context and explores the literature surround large clearances within the high pressure stages of industrial axial compressors.

Chapter 2

Literature Survey

2.1 Introduction

This chapter explores the literature surrounding tip clearance flows within industrial axial compressors. Specifically this chapter will concentrate on the over tip leakage flows within industrial axial high pressure compressors (HPC's). The other flows affecting the tip clearance flow will also be explored with an initial description of how loss through the compressor is generated. Much of the published tip leakage specific work involves aero-engine applications. The industrial axial compressor specific literature was much smaller and so aero-application literature is related to the industrial compressor context. High pressure low speed specific literature was also limited and so much of the following literature involves transonic compressor stages. To distinguish the need for this work the tip clearance flow differences between the low pressure and high pressure stages will be explored.

Experimental linear cascade testing and computational fluid dynamics (CFD) techniques were used for this work and so these methods and their uses will be explored and the different tip clearance modelling techniques. The difference between linear cascades and rotating machines will be discussed. Finally methods for reducing the adverse effects of tip leakage and endwall flows will be reviewed, especially focusing on casing treatment methods. A selection of the more promising methods will discussed and examined for there applicability within HPCs.

2.1.1 Wider Impact of Turbomachinery

Industrial gas turbines are used to generate electrical power. The principles of operation are similar to aero engines and well known; air is compressed (Compressor), fuel is added and combusted (Combustor), then the hot gasses are passed through a turbine. The turbine then drives the compressor and a generator to produce electricity. In the case of an aero engine the turbine drives the compressor and a fan to provide the propulsion. Although in principle the machine is simple, in reality it is very complex and requires huge effort in the design and operation. Operational efficiency is of paramount importance to ensure an economically and environmentally sustainable plant. A large gas turbine may produce in the region of 300MW of power, for example Alstom Power's GT26 produces a gross electrical output of 288.3MW which when used in a combined cycle power plant will produce more than 400MW. The overall efficiency of such a plant is therefore important; a 1% decrease in efficiency from a 400MW plant will reduce the power output by 4MW. This is approximately the size of two large wind turbines and would incur a significant penalty in profits. Not only is there a penalty in profit but also of harmful emissions to the atmosphere which can be lowered through efficiency increase as well as new technologies. This explains the motivation behind this work.

2.1.2 Industrial Axial Compressor Design

The purpose of the compressor is to increase the total pressure for the combustor. Air enters, usually at atmospheric pressure and exits to the combustor at an increased pressure. The aim of this is to create the highest possible pressure for a given work input. Axial compressors contain rows of rotors and stators, the rotors rotate with the rotor and the stators are fixed within the casing, a rotor and stator pair is termed a stage. Within an industrial compressor the stages can be classed within three sections; the low pressure (LPC), intermediate pressure (IPC) and high pressure (HPC) stages. Typically there may be upwards of 30 stages within the compressor and a pressure ratio larger than 1:30 as found within Alstom Power's GT26.

Industrial engines like the GT26 have a single rotor; this is due to the size of

such engines and the mechanical challenges and cost of splitting the rotor on to several shafts as undertaken within aero engines. The consequence is that all the parts must rotate at the same speed making it difficult to design to an optimum for every stage and therefore a compromise is required. Another restraint is that the rotational speed must match the generator which for most geographical locations needs to be 50 or 60Hz. Other requirements for the compressor exist, including: high durability; high efficiency; size and weight; cost of design and manufacture; reduced development and testing; and secondary services e.g. bleeding of the fluid prior to the HP. All of these require a compromise in design, for example the optimal design for aerodynamic efficiency may not be practical from a mechanical and engine life perspective.

The early LPC stages take the air from the inlet, usually at atmospheric pressure, and significantly compresses it. The flow within these stages usually has a Mach Number greater than unity meaning that the outer section of the passage is dominated by shocks. The flow within these stages is therefore sensitive to the boundary conditions and usually where the compressor will stall. The IPC stages take the pressure from the LP stages and further increases the pressure, within these stages the flow has a Mach number less than unity and therefore is inherently more stable posing less of a problem to the compressors stability.

The air enters the HPC stages from the IPC and exits to the combustor. Typically, as with the GT26, there may be 6 stages. The stage loading within the HPC is low and may only increase the pressure over the 6 stages by only 1:1.5. To ensure a relatively constant axial velocity through the compressor with increasing fluid pressure and density, the annulus area is reduced. Also to keep a high blade speed and therefore the work done high the hub radius is increased. Within the later stages, because of the low loading and therefore small change in density, the change in annulus height within the HP is small.

At the end of the blades, due to the relative motion, a clearance exists. Within the LPC the clearance is relatively small compared with the span or chord but within the HPC, because of the short length of the blades, the clearance is relatively large. The size of the clearance is set by thermal expansion and movement of the

blades. These clearances and the flow features that follow create loss and affect the operating condition of the compressor. The causes of loss within a compressor is explored next followed by the flow physics of the flows through the compressor.

2.2 Loss

The loss within turbomachinery is now considered. Losses directly influence the efficiency of the compressor. As argued by Denton [1993] loss sources in turbomachinery are difficult to quantify and therefore it is important to have a physical understanding of the flow and origins of loss. For adiabatic flow (as can be assumed in compressors) loss results in a rise in entropy and reduction in stagnation pressure. Therefore the loss reduces the stagnation pressure rise through the compressor. Cumpsty [1989] states that "at microscopic level the losses may be thought to have a single cause, viscous shearing leading to a rise in internal energy". He then groups possible loss sources as; drag at solid surfaces, mixing, shock and shear work. Cumpsty [1989] and Denton [1993] thoroughly explored the loss within turbomachinery and the following overview is mostly taken from these two sources. It is important to note that if the system were adiabatic and therefore no heat transfer to or from the system the only loss is as a result of the viscosity of the fluid. If there was no viscosity then there would be no loss.

Drag at Solid Surfaces: The loss caused by drag at solid surfaces is the dominant loss source for the mainstream (mid-span) blade. This loss is a result of the flow over the blade and through viscosity creates a skin friction drag and a pressure drag. A good description of the flow over an aerofoil and the drag associated with it was given by Massey and Ward-Smith [1998]. The drag and therefore the loss can be calculated by considering the wake momentum thickness without considering the detailed flow physics.

Mixing: The sudden enlargement of a pipe is a standard example of a thermodynamically irreversible process due to mixing. Mixing refers to the mixing of one fluid with different properties for example temperature, pressure or velocity, and not mixing of different fluids. In turbomachinery the mixing is much more complicated

and usually three-dimensional. For example the tip clearance flow undergoes mixing with the mainstream flow. Essentially non uniformity in the flow is what creates mixing loss. This process continues to occur downstream of the blade row and in to the next row or beyond.

Shear Work: Shear work takes place whenever there are velocity gradients and as such is the source of loss within mixing. The differentiation here is that such velocity gradients are encountered when there are boundary layers, wakes and vortices. Shear work is only of concern when the velocity gradient is significant or turbulent flow is encountered.

The flow around the trailing edge of an aerofoil is an example of mixing within turbomachinery. For minimum loss, an aerofoil which creates lift through non uniformity of the flow on the suction and pressure surfaces must decelerate the flow on the suction surface to allow for a minimum velocity gradient at the trailing edge when the two flows meet. If the velocity is the same on both surfaces at the trailing edge then the Kutta condition will hold and minimum loss will be incurred.

Shock Losses: This thermodynamically irreversible process produces a reduction in stagnation pressure. If the shock is strong and there is only one shock then the largest loss is encountered. However with a weak shock or series of shocks as often found within industrial compressors the loss can be small and the flow nearly reversible. One of the more serious aspects of a shock is the ability to separate the blade's boundary layer; this may create a large boundary layer downstream and consequently its contribution to the overall loss can be significant. Within the HPC shocks are not encountered. Therefore findings and literature from the early stages may not be appropriate for the HPC if they involve shock mechanisms.

2.3 Flows through a Compressor

Gallimore [1999] outlines some of the basic principles and rules associated with the design of axial compressors. This was principally for aero engines but much of the paper is still relevant for industrial machines. Cumpsty [1989] presents another more in depth look at the compressor.

The mainstream flow of a compressor can be considered as two-dimensional (2-D) flow and so classical aerofoil theory can be used to predict the flow. This was historically the normal geometrical starting point for compressor design; where the blades were stacked without accounting for secondary flows but only the radially changing blade velocity and therefore the radially changing inlet angle. If the blades are relatively long the loss produced by the blade profile in the mainstream flow is the largest loss source and this holds for the early low pressure stages.

Within the axial compressor, or more generally turbomachinery, there are numerous flow structures other than the mainstream flow which usually result in loss. Figure 2.1 taken from Lakshminarayana et al. [1982] indicates these flow structures. These loss sources are traditionally grouped as 'profile loss', 'end wall loss' and 'leakage loss'. The percentage that each loss attributes to the total loss varies between stages. In the LPC the blades are long, therefore the percentage attributed to the endwall loss is small and the profile loss is dominant. Within the HPC the blades are short thus the endwall and leakage losses are more important. It is clear however that each source of loss does not act independently. Other than the main gas path losses, as discussed, there are many other loss sources including fluid leakage, step and gaps.

Profile loss Profile loss is the loss generated by the blade's boundary layer and the trailing edge.

Endwall loss Endwall loss can be referred to as 'secondary loss', or sometimes, as with Gregory-Smith [2003], is used as a term to encapsulate all the loss sources within the endwall region. This will include the tip leakage loss, secondary loss and endwall boundary layer; the blade profile loss within this region may also be included. Due to the inseparable interactions of each loss source the latter definition is used in this thesis. These flows are 3-D and require significant effort to understand and predict. The percentage that each endwall loss source attributed to the total endwall loss varies from stage to stage and between geometrical designs.

Overall Loss - Many attempts have been made to predict the overall loss. Most of these have attempted to mathematically account for each source of loss in turn. Koch and Smith [1976] attempted one such method. They accounted for four

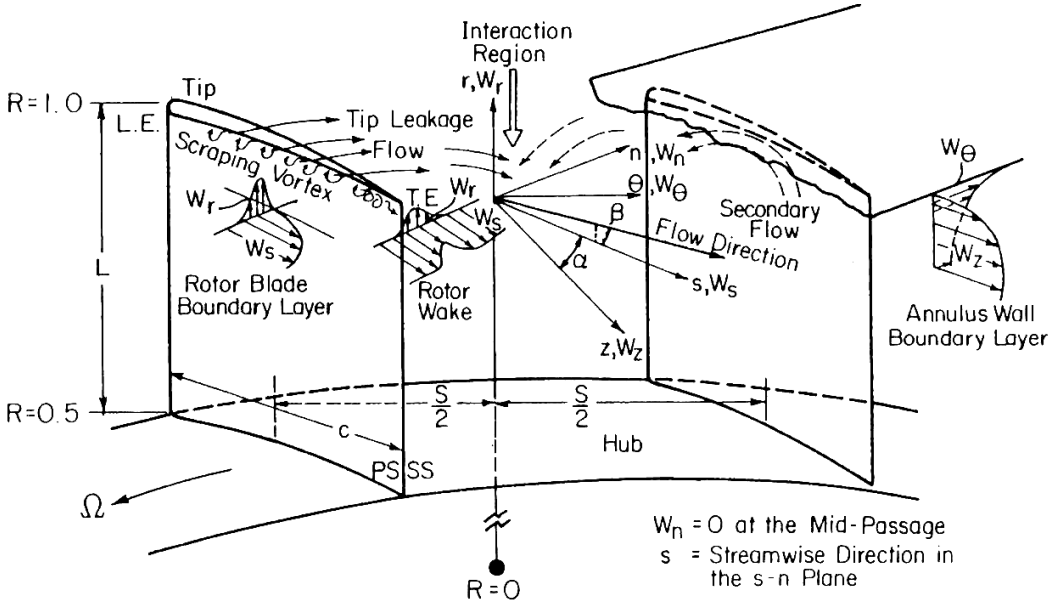

Figure 2.1: *Flows Within the Endwall Region of a Compressor (Lakshminarayana et al. [1982])*

sources of loss; blade profile loss, endwall boundary layer loss, shock losses and part span shroud losses. They employed correction factors for each form of loss to match the results with experimental data. More recently 3-D CFD calculations have aided with the calculation of the total loss and this has been undertaken by many authors as well as becoming common practise within industry.

2.3.1 2-D / Profile flow

Simplistically the flow at mid-span can be considered to be 2-D. Cumpsty [1989] gives a comprehensive review of the flows over an aerofoil. The profile loss across a subsonic aerofoil is due to the boundary layer formed over the blade surface and the separation at the trailing edge. Most of this loss occurs on the suction surface where the boundary layer is thicker. For high speed sonic blades the boundary layer interacts with the shock resulting in large losses. The boundary layer along the blade surfaces can usually be considered to be laminar at the leading edge and then they may go through transition to turbulence or separate. On the pressure surface the laminar region may remain to the trailing edge but on the suction surface it will not. The suction surface laminar region may only be short before transition but

it will exist even under highly turbulent flow. The boundary layer transition and separation is dependent on Reynolds Number, pressure gradient, viscosity, surface roughness and unsteadiness of the oncoming flow and as such is quite complex but well known (e.g. Cumpsty [1989]) and not discussed in detail here.

2.3.2 Endwall Flows

'Endwall flows' is the generic name for all flows created by fluid interacting with the hub or casing and can be seen in Figure 2.1 taken from Lakshminarayana et al. [1982]. In this region the flow over the blade can no longer be considered 2-D. Much work has been undertaken concerning endwall flows in turbines and compressors. The differences between the flows in a turbine and compressor include: compressor blade turning is much lower, therefore the secondary flows are weaker; within a compressor the boundary layers are decelerated rather than accelerated and therefore separations are more likely to occur; the compressor's incoming boundary layer is much thicker; and the stability of a compressor is lower with surge and stall being an issue. The secondary flows nearly always have the effect of under turning the flow and increasing losses. Turning of the fluid through the stage can be directly linked to the power of the stage and so the mechanics of the under turning close to the end walls results in decreased pressure rise.

This sub-section will discuss all of the endwall flows apart from the detailed leakage flow. This is because the main thrust of this work is aimed towards the leakage flow. It is however important to remember that as discussed by Denton [1993] the endwall flows can not be considered to act independently.

Inlet Boundary Layer

Within the endwall region a significant low momentum region exists at inlet to the blade row on the hub and casing, and this is termed the boundary layer. Within the LPC the inlet boundary layer region is small as a percentage span but in the HPC it can consume a significant proportion of the annulus height (typically 10%). Hunter and Cumpsty [1982] found this to consist of low axial velocity (low dynamic pressure) and high loss fluid. For a rotor row this decreased axial velocity results in

a higher inlet angle within the endwall boundary layer. On the contrary at inlet to the stator a decrease in inlet angle occurs. The thickness of the inlet boundary layer was shown, for example Wagner et al. [1985a], Wagner et al. [1985b] and Brandt et al. [2002] to significantly affect the row performance.

Inlet skew is the increased angle at the inlet to the row on the endwalls and this exists within the inlet boundary layer. It is created by a combination of the axial velocity deficit as described above, the upstream walls motion, the upstream rows endwall flows and the change in frame of reference between the rotor and stator. The direction of skew is generally of an increase in incidence on to the blade. The skew and thickness of the endwall boundary layer entering a row are dependent on the upstream rows and therefore a product of the following end wall flow features.

Passage Vortex

The formation of the passage vortex is well known and has been described by many authors including Denton [1993], Cumpsty [1989] and Gregory-Smith [2003]. More fundamentally 'Classical Secondary Flow Theory' can be used as a way of explaining and predicting the passage vortex, for example Came and Marsh [1974] and Marsh [1974]. The formation of the passage vortex and resultant corner stall is shown in Figure 2.2 which is a figure revamped from Gregory-Smith [2003].

Within the blade passage the primary flow is turned by the blades and so establishes a pressure field between the blades. The velocity within the boundary layer on the endwall is lower than the free stream velocity therefore the pressure gradient across the blade passage forces the boundary layer flow to follow a tighter radius of curvature. This over-turns the flow within the endwall boundary layer. Crossflow is then produced by the components of velocity locally perpendicular to the free stream flow. Away from the casing/hub there is a counter balancing flow from the suction to the pressure surface which gives a vertical flow at exit of the cascade. This is termed the passage vortex and as a result there is an area of increased tuning away from the wall.

The inlet skew has the effect of opposing the endwall crossflow reducing the passage vortex. As explained by Cumpsty [1989] if the stagger is high then the

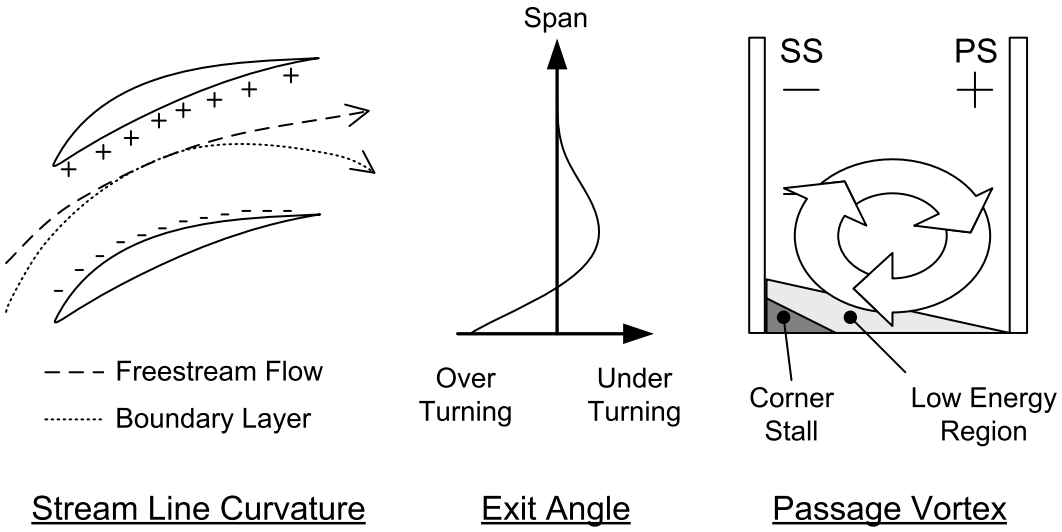

Figure 2.2: *Formation of Passage Vortex and Corner Stall*

camber is usually small therefore the passage vortex is weaker due to the reduced turning, resulting in under turning at exit in the endwall region. On the contrary if the stagger is low the blade camber tends to be high resulting in over-turning due to the larger passage vortex. This therefore affects the skew of the boundary layer on to the next blade row.

Corner Stall

The low energy high entropy fluid within the boundary layer is moved via the passage vortex's crossflow against the corner of the wall and blade's suction surface, as seen in Figure 2.2. This results in an accumulation of low energy fluid, and coupled with the overall pressure rise often combines to form a separated region, termed corner stall. This creates a large blockage in the endwall regions and may interact with the suction surface along a significant length of the span. The corner stall may account for a significant proportion of the total stage loss. The size of the corner stall and the overall loss created is affected by the design and the flows within the compressor. Hah and Loellbach [1999] gave a good insight into the formation of the separation and the flows within the separation. Gbadebo et al. [2007] further investigated the corner stall in detail and in particular the effect of tip clearance on corner stall, which for larger clearances was shown to completely suppress the 3-D separations, a result also found by Dong et al. [1987].

Hah and Loellbach [1999] investigated the hub corner stall. They reported that with increased rotor loading the corner stall moves further upstream along the chord. This increased loading significantly altered the flow downstream and changed the angle of attack at the leading edge of the stator. A severe flow separation on the stator suction surface then occurred close to the hub. As with all secondary flows the downstream rows are affected. Increasing the inlet endwall skew opposes the passage crossflow, therefore reducing the secondary flows and corner separation; but also increases the blade tip loading within the skew.

Horseshoe Vortex

The horseshoe vortex is widely understood (e.g. Eckerle and Langston [1987]) and forms around all blunt bodies protruding out of a shear flow. Within compressors this occurs at the junction between the end-wall and the blade's leading edge and so it is usually formed at the rotor hub and stator casing. A partial/weak horseshoe vortex may occur at the blade tip if the blade protrudes into the boundary layer.

The strength of the horseshoe vortex depends on the blade's leading edge thickness. Therefore within the a compressor it is usually a weak feature and because of the non symmetrical nature of the blade the strength of each leg will be different. As explained by Cumpsty [1989] the suction surface leg will travel along the suction surface corner and the pressure surface leg will move across the passage impinging on the adjacent blade's suction surface corner. This results in two oppositely rotating vortices within the suction surface corner region. Gbadebo et al. [2007] clearly shows the formation and existence of a horseshoe vortex within a compressor cascade with small clearances, and the trajectory of the suction surface leg along the blade at the boundary with the corner separation region. With clearances larger than the boundary layer the horseshoe vortex was no longer evident.

2.4 Compressor Tip Leakage Flows

The tip clearance allows for the passage of fluid over the tip of the blade which is termed tip leakage flow. These flows have been widely investigated both experimen-

tally and computationally as they are a significant cause of compressors instability and loss. The clearance gap is usually defined as a relative clearance of either the annulus height or the chord length. In the LPC stages where the blades are long the tip clearance size is generally within 1% of the annulus height but within the HPC the clearance may be as large as 6% of annulus height. Note that the absolute tip clearance may be of similar size but the relative clearance within the HPC is much larger; since both the span and chord are shorter. This holds for both relative clearance definitions.

The reason for the requirement of the absolute clearances size is to ensure a clearance between the casing and the tip at all working conditions. Rubbing of the blade on the casing may cause significant damage and a lengthy shut-down of the machine. Thermal and centrifugal effects mean that the blades will change in size Cumpsty [1989] explains that the compressor tip clearance size will change during operation due to the temperature of the components. Furthermore the annulus may not be fully concentric therefore the tip clearance will vary around the rotor. Freeman [1985] showed that the pressure rise was dependent on the integrated clearance around the annulus and therefore independent of the concentricity of the annulus. The stall margin was dependent on the concentricity and the largest clearance over a sector determined this.

Considerable research has been undertaken concerning tip clearance flows; Peacock [1982], Peacock [1983] and Cumpsty [1989] summarised much of the early work. Cumpsty [1989] describes some work by Freeman [1985] who investigated the effect of tip clearance size on the performance of a 6-stage high pressure aviation compressor. He showed that a variation in tip clearance gap of 1% to 3% chord resulted in a significant performance change. At small clearance values ($< 1\%$ chord as found by Storer and Cumpsty [1991]) the tip leakage flow can prevent corner stall and as a consequence reduce the blockage and increase the efficiency. Many other authors have shown this to occur, for example Inoue et al. [1986] showed the optimum to be less than 1% Chord. Above this small clearance the effects of increasing the tip gap are extremely detrimental resulting in a fall in pressure rise and efficiency, and shift of the surge line towards higher mass flows.

The flow within the tip clearance is highly complex and varies significantly along the compressor due to the geometry, presence of shocks and the state of compressor throttling. Lakshminarayana et al. [1982] attempted to indicate many of these flows in Figure 2.1 on Page 12. Simplistically the tip clearance allows for a pressure driven jet to pass across the tip of the blade, this flow (termed 'tip leakage flow') then rolls up in to a tip leakage vortex which then passes out of the passage to the next blade row.

Significant loss occurs within the tip leakage flows. The origins of this loss include: shear stress loss on the endwall and blade surface; mixing loss within the jet and the shear flows; secondary loss due to the formation of the tip leakage vortex; and mixing loss of the leakage flow with the mainstream flow. The vortex losses may occur well downstream of the row and pass into the next row.

2.4.1 Flow Through the Clearance

There are two mechanisms responsible for the tip leakage flow. Principally the flow is pressure driven. Storer and Cumpsty [1991] found the chord-wise distribution of the flow across the tip to be dependent on the static pressure field close to the blade tip. For their geometry the blade loading was at its highest in the forward part of the blade and so the tip leakage flow was stronger there. Secondly, the viscous stresses caused by the relative motion between the blade and the endwall, drag the fluid through the clearance which assists the strength of the tip leakage flow.

The flow enters the tip clearance from the pressure side of the blade and separates from the blade tip to form a strong jet as illustrated by Glanville [2001] in Figure 2.3. This separation creates a contraction of the leakage jet. The contraction ratio as explained by Denton [1993] depends on the radius of the blade tip pressure surface corner, but he give a nominal value of 0.6.

Compressor blades are generally thin and therefore the clearance jet is unlikely to reattach to the blade tip. Without reattachment the separation creates a vena-contracta feature over the tip of the blade. Glanville [2001] stated that for reattachment of the separation on to the tip of the blade the aspect ratio (tip gap height divided by maximum blade thickness) must be lower than 0.4. For a lower aspect

ratio gap, reattachment of the flow on to the blade tip occurs; this produces mixing creating loss within the tip gap and a separation bubble close to the PS blade edge. Storer and Cumpsty [1991] also investigated the flow through the clearance and found that without reattachment the ideal vena-contracta model was valid and predicted the streamlines through the clearance well.

Tang et al. [2006] thoroughly studied the leakage flow within the blade and casing gap giving insight into the velocity profile within the gap. They also found separation and a vena-contracta for their larger clearance (3.30% Chord) and reattachment for their smaller clearance (1.65% Chord). HPC blades are thicker but the clearance is also larger and so the reattachment of the clearance flow onto the end of the blade is generally prevented. Within the separation over the tip edge a 'tip separation vortex' is formed, as termed by Kang and Hirsch [1995] and also investigated by Tang et al. [2006]. The tip separation vortex convects low energy fluid towards the point of minimum pressure along the blade tip and then moves in to the passage.

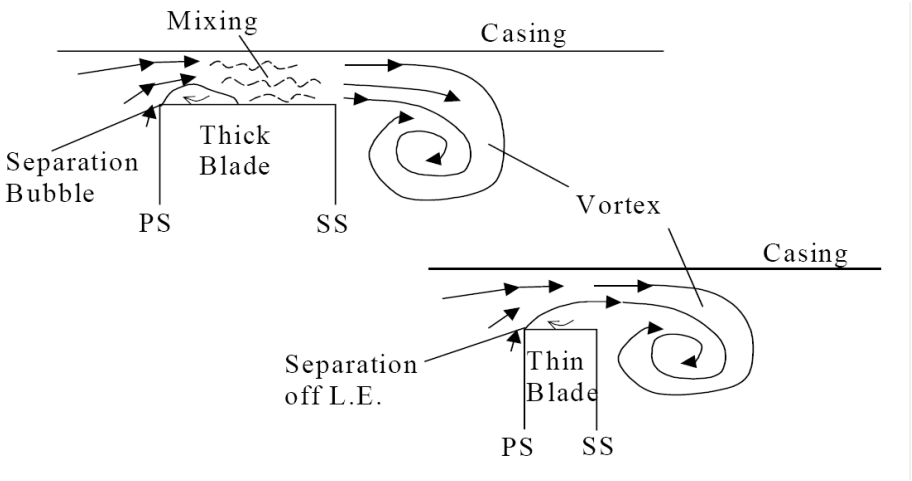

Figure 2.3: *Leakage Flow Over Blade Tip (Glanville [2001])*

2.4.2 Formation of Leakage Vortex

The tip leakage flow jet exiting the clearance interacts with the cross passage, secondary flow and the incoming boundary layer. This interaction is very complex and causes the tip leakage flow to roll up in to a vortex which is termed the 'tip leakage vortex'. Some of the leakage flow passes over the tip leakage vortex and interacts

with the passage vortex and through shear on the endwall forms a second counter rotating vortex termed the 'induced vortex' (labeled 'I' in Figure 2.4(b)). This was illustrated well by Van Zante et al. [2000] (Figure 2.4) for a transonic rotor. The leakage vortex may contain negative axial flow which has been shown through many studies, for example Inoue et al. [1986], Saathoff and Stark [2001], Brandt et al. [2002] and Saathoff et al. [2003]. The actual flow angle depends on the geometry and throttling level of the stage.

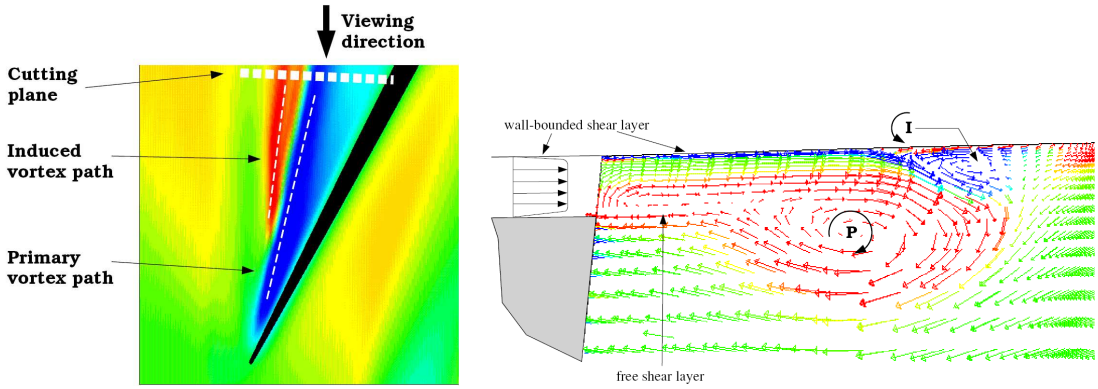

(a) View From Casing, Axial Velocity *(b) View on to Cutting Plane*

Figure 2.4: *Formation of Leakage and Induced Vortex from Van Zante et al. [2000]*

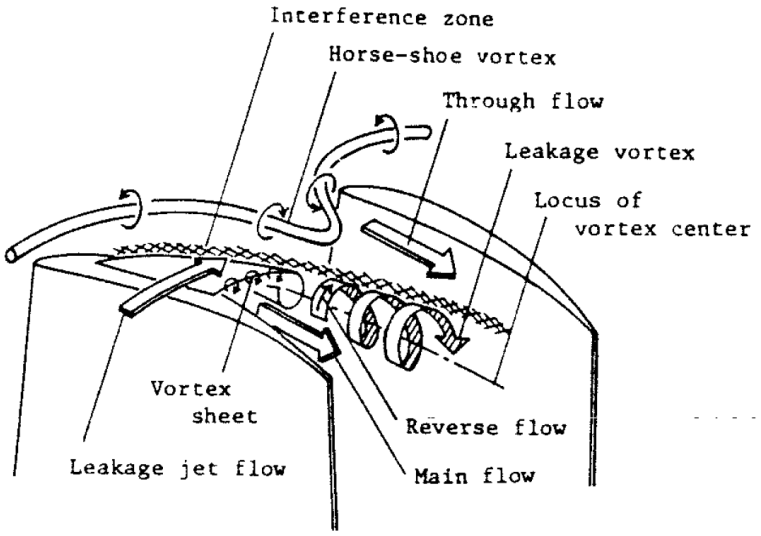

Figure 2.5: *Structure of Leakage Flow (from Inoue and Kuroumaru [1989])*

The formation of the induced vortex is not always reported, as the strength of this vortex depends on the velocity difference between the leakage jet flow and the

wall motion. Furthermore there are several different explanations in the literature of what appears to be the same feature: Inoue and Kuroumaru [1989] termed the region the 'Interference Zone' as seen in Figure 2.5; Lakshminarayana et al. [1982] (Figure 2.1) termed it the 'Interaction Region'; other explanations associate it with the secondary vortex. Saathoff and Stark [2001], Brandt et al. [2002] and Saathoff et al. [2003] also showed this feature and all these explanations appear to involve the same feature.

Figure 2.4 (from Van Zante et al. [2000]) indicates only a small secondary flow, which is counteracted by the tip clearance flow. An induced counter rotating vortex can be seen at the interface between the leakage vortex and the secondary flow. This is developed by the wall shear layer and the interaction of the cross passage flow; its strength depends on the difference between the tip clearance flow velocity and the end-wall velocity. For a transonic rotor, as for Van Zante et al. [2000], the induced vortex is much stronger than for a subsonic rotor. Van Zante et al. [2000] showed that the induced vortex inhibits the migration of the tip clearance vortex across the passage to the pressure surface of the adjacent blade. Walker et al. [2005] showed that for a stationary subsonic rotor and large tip clearances (8% span) an induced counter vortex was observed. With a moving endwall no induced vortex was observed for the same tip clearance. This was because the leakage flow was too large and completely suppressed the cross passage flow and the wall shear flow.

The HPC leakage flows can consume a significant portion of the span. For example Foley and Ivey [1996] showed that two dimensional flows for their four stage research compressor could be assumed between only 40 and 85 percent of the annulus height. This creates a blockage which effectively reduces the passage area and decreases the pressure rise across the stage. Hunter and Cumpsty [1982] investigated the increase in the boundary layer size across a low speed rotor with varying clearance, flow coefficient and inlet boundary layer thickness. They investigated clearances up to 10% of the chord finding a significant increase in blockage, in the form of low axial velocity and underturning, with increased clearance. Most of the blockage they accounted to the clearance vortex.

The tip leakage vortex can be described as two separate vortices; for example,

as found by Songtao and Zhongqi [2002]. The first emanating from the forward part of the blade tip forms a strong loss vortex core. This initially closely follows the suction surface with the favourable blade pressure profile and then at the peak loading when the blade pressure gradient becomes adverse moves away from the blade surface into the passage. After the first vortex leaves the suction surface the remaining tip leakage flow wraps around the core vortex forming a significant blockage. This second weaker vortex may pass across the passage impinging on the PS of the adjacent blade and passing through its clearance.

The tip leakage vortex is unsteady, especially at high speed, and becomes more so towards the stability limit. Mailach et al. [2001] investigated this using a four stage low speed compressor and linear cascade. They showed that close to the stability limit the leakage vortex trajectory fluctuates significantly from the normal trajectory too moving around the leading edge of the adjacent blade, and so influencing the incoming flow of the next blade. This unsteady short length scale pattern was shown to propagate along both of Mailach's experimental rigs. This is the starting point of stall and generally moves from multi stall cells, as described above, to full stall. This is a huge area of research and as such is not discussed in more detail within this thesis.

2.4.3 Influence of Tip Clearance Size

The point at which the initial tip leakage flow rolls up into a vortex was investigated by Storer and Cumpsty [1991]. They found as previously discussed that the pressure profile significantly affects the tip leakage flow and so because the loading changes with clearance size so does the tip clearance vortex. They reported that as the tip clearance was increased the roll-up of the clearance vortex moved downstream. This was found to be as a result of the increased pressure from the mainstream flow at inlet. They also found that the blade force near the tip increased with tip clearance, which was a consequence of a strengthening of the vortex and an increase in the blade pressure loading.

Storer and Cumpsty [1991] showed plots of blade loading at 2% chord from the blade tip. The effect with different clearances was as follows. Storer's tip loading and

blade contour plots are shown in Figure 2.6 for 0% and 4% tip clearance. Without clearance the suction surface had an increase in pressure, and therefore a decrease in loading which was shown to be due to corner separation. With clearance the pressure profile at the blade tip showed a marked difference. On the pressure surface the loading was lower, especially at the leading edge, and on the suction surface there was an increase in pressure at the leading edge and decrease in pressure after 20% chord. This change moved the suction surface minimum pressure and therefore the maximum blade loading downstream along the chord. Another effect was to increase the loading on the tip end so that for the 4% tip clearance the blade loading at the tip was similar to mid-span. The loading change at the tip with clearance was found to be due to the influence of the leakage vortex.

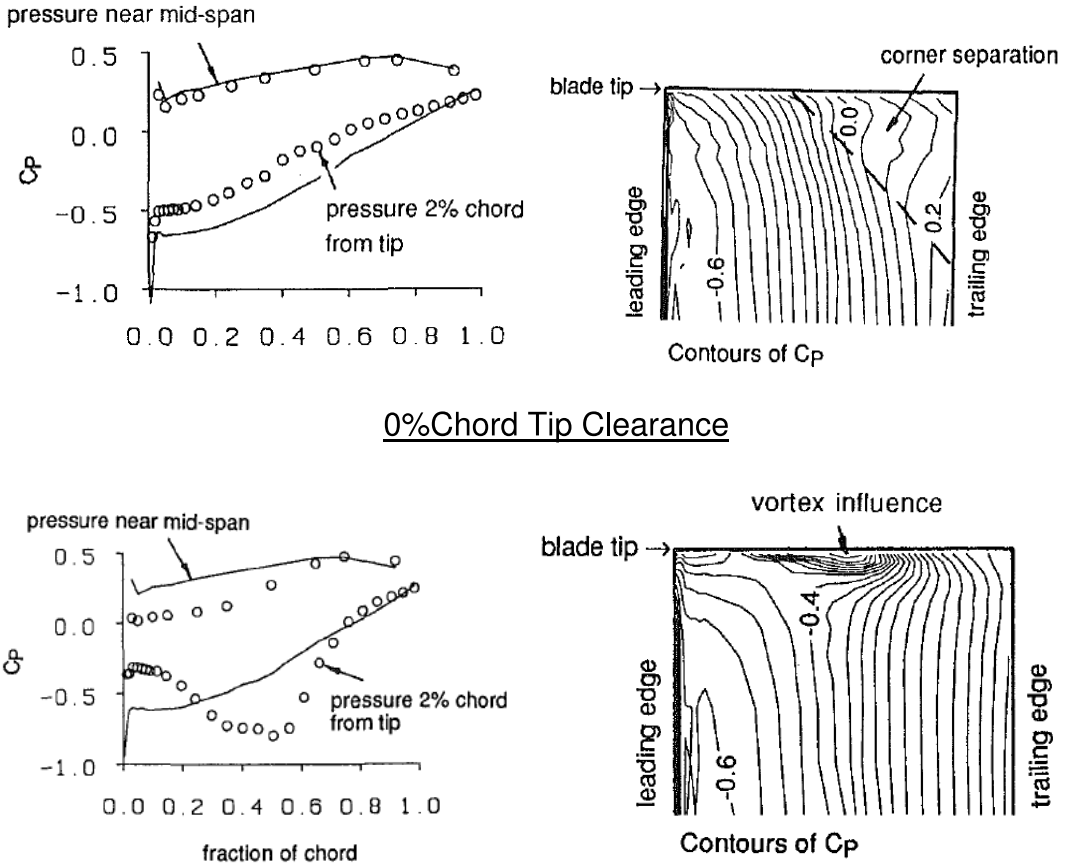

Figure 2.6: *Blade Tip Loading (from Storer and Cumpsty [1991])*

Foley and Ivey [1996] also found a decrease in suction surface pressure and increase in loading close to the tip; the reason for this was shown to be the radial flow of the leakage vortex on the suction surface. Pandya and Lakshminarayana [1983] investigated the flows within the passage and for their geometry the roll up occurred close to the mid-chord which is typical of HPC blading; LPC blading tends to be more front loaded and therefore roll up occurs earlier. A positive influence of the clearance flows was a removal of the corner separation as seen in Figure 2.6.

The trajectory of the tip leakage vortex is dependent on the row geometry, speed and throttling condition. Chen et al. [1991] found that the vortex trajectory was independent of the tip clearance value but did depend on the blade loading. Usually, at the operating condition, in highly loaded transonic rotor rows the leakage vortex moves across the full length of the passage and impinges on the adjacent blades pressure surface. However in the HPC stages, at operating condition where the rotor rows are lowly loaded, the tip leakage vortex will remain close to the suction surface and move out of the passage without affecting the adjacent blades pressure surface. The degree of migration depends on the loading of the blade. As the flow coefficient is reduced the blade incidence rises and so the blade loading rises. This strengthens the pressure driven jet increasing the strength of the leakage vortex.

Hunter and Cumpsty [1982] conducted tests on a low speed rotor with 3 different flow coefficients. They found that as the flow coefficient was reduced the tip leakage vortex moved across the passage and impinged on the pressure surface of the next blade. When this occurred, a significant blockage was established, with low dynamic head fluid close to the pressure surface and end-wall corner. The blade wake was shown to increase in size also. If the clearance vortex passed over the front of the adjacent blade then stall of the rotor occurred. Saathoff and Stark [2001] and Saathoff et al. [2003] showed through oil film plots that the leakage vortex was bounded by incoming separation (which as previously discussed may be termed the induced vortex) and this could be seen to occur far upstream of the leading edge at stall.

2.4.4 Influence of Inlet Boundary Layer

The effect of the inlet boundary layer on tip leakage flows is significant. Choi et al. [2005] found computationally that at design condition (for his single compressor rotor) the tip clearance flows and hub corner stall are similar and therefore are not affected by the tip clearance. However when operating at near stall, there was a significant effect from the boundary layer thickness. Brandt et al. [2002] computationally investigated this and used the results of Saathoff and Stark [2001] for comparison with a view to further their work to include varying the inlet boundary layer thickness. They found that increasing the boundary layer thickness moved the vortex roll-up point upstream and increased the trajectory angle towards circumferential and increased the total pressure loss. Furthermore they found that the displacement of the roll-up point is more sensitive with thin boundary layers. This was found to be opposite to varying the tip clearance, as discussed previously by Storer and Cumpsty [1991]; if the boundary layer thickness was kept the same then the roll-up point moved downstream with increased clearance. Increasing the boundary layer thickness increased the loss and blockage in the endwall region. These findings were similar to Brandt et al. [2002].

2.4.5 Influence of Leakage Vortex on Row Exit

The effect of endwall and leakage flows are generally considered by pitch mass averaging to give a two-dimensional span-wise profile, and area averaging to give a total loss value upstream and downstream of the row. Inoue et al. [1986] carried out studies of a test rotor with NACA 65 profile and varied the tip clearance up to 5mm (approximately 4.4% tip span). At inlet they showed that with increased clearance, an increased inlet yaw angle at mid-span but decreased yaw angle towards the casing occurred; this they attributed to the increased blockage and redistribution of the flow towards the mid-span. To remove the inlet angle offset with increased tip clearance size they altered the throttling setting to match the inlet angle at mid-span. At exit (as seen in Figure 2.7 they found a redistribution of flow towards the mid-span indicated by the increased axial velocity, resulting in a reduction in velocity on the

casing. This was also seen with the exit angle, where for their larger clearances there was an increase in turning at approximately 0.95% span and a large under turning of approximately 20° on the casing. They also plotted the total pressure loss coefficient. At mid-span there was only a marginal change due to the matching of the inlet yaw angle. With tip clearance a slight reduction in loss at 90% span and then loss increase at the leakage vortex peak followed by a smaller loss on the endwall. This large under turning and low energy fluid is then passed into the next row and is one of the causes of endwall skew.

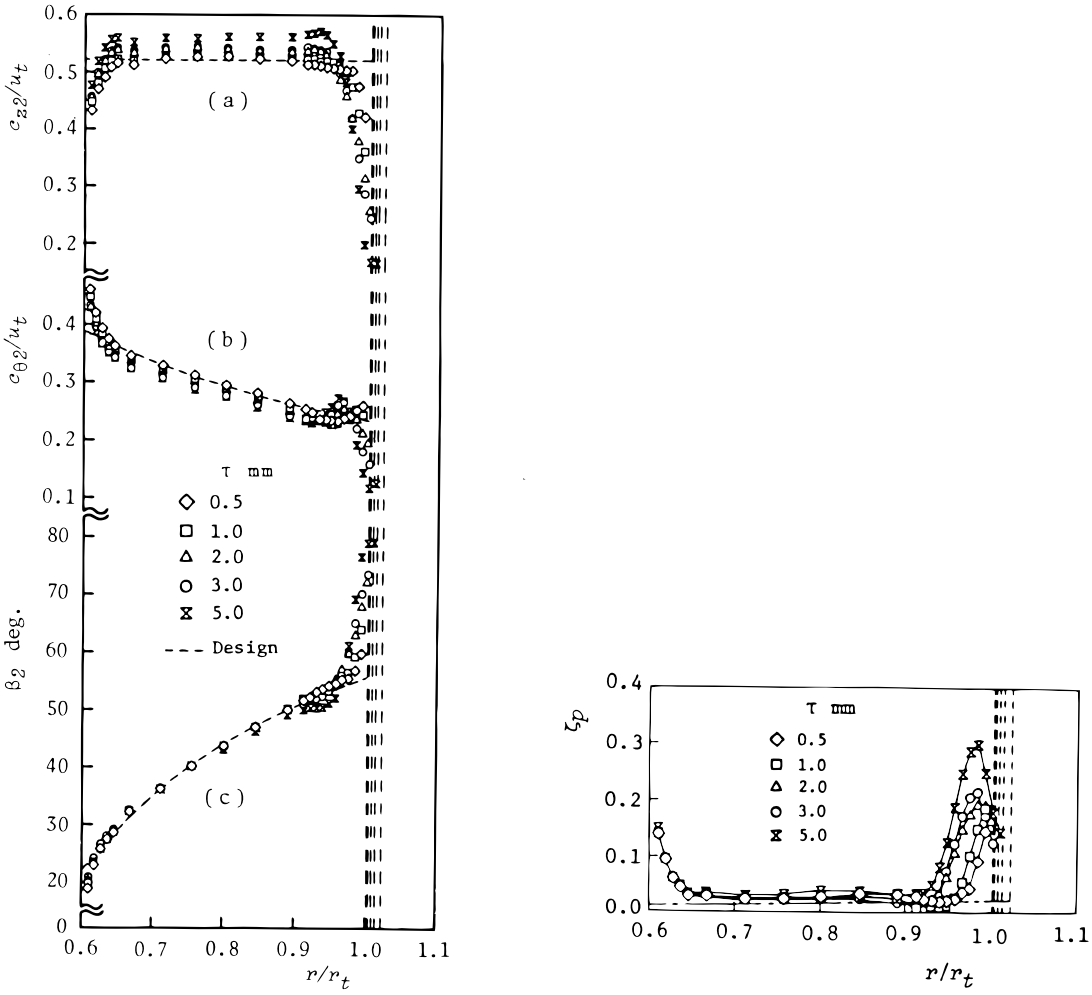

(a) *Distributions of Axial Velocity, Tangential Velocity and Relative Velocity*

(b) *Distributions of Total Pressure Loss coefficient Through Rotor*

Figure 2.7: *Flow at exit of a Rotor Row (from Inoue et al. [1986])*

2.4.6 Leakage Flows in High Speed Rotors

In the LPC rotor the leakage vortex is somewhat different to the IPC or HPC. This is because of a combination of the blade geometry, rotor loading and speed. Unlike the HPC the leakage vortex core emanates from the leading edge of the blade and then passes through the passage. As previously mentioned, the remaining leakage flow from the rest of the blade wraps around the leading edge vortex core and will impinge on the adjacent blades PS.

Within high speed rotors, above Mach 1, shocks occur within the passage; their interaction with the tip leakage vortex has been studied widely. Much of this work has concerned the NASA Rotor 37 as representative aero-engine geometry, for example Suder [1998], Gerolymos and Vallet [1999] and Suder and Celestina [1996]. The shock-vortex interaction is a major source of loss in axial compressors because the shock forces the leakage vortex to burst and leads the row to stall. As described by Schlechtriem and Lotzerich [1997]: "*The location of the shock-vortex interaction is a function of the back pressure. If the back pressure reaches a certain level the position of the interaction of the shock with the tip leakage vortex moves upstream and the burst vortex no longer heals up. The end-wall blockage grows rapidly and the compressor stalls. In this case the blockage extends upstream of the leading edge*". The vortex breakdown is due to the sudden flow deceleration across the shock.

2.4.7 HP Specific Tip Clearance Flows

As previously discussed the tip clearance gap within the high pressure stages of industrial machines are relatively large. Only limited literature, has concerned clearances of the size of interest. One of the few papers is by Hunter and Cumpsty [1982] who varied the tip clearance of a low speed rotor from 1% to 9.2%. They found that the blockage significantly increased with tip clearance and with blade loading. Downstream traverses showed that the under-turning through the cascade was significantly increased and therefore the pressure rise was decreased. They also examined the effect on stall coefficient and due to the increased blockade the stall coefficient also increased and stall occurred earlier. Layachi and Bölcs [2002] used two

different clearances the largest being 4.8% chord, their results showed a significantly thicker boundary layer through the entire stage.

2.4.8 Other Tip Vortices

Also shown in Lakshminarayana's (Lakshminarayana et al. [1982]) plot (Figure 2.1) is the 'Scraping Vortex' which travels along the pressure surface tip of the blade. The formation of the scraping vortex arises from the inlet skew within the inlet boundary layer. This will not arise if the tip clearance is larger than the boundary layer thickness and the mainstream incidence is low. The Scraping Vortex can be thought of as one leg of the horseshoe vortex which can partially exist when a tip clearance exists. It tends to be a weak feature and so having little effect. The high skew boundary layer flow associated with the creation of the scraping vortex on the contrary does have a large influence on the endwall flows.

2.4.9 Multi Row Effects

Axial compressors consist of many rows in succession. Therefore each row cannot be considered to act independently and must be matched to the row upstream and downstream. Furthermore the interactions between rows are highly unsteady. Many authors have considered this, including Cumpsty [1989], Horlock [1995] and Denton [1993]. All the flows within the row affect the downstream flow and these include; the mainstream flow, wake, leakage flows, hub/casing separation, and secondary flows. Within a tip leakage flow context, the tip leakage flows/vortices will pass into the next row affecting the performance of that row. Conversely the row in question will also be affected by the upstream rows hub/casing clearance flows.

As previously examined the flow at rotor exit will vary along the span and so the following row must be designed to allow for this. The rotor tip leakage has the effect of reducing the incidence on to the stator root while the skew effect increases the incidence. The net effect depends on the design and operating condition. Clearly the unsteady interactions between rows are of much interest, but are not examined in detail here. One such multi-row unsteady effect is the relative circumferential

position of the blades which is termed clocking. Layachi and Bölcs [2002] showed that the effect on efficiency of varying the stator clocking was within 0.7% and 1.5% depending on the turbulence model used within their simulations.

2.5 Linear Cascade Testing

Linear cascade testing allows for simplification of the real machine which aids the study of turbomachinery flows both experimentally and theoretically. Therefore traditionally linear cascade testing has been of great use to understand compressor flows. However the simplified flow may also make the result non-realistic if not properly understood. Cumpsty [1989] describes the use of linear cascades and 'Cascade Aerodynamics' a book by Gostelow [1984] explores cascades and cascade testing in detail. Gostelow defined the cascade as an "*infinite row of equidistant similar bodies*" which in turbomachinery are usually aerofoil. The challenge comes when the cascade is not infinite and therefore the flow will be non uniform along the length. For this reason a compromise between the length of the cascade and its size has to be met to fit the wind tunnel powering the cascade. Linear cascades have a significant role to play in compressor and turbine testing. The greatest advantage, as well as the relatively cheap cost, is that many measurement techniques are possible within the cascade that are not within rotating machines. For example, detailed pressure measurement within a rotating passage.

Brandt et al. [2002] showed that the results may be closely related to the rotating case. Within linear compressors the flow at inlet is what Cumpsty [1989] terms 'collateral flow' which means that the flow direction within the boundary layer is uniform and as such can be considered as a normal boundary layer. This boundary layer also tends to be un-representatively thin. Within real machines there is significant inlet end-wall skew. The cascade's relatively thin inlet boundary layer also poses additional problems. In a rotating machine the high skew flow over the tip of the blade will normally cause a separation along the blade suction surface corner. Conversely with the linear cascade having a thin and low skew inlet boundary layer the final part of the blade corner region may only reach boundary layer transition.

2.6 CFD Tip Clearance Modelling

Most of the work undertaken on tip clearance flows since the late 1980's has included some CFD or numerical analysis. Computations are now common place and testing is only undertaken where necessary. The reason for this is mostly due to the low cost and effort required in CFD but also because experimental measurements close or within the tip gap are very difficult and with rotation almost impossible. Experimentation is however still required, even though CFD has huge time saving advantages over experimentation, the CFD models must be compared to experimental data so that the results can be trusted. For example the loss is hard to predict quantitatively using CFD.

As described by Van Zante et al. [2000] and also investigated by Gupta et al. [2003]; there are currently three general methods for treating the tip clearance gap:

1. Assume flow periodicity across a non-gridded region above the blade tip (Figure 2.8(a)).

2. Rounding the blade tip by distorting an H-type grid to fill the gap over the blade i.e. pinch tip (Figure 2.8(b)).

3. Fully gridding the gap with a separate gridded block.

It is advantageous in order to save computational power to use the technique which uses the least number of cells possible. For this reason the above list is in order of computational time preference, but unfortunately also in order of increasing accuracy. One difficulty of using a pinch tip model is that the grid around the tip can be of poor quality. This can have the result of creating numerical loss, thus over-predicting the loss.

The use of the first method can be assumed to be reasonable when considering the flow as a vena-contracta. However the tip clearance must be set to that of the vena-contracta's minimum thickness or a discharge coefficient must be employed. This is because the first method will over estimate the size of the actual tip clearance flow.

The pinch tip model attempts to model the leakage jet as a vena-contracta. One problem with this method is that it is difficult to know the size of clearance that is

being modelled without calibration of the mesh to experimental data. Storer and Cumpsty [1991] compared this method in Figure 2.9 to the flow around a square edge and showed that the results were comparable. Therefore this method is reasonable but only if the flow remains separated over the entire tip of the blade which, as discussed earlier, occurs for a relatively large tip clearance or thin blade.

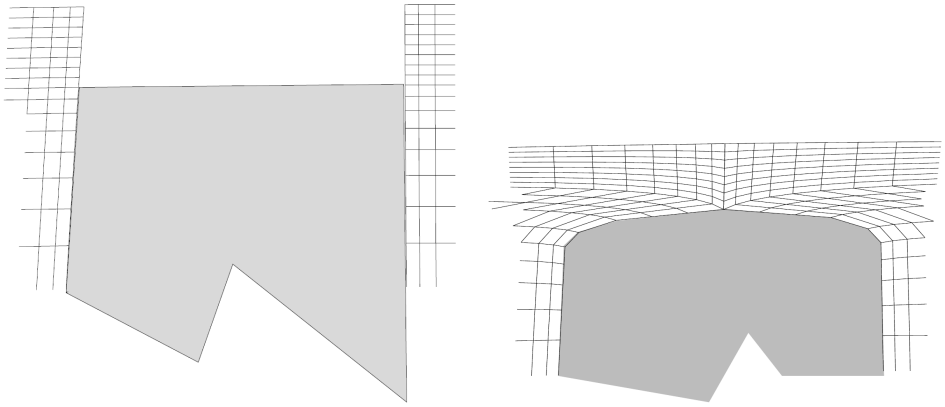

(a) *Non Gridded* ***(b)*** *Pinch Tip*

Figure 2.8: *Tip Clearance CFD Modelling Techniques (from Van Zante et al. [2000])*

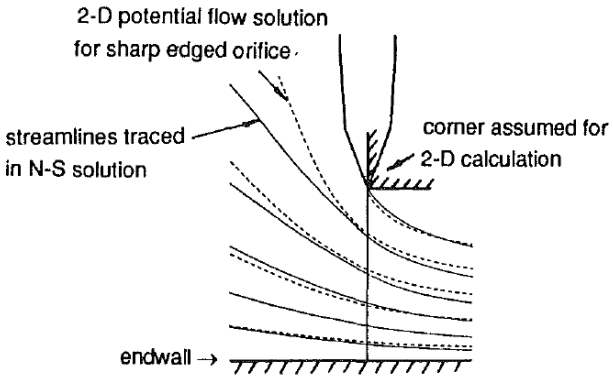

Figure 2.9: *Blade Pinch Tip Modelling from Storer and Cumpsty [1991]*

Modelling the tip gap fully, has advantages as it removes the unknown contraction size of the vena-contracta over the tip of the blade tip and therefore allows for the correct clearance size to be modelled. This however uses significant computational time due to the required cell number and requires multi-block CFD codes. Gupta et al. [2003] and Van Zante et al. [2000] conclude that fully meshing the tip

leakage area is the superior method. Gupta found that this method more accurately predicted the pressure rise through the clearance and as such better predicted the row pressure rise. They also found that mesh clustering in the casing region, which every tip model used, was necessary to resolve the shear layer interactions and therefore the leakage vortex trajectory. The pinch model and non-gridded model both were shown to over predict the pressure rise and loss through the tip. Gupta et al. [2003] suggests that the pinch model can produce reasonable results if the grid resolution is reasonable and the tip shape is set correctly.

2.7 Loss Reduction Techniques

Methods of loss reduction within axial compressors is a vast research area. Many methods have been proposed and investigated which try to reduce secondary and tip clearance flows; as with tip clearance flow these techniques have mostly been proposed within the LPC as methods for prolonging the onset of stall. Minimising the blade clearance, historically, is the primary method to reduce the effect of the tip leakage flow. This however cannot be done to a successful level within the HPC, the subject of this thesis. Therefore other techniques must be examined.

The different techniques can be widely defined within two categories; 3-D blading design, and end-wall treatment. Some of these methods are now explored.

2.7.1 3-D Blade Design

3-D blade design generally aims to reduce the blade loading near the end of the blade or to modify the blade chord-wise loading distribution. This facilitates the reduction in secondary flow and tip clearance flows because they are both, as previously discussed, controlled by the local blade loading at the tip of the blade. The main blade modifications may include; dihedral, sweep or blade profile modifications (e.g. re-cambering). Dihedral is the movement of the blade perpendicular to the chord, whereas sweep is movement along the chord. The optimum 3-D design is difficult to obtain and requires significant effort to achieve across all compressor operating conditions. Therefore a great deal of work is ongoing to find a sustainable design

method to obtain the optimum design. One example of the application of sweep and dihedral is by Tschirner et al. [2006] who showed that through 3-D blade design significant changes can be made to the efficiency and operating conditions.

Dihedral is defined as being positive if the blades suction surface has an obtuse angle with the endwall. This results in a component of blade force on the fluid towards the endwall raising the endwall static pressure and so reducing the endwall Mach Number and velocity on the suction surface of the blade tip. The effect of the increased pressure is a reduction in the cross passage pressure/flow reducing the secondary flow (passage vortex) and a reduction in the cross blade tip pressure difference, reducing the tip clearance flow. The reduction in blade loading and cross passage secondary flow also has the effect of suppressing the corner stall reducing the blockage. Gallimore et al. [2002] numerically investigated the effect of positive dihedral (bowed blades). They found that an increase in pressure surface loading (increased static pressure) with positive dihedral occurred but this was outweighed by the larger increase in SS static pressure giving an overall increase in blade loading at the tip. At the hub there was a reduction in corner stall but the span-wise redistribution affected the mid-span resulting in an increased wake thickness.

The effects of dihedral are not always positive. Fischer et al. [2004] showed that the use of strongly bowed stators for the last two stages of a 4-stage axial compressor worked as expected reducing the endwall loading and increasing the mid-span loading. At high loading the dihedral had the overall effect of increasing the efficiency and pressure ratio, but below the operating point the increase in mid-span loss outweighed the reduced end-wall loss resulting in an overall decrease in efficiency at nominal operating point.

Sweep is defined as being positive if there is an obtuse angle between the leading edge and upstream endwall. Therefore if the blade is leant forward from the hub (forward sweep) there is a negative sweep at the hub and positive sweep at the casing. Sweep is usually used within transonic rotors, where the effect is to move the shock. The effect of positive sweep is to bend the suction surface streamline towards the endwall and to bend the pressure surface streamline away from the endwall. This has the effect of opposing the secondary flow. Positive sweep also has

the effect of redistributing the loading towards the trailing edge. Again the effect of three-dimensional design on the mainstream flow must always be considered because the three-dimensional effect changes with operating condition. Corsini and Rispoli [2003] showed this; they investigated the use of forward sweep on a low speed fan. This had the positive effect of reducing the secondary flow and tip clearance flow at low flow coefficients. However at high flow coefficients the efficiency reduced because of increased diffusion towards the casing.

Blade profile modification techniques are methods that change the blade shape to allow for or oppose the endwall flows. These techniques include re-cambering and leading edge bulbs. Re-cambering involves altering the blade shape close to the endwall to match the inlet flow angle within the boundary layer; the blade exit angle may also be changed to allow for the different exit angle. This method is often known as 'end-bends'. The term leading edge bulb describes the thickening of the leading edge. The mechanism as investigated by Müller et al. [2003] is to strengthen the suction side horseshoe vortex, which opposes the secondary flow passage vortex. As the horseshoe vortex does not occur if there is a tip clearance and as the tip leakage flow suppresses the passage vortex this method is only of use at the root of the blade (i.e. rotor hub or stator casing). Using both numerical and turbine cascade experiments (without skew), they found that a significant reduction in loss was achieved with the implementation of leading edge bulbs.

The blade profile modifications methods above are used in the first instance to suppress the corner separations and in the second instance to suppress the secondary flows. There have been a number of blade profile modification techniques suggested to reduce the tip clearance flows. Wisler [1985] referred to a number of these ideas, which include grooves on the blade tip, winglets and squealer tips. The only method that appears to be widely used is the squealer tip; however the use of this is for mechanical reasons to reduce the contact area during a rub. No literature that the author is aware of, assesses any of these techniques within compressors. However some similar studies within turbines have been undertaken, for example Booth et al. [1982]. Who found that there use was somewhat inconclusive.

Jia et al. [2001] numerically investigated a chord-wise linear variation in tip gap.

He found that if a stator tip gap is linearly increased from the leading to the trailing edge then the overall efficiency was increased compared to a uniform clearance with the same circumferential leakage area. His increase in gap was between 0.7 mm to 2 mm from leading to trailing edge. As previously discussed he found that with a small clearance ($< 1\%$ Span or $< 1.5\%$ Chord) the leakage flows had the effect of suppressing the secondary passage vortex increasing the efficiency, but with larger clearances the effect was to reduce the efficiency and performance. There was no mention as to the effectiveness of the expanding tip clearance with large tip clearances or why such a technique would be used at all in a real machine. It would appear from their figures, that the efficiency with a constant clearance at the lowest value of the expanding clearance was higher than the efficiency with the expanding clearance, therefore the smaller constant gap would appear superior. They did report however that the technique prolonged the onset of the tip leakage vortex roll up which maybe the intended application.

2.7.2 Endwall Treatment

Endwall treatments use the shaping of the endwall to alter the flow through the passage with the aim of increasing the operating range of the compressor. Two notably different classifications exist; endwall profiling and casing treatments. Endwall profiling describes the contouring of the endwall to reduce the secondary passage vortex and would normally be used at the blade root, or within a shrouded compressor on both the casing and hub walls. For this reason the method may also be classed within 3-D blade design. Casing treatments are generally modifications to the casing of a rotor, or the stator hub, the main motivation being to improve the stall margin by suppressing the blockage primarily due to the tip clearance vortex, but also the endwall flows more generally.

2.7.3 Endwall Profiling

As end-wall profiling is not associated with the tip of the blade it is not reviewed in detail. Hoeger et al. [2002] used end-wall profiling on the hub of a transonic rotor

cascade. Their technique employed a concave contour on the end-wall close to the pressure surface and linear profile at the suction surface. This enhanced the pressure close to pressure surface enhancing the cross flow. The mechanism therefore was to locally reduce the Mach number and consequently the shock losses. end-wall non-axisymmetric profiled end-walls have been used successfully in turbines e.g. Gregory-Smith et al. [2001] and similarly have now been implemented into aero-engines. The concept has been to raise the pressure near the suction surface and lower it near the pressure surface, reducing the cross passage pressure gradient which drives the passage vortex. This method should also work for compressors and as an outcome reduce the corner separation, reducing the blockage. Recently Harvey [2008] & Harvey and Offord [2008] applied profiled end-walls to a compressor and reported promising results.

2.7.4 Casing Treatment

Casing treatment has been of interest since the early 1970's as a method to reduce the blockage within the blade tip region, hence improving the stall margin. Most casing treatments attempt to shift, remove or suppress the blockage caused by the tip clearance vortex. Most work has been undertaken for transonic fans or rotors and therefore their use within the HPC can only be considered. Passive casing treatments often include (as seen in Figure 2.10 taken from Cumpsty [1989]) axial, circumferential or angled slots, or may for example have a honeycomb structure. These slots may be cut perpendicular or at an angle in to the casing. Another casing treatment could be trenching where by the tip of the blade is recessed in to the casing. Passive casing treatments remove flow from the high pressure regions and then reintroduce the flow where the pressure is low; this helps to reduce the tip clearance flows. The above mentioned techniques are all passive. Other techniques are active. Active control uses features such as injection or suction to suppress instabilities and secondary flows.

Some of the above treatments are good candidates for HPCs such as those of interest within this thesis. Only passive axial and circumferential grooves, and their variations are examined within this review. This is because they show potential for

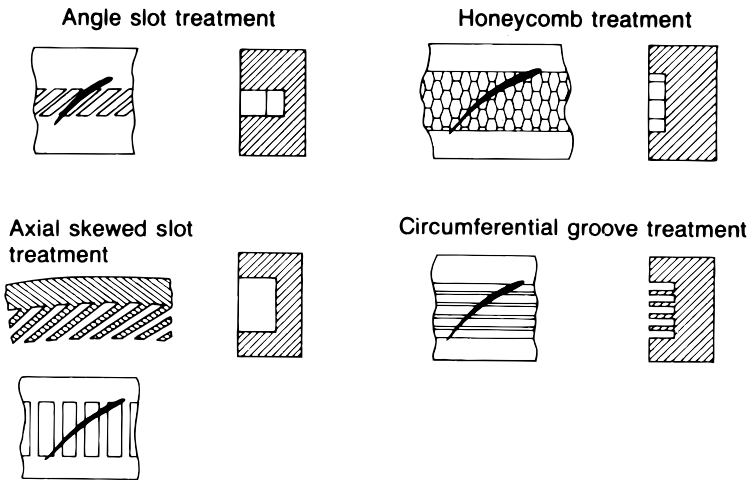

Figure 2.10: *Examples of Passive Casing Treatment (from Cumpsty [1989])*

controlling the tip clearance flows and therefore increasing the surge margin while being simple and potentially cost effective to implement within the real machine.

Casing treatment methods have typically resulted in reduced efficiency, because the flow mechanisms absorb energy. However some recent work has reported only a modest reduction in efficiency. A method that works within one part of the compressor may not work within the other because the treatments are flow specific and may rely on shock interactions. As stated by Cumpsty [1989], "*not all treatments are effective and some can in fact worsen the flow*". He also states that, "*Casing treatment is only effective when it is installed where the rate of increase of local blockage and perhaps deviation with decrease in flow rate is rapid; often this is near the rotor tips but it need not always be*". Therefore casing treatment is only of use if the region that it is implemented in the region that causes the compressor to stall. For example a compressor may stall from the hub if the growth of the hub corner separation occurs first in which case end-wall profiling may be a better option within that row. Much of the literature, e.g. Cumpsty [1989] and Johnson and Greitzer [1987], explains that the compressor row must undergo 'wall stall' and not 'blade stall' within the end-wall region for the casing treatment to be effective.

Honeycomb

Honeycomb structures are perhaps the simplest idea. The flow enters the individual cell when the pressure is high and then emerges when the pressure is low as the blade passes over the cell. For this method to work the flow clearly has to be compressible (transonic) with reasonably high pressure changes and therefore at high Mach Numbers. These conditions are only found in the earlier stages of the industrial axial compressor and therefore this technique will not function within the HPC.

Axial Slots

Axial slots are slots parallel to the rotational axis and can be skewed radially and/or axially. Skewing of the slots allows for alignment with the flow at exit from the slots. As far as the author is aware all the work using casing treatment, and in particular axial slots has been undertaken within rotating experimental rigs or more recently using 3-D computational methods. Much of the experimental work has been undertaken using stator casing treatments to avoid instrumentation difficulties in the rotating frame. This work can then be related to the casing due to the end-wall flow similarities between the rotor casing and the stator hub. Many positions and angles of axial slots have been attempted, but the optimum geometry appears to be very much row specific. The lean towards the pressure surface gives the best increase in stall margin with a lean to the suction surface giving a decrease in stall margin.

With most of the early attempts, e.g. Smith and Cumpsty [1984] or Johnson and Greitzer [1987] the slots covered a significant proportion of the axial chord and were positioned between the leading and trailing edges. Johnson and Greitzer [1987] used a previously proven design by Takata and Tsukuda [1977] and implemented on both the rotor and hub walls. Johnson's research compressor was low speed with a rotor tip Mach Number of 0.24. Therefore the working mechanism did not require compressibility and as tentatively concluded by Cumpsty [1989] the unsteadiness of the blade passing the slots was not important.

The working mechanism behind axial slots is a removal of the high pressure flow

towards the trailing edge and then a recirculation within the slots towards the front part of the blade close to the leading edge. The flow, as found by Johnson and Greitzer [1987], leaves the axial slot with a high velocity jet (compared to the inlet end-wall axial velocity) which he suggests was strongest if the slots are leaned facing the blade pressure surface.

One of the first reported attempts to model axial slots was undertaken by Crook et al. [1993], the slots extended from 5% to 95% of axial chord and at 60^0 to the perpendicular; similar to those of Johnson and Greitzer [1987]. They modelled the flow using a steady extraction at the trailing edge and injection at the leading edge. From their calculation they determined that the suction of low total pressure fluid at the trailing edge and suppression of the leakage vortex blockage due to the excitation from the inlet jet at the front of the passage, delayed the stall by reducing the blockage. This method however provided no understanding of the flow structures within the slots.

A more recent study by Wilke and Kau [2002] used steady simulations to model the use of axial slots perpendicular to the casing within a transonic compressor. For their case they aimed to suppress the tip clearance vortex in such a way as to prevent the bursting of the vortex due to the shocks and thus the high static pressure region within the tip clearance region creating the blockage. They found that the high pressure rear end of trailing vortex moved into the slot creating a slot vortex which then exited the slot and suppressed the rolling up of the tip clearance flow close to the leading edge when the pressure was low. Wilke and Kau [2002] stressed the use of unsteady simulations to capture the full effects of slots because of the relative movement of the blade and slots.

Other recent studies include Emmrich et al. [2007], Lin et al. [2008], Ning and Xu [2008], Lu et al. [2006b,a, 2008]. Lu et al. [2008] presents several casing treatment designs as variations to purely axial slots; these included angled slots (i.e. not parallel to axial) and bend skewed slots which are a combination between both methods. They suggested that all these methods improved the stall margin. The bend skewed slots gave the best stall margin improvement with the lowest efficiency penalty. He also found that the driving force, as previously discussed, behind the

improvement was the recirculation within the slots from high pressure regions to low pressure regions.

Axial slots have successfully been implemented to raise the surge margin of many compressor designs, with a full spectrum of Mach Numbers; most recent work however has been undertaken concerning transonic stages. All of the work until recently, has employed rotating experimental rigs due to the interaction of the slots with the blades. This has lead to difficulties finding optimum designs because of the unknown flow mechanisms within the slots. Recently computational techniques have given insight in to the flow patterns within the slots allowing for designs that minimize the losses as well as the surge margin.

The author has found no literature that uses axial slots or similar within HPCs, such as those found in industrial compressors, with large tip clearances. The performance of axial slots for this application is unclear, however the author hypothesises that because of the highly skewed thick boundary layer flow that passes directly over the tip of the blade and the low blade loading, the wall pressure difference will not be significant enough to create the required recirculation within the slots. To investigate this method, experimental rotating machines or computational simulations would be required. Therefore and because of the facilities available to the author this method is not investigated within this thesis but may have potential within HPC's if the pressure differences within the wall region are large enough.

Circumferential Grooves

Circumferential grooves are another widely researched passive end-wall treatment. Again, as with the axial slots, the idea is to remove the high pressure low momentum fluid and inject it back in to a lower pressure region. Practical use of circumferential grooves has been limited due to a lack of detailed understanding; their research being limited to a few experimental investigations. Since 2002 there has been an increased interest in circumferential grooves, possibly because of improved computational techniques allowing for enhanced detailed understanding of the working mechanism.

Rabe and Hah [2002] and Wilke and Kau [2002] both investigated such treatments on transonic rotors and both reported significant stall margin improvements. Rabe and Hah [2002] concluded that the additional radial and tangential flows created within the grooves caused additional mixing and loss which reduced the efficiency. As a consequence they found a thickening of the row boundary layer and a movement of the shock upstream. They also reported that unlike subsonic rotors were the grooves are usually deep, shallow grooves were more effective and that two grooves close to the leading edge were better than five grooves of any depth covering the majority of the chord. They suggested that the "*working mechanism by which circumferential grooves increase compressor stall margin is an alteration of the local flow distribution near the pressure side of the leading edge*" and that "*the effectiveness of the grooves can be measured by how much they reduce flow incidence on the pressure side of the leading edge*".

Wilke and Kau [2002] used two circumferential groove designs, the first design contained four grooves equally spaced with the tip chord and the second had eleven grooves with a more stretched height to width ratio. They found that the first configuration had the best results for all speeds and that close to stall an improvement in efficiency occurred. The second configuration with eleven grooves gave poorer results and significantly decreased the efficiency. They attribute the improvement in stall margin to a weakening of the rolling up mechanisms of the tip leakage vortex. This delayed the vortex breakdown which lead to stall. As a development to the design they tried only modelling the first configuration with either the first or last two slots blanked and found that there was no longer an increase in stall margin. This was because the vortex was able to form unhindered in the area without slots. Computationally Wilke and Kau [2002] point out that steady simulation is appropriate for circumferential treatments but for axial treatments it is not.

The NASA Rotor37 is a high pressure ratio transonic compressor rotor, and numerous researches have implemented circumferential grooves on to it. Such studies include Beheshti et al. [2004], Chen and Fu [2005] and Huang et al. [2008]. All three papers reported an increase in surge margin and decrease in stall for some, but not all, of the tested configurations. Chen and Fu [2005] employed two different

configurations, firstly one groove placed close to the leading edge and secondly seven grooves equally spaced across the entire axial chord. They found that only the seven grooved design delayed stall and extended the surge margin (a similar result to Wilke and Kau [2002]). Huang et al. [2008] numerically investigated many combinations of slot position. For the Rotor 37, which has a tip clearance of 0.47%, the following effect of the grooves was found: at the leading edge to 10% axial chord the grooves had almost no effect on the stall margin as they had limited effect on the important flow structures; between 15% and 40% chord the grooves influenced the tip leakage vortex trajectory reducing the blockage and controlled the tip leakage vortex shock breakdown; from 45% to 80% chord the grooves suppress the trailing edge separation found with small or no clearances. Huang et al. [2008] therefore suggested that with small tip clearances grooves between 10% and 90% chord should be used, and with larger clearances grooves between 10% to 45% chord can be as effective as they only affect the flow attributed to the tip clearance vortex.

Müller et al. [2007, 2008] successfully increased the stall margin, using circumferential casing treatment within a transonic rotor of an experimental single stage test rig. Figure 2.11 is a picture taken from Müller's 2007 paper showing their six deep groove configuration. Müller et al. [2007] presents stage characteristics for several designs with varying groove number and depth. They found that six deep grooves spanning almost the full axial chord incurred the largest increase in surge margin. He reported an increase in stage efficiency which he attributed to a positive effect on the stator inlet and so having an overall stage efficiency increase. The increase in efficiency was a result of the positive effect of the casing treatment outweighing the increased losses within the grooves.

Müller et al. [2008] further investigates the flow patterns surrounding circumferential grooves. Using unsteady piezoresistive pressure sensor measurements on the casing he showed that at near stall the tip leakage vortex trajectory was significantly altered by the casing treatment. Usually at near stall the tip clearance vortex hit the front part of the adjacent blade's pressure surface, but with the casing treatment the trajectory was similar to the normal operating condition and remained close to the suction surface. Müller et al. [2008] differentiated between the tip leakage

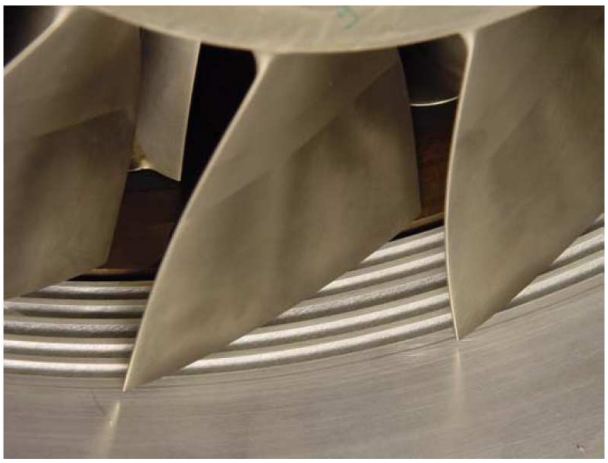

Figure 2.11: *Müller's Circumferential Six Groove Design ("Darmstadt Rotor-1 with CG6d Casing" from Müller et al. [2007]*

core vortex (emanating from close to the leading edge of the blade) and the later vortex emanating from further along the blade. He found that the over tip leakage vortex, that would normally have a trajectory that impinged on to the adjacent blade and close to stall remained close to the suction surface as if under normal operating conditions. This shift in trajectory reduced the blockage and therefore the operating range. Müller offered as an explanation a reduction in circumferential tip clearance flow, which numerically he found to have a mass flow reduced by 60% with the grooves compared to the smooth casing. The reason for this was due to the reduced pressure gradient across the blade tip and the radial flows in to and out of the grooves suppressing the over tip leakage flow.

Circumferential casing treatment grooves have been successfully applied to low speed compressor rows. Lu et al. [2006b] as discussed earlier investigated axial and circumferential slot configurations. Their circumferential slot design consisted of 5 equally spaced grooves between 8% axial chord upstream and downstream of the blades LE and TE. He found, as with Müller et al. [2007], that the extension in surge margin was a result of a repositioning of the tip clearance vortex towards the suction surface of the blade due to a decreased tip clearance flow brought about by a reduction in the blade tip loading.

Perrot et al. [2007] undertook a CFD-based investigation again of five equally spaced grooves. They found that the grooves, as previously discussed, removed

the cross tip low momentum fluid within the boundary layer and inject it back in to the passage. The fluid entering the passage disturbed the tip leakage backflow and limited the spreading of the leakage vortex towards stall. He evaluated the contribution of each groove to the overall performance gain. The first three grooves were found to have the largest contribution at high throttling with the last two grooves only having a small contribution. The first groove was found to increase the stability while the second was found to increase the performance. The third groove added to both the overall efficiency and performance gain reaching the same improvements as with the five grooves. Close to stall the last three grooves were found to have a negligible effect, but for lower throttling levels they were found to have a positive effect justifying their existence.

More advanced groove configurations have been investigated, for example Yu [2004] tested several groove configurations within a ten stage subsonic aviation compressor. The configurations included: constant groove depth with changing axial location; linearly changing groove depths both deep to shallow and shallow to deep, again varying the axial location; and finally three other advanced designs were tried with varying depths including two where the blades were entrenched. They found that changing the groove depth was important in order to obtain increased stall margin this however involved significant effort to assess the optimum design for each row/geometry. The author's observation is that Yu's results showed that there was a significant dependence on the location of the grooves with varying depth but with a constant depth there was not. Therefore for a robust design constant depth grooves may be superior.

To summarise, the use of circumferential grooves have been widely investigated. For subsonic and transonic compressors a positive effect on performance and efficiency has been demonstrated with the correct design. Circumferential grooves appear to be appropriate for HPC geometry. As far as the author can find, no studies have been undertaken concerning large tip clearances, comparable to the size within this thesis. This method may have potential within the HPC stages explored within this work.

2.8 Conclusions

This chapter has explored a selection of literature surrounding the tip leakage flows within axial compressors. Large tip clearance flows within the HPC are the subject of this thesis. It is clear that there is little literature available on the subject, which illustrates the contribution that this thesis can make to the subject.

Two different cascades were used within this thesis and the description of which follows. These cascades vary in geometry and allow for the investigation of clearance flows. Computational simulations of the cascades was also employed to further the experimental work. A pinch tip method is used to mesh the tip of the blade. This methods appears valid from the available literature if the over tip leakage flow remains unattached over the end of the blade as in the HPC.

Circumferential casing treatment appears to show potential for use within high pressure compressors. As the working mechanism does not rely on the relative movement of the casing and the blade, then linear cascades may be an appropriate method of investigation. This will be investigated in Chapter 6.

The next chapter (Experimental Methods and Techniques) will present the two cascades used for this thesis.

Chapter 3

Experimental and Computational Methods and Techniques

This chapter describes the low speed linear cascade test facilities used within this thesis. Two linear cascades were used, one which was adapted for tip leakage flow investigation (Build-A) and the other bespoke for this work (Build-B). Build-A consists of low stagger relatively high turning geometry, and Build-B had more engine representative geometry with relatively high stagger and lower turning. Both linear cascades attached to the exit of the same wind tunnel. This chapter includes the following; instrumentation and data processing, wind tunnel arrangement and flow quality, Build-A low stagger cascade and Build-B engine representative cascade.

3.1 Instrumentation

The measurement techniques used were 5-hole pneumatic pressure probe measurements and blade static pressure measurements; the use of these measurement techniques is well known and as such only a brief overview is included. Automated data acquisition techniques were used and controlled using in-house software named 'Durham Software for Wind Tunnels'; post processing of the raw data was also undertaken using this software. The program suite is written in C and was operated in Windows XP. A user manual existed within the School of Engineering for the use and application of this software. Figure 3.1 shows the instrumentation attached

to Build-B. Of note are the instrumentation trolley, probe, traverse equipment and stand. The instrumentation trolley consisted (from the bottom) of a PC, uPic (motor controller), power supply, logging card, motor driver and pressure transducers.

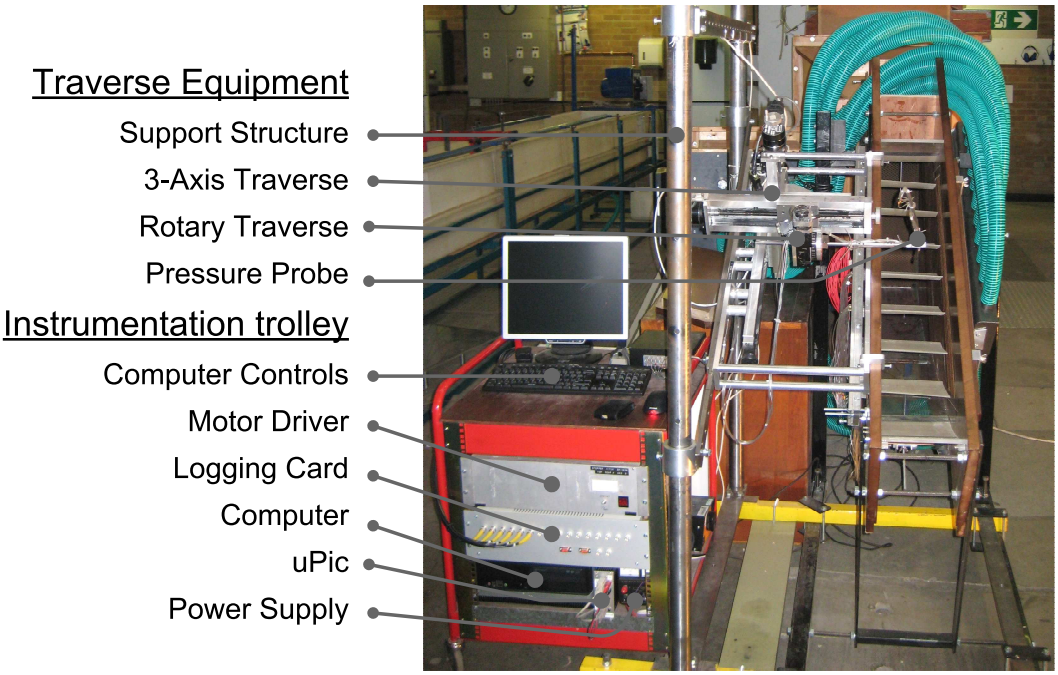

Figure 3.1: *Instrumentation*

A bank of six pressure transducers with a range of ±1000 Pa were used. The pressure transducers were calibrated by applying a series of known pressures and measuring the resultant voltage. A linear relationship between voltage and pressure was then assumed and the gradient calculated. The gradient was then used to calculate the pressure from each measured voltage. For each set of measurements taken, datum voltages were measured at atmospheric pressure with the wind tunnel switched off. These datum values were used as the offset datum voltage due to transducer drift and as such added or subtracted from the following measurements.

3.1.1 Pressure Probe Measurements

Two conventional five hole pressure probes were used within this work. The upstream traverse probe was long enough to pass through the cascade and featured a bend close to the end to enable the head to reach the required location. This

probe was used for the upstream traversing of Build-A and all the traversing of the Build-B. A shorter, straighter probe was used for the downstream traverse of Build-A.

The upstream total pressure was used as the datum pressure for all measurements taken. This was measured using a pitot-probe upstream of the cascade at mid-span and 1.0 Cx upstream. The reference pressure for each pressure transducer was therefore connected to the upstream total pressure. The upstream total pressure referenced to atmospheric pressure was also measured and used as the datum dynamic head. This was equivalent to the upstream total pressure to downstream static pressure and equal to the isentropic dynamic head and as such could be used to calculate the isentropic exit velocity.

A good description of the use of five hole probe data techniques was given by Ingram [2003] and, Ingram and Gregory-Smith [2006]. Although his coefficients were slightly different to those used within this work the techniques were the same. The principle of five-hole pressure probes was straightforward; in general the hole that was aligned with the flow will measure a higher pressure than the other holes. If the pressure difference between the holes is known for specified angles then the flow angle on to the probe was calculated through calibration. Furthermore the total and static pressure and therefore the velocity were similarly calculated. The difference in pressure between the holes depends on the exact geometry of the probe head and any probe head imperfections. At high flow angles the probe may not produce accurate readings and so if the flow deviates outside the calibrated region ($\pm 30^\circ$ yaw and pitch) an error was reported and no data was recorded for that point.

Calibration was undertaken by moving the probe about the probe head through a known set of angles and recording each of the five hole pressures. These pressure values were then used to calculate coefficients of yaw, pitch, dynamic pressure and total pressure. A calibration rig was used to do this which consists of a fan that supplied air to a smooth nozzle which exhausted a uniform jet over the probe head to atmosphere. Also measured was the nozzle total pressure and static pressure for each measured angle; these were measured either side of the nozzle and therefore nozzle calibration was required and applied to ensure that the measured values

corresponded correctly to the value at the probe tip. For this work the probe pressures were measured relative to the upstream total pressure, therefore the value of the total pressure used for the coefficient calculation was set to zero plus the nozzle calibration offset. The coefficients obtained for each angle were then used to generate a calibration file. If the average pressure of the 4 outer holes was found to be higher than the central hole, the coefficients were considered to be inaccurate and therefore the probe was reported to be out of range within the calibration file.

The measured flow angle and pressure on to the probe within the cascade were found by reversal of the coefficients. These reversed coefficients were used to interrogate the calibration file and through linear interpolation between the calibration grid points, the angle and pressures that corresponded to the individual probe pressure condition was found. If the probe was out of range an out of range fault code was reported for the data point and the values set to zero.

Traverse Equipment and Probe Installation

The probe was manoeuvred using a 3 axis automated traverse to set the x, y and z location. The probe yaw angle could be altered using a rotary actuator but no probe pitch angle control was available. This equipment was mounted on a support frame, adjacent and attached to the cascade. Figure 3.1 shows the traverse equipment fitted to Build-B. Further details of the traverse set up and location are shown in Section 3.4, for Build-B. The definition of the probe angle and flow vector are shown in Figure 3.2 taken from the software manual. The probe was attached to the traverse equipment via a clamp which attached via a rod in the radial axis to the rotary actuator. The probe was moved through the clamp to set the axial range of the probe. To set the probe angle the probe was positioned parallel with the exit of the cascade (90° yaw) and then rotated to the required probe angle. The head position was then set using a jig of known position relative to the datum.

Post Processing

Post processing of the logged data was undertaken using programs within the 'Durham Software for Wind Tunnels' software suite, some of which were written

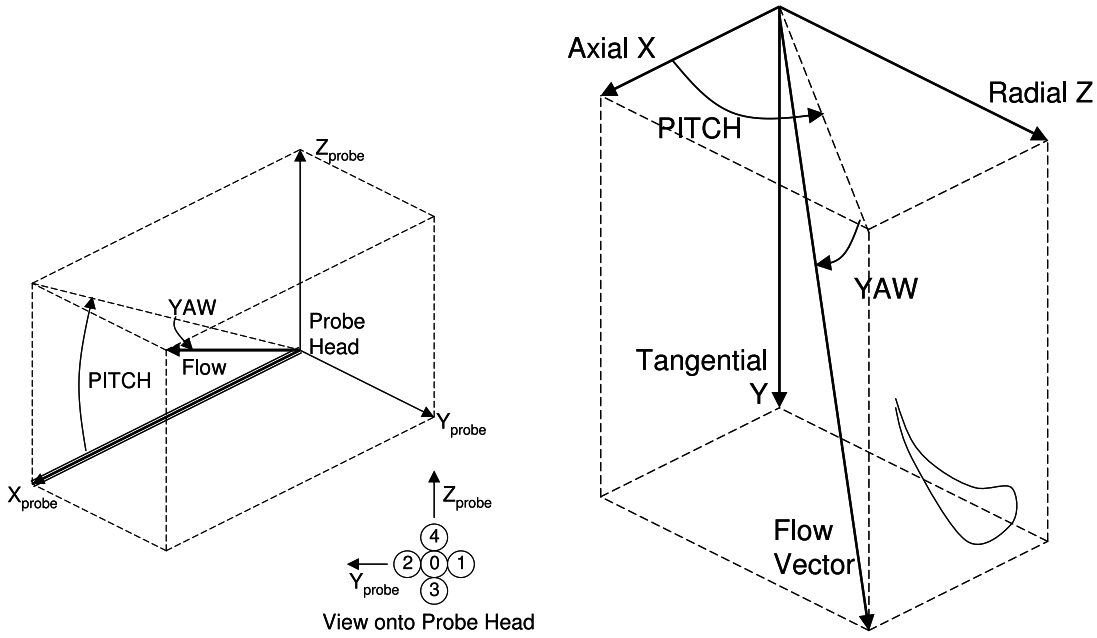

(a) *Probe Angle* ***(b)*** *Flow Angle*

Figure 3.2: *Definition of Flow Vector (from 'Manual for Durham Software for Wind-Tunnels Version 2.0')*

especially for this project. Initially the 'TravLogVolts' program moves the probe through the traverse grid and outputs voltages for each point. The voltages are then converted to pressure using 'ApplyCal' and the probe calibration applied using 'Apply5hCal'. This outputs values of 'PDynRefMeas' as the datum pressure (total pressure upstream - atmospheric pressure) and, 'Yaw', 'Pitch', 'P_0', 'P_{dyn}', 'P_s', 'V', 'V_x', 'V_y', and 'V_z' at the probe head for each grid point. The raw data of voltage and pressure for each hole also remained in the calibrated file. Tecplot, a commercial and widely used graphical plotting program, was used to create contour plots of the data files. The pressure loss coefficient was calculated within Tecplot and was defined as:-

$$Cp_0 = \frac{P_{T,\text{upstream}} - P_{T,\text{local}}}{\frac{1}{2}\rho V^2_{\text{isentropic}}} = \frac{P_{T,\text{upstream}} - P_{T,\text{local}}}{P_{T,\text{upstream}} - P_{\text{atmospheric}}}, \tag{3.1}$$

Pitch Mass Weighted Averaging

Pitch averaging of the previously mentioned variables, including the pressure loss coefficient, was undertaken using the program 'PitchAverage' which was written for this project. The pitch averaging was undertaken using standard methods with each

variable being weighted using the axial velocity (V_x). The tangential pitch averaged boundaries were different for each cascade. The pitch averaging was undertaken using the trapezium rule which was sufficiently accurate.

The pitch averaged pressure loss coefficient was as follows, where h was the pitch:

$$\overline{Cp_0} = \frac{\int_0^{\mathrm{h}} Cp_0.V_x.dt}{\int_0^{\mathrm{h}} V_x.dt}. \tag{3.2}$$

The pitch averaged velocity (V) and its components; axial (V_x), tangential (V_y) and radial (V_z) were:

$$\overline{V} = \frac{\int_0^{\mathrm{h}} V.V_x.dt}{\int_0^{\mathrm{h}} V_x.dt}, \tag{3.3}$$

and the pitch averaged axial velocity was:

$$\overline{V_x} = \frac{\int_0^{\mathrm{h}} V_x.dt}{\int_0^{\mathrm{h}} .dt}, \tag{3.4}$$

and the yaw angle was calculated as:

$$\overline{\alpha} = \arctan \frac{\overline{v_y}}{\overline{v_x}}. \tag{3.5}$$

This method of calculating the yaw resulted in the pitch mass averaged yaw corresponding to the correct tangential momentum and mass flow.

Area Mass Weighted Averaging

The area averaging was undertaken using the trapezium rule and weighted using the pitch averaged axial velocity which was undertaken within a 'Microsoft Excel' spreadsheet. In general, within this work, this was undertaken from mid-span to 5mm (2.6%-span) from the casing. 5mm was the limit of the traverse from the casing and therefore introduced a small unavoidable error in the results. Extrapolation up to the casing would have been possible, however because the flow variation close to the casing was large this would have been an unreliable method and had no advantage over the method used. Area averaging was undertaken using the trapezium rule to solve the following equations:

The area averaged loss was:

$$\overline{\overline{Cp_0}} = \frac{\int_{0.5\mathrm{S}}^{\mathrm{S}} \overline{Cp_0.V_x}.dr}{\int_{0.5\mathrm{S}}^{\mathrm{S}} \overline{V_x}.dr}. \tag{3.6}$$

Area averaged axial velocity was:

$$\overline{\overline{V_x}} = \frac{1}{0.5S} \int_{0.5\mathrm{S}}^{\mathrm{S}} \overline{V_x}.dr. \tag{3.7}$$

Area averaged tangential velocity was:

$$\overline{\overline{V_t}} = \frac{\int_{0.5\mathrm{S}}^{\mathrm{S}} \overline{V_t.V_x}.dr}{\int_{0.5\mathrm{S}}^{\mathrm{S}} \overline{V_x}.dr}. \tag{3.8}$$

Again the area averaged yaw was calculated from the area averaged tangential and axial velocities.

$$\overline{\overline{\alpha}} = \arctan \frac{\overline{\overline{V_y}}}{\overline{\overline{V_x}}} \tag{3.9}$$

Vector plots

Projected 2-D secondary vector plots were used within this work; the advantage was to remove the primary velocities and therefore visualize the secondary flows. This was undertaken by projecting the velocities on to the 2-D plane of interest and then subtracting the pitch averaged mid-span projected value. The secondary flows for Build-B were at a high angle to the axial measurement plane and therefore the tangential velocity was too high for this technique to be used. Altering the viewing angle so as to look along the cortex aids with this but this is difficult to plot. For this reason meaningful 2-D velocity vectors were not possible and therefore not used for Build-B.

3.1.2 Blade Static Pressure Measurements

Blade static pressure measurements were undertaken for both cascades. Each instrumented blade consisted of several tubes running radially along the length of the blade which had 1.6mm diameter tapings at several span-wise locations. To limit the measurements to one span-wise tapping row the other rows were sealed using tape. Again the automated measurement of the pressure within these tubes was undertaken using 'Durham Software for Wind Tunnels'. Each blade pressure

tube was linked through a scani-valve to one of the pressure transducers; this allowed for many tubes to be linked to one transducer and automatically measured in turn. This was undertaken using the program 'logScani' which controlled the valve and measured the pressures. Also measured and recorded were the upstream total and the atmospheric static pressures. The relative dynamic head was again defined as upstream total minus atmospheric static pressure. The program 'logScani' outputted the voltage and pressure for each measurement and calculated the pressure coefficient which was defined as:

$$Cp = \frac{P_{S,\text{local}} - P_{S,\text{atmospheric}}}{\frac{1}{2}\rho V^2_{\text{isentropic}}} = \frac{P_{S,\text{local}} - P_{S,\text{atmospheric}}}{P_{T,\text{upstream}} - P_{S,\text{atmospheric}}}, \tag{3.10}$$

Plotting these values of both blade surfaces against the axial chord gives the blade loading profile. Integrating the blade loading profile gave the blade loading coefficient and this was integrated using the trapezium rule. The loading coefficient was calculated using:

$$C_L = \frac{1}{C_x}\int_0^C (Cp_{\text{PS}} - Cp_{\text{SS}})dx \tag{3.11}$$

This was solved using the trapezium rule, where 'dx' was the change in axial distance between the data points. Integrating the loading coefficient along the blade span indicated the blade loading. Again this was undertaken using the trapezium rule and the boundaries were from mid-span to the last tapping row at the tip of the blade (2% span from the tip of the blade):

$$\overline{C_L} = \frac{1}{0.5S}\int_{0.5S}^{1.0h} C_L.dr \tag{3.12}$$

3.1.3 Measurement Error

All measurement entails error. The 5-Hole probe was the largest error sauce within the experimentation. This was caused by the probe positioning both within the calibration and experimental rig. It was estimated that the angle set-up within each rig was within $\pm$ 0.5° and therefore the resultant angle measurement was within $\pm$ 1° in both the yaw and pitch direction. As the probe angle was only set at the start of a each measurement campaign this error was eliminated for each set of data in relative terms. The Cp_0 error was within $\pm$0.05.

3.2 Wind Tunnel Arrangement and Flow Quality

The open flow, low speed wind tunnel as shown in Figure 3.3 consisted of an 11Kw fan which diffused in to a large settling chamber. A gauze screen within the settling chamber equalized the total pressure. The flow exited the settling chamber through a 7.5:1 contraction ratio nozzle through a section of 0.25x0.8m. The exit flow velocity of the tunnel was controlled through the the fan speed. Details of the flow quality are shown when describing Build-A. Yang [2004] described the design of the tunnel and the first linear cascade (Build A) in more detail.

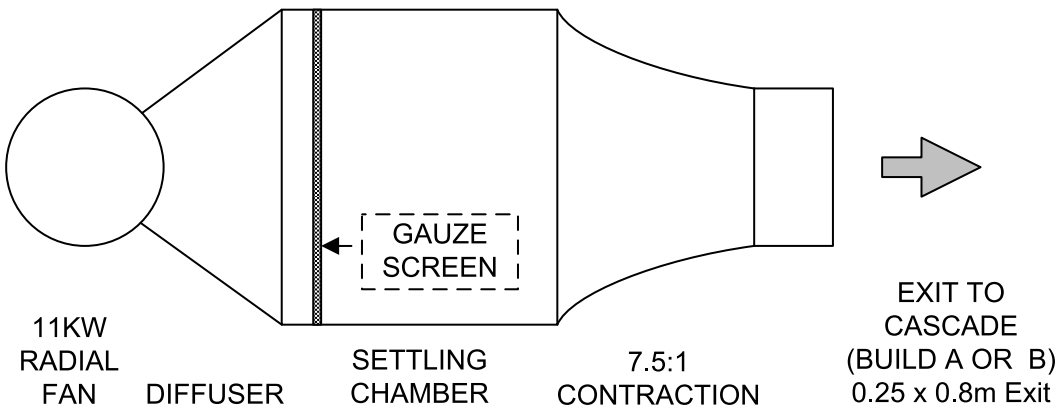

Figure 3.3: *Wind Tunnel Schematic (Not to Scale)*

3.3 Low Stagger Cascade (Build-A)

3.3.1 Cascade Geometry and Details

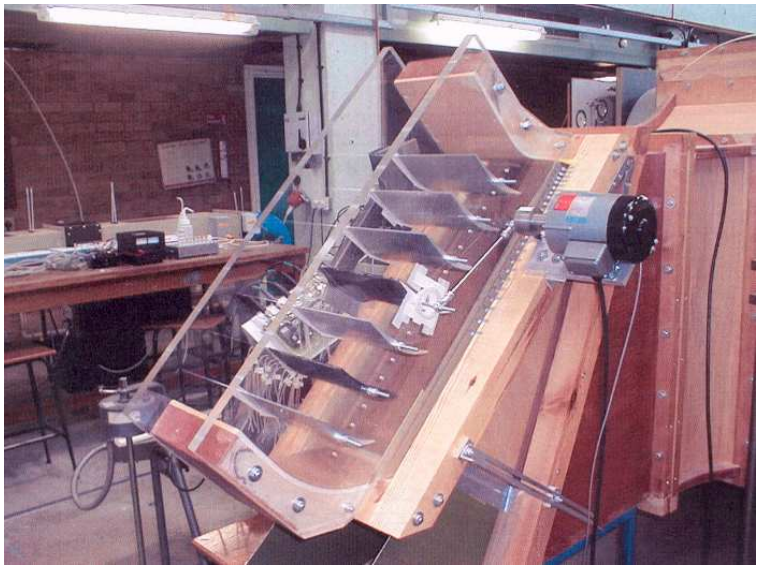

Figure 3.4: *Build-A Photograph from Yang [2004]*

As previously stated the first cascade was modestly adapted for the study of tip leakage flow from its previous use for unsteady CFD validation, undertaken by Yang [2004] and a picture of which is shown in Figure 3.4 and a schematic drawing in 3.5. The cascade located at the wind tunnel exit exhausted to atmosphere one axial chord after the trailing edge. Seven aerofoils including profiled upper and lower boundaries gave eight passages in total; allowing for reasonably periodic flow. Hinges at the top of the cascade enable the geometric inlet angle to be altered. A movable bottom splitter plate (aligned horizontally) allowed for the vertical change in inlet height due to the change in cascade angle; the split flow passed to atmosphere below the splitter plate. The bypass diffusion could be controlled by altering the bypass diffuser. A side wall boundary layer bleed was located one axial chord length upstream of the leading edge. The bleed plate was 3mm thick ensuring minimum interference on the flow.

The controlled diffusion aerofoil used was that as designed by Sanger [1983] and intensely tested in open literature including Sanger and Shreeve [1986]. Blade properties are shown in Table 3.1 and the profile is shown in Figure 3.6. Two of the

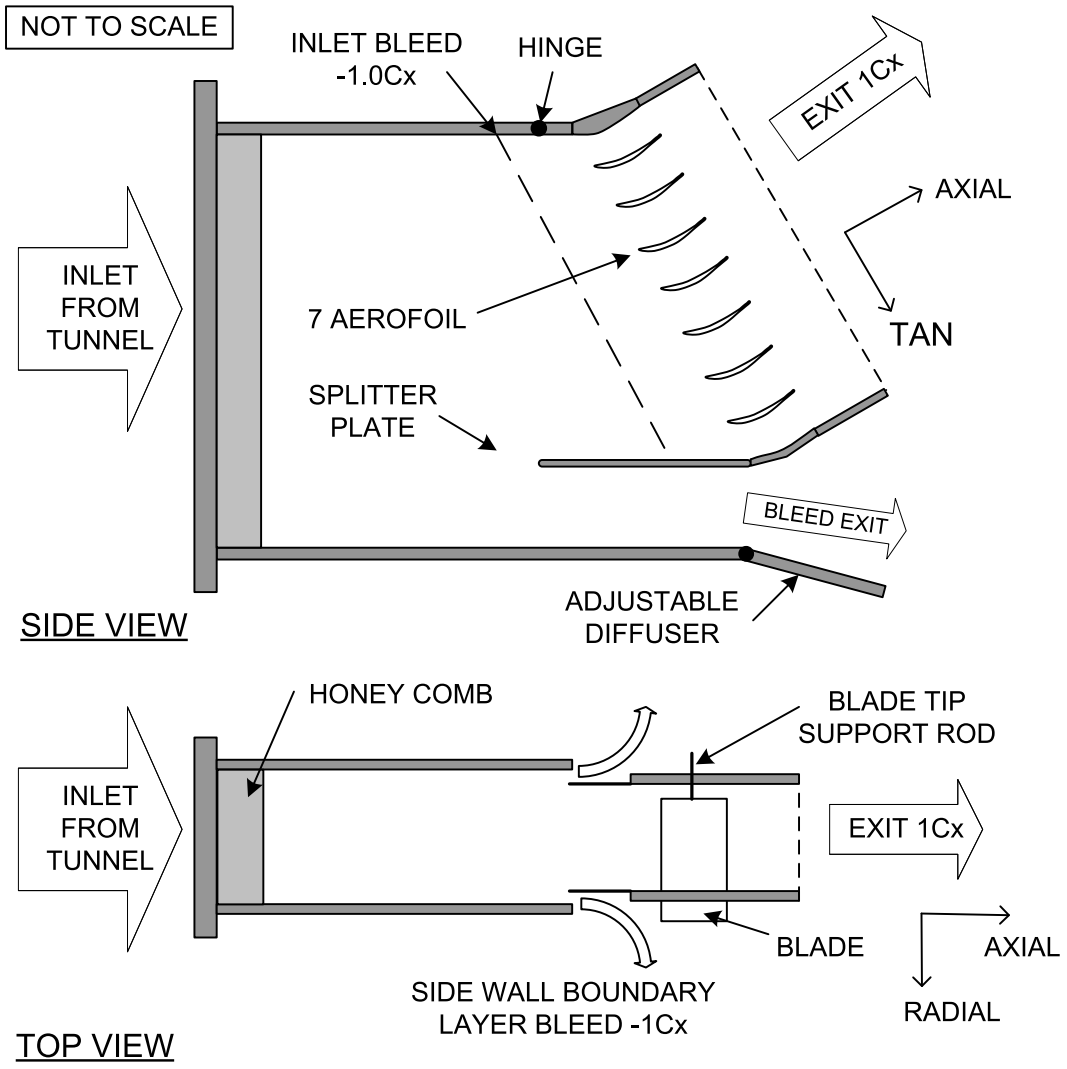

Figure 3.5: *Build-A Schematic*

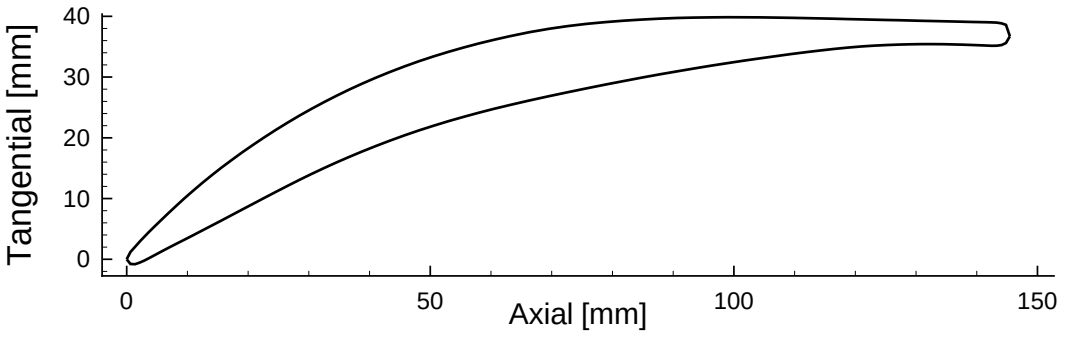

Figure 3.6: *Build-A Blade Profile*

blades were instrumented, these being the central blade and one other which could be moved in to any blade location. Pressure tapings at various radial locations (20, 50, 70, 90, 95 and 98% span wise sections) were positioned on both surfaces of the

blade. There were 14 pressure tappings on the suction surface and 10 tappings on the pressure surface.

Passing the blades radially through the hub enabled the TC value to be altered and supported at the hub end of the blade. The blade tips were supported using a 3mm threaded bar fixed in the end of each blade and passed through the casing wall. Due to the size, the tip suspension bar was assumed to have little effect on the blade loading close to the tip; Build-B did not use such an arrangement and similar blade tip loading features were found, therefore this assumption was reasonable. Within the CFD the tip suspension bar was not accounted for.

Number of Aerofoils	7
Pitch	0.09 m
Blade Span	0.19 m
Stager Angle	14.2°
Inlet Flow Angle (Nominal)	37.5°
Isentropic Exit Velocity	19.5 m/s
Reynolds Number Based on Chord	1.95×10^5
Side Wall Bleed Location	1 Cx Upstream
Pitot-Probe Location	1 Cx Upstream
Aerofoil Type	Controlled-Diffusion Blade
Chord Length, C	0.15 m
Aspect Ratio, h/C	1.27
Maximum Thickness	0.07C
Leading Edge Radius	0.00132 m
Trailing Edge radius	0.00186 m
Solidity (C/S)	1.67

Table 3.1: *Build-A Properties*

3.3.2 Tunnel Exit Flow Conditions

The tunnel exit flow was assessed using a 5-hole probe traverse at the exit of the tunnel. The cascade was removed at the hinge and the traverse was carried out downstream of the honeycomb section; the measurement plane location and axis definition are shown in Figure 3.7. Yaw was defined as the angle up and down, between the x and y axis. Pitch was defined as the side to side angle between the x and z axis. The tunnel exit was 0.25 × 0.8 m.

A traverse filling the majority of the tunnel exit was undertaken along the traverse plane as shown in Figure 3.7. One dimensional sample results (defined in Figure 3.7) of the exit traverse are shown in Figure 3.8. It was assumed that the high and low pitch values ($< 3°$ & $> 3°$) close to the wall were as a result of a 5-hole probe error. Since the size of the probe was thicker than the boundary layer the probe measured an incorrect flow angle. The results showed that the yaw and pitch were between $\pm 1°$ for the majority of the main stream flow and so the flow angle was reasonably uniform throughout the exit of the wind tunnel. The total pressure coefficient was within +0.1 and -0.02 across the tunnel exit. A rise in total pressure close to the hub wall (z = 0) existed, however as this was not the wall of interest and did not affect the results. The variation in exit flow was acceptable for this work.

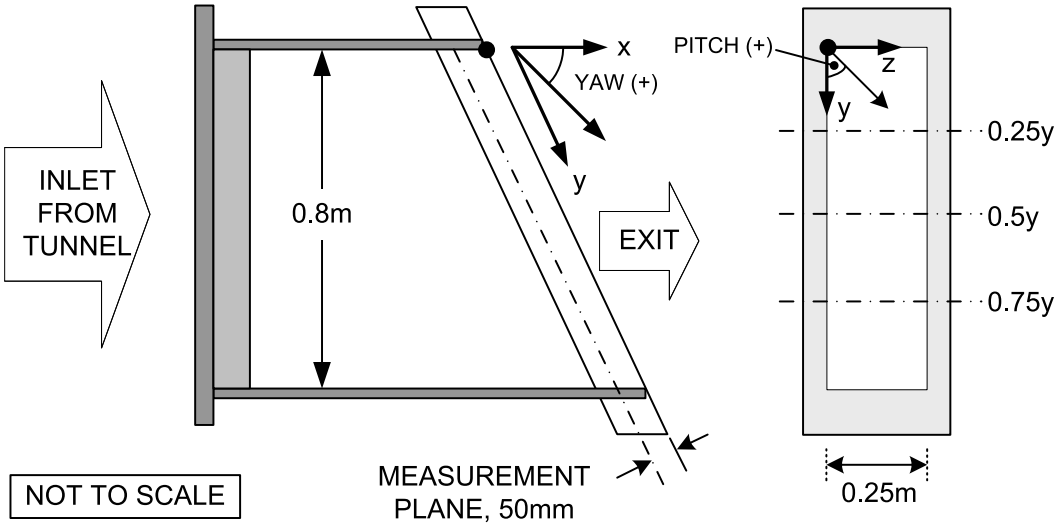

Figure 3.7: *Tunnel Exit Measurement Plane*

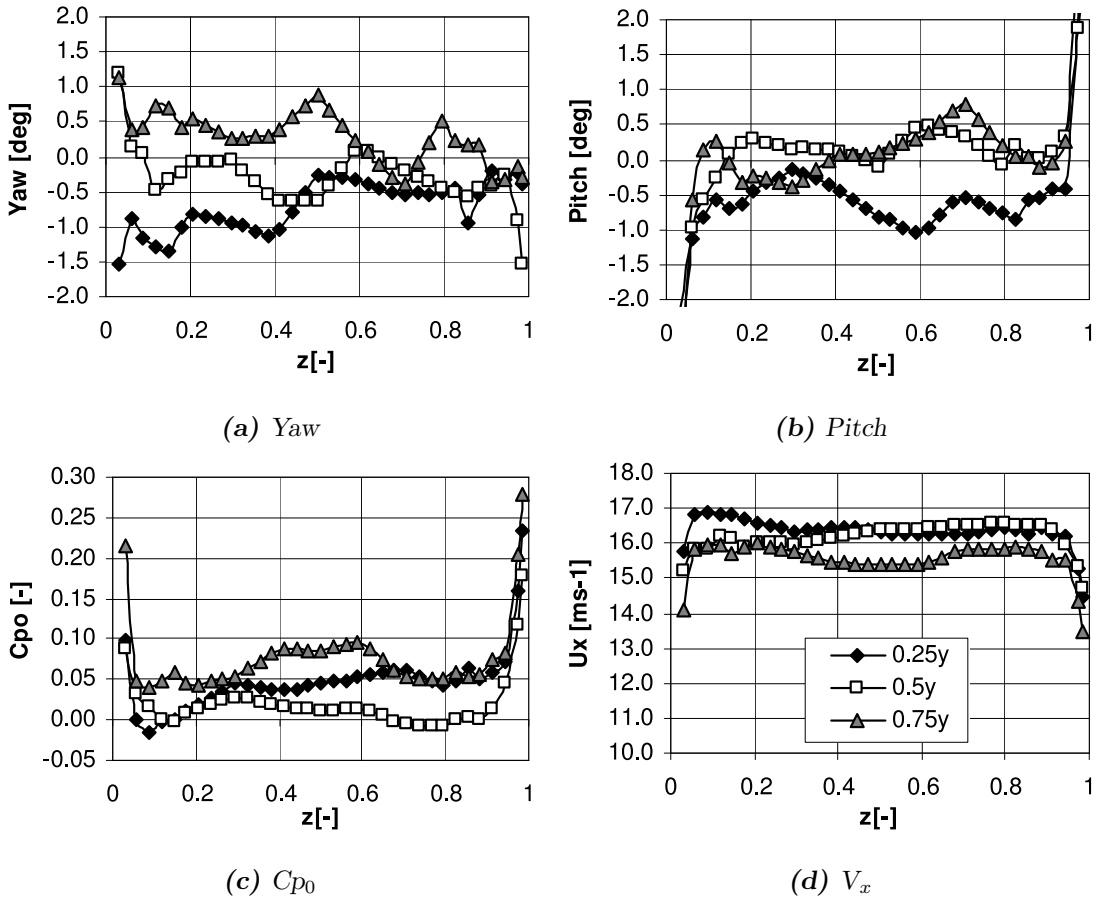

(a) *Yaw* *(b)* *Pitch*

(c) Cp_0 *(d)* V_x

Figure 3.8: *Tunnel Exit Conditions*

3.3.3 Cascade Traverse Locations

The inlet and exit traverse locations are shown in Figure 3.9 along with the grids used. Also shown is the co-ordinate system; x was defined as axial, y was tangential and z was radial. The origin was defined as the trailing edge of the central blade at the hub. Four blade passages at inlet and 2 passages at exit were traversed. Pitch averaging was undertaken across both exit traverses and all four inlet traverses.

The upstream traverse was undertaken by inserting the probe through the blade row and therefore the traverse area was limited for a given probe angle. The inlet traverse was located at 0.5Cx (72.5 mm) upstream of the leading edge and extended to cover the inlet of the central 4 passages. Two traverses at different probe angles covered the majority of each passage area, however there was a small area not covered by the inlet traverse. The grid extended to 5 mm from the wall.

The exit traverse was undertaken at 1.2Cx (29 mm) downstream of the trailing

edge. Two blade passages were covered from mid passage to mid passage of the central blade and the blade below it. This traverse location was chosen so that the pitch averaging boundaries would not coincide with the wake.

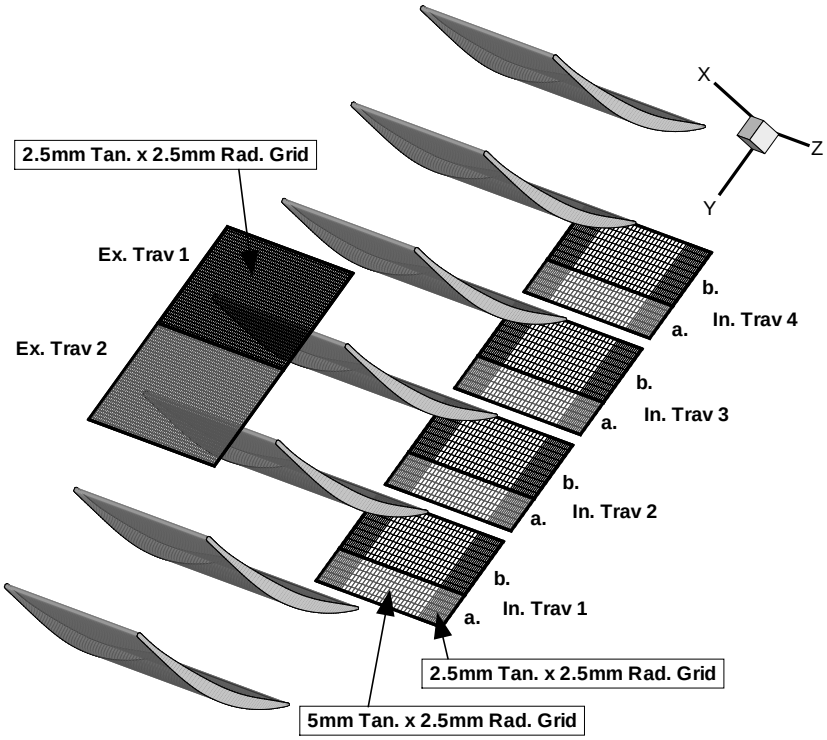

Figure 3.9: *Build-A Measurement plane*

3.3.4 Cascade Inlet Flow Conditions

Significant effort ensured high quality inlet flow conditions to the cascade (Build-A). This included: adaptation of the inlet casing and hub bleed plates to a 3 mm aluminium sheet ensured a periodic boundary layer; control of the side wall bleed rate, control of the incoming periodicity through the bottom bypass diffuser angle; and altering the cascade's geometrical angle to match the required inlet flow angle. The inlet flow to the cascade was conditioned to ensure uniform periodicity and an inlet flow angle of 37.5° at an inlet traverse location of 0.5Cx upstream of the leading edge (0.5Cx downstream of the bleed).

The inlet flow angle was found to have a deviation to the geometrical angle of approximately 5°. To allow for the offset the cascade geometrical angle was set to

42.5°. This offset requirement was attributed to the finite number of blades in the cascade, further mention of which will be made in Section 5.1.6 on page 138. Good practice was found to include the angle of the bottom plate (set horizontal), the bottom diffuser angle and the diffusion of the side-wall bleeding being accurately set. The inlet pitch mass averaged yaw and total pressure loss, pitch averaged over the central four passages, can be seen in Figure 3.10(a). A significant boundary layer with low total pressure and high skew on the walls was evident which was attributed to the sidewall bleed pushing the flow down. Also of note was the increase in total pressure and decrease in yaw towards the hub. Only the outer 50% span was of interest so this was unimportant and the inlet condition was reasonable for the measurement campaign.

Figure 3.10 also shows contour plots of Cp_0 (Figure 3.10(b)) yaw (Figure 3.10(c)) and V_x (Figure 3.10(d)). The increase in Cp_0 and decrease in yaw within the hub side of the cascades inlet was evident within the contours and this was accompanied with an increase in axial velocity. The increased total pressure in the hub region at tunnel exit (Figure 3.8) was responsible for this. Generally the total pressure increased and the angle decreased towards the bottom of the cascade. In the top left hand corner the location of the pittot-probe was visible by the high loss region, low yaw angle and low axial velocity.

Considering the multi-row case with highly skewed flow at the wall these inlet conditions were deemed acceptable, however not engine representative. Generally the boundary layer will typically extend 0.2 span from either wall. For this cascade the boundary layer thickness was less than 0.1 span but the boundary layer's skew of $\approx 10°$ on the casing was representatively high.

3.3.5 Cascade Exit Flow Conditions

The cascade exit total pressure coefficient (loss) across both passage exits is shown in Figure 3.11. A reasonable tangential similarity was observed between passages demonstrating periodic conditions. However there was a difference between the hub and casing; on the casing (right hand side of the plot) there was clear evidence of an accumulation of high loss fluid on the suction/casing hub junction and a

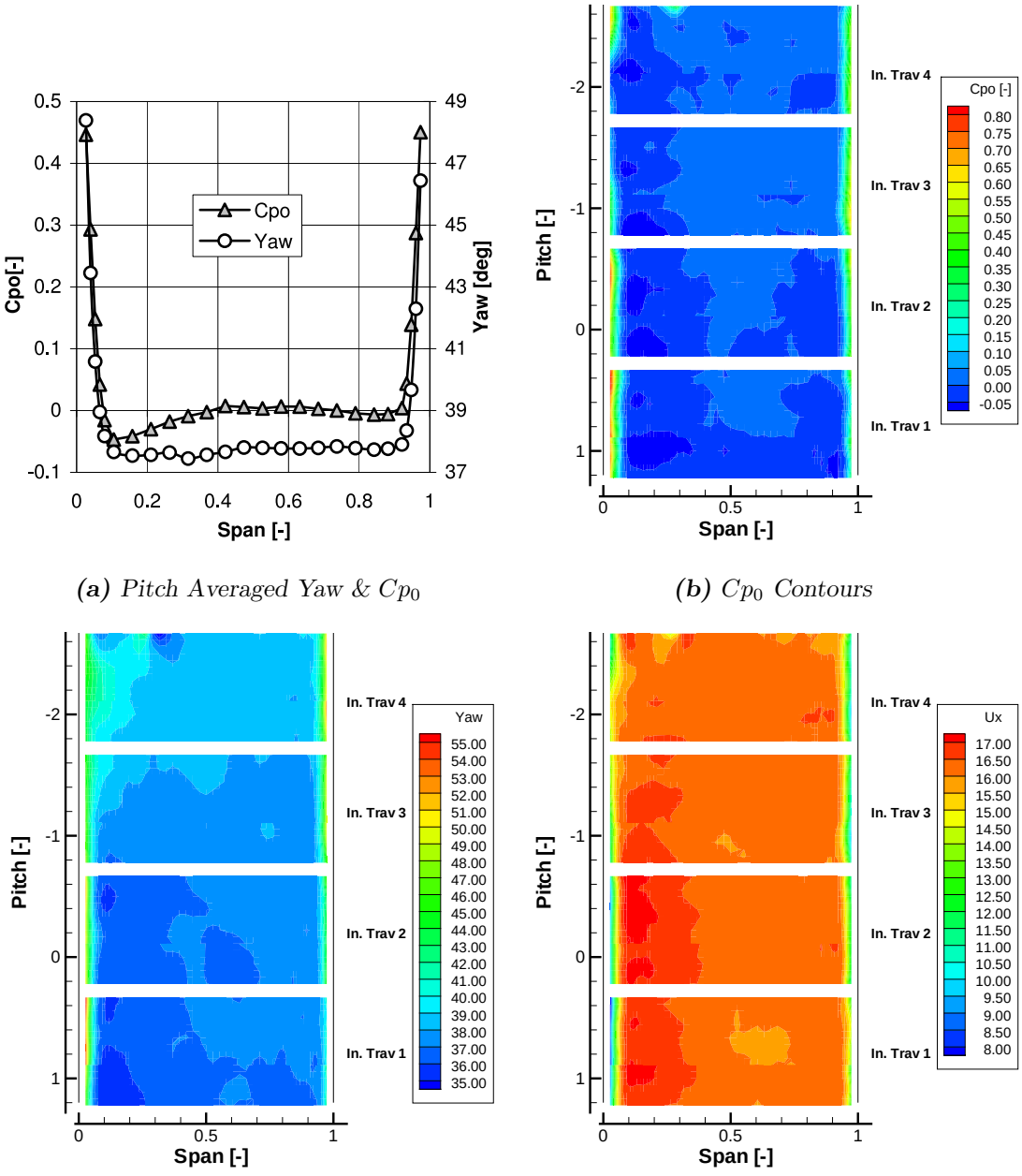

(a) Pitch Averaged Yaw & Cp_0

(b) Cp_0 Contours

(c) Yaw Angle Contours

(d) Vx Contours

Figure 3.10: *Build-A Inlet Flow Conditions*

passage vortex close to the corner, indicating a corner separation. On the hub however the passage vortex filled much more of the passage and the loss was more uniform across the pitch. The reason for the difference in hub and casing flow was found to be as a result of atmospheric air passing in to the cascade from the gap between the blades and the hub-wall preventing the accumulation of low energy fluid and therefore preventing the corner separation. This plot demonstrated reasonable

periodic conditions and because the area of interest was the casing and not the hub these conditions were acceptable for tip leakage investigation.

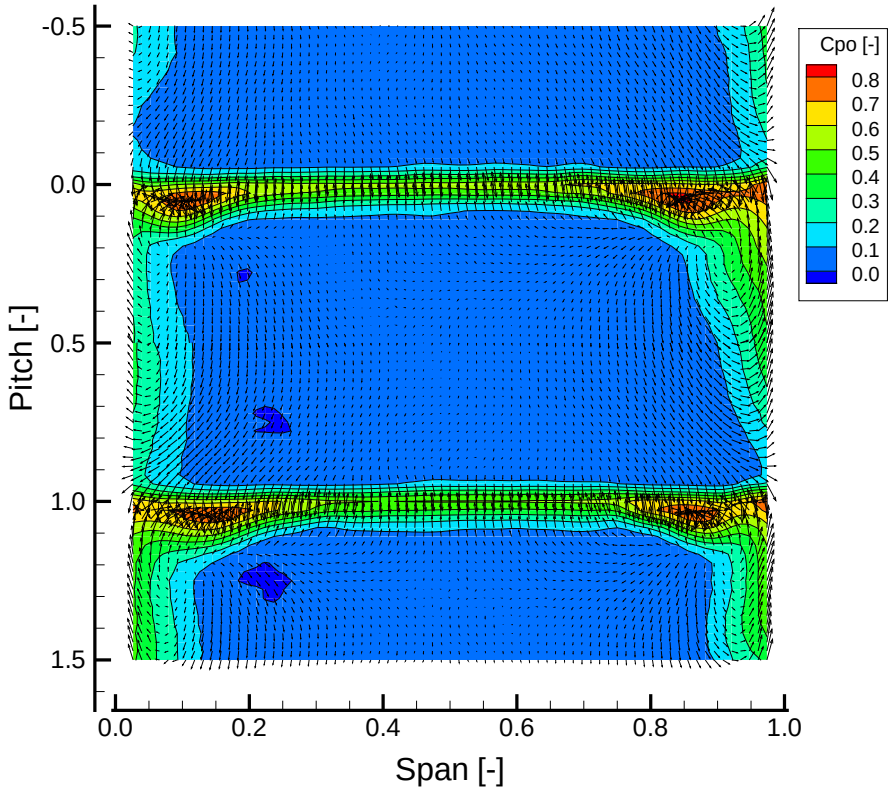

Figure 3.11: *Build-A Exit Traverse Cp_0 Contours with 0%TC*

3.3.6 Cascade Loading (Diffusion Factor)

As described by Cumpsty [1989] the blade loading can be assessed using the Diffusion Factor. This can be calculated using:-

$$DF = 1 - \frac{V_2}{V_1} + \frac{\Delta\ V_\theta}{2\sigma\ V_1} \tag{3.13}$$

where:-

$$\sigma = \frac{BladeChord}{BladePitch} = Solidity, \tag{3.14}$$

V_1 and V_2 are the velocities into and out of the blade row respectively, and $\Delta\ V_\theta$ is the change in whirl velocity or tangential velocity. Diffusion factors of 0.6 generally indicates blade stall and 0.45 may be taken as a typical design value. With

incompressible flow with constant axial velocity this can be simplified to:-

$$DF = [1 - \frac{\cos\ \alpha_1}{\cos\ \alpha_2}] + \frac{\cos\ \alpha_1}{2\sigma}(\tan\ \alpha_1 - \tan\ \alpha_2). \tag{3.15}$$

Using this second equation the diffusion factor for this cascade at mid-span with zero clearance was 0.32. This was calculated using the mid-span design inlet angle of 37.5° and the measured exit angle of 5.6°. Therefore this cascade was moderately loaded.

3.4 Engine Representative Cascade, (Build-B)

The second cascade (Build-B) attempted to simulate tip leakage flows with engine representative geometry and inlet conditions. The blade geometry used was that of Build II of the Dresden 4-Stage Low Speed Research Compressor (DLSRC), this geometry was representative of a typical HPC. Details of the LSRC are given by Boos et al. [1998], and Müller and Vogeler [2007]. The blade geometry was that of the casing section and in the cascade it was scaled by 1.75 in the circumferential plane. Radially the cascade span was 180 mm and so the scaling was 1.5 from the DLSRC, which was the maximum size possible to mate with the existent wind tunnel. At mid-span the inlet flow axial velocity was approximately 15 m/s.

A requirement of the cascade design was to provide realistic inlet conditions which were chosen to match those at inlet to rotor 3 of the DLSRC 'Build II'. The aim for the natural inlet condition of the cascade was to have an inlet angle of 55° at mid-span and a natural boundary layer on the casing (low skew). With the realistic inlet boundary condition (high skew) the aim was to have an increase of 10° yaw on the casing with a linear distribution up to the nominal inlet angle at 80% span.

Figure 3.12 shows the inlet yaw angle upstream of rotor 3 of the DLSRC (dashed line). The ideal linear cascade inlet boundary layer as aimed for with this work is shown by the solid line. To achieve these inlet conditions upstream tangential injection was implemented and details of which are presented below.

3.4.1 Cascade Geometry and Design

This bespoke cascade was designed by the author and built within the School of Engineering workshops. Figure 3.13(a) and Figure 3.13(b) show a mid-span section of the cascade on to the hub and casing walls respectively; Figure 3.14 shows a picture of the cascade. Table 3.2 gives some of the cascade and blade dimensions. Manufacture and assembly of the entire cascade was undertaken over 8 weeks. The materials used included Perspex, Plywood, Medium Density Fibreboard (MDF) and softwood along with steel and aluminium fastenings. The design allowed for easy assembly and disassembly of the entire test facility to accommodate for and future

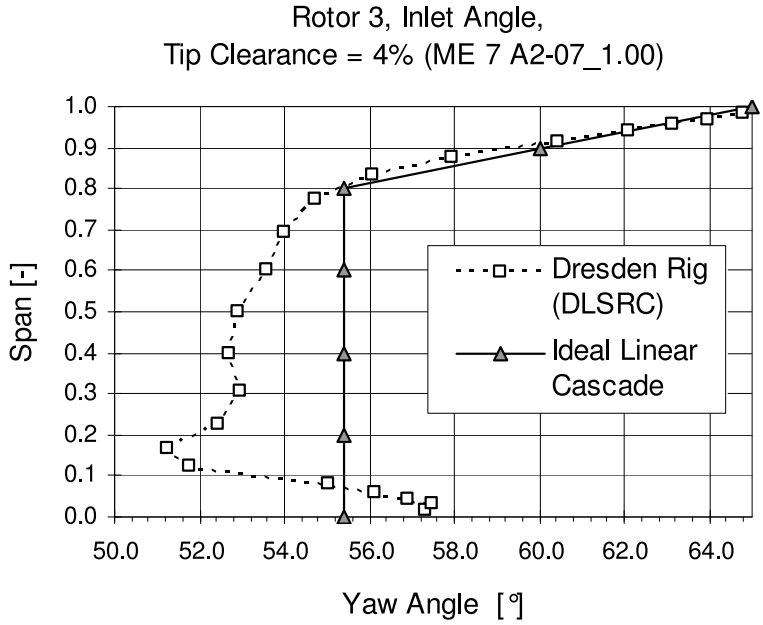

Figure 3.12: *Linear Cascade Inlet Flow Angle Derivation*

alterations. Further details of the design and design requirements can be found in Williams et al. [2007b].

The blades were manufactured using rapid prototyping technology within the department. This technique enabled the blades to be manufactured quickly and instrumented without intensive machining, making this technology ideal for a low speed linear cascade.

The cascade had 8 movable blades which passed through the hub and were cantilevered from a plate; the variable position of the plate along the fixing studs allows for the variation of tip clearance size. Two fixed blades formed the top and bottom passages of the cascade giving 8 passages in total. Variable exit diffusers were located at the trailing edge of the top and bottom blades to control the cascade periodicity through the exit diffuser angle.

Removal of the tunnel hub and casing boundary layer was accomplished by bleeding 2.5 axial chord lengths upstream of the blade leading edge. The bleed had a width of 20 mm and spanned the full length of the cascade. The cascade was hinged around the leading edge of the top blade to allow for a change in incidence during set-up of the inlet conditions. Once chosen, the cascade angle was permanently set to a geometrical blade inlet angle of 58°. Top and bottom inlet horizontal split-

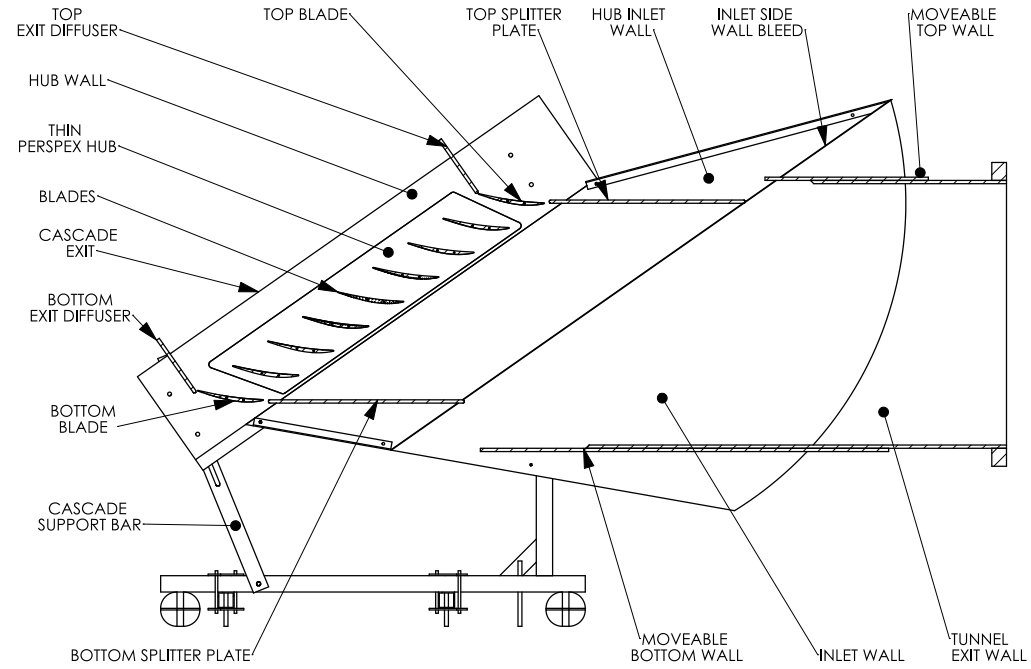

(a) *View on to Hub*

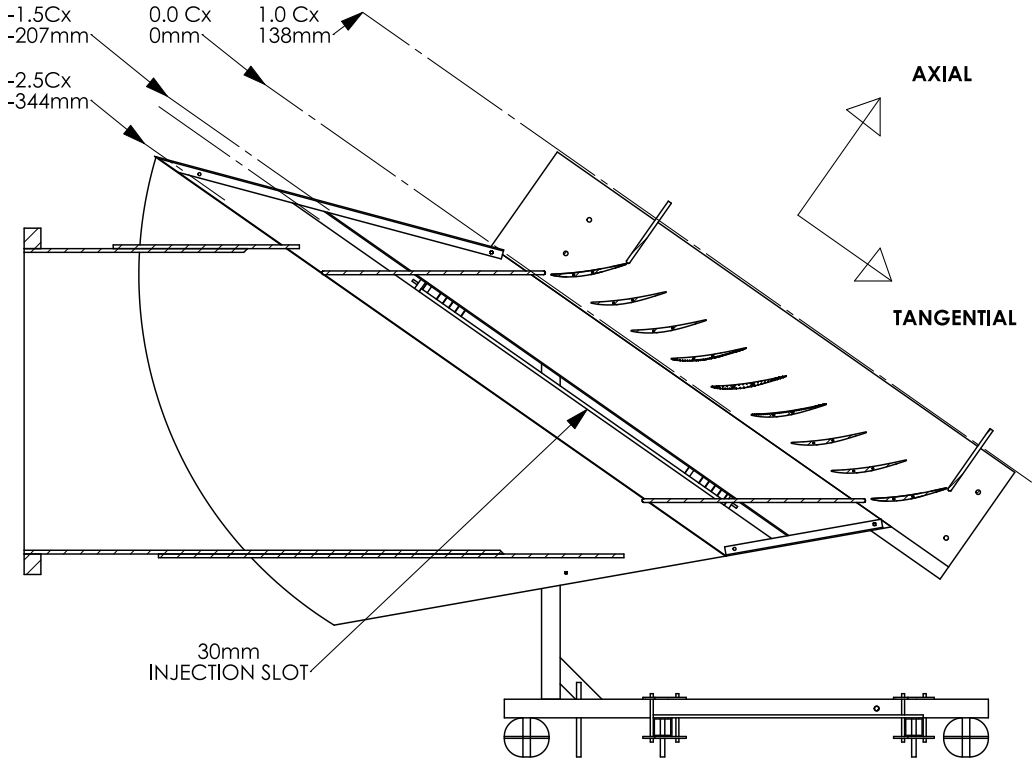

(b) *View on to Casing*

Figure 3.13: *Build-B Sectional View*

Figure 3.14: *Picture of Build-B*

ter plates allowed for changes in cascade angle and removal of the top and bottom tunnel boundary layers. These were set horizontally and extended 3 chord lengths upstream. Suction of the splitter plate boundary layer upstream of the top and bottom blades was available but not used and therefore blanked off.

Control of the inlet boundary layer flow angle was implemented by injecting air through a slot located at -1.5Cx, that is 150% of axial chord upstream of the blade leading edge. The slot width could be controlled up to a maximum of 30 mm. For the first configuration without injection the slot was blanked to create a smooth casing. The injection took place over 95% of the cascade tangential length starting from the top. The inlet traverse was located at 0.5Cx upstream of the blade row which was therefore after the injection slot.

The effect of skew at inlet was investigated using two inlet flow configurations. The first used the natural inlet boundary layer of the cascade (2° skew, 10% span thickness, labelled 'Low Skew') and the second had a more engine representative inlet boundary layer (10° skew, 20% span thickness, labelled 'High Skew').

Number of Aerofoils	7
Number of Passages	9
Aerofoil Pitch	131.25 mm
Cascade Annulus Height	180 mm
Upstream Side Wall Bleed Location	-2.5Cx from leading edge
Inlet Injection Location	-1.5Cx from leading edge
Pittot-Probe Location	-1.0Cx from leading edge
Cascade Exit	2.0Cx from leading edge
Inlet Flow Angle (Mid-Span)	55°
Cascade Reynolds Number	3.622×10^5
Aerofoil Chord (C)	204 mm
Aerofoil Axial Chord (Cx)	140 mm
Stager Angle	46.5°
Aspect Ratio (Span/C)	0.88
Solidity (Chord/Pitch)	1.55
Inlet Velocity	23 m/s

Table 3.2: *Build-B Properties*

3.4.2 Inlet Injection Design and Implementation

As discussed, to achieve the casing inlet skew, upstream tangential injection was implemented. The feasibility of this method was investigated using both analytical and computational techniques and shown to be a practical method. Analytically this involved matching the casing boundary layer with the slot's tangential injection momentum and energy. Computationally a commercial CFD package (Fluent) was used to investigate the effect of slot width and flow angle. Both methods showed that the the use of injection for controlling the inlet boundary layer thickness and angle was feasible, but they were not deemed sufficient to choose an exact injection design. Therefore geometrical flexibility was essential in the design. Details of this process can be found by Williams et al. [2007b].

A schematic of the injection system is shown in Figure 3.15. Within the injection

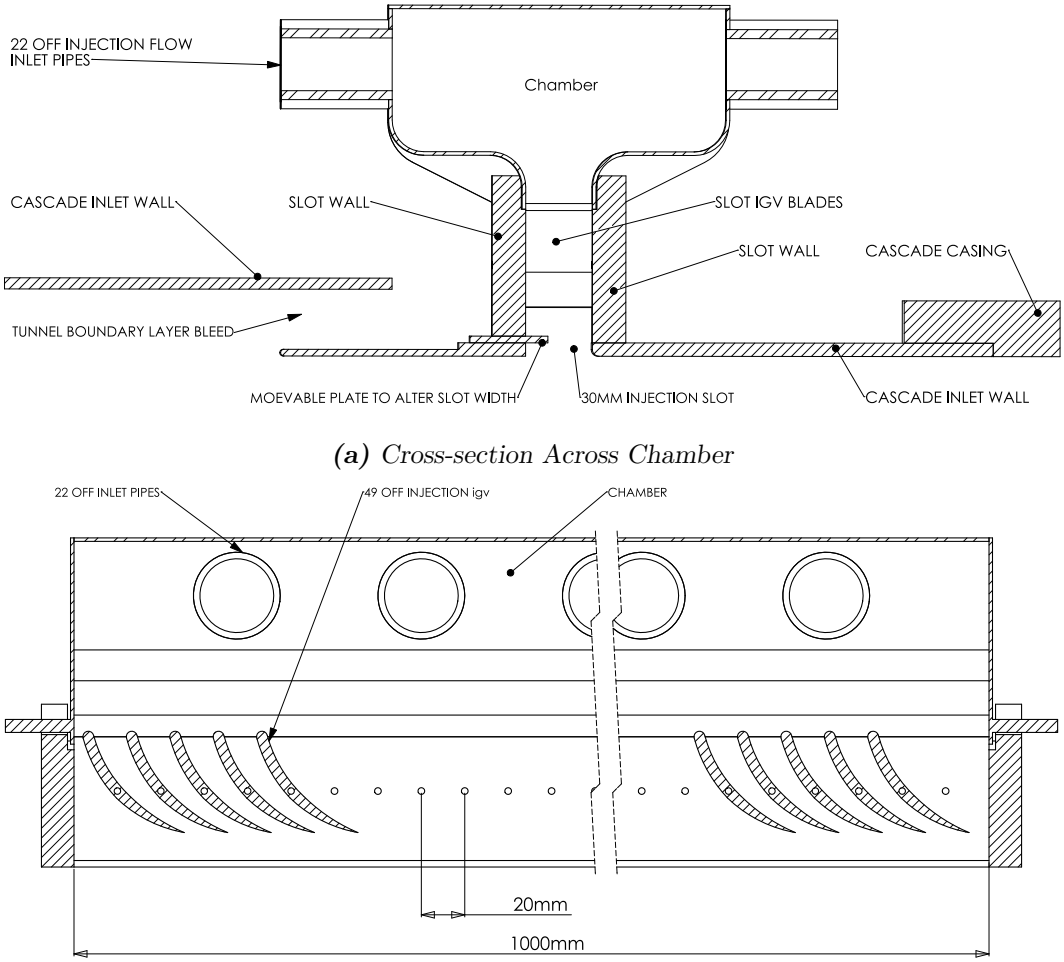

(a) *Cross-section Across Chamber*

(b) *Cross-section Along Chamber*

Figure 3.15: *Injection System Drawings*

slot forty nine injection guide vanes (IGV's) could be altered to give a geometrical exit angle between 5° and 40° to the casing wall. Twenty two pipes supplied air to the slot, which were in turn supplied from a fan via a settling chamber. The fan speed could be altered to vary the injection mass flow rate. At either end of the injection slot the flow was affected by the slot end plates, however because this occurred away from the measured passages it was considered to have a negligible effect on the results.

To obtain the desired inlet flow boundary layer the slot width, IGV angle and injection mass flow were systematically varied. This process is not documented within this thesis, further details of the procedure undertaken can be found within Williams et al. [2008b]. It was necessary to alter the IGV angle along the length of

the injection slot to improve the boundary layers periodicity. The IGV angle was set to 10° at the top of the cascade and 5° at the bottom. A fan speed of 30 Hz was chosen which approximated to a mass flow of 7.5% of the tunnel mass flow rate. The slot width was set to 30 mm. With the final injection arrangement the mid-span variation was approximately 1° and the casing variation was around 6° across the length of the cascade. At inlet to the passages of interest, and as used for the inlet pitch averaged data, the casing variation was only 4°.

3.4.3 Instrumented Blade

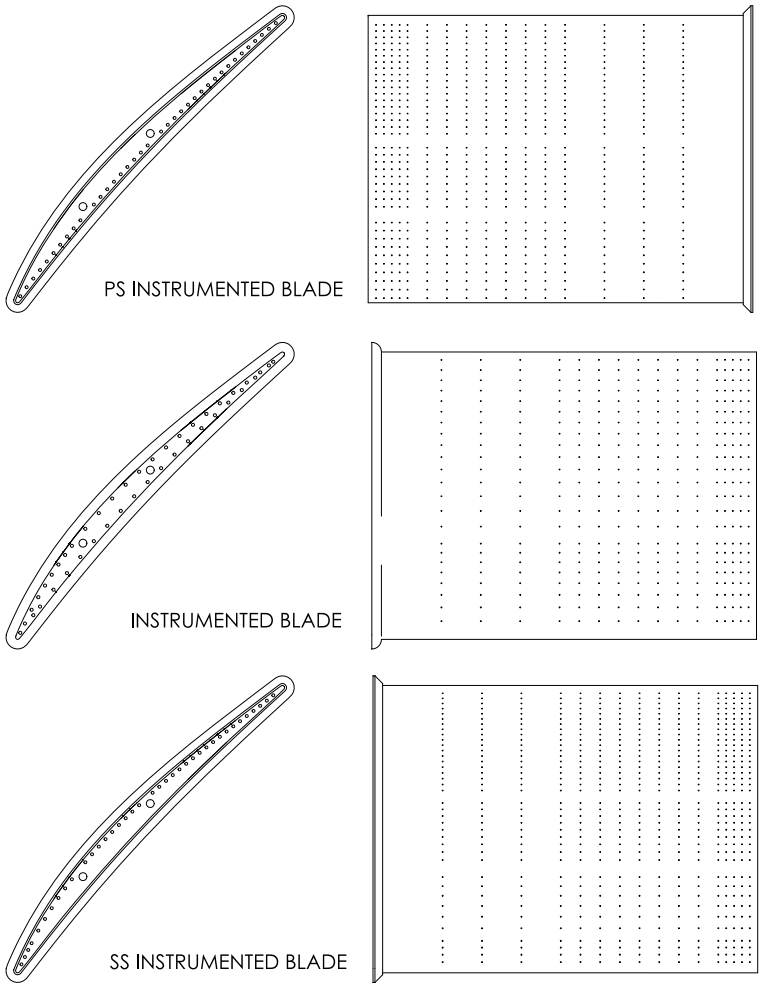

Figure 3.16: *Build-B Blade Profile & Instrumentation*

As previously stated the geometry was that of the casing section of the LSRC scaled by 1.75. This was the maximum scaling possible to allow for 9 passages

and the required angle variation at exit of the tunnel. Three of the blade were instrumented (Figure 3.16) with pressure tapings; the central blade had pressure tapings on both the pressure surface (PS) and the suction surface (SS), and the blades either side of the central blade had static pressure tapings on the surface closest to the central blade. The 1.6 mm tapings connected to tubes which ran the length of the blade and protruded through the hub. The taping holes were located in constant span-wise rows along the blade. The span-wise spacing was as follows, from the tip; 2% chord for the first 10% chord, 5% chord up to 50% chord and 10% chord up to 80%. Therefore sixteen tapping rows existed along the blade. Tape was used to isolate the end of the tubes at the tip of the instrumented blades and to cover the unused taping rows. Pressure measurement was also possible on the tip of the blade due to the pipes running the full length of the blade. This was therefore around the edge of the blade as can be seen on the end of the instrumented blade in Figure 3.16.

3.4.4 Cascade Traverse Locations

Inlet traverse

The inlet and exit traverse locations are shown in Figure 3.17. The datum was defined as the trailing edge of the central blade on the hub; x was axial, y was tangential and z was radial. Similar to the first cascade the upstream traversing was undertaken 0.5Cx upstream of the leading edge by positioning the probe through the blades. For each passage inlet the grid was split in two, with two probe angles for each passage inlet. The traverse limit was 5 mm from either wall and the measurement grid density was 5 mm $\times$ 4 mm (Tangential x Radial) within 45 mm (25% annulus height) from both cascade walls and 5 mm $\times$ 10 mm for the central region of the annulus. While examining the cascades periodicity, pitch averaging was undertaken for each individual passage. For the inlet condition, as shown in Figure 3.20, pitch averaging was undertaken across the inlet to the central 4 passages ('In. Pass-2' to 'In. Pass2', as defined in Figure 3.17).

Exit Traverse

Two axial exit traverse locations were used, 1.2Cx and 1.5Cx. A selection of results from 1.5Cx are included in the appendix. Three passage exits were covered and the boundaries of each were axially in-line with the trailing edge of each blade as shown in Figure 3.17. The mesh density was 2.5 mm × 2 mm within 30 mm of the walls and 2.5 mm × 5 mm for the central region. For the results with tip clearance, only the outer half of the cascade was measured.

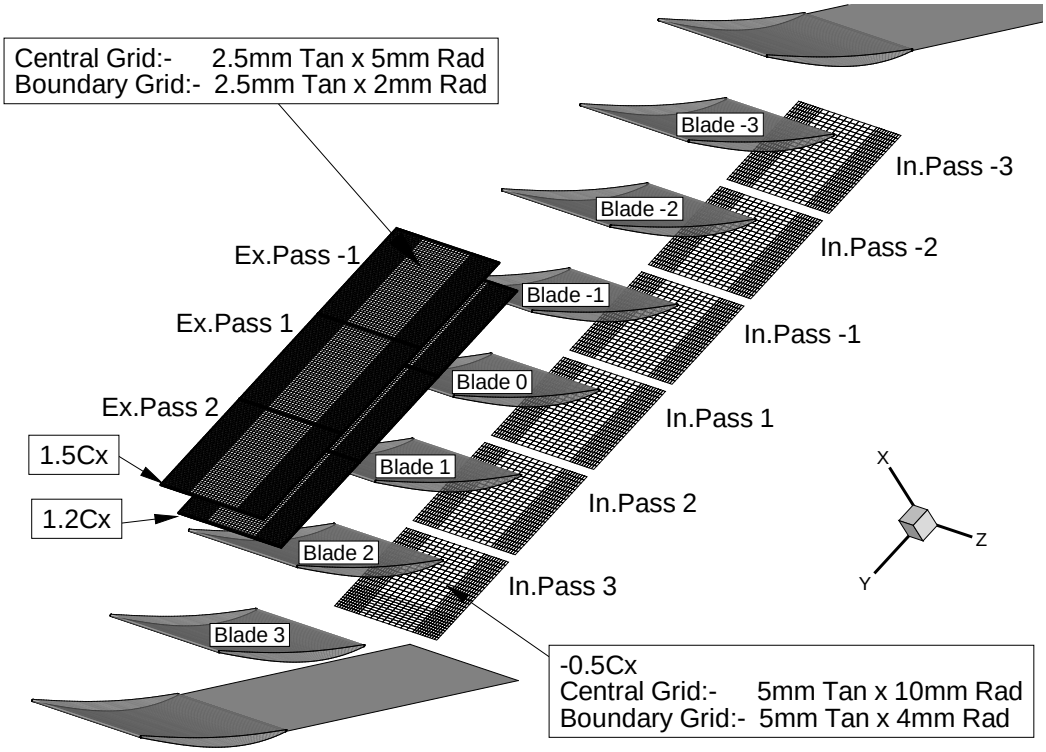

Figure 3.17: *Build-B, Measurement Plane*

General practice would require the choice of pitch averaging boundary to be a tangential location with low loss. However the changing flow structures with clearance and absence of a low loss pitch-wise region, prevented this. Therefore pitch averaging was undertaken across all 3 passages. This method gave similar results to the central passage if the pitch averaging boundaries were moved to be relative to the same flow feature for each tip clearance measured. Unfortunately this method prevented the comparison between the two downstream traverse planes because different flow structures were captured between axial locations.

Internal traverse

Internal passage traversing, from 0.3Cx to 1.0Cx, was undertaken as shown in Figure 3.18. This was undertaken within 'Pass1' which related to the central blade's tip leakage flow. The tip leakage flow within the passage was fully covered by the traverse region. However the manoeuvrability within the passage, due to the size and geometry of the probe, prevented full pitch-wise traversing within the pressure surface region towards the front of the blade row. No traversing within the clearance region was undertaken. Again only the outer half of the cascade was measured and the mesh density was the same as for the exit traverse.

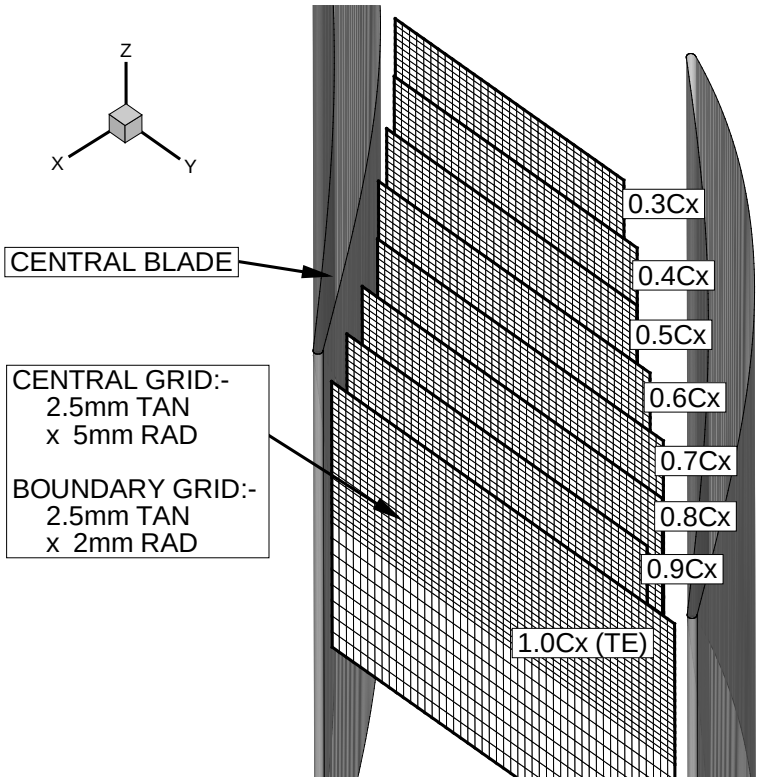

Figure 3.18: *Internal Measurement Plane*

3.4.5 Cascade Inlet Flow Conditions

High quality uniform periodic flow was ensured at inlet to the cascade. Details of the process are not included but a brief overview can be found by Williams et al. [2008a,b]. Again, similar to the first cascade, the inlet flow angle at the inlet

traverse plane did not correspond to the geometrical angle but instead varied by $\approx 5°$ from the cascade geometrical angle which was set to 58°. A significant reduction in periodicity occurred with a geometrical angle above this value. The inlet flow conditions shown here are as used for the measurements. Figure 3.19(a) (low skew inlet) and 3.19(b) (high skew inlet), show the change in pitch averaged yaw angle for each passage inlet as defined in Figure 3.17. At mid-span with the low skew inlet the cascade had a 2° variation in yaw angle, 0.02 variation in loss coefficient (Cp_0) and 1 m/s variation in axial velocity along the length of the cascade. The pitot-probe wake, observed at the top of the cascade, was the exception to this. The high skew inlet reduced the mid-span yaw variation to 1° while the loss and axial velocity variation were similar.

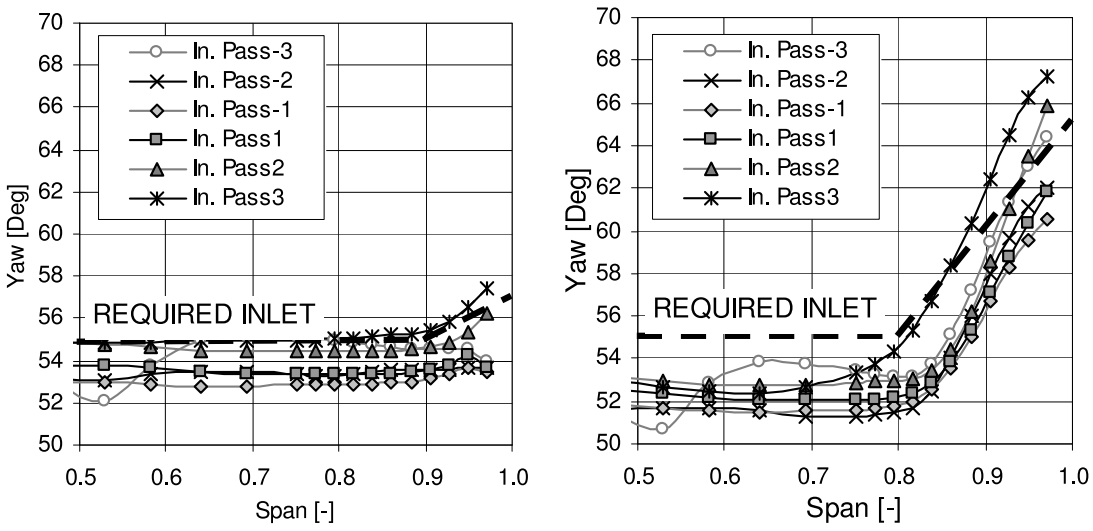

(a) *Low Skew Inlet* ***(b)*** *High Skew Inlet*

Figure 3.19: *Pitch Averaged Inlet Yaw Angle (Averaged Individual Passages)*

Figure 3.20 presents the pitch averaged axial velocity, yaw angle and loss across the inlet to the central four passages for both inlet skew conditions with no tip clearance. At mid-span (0.5 span) there was little difference between the axial velocity and Cp_0 for the different inlet boundary conditions. The yaw angle with increased skew was approximately 1° higher than without, which was due to a redistribution of mass flow away from the casing brought about by the increased boundary layer blockage. Both inlet conditions had a lower mid-span inlet angle than required and

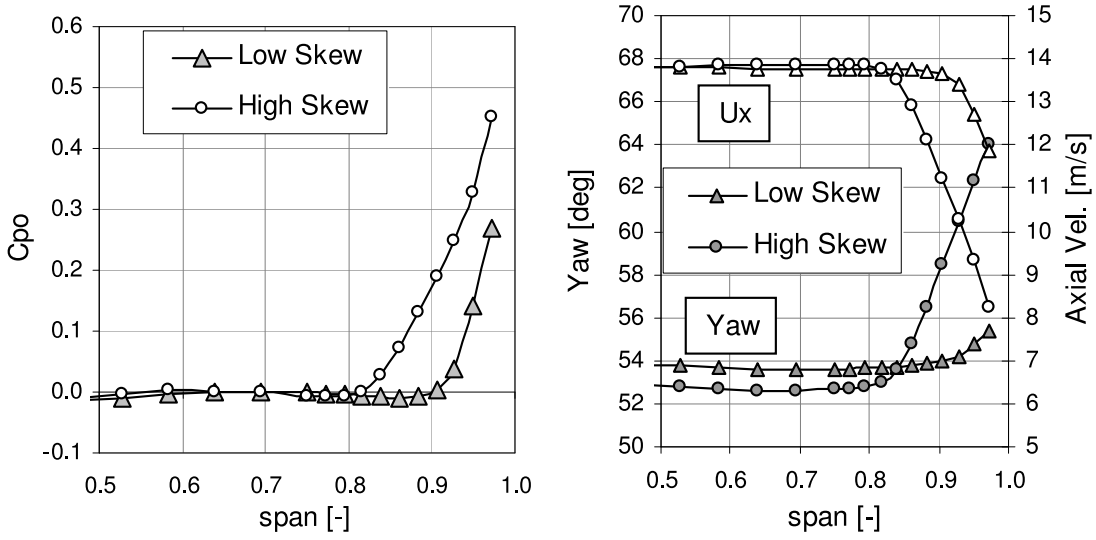

(a) Cp_0 *(b)* Yaw & v_x

Figure 3.20: *Pitch Averaged Inlet Conditions (Averaged Central Four Passages)*

this will be discussed in Section 5.1.6 on Page 138. Towards the casing the increase in yaw angle, although offset, was reasonably close to the required profile. The axial velocity and total pressure boundary layer profiles were both acceptable. A constant fan speed was used for all clearance values and both inlets throughout the measurement campaign.

3.4.6 Cascade Exit Flow Conditions

The loss at the cascade exit (without clearance) is shown in contour form in Figure 3.21 and pitch averaged form in Figure 3.22(a). The effect of the pitot-probe was clearly visible downstream and a large loss in the hub region of the bottom passage existed; this was however far from the area of interest and therefore not influential. The pitch averaged results in Figure 3.22 enlightened the difference between the passages. In general there was slightly more blockage corresponding to lower axial velocity, more loss and increased yaw angle at the hub. This was a result of atmospheric air entering the cascade through the hub from the gap between the blade and the hub. The central 4 passages had good periodicity, an increase of less than one degree in yaw from Pass2 to Pass-2 and a change of less than 0.5 m/s reduction in axial velocity existed. These exit results were deemed reasonable and fit for the

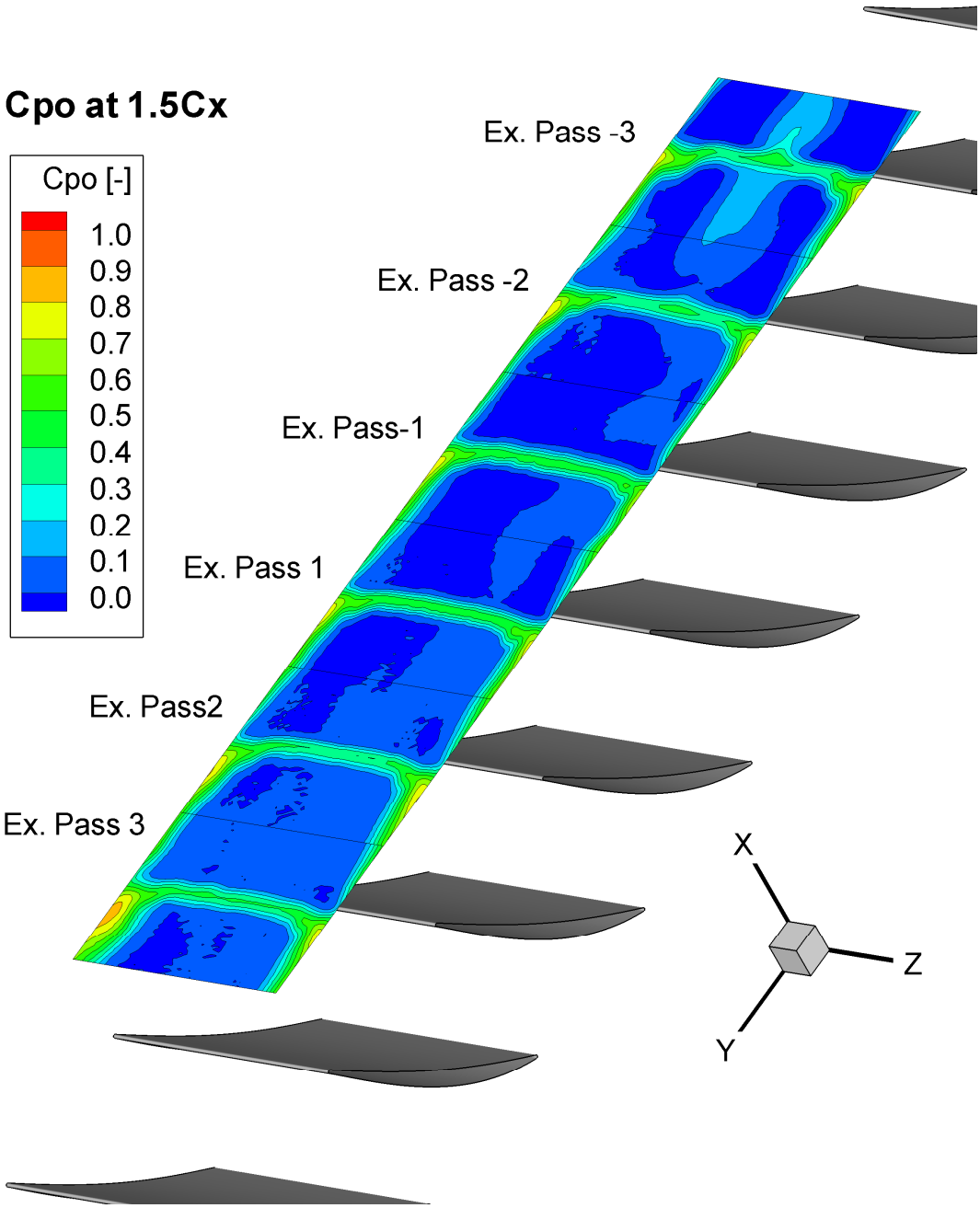

Figure 3.21: *Exit Total Pressure Loss Contours*

purpose of tip leakage investigation.

3.4.7 Cascade Loading (Diffusion Factor)

The method for calculating the diffusion factor was given in Section 3.3.6 on Page 63. The diffusion factor for Build-B was 0.29 which was calculated using (equation 3.15) and the designed inlet angle of 55° and measured exit angle of 43°.

3.5 Computational Methods

This section describes the computational methods and grids used within this thesis.

3.5.1 Code

The computations within this thesis were undertaken using a code developed by He at Durham University called TF3d-20. A good description of the code structure can be found by He [2000]. The code iteratively solved the Reynolds averaged 3D unsteady compressible Navier-Stokes equations. Turbulence closure was achieved the using the Spalart-Allmaras model (Spalart and Allmaras [1992] for the majority of this thesis. Section 4.1 used the Baldwin and Lomax model(See Baldwin and Lomax [1978] turbulence model instead. The governing equations were discretized in space using the cell centred finite volume scheme which were integrated in time using the explicit four stage Runge-Kutta method. To accelerate convergence multi-grid and local time stepping was used. Boundary layer trips were located on the blade SS and the casing to ensure a turbulent boundary layer and convergence.

For the results within the rest of this thesis the code was run to at least 5000 time which ensured convergence with a maximum axial velocity change between time steps less than 0.001 and the difference between inlet and outlet mass flow rate of less then 0.05%.

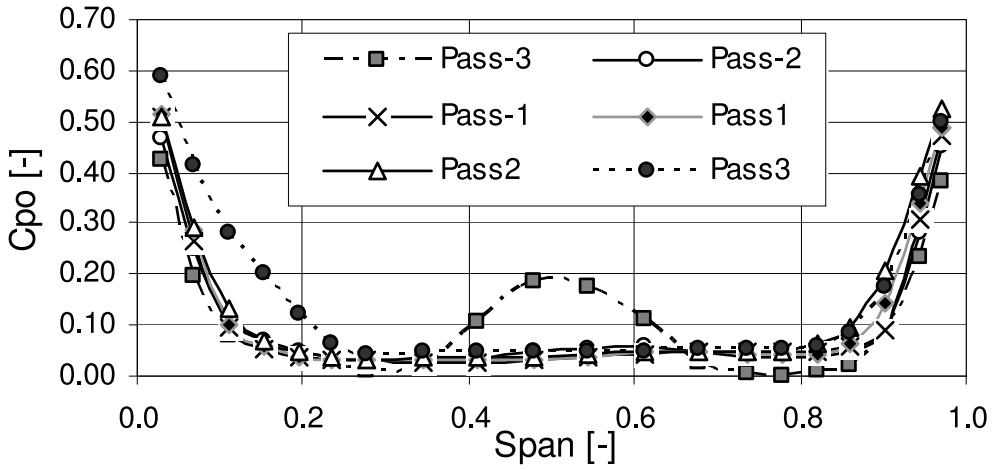

(a) Cp_0

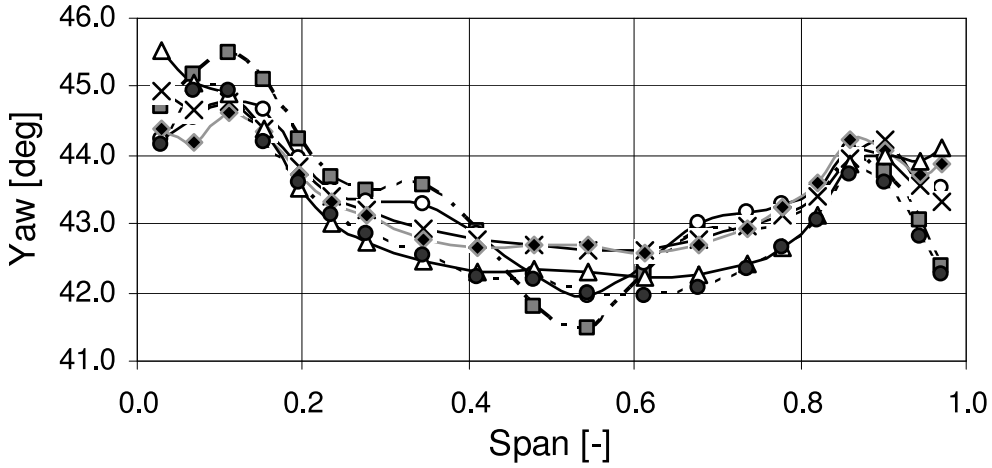

(b) *Yaw*

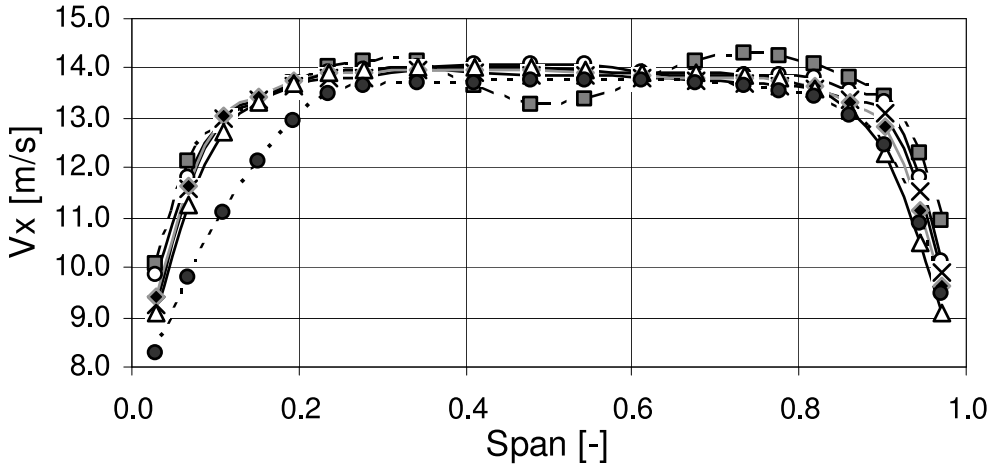

(c) U_x

Figure 3.22: *Pitch Averaged Exit Flow Conditions (Averaged Individual Passages)*

3.5.2 Build-A CFD Method, Effect of End Wall Motion

This section describes the mesh and settings used to investigate the effect of end wall motion in Chapter 4, Section 4.1 starting at Page88.

Grid

A structured H-mesh type grid was used and the blade tip was modelled using the pinch tip method. The grid extended 1 axial chord length upstream and two axial chord lengths downstream. The long mesh downstream was to allow for mixing of the tip clearance vortex before reaching the computational domain exit. The mesh extended at an angle of 37.5° upstream and 0° downstream with reference to the axis which matched the inlet and approximately match the outlet flow angles. There were 156 axial, 60 span-wise and 41 axial mesh cells giving a total of 383760 mesh cells. The blade profile was based on the measured cascade geometry (rather than the nominal coordinates). To approximate a linear cascade within the CFD the cascade hub radius was specified as 100 m.

The grid was the same for all clearances and to change the clearance the blade was made shorter within the grid through specification of the blade tip radius. In the span-wise direction the casing mesh spacing was such that a fine grid captured the tip clearance flow for up to a tip clearance of 10% span. Figure 3.23 shows the pinch tip mesh with a 6% tip clearance (6%TC) at 90% axial chord. A uniformly fine mesh existed close to the casing and each cell was 0.5% span and so with 6% tip clearance there were 12 cells in the tip clearance between the casing and the blade tip. The pinch was spaced over two percent of the span i.e. over 4 cells. The fine mesh extended to 12% tip clearance (26 cells). Beyond this the mesh spacing expanded towards mid-span before becoming finer again close to the hub. Cell stretching was kept within a ratio of 1.3 and the pinch angle lower than 60°. The same axial and pitch wise spacing was used for all clearances. Smaller cells on the blade surface and at the leading and trailing edges captured the flow features whilst not creating numerical instability.

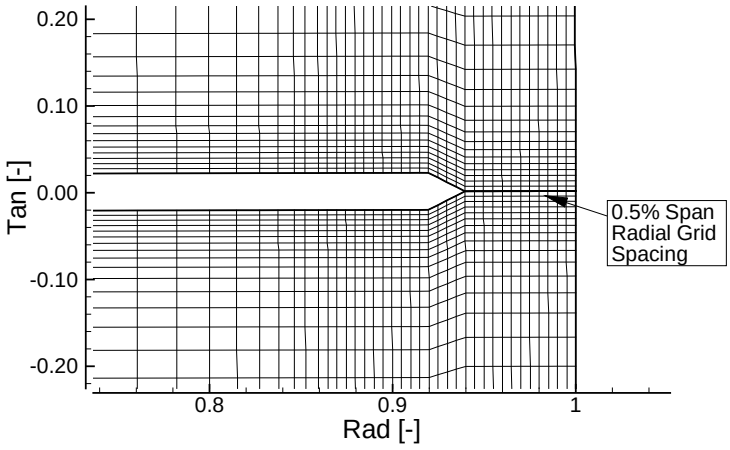

Figure 3.23: *Pinch Tip Grid at 0.9Cx*

Boundary Conditions

The boundary conditions for this section were taken from design conditions provided by Yang [2004]. No inlet boundary layer was specified.

A radially uniform inlet profile was specified across the full span. For the stationary case a yaw angle of -37.5°, stagnation pressure of 1.01575 bar and total temperature of 293 K were specified. The static pressure at exit was 0.99 bar on the hub. The exit static pressure was chosen to give an inlet axial velocity 3 times higher than within the linear cascade, which ensured convergence. To ensure the correct operating condition the Reynolds Number was set the same as the experimental cascade operating condition and therefore ensuring the correct fluid viscosity.

For the rotating case the inlet conditions were set to ensure the same cascade loading and inlet conditions. Therefore the stagnation pressure at inlet was 1.00310 bar with an inlet (absolute) flow angle of zero. To ensure the same velocity triangle as for the stationary case, the rotational speed was 4.355 rpm.

3.5.3 Build-A CFD Method

Following the experimental campaign the computational results were revisited from those used to investigate the influence of casing motion and the code settings and mesh improved. This process was undertaken to ensure that the solution was as accurate as possible.

This section describes the mesh and settings used in Chapter 4 other than Section 4.1.

Grid Details

A structured H mesh was used and the tip clearance was modelled using the pinch tip method introduced previously. Although other more accurate methods could have been available with another code, this method offered reasonable results without adding complexity and increasing computational time. To avoid excessive numerical instabilities around the pinch tip the pinch angle was limited to sixty degrees from the radial direction (as shown in Figure 3.24). The tip clearance was defined as the distance between the tip of the pinch and the casing. This clearance size definition may explain some of the discrepancy between the experimental and computational results; as previously explained in the literature review (Chapter 2 Section 2.6 on Page 30) the selection of the correct clearance size is essential for a pinch tip model to accurately predict the flows. Generation of the grid was undertaken manually using a combination of Matlab and Microsoft Excel.

The hub was defined as an inviscid wall thus ensuring no hub boundary layer and therefore preventing the formation of hub secondary flows. To approximate a linear cascade the hub radius was set to 100m and with a specification of 6981 blades the correct pitch of 90mm was realised. The computation was steady state and therefore only one passage was required and solved.

Grid Dependency

A mesh dependency study was undertaken to develop a mesh capable of solving the physical flows using the experimental data as an objective. This study is not documented here.

In general it was found that the grid dependency diminished with increased tip clearance which was found to be as a result of a reduced interaction between the leakage flow and the casing. The pitch-wise grid was found to have little effect at mid-span as long as the blade boundary layer mesh size was reasonable. To prevent diffusion of the tip clearance vortex the mesh within the endwall region was the

finest mesh possible without instability, and therefore a balance had to be obtained. Within the tip clearance it was found that if the pitch-wise grid was too fine then convergence was poor due to instabilities. Therefore, as seen in Figure 3.24, the pitch mesh was made uniform at the casing and then linearly distributed until the start of the pinch. This method decreased the the cell size within the pinch clearance and increased the cell size at mid-pitch. The radial spacing of the mesh had the largest effect on the endwall qualitative result while the axial spacing had the largest effect at mid-span. The grid dependency study found that there was a 15% change in Cp_0 loss at 1.2Cx between the grids investigated.

Final Grid

Figure 3.24 shows the grid used for the 6%TC case. A plot of constant radius is shown in Figure 3.24(b). The inlet mesh angle was 37.5° which followed the inlet flow angle and was 0.5Cx long. Downstream the mesh extended to 2.0Cx after the trailing edge at an angle of 0° or axially; this was reasonably close to the exit flow angle. The maximum cell expansion was 1.3 in any direction to avoid numerical instability.

Figure 3.24(a) shows the mesh along a constant axial plane; within the end-wall region a uniform radial distribution of 0.25% span existed for the outer 12% span. The grid spacing then gradually expanded until the cells were approximately 2.5% span, after which the distribution was constant.

To maintain a reasonably fine grid within the mid pitch casing region the pitch spacing was constant on the casing and expanded up to the pinch end. For the remainder of the span the pinch mesh distribution was spaced with a finer grid on the blade surface and coarse grid at mid pitch.

Boundary Conditions

At inlet the yaw angle and total pressure were set to be the same as for the experimental inlet conditions for the outer 50% span, which were shown in the experimental set-up in Section 3.3.4. From the hub to mid-span the inlet conditions were uniform as this flow was not of interest.

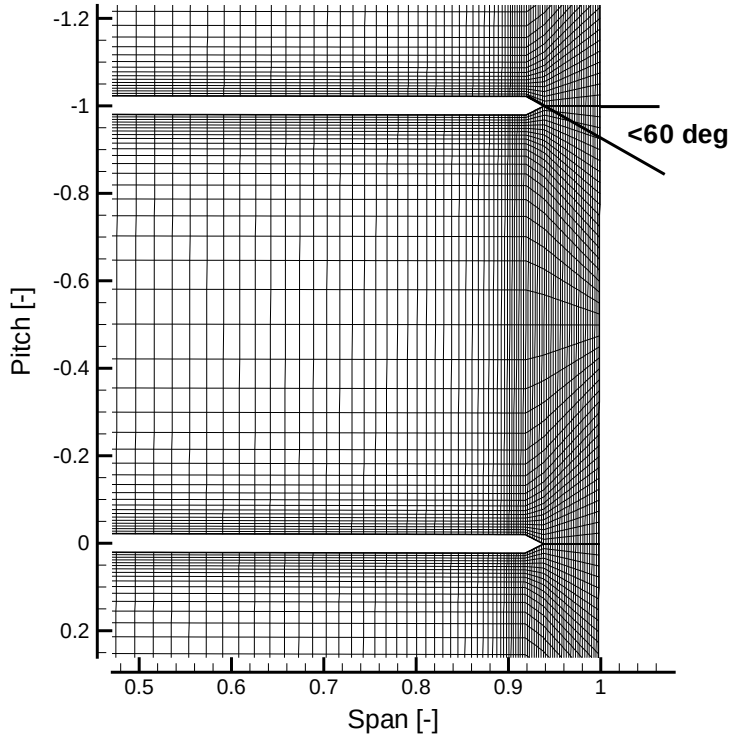

(a) K Plane

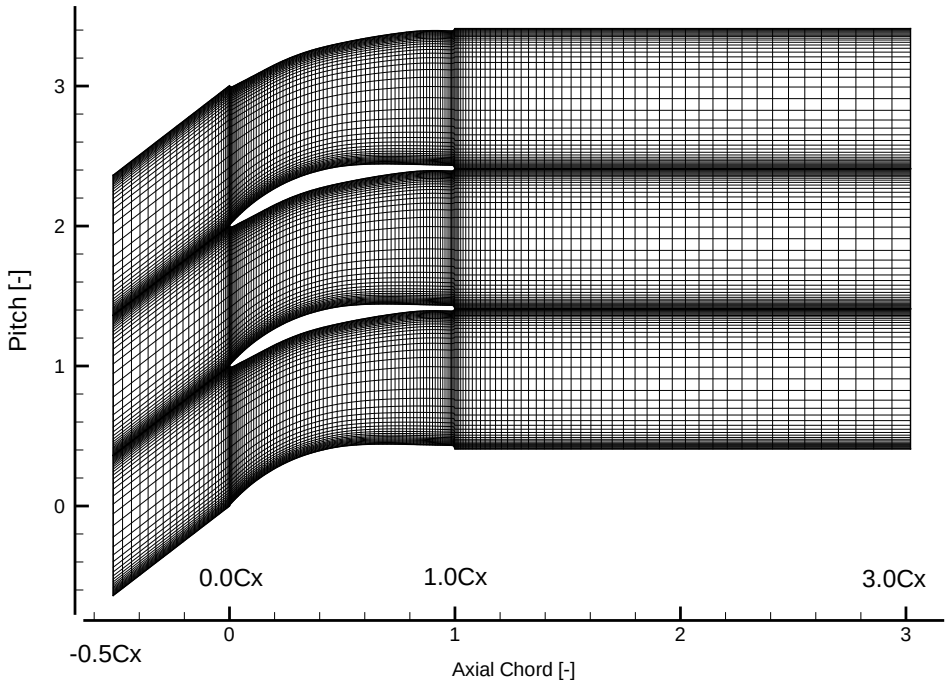

(b) J Plane

Figure 3.24: *CFD Grid for Build-A Computations with 6%TC*

At outlet the static pressure was specified at the hub and the span-wise variation was determined within the code through radial equilibrium. The outlet static pressure relative to the inlet total pressure controlled the mass flow rate and therefore the inlet velocity. To ensure convergence the back pressure was set to ensure the velocity was approximately three times higher than for the experimental rig. This was required because the CFD code used was a density based solver and therefore unable to predict low speed applications. To ensure the correct fluid viscosity and therefore the correct working conditions the Reynolds Number was set as for the experimental cascade ($Re = 1.91 \times 10^5$). The CFD code (TF3d-20) then established the fluid properties from the initial estimate of inlet velocity.

3.5.4 Build-B CFD Method

A similar mesh was used as for Build-A in Section 3.5.3 on Page 81. The mesh extended half an axial chord (-0.5Cx) upstream of the leading edge and 2 axial chords downstream of the trailing edge (3.0Cx). There were 145 axial, 41 tangential and 118 radial mesh cells per passage giving a total of 701510 cells per passage. Again a pinch tip model was used and the cells within the gap were 0.25% span high. As an example with 6%TC case the clearance consisted of 24 cells between the casing and pinch tip.

At inlet the yaw and total pressure were specified as measured in the experimental cascade for both inlet conditions. As with the previous cascade only the outer half of the cascades inlet profile was specified; the inner half was assigned the mid-span value. To avoid hub wall secondary flows the hub was specified as a frictionless wall. The inlet Reynolds Number (3.6221×10^5) was specified as for the experiment. The static pressure at exit was specified to set the mass flow; again this was purposefully set low to increase the mass flow and therefore aid convergence. As the turbulence code used was the Spalart-Allmaras model (Spalart and Allmaras [1992]), tripping of the boundary layer was required and this was undertaken on the casing and both the SS and PS of the blade. The trip on the PS was required for convergence due to a negative incidence angle on to the leading edge of the blade.

3.6 Summary

This chapter has presented the two linear cascades used within this thesis and the computational methods used. Build-A consisted of low stagger high turning blading and Build-B consisted of high stagger low turning blading. Build-B had a unique upstream tangential injection system to control the inlet boundary layer, details of which were given. Details of the cascades construction, set-up and flow quality were presented. Details were also given of the computational code, boundary conditions and grid.

The following chapter (Chapter 4) presents experimental and computational results from Build-A and Chapter 5 presents the results obtained from Build-B.

Chapter 4

Build-A, Results and Discussion

This chapter presents a selection of the results obtained from the low stagger geometry cascade (Build-A) using experimental and computational techniques. The leakage flow physics and the effect of clearance size will be explored for this geometry. Firstly the effect of endwall motion with different clearances will be investigated to assess the cascade results relevance within a real machine. The computational fluid dynamics (CFD) methods used are then explored and best practice for the grid density and the code settings established. Experimental downstream traverse and blade static pressure results will be presented and used for computational validation. Both the experimental and computational results will be used to examine the effect of tip leakage size on the leakage flows and row performance. The 6%TC case will be further explored to investigate the physics of large clearances; the choice of clearance value was due to the applicability within the real engine. Discussions and conclusions will be undertaken for this geometry.

Within this work the tip clearance was defined as the percentage of cascade span (annulus height). Table 4.1 shows the conversion to absolute and percentage chord values.

% Cascade Span	0	1	2	4	6	8	10
Tip Clearance (mm)	0.0	1.9	3.8	7.6	11.4	15.2	19
% Blade Chord	0.00	1.27	2.53	5.06	7.6	10.1	12.6

Table 4.1: *Build-A Tip Clearance Size Definition*

4.1 Effect of End Wall Motion

As discussed within the literature survey linear cascades generally, and within the current work, have a stationary wall (casing). However real rotors have a relatively moving casing due to the rotor rotation. Tip leakage flows are affected by this motion and so therefore it is essential to understand the differences between the real case and the cascade. This section therefore investigates the effect of relative casing motion using CFD. The effect of rotation on the radial flow was ignored. For a rotating machine, in the relative frame of motion, the flow on the end wall does not fall to zero but to the speed of the end wall. For a compressor this motion is in the same direction as the pressure drop from PS to SS resulting in an increase in the tip clearance flow.

Details of the CFD code, boundary conditions and grid used within this section were shown in Section 3.5.2 on Page 80. The boundary conditions for this section were taken from design conditions provided by Yang [2004]. This work also looked at the leakage flows in more detail however they were superseded after experimental data became available therefore only the relevant data for the investigation of wall motion is explored.

4.1.1 Results

A selection of results to investigate the effect of a relatively moving wall on the tip leakage and endwall flows follow. Figure 4.1 shows loss contours and velocity vectors at 0.9Cx with and without motion for 1%TC and 6%TC. Figure 4.2 shows the pitch averaged loss and yaw angle downstream of the cascade at 1.2Cx with and without motion for clearances from 0%TC to 10%TC. At 1%TC the loss contours are significantly affected by the motion but for the large 6%TC the difference is less significant.

It should be noted that if the fluid were inviscid then the wall motion would have no effect on the leakage flows as it would be a purely pressure driven jet. However through friction the wall rotation does have an effect. With 1%TC and without rotation (Figure 4.1(a)) three vortex structures were clearly observed. These

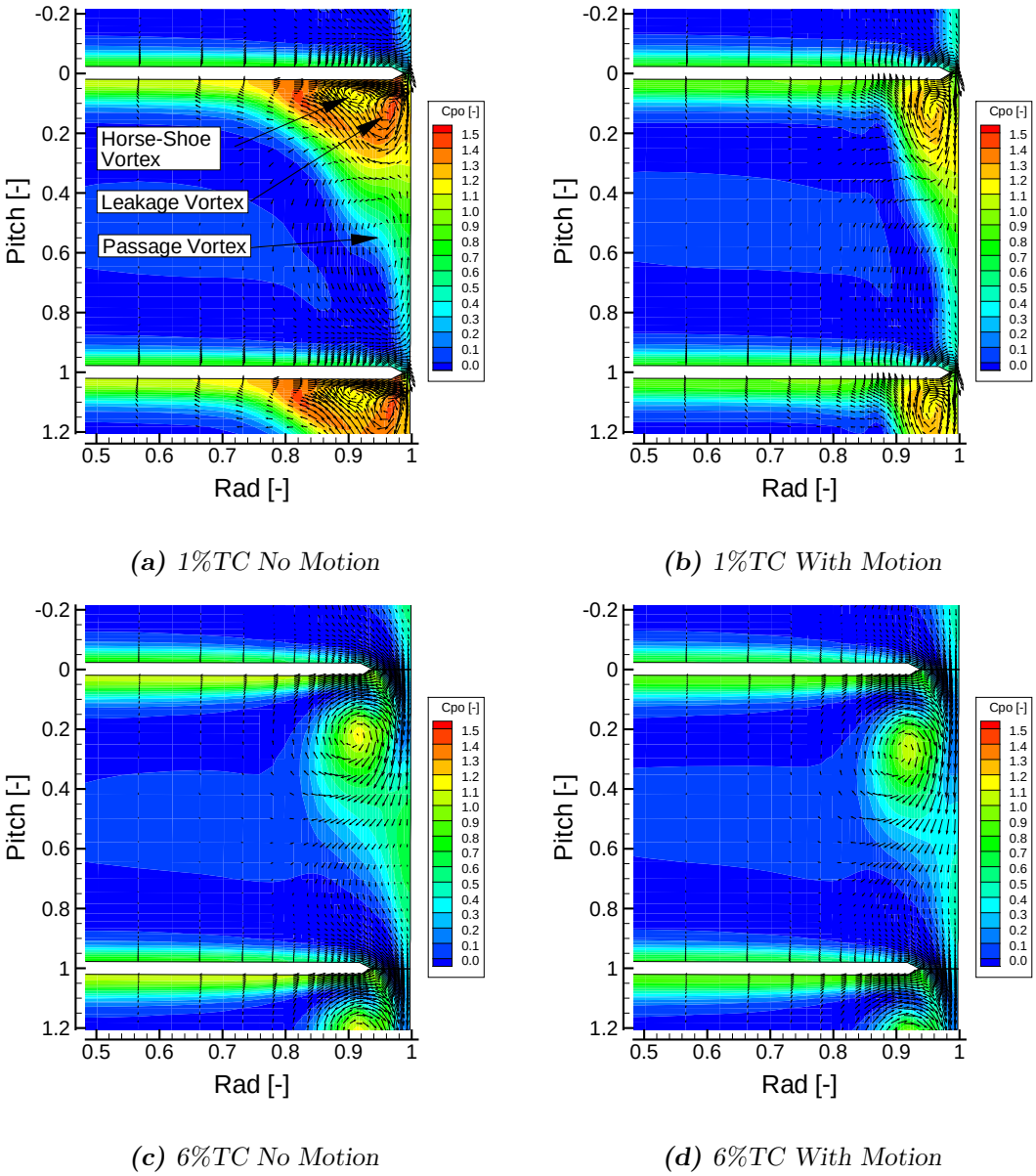

(a) 1%TC No Motion

(b) 1%TC With Motion

(c) 6%TC No Motion

(d) 6%TC With Motion

Figure 4.1: *Effect of Casing Motion, Cp_0 Contour Plots at 0.9Cx*

were the passage vortex, leakage vortex and horse-shoe vortex. As expected both the leakage vortex and suction surface leg of the horseshoe vortex rotated counter-clockwise looking from downstream which was the same as the leakage vortex and opposite to the passage vortex. This flow structure represented a corner separation as discussed in the literature survey.

The leakage flow magnitude increased with endwall motion, which was due to the endwall motion pulling the flow through the clearance gap, this energised the flow within the corner region preventing the corner separation. The high loss/blockage

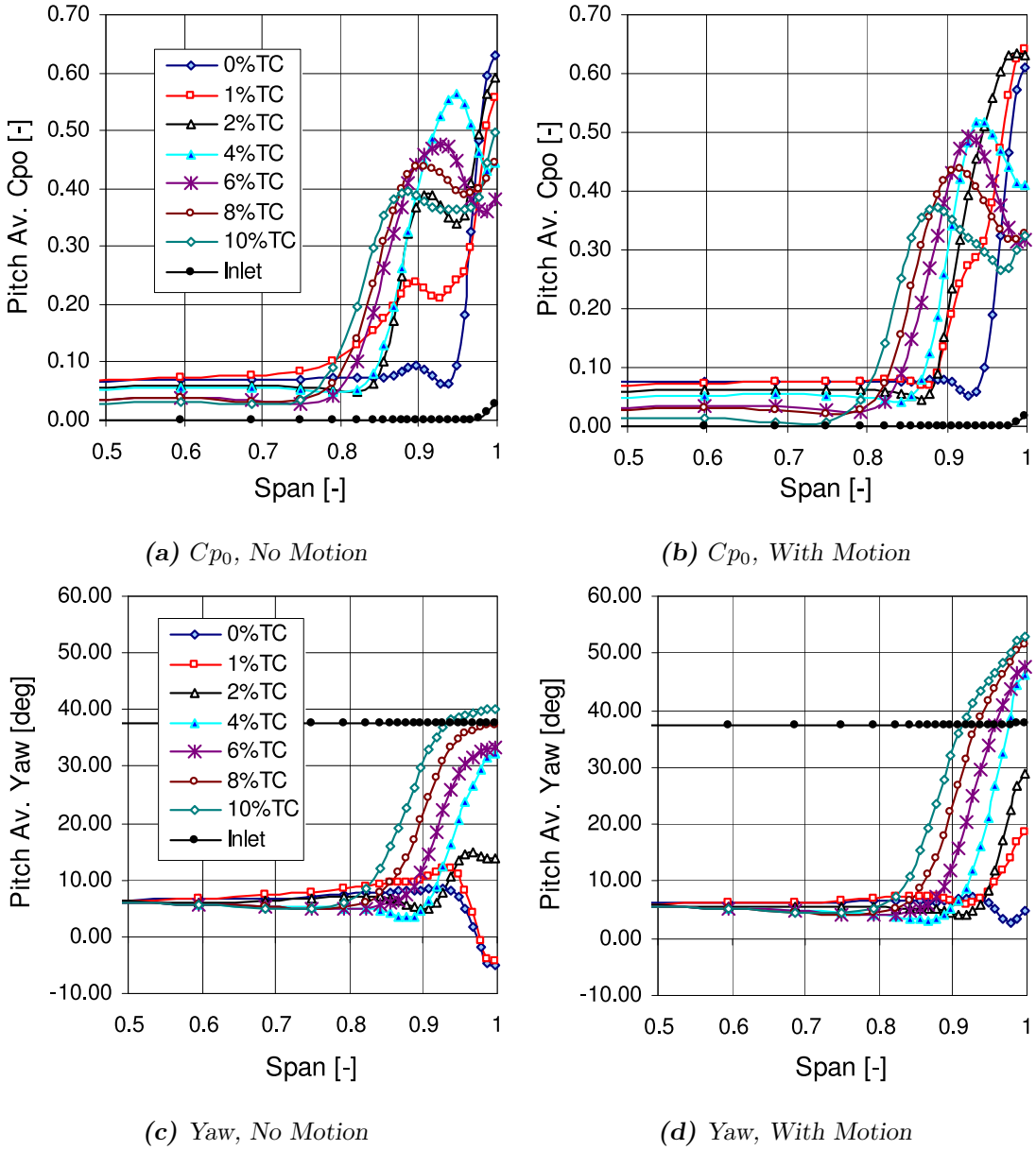

(a) Cp_0, *No Motion* *(b)* Cp_0, *With Motion*

(c) *Yaw, No Motion* *(d)* *Yaw, With Motion*

Figure 4.2: *Effect of Casing Motion, Pitch Averaged Yaw &* Cp_0 *at 1.2Cx*

region was therefore reduced and the passage vortex and its blockage was eliminated by the increased leakage flow as an outcome of the motion. These flow features were apparent in the pitch averaged plots (Figure 4.2). With 1%TC the loss on the casing was slightly reduced by the rotation but the yaw angle was significantly underturned with and exit angle of $\approx -20°$ (under turned by $\approx 13°$) compared to an over-turned exit angle of $\approx +5°$ (over-turned by $\approx 12°$). There was an increased area of loss close to the wall with motion and the loss due to the corner separation was eliminated. Away from the wall (approximately 0.9 span) the angle underwent

a small over-tuning with motion but small under-turning without motion.

For the larger 6%TC the differences were less significant and the contours show a significant leakage vortex with and without motion. The trajectory of the vortex centre with the endwall motion moved a little further across the passage away from the SS and slightly closer to the wall. With motion an increased leakage flow moving unhindered across the passage occurred and the relative velocity gradient on the end wall was reduced. These two effects eliminate the formation of the induced vortex which was present without motion. Although a higher loss region still existed this reduced the loss magnitude associated with the induced vortex. With motion the peak loss associated with the leakage vortex was similar in magnitude but tangentially elongated and enlarged therefore increasing the total loss (Figure 4.2). The loss on the casing was lower with the motion, this was because in the relative frame the wall exerted work on the fluid and therefore introducing energy in to the fluid. Without motion the yaw angle was significantly under-turned by the leakage flows. With wall motion the flow was further under-turned; in fact the yaw angle on the casing was lower (approximately 10°) than at inlet. The flow was therefore skewed by the motion of the casing at exit of the row.

A similar pattern was observed for the other clearances shown in the pitch averaged plots (Figure 4.2). The flow pattern within the endwall region was found to be significantly different for the values of clearance above and including 4%TC. In general the flows below this clearance were strongly affected by the casing motion, but above they were only mildly changed. For the larger clearances the effect of the motion was small and mostly observed by increased skew at inlet as shown in Figure 4.3.

The wall motion altered the blade loading as seen in Figure 4.4. The effect for the larger tip clearances was small but for the small tip clearances the blade loading at the end of the tip was significantly increased. The reason for this was partly due to the increased skew at inlet and also the change in leakage flow patterns.

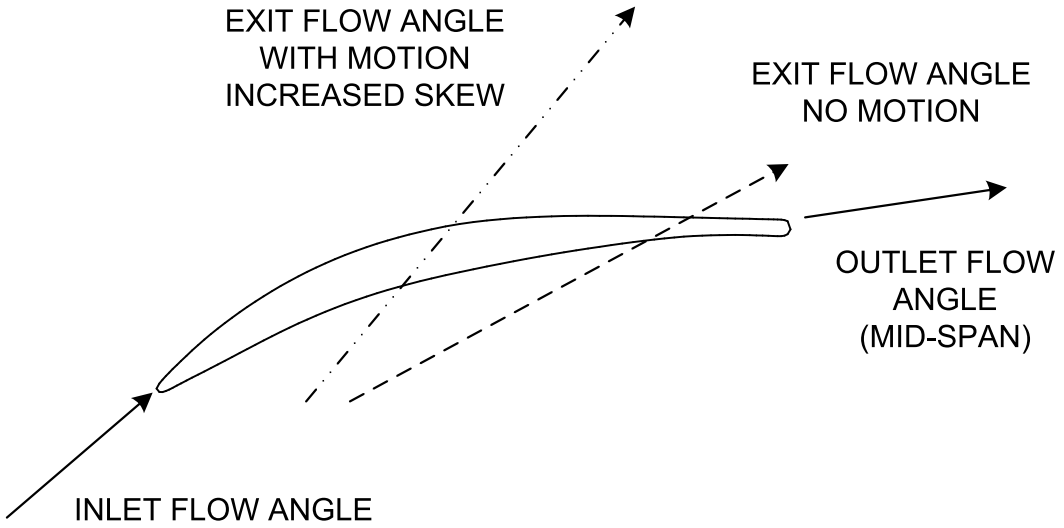

Figure 4.3: *Effect of Motion on Exit Skew Angle*

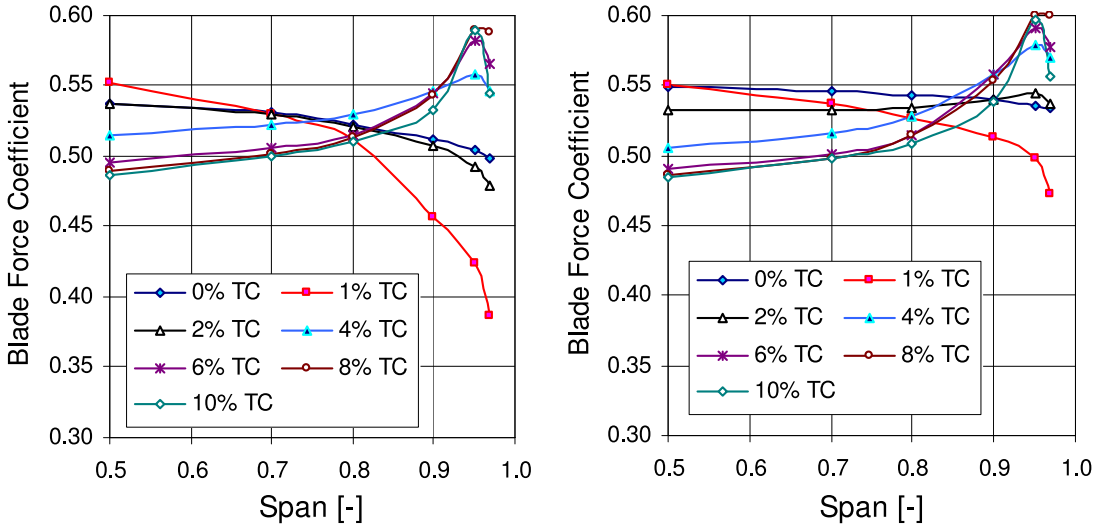

(a) *No Motion* ***(b)*** *With Motion*

Figure 4.4: *Effect of Casing Motion on Blade Loading*

4.1.2 Conclusions

With a small ($\leq$ 4%TC) a significant effect of endwall motion was found but with a large clearance the influence was small. This was a helpful outcome, for the large clearances within this work the effect of motion was limited and could be predicted. The rotation therefore was found to have little effect on the conclusions. The summarised moving endwall effects follow:

Small Clearance $\approx< 4\%TC$**:** The endwall motion changes for small clearance

were due to the increased inlet angle (inlet skew) and the increased leakage flow strengthening of the leakage vortex and therefore suppression of the corner stall. The loss distribution was therefore changed and the flow was under-turned as opposed to over-turned without motion. An increase in blade loading towards the tip also occurred but was lower than the 0%TC case.

Large Clearance $\approx> 4\%TC$: With a large clearance the end wall motion had little effect on the clearance vortex strength. However the vortex trajectory was altered, a slight pitch-wise shift across the passage and radial shift towards the casing occurred. The loss on the endwall was reduced by the motion, and this was a result of the suppression of the counter rotating vortex and the wall doing work on the flow in the relative frame. The flow underwent further under-turning at exit with endwall motion. In fact the flow had a lower angle than at inlet resulting in more highly skewed flow at exit of the cascade.

The predictable and reduced effect of casing motion with large clearance values justifies the use of a linear cascade for endwall secondary flow investigations. A small shift in vortex trajectory, increased exit skew angle, reduction in loss and increased blade tip loading occurred with wall motion. The remainder of this chapter will explore the effect of clearance size on the tip clearance flow structures and there influence on the rotor performance.

4.2 Experimental Results and CFD Validation

The experimental results obtained from the low stagger cascade are now given. These are compared with the computational results for CFD validation. Results were obtained for a datum of 0%TC clearance and for three different clearance values (1%TC, 2%TC and 6%TC). Details of the computations including the code, boundary conditions and grid were shown in Section 3.5.3 on Page 81.

4.2.1 Downstream Traversing

Previously the measurement grid at 20%Cx downstream of the trailing edge was presented and to indicate the cascade's periodicity the 0%TC (Figure 3.11 on Page

63) case loss contours shown. Here Figure 4.5 shows the loss contours for each of the measured clearances including the datum. Figure 4.6 presents the pitch averaged yaw (Figure 4.6(a)), loss (Figure 4.6(b)) and axial velocity (Figure 4.6(c)); and included are the CFD results. Secondary vectors are included on the contour plots; these secondary vectors were vectors corrected by the average mid-span values as discussed in Section 3.1.1 on Page 52. Similarly the pitch averaged values were zeroed at mid-span to emphasize the effect of the endwall flows. For clarity, the contour level boundary was reduced for the no tip clearance case.

With no clearance, and therefore no leakage, the secondary flow was clearly observed. over-turning existed close to the wall and under-turning occurred further away from the wall. This accumulated high loss fluid on the suction surface corner region. The existence of a corner separation was probable but not clearly visible from these results. The blockage was clearly evident in Figure 4.6(c) with reduced axial velocity on the casing and increased axial velocity at mid-span.

The computational pitch averaged results compared well with the experimental data (Figure 4.6). Quantitatively the results showed a good comparable pattern. Qualitatively the yaw angle was reasonable but the loss was slightly over predicted. The 0%TC and 6%TC cases showed the best comparison with the smaller tip clearances (1%TC and 2%TC) showing poorer comparisons.

4.2.2 Blade Static Pressure Measurements

The experimental and computational blade pressure coefficient profiles are shown in Figure 4.7 for 50%, 90% and 98% spanwise sections from the tip respectively. Without clearance the blade loading showed good agreement between experimental and computational results, which was also the case with the large 6%TC case. For the smaller clearance of 2%TC the agreement was not so good. This difference at 2%TC may have been due to the computational grid not being optimised for small clearances and also the pinch tip not capturing the flow structure correctly.

A similar pattern was followed with the CFD as with the experimental results. Generally the experimental peak suction surface pressure was slightly lower than for the CFD suggesting a lower incidence angle. Experimentally a higher pressure on the

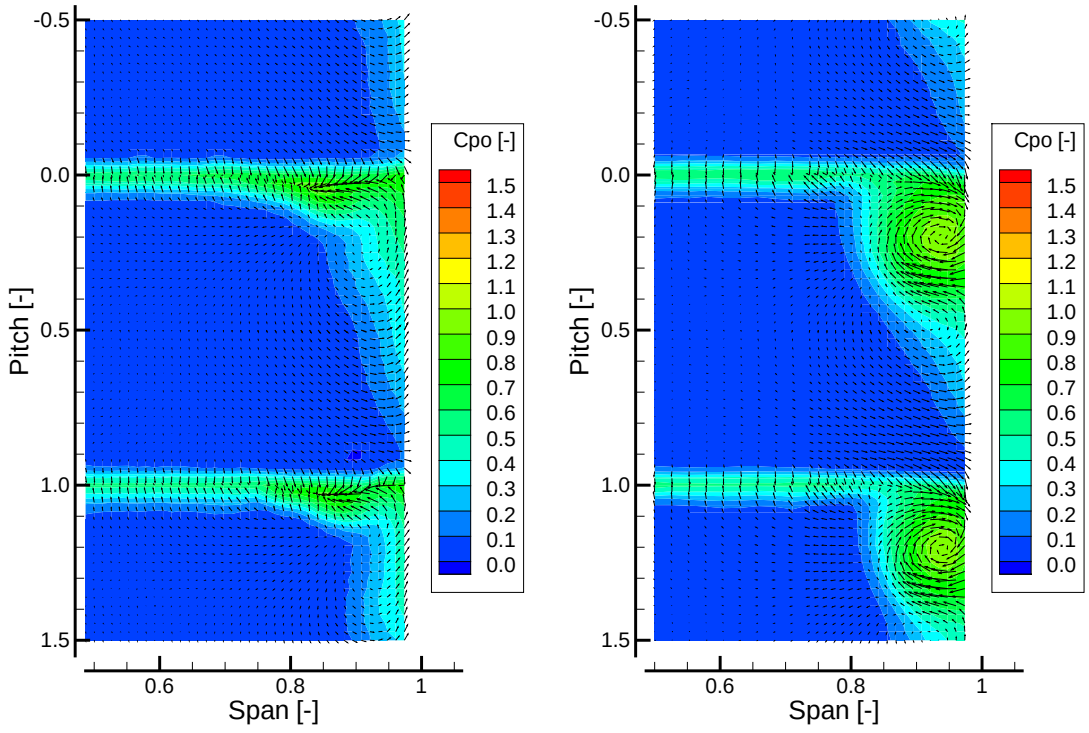

(a) 0%TC *(b) 1%TC*

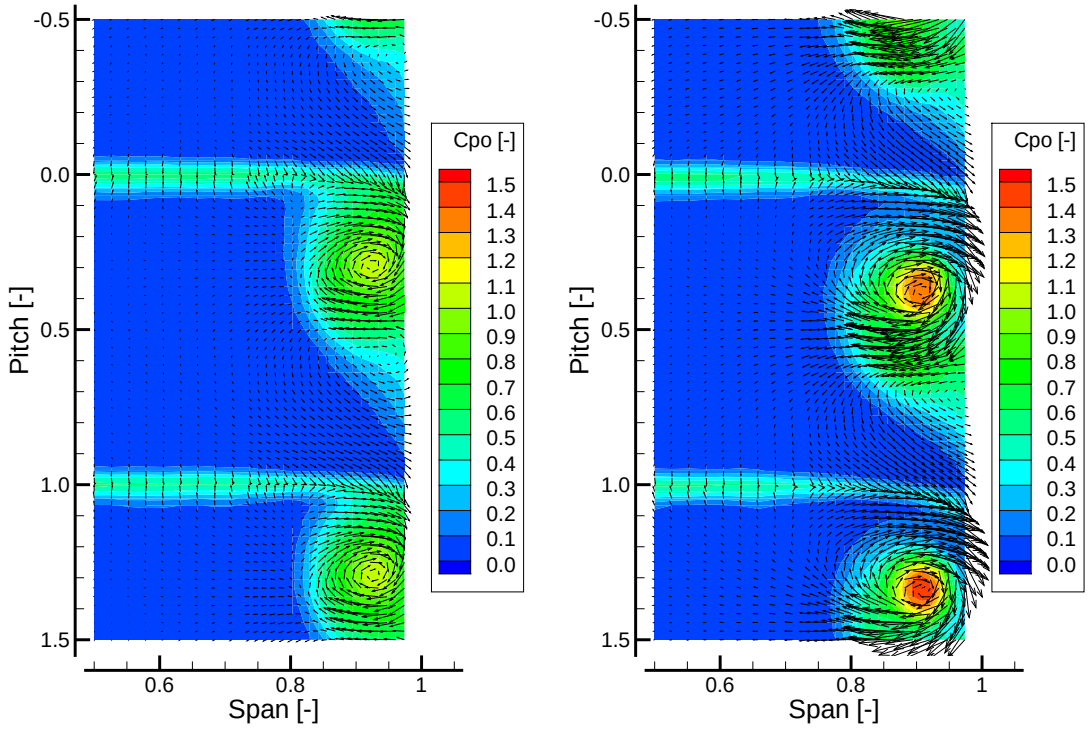

(c) 2%TC *(d) 6%TC*

Figure 4.5: *1.2Cx, Experimental Cp_0 Contours & Velocity Vectors*

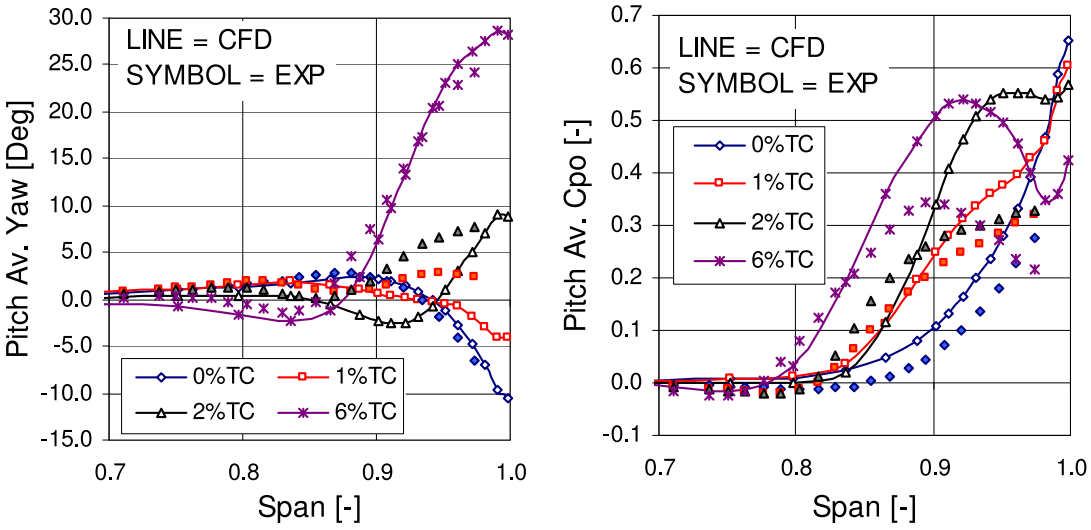

(a) *Yaw* *(b)* Cp_0

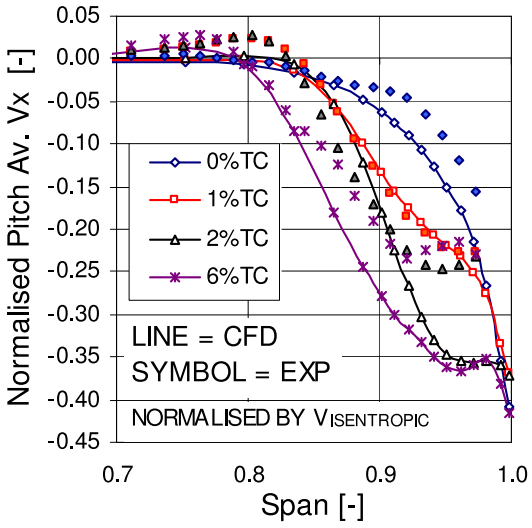

(c) V_x

Figure 4.6: *1.2Cx, Experimental Pitch Mass Averaged Results*

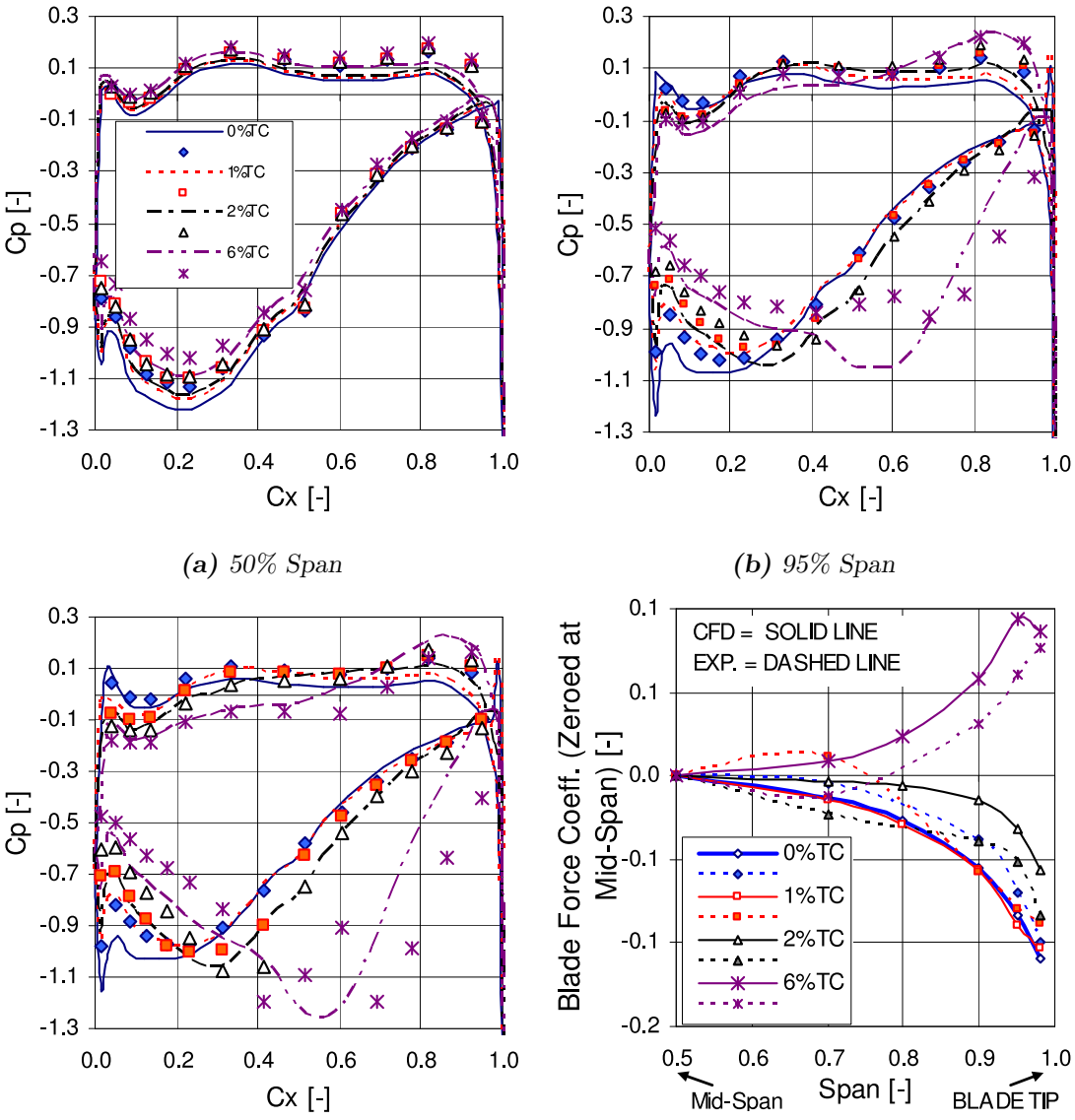

(a) 50% Span

(b) 95% Span

(c) 98% Span

(d) Blade Force Coefficient

Figure 4.7: *Experimental Blade Pressure Coefficient Plots*

rear part of the pressure surface exists. At 98% span and 6%TC the experimental data showed a high pressure region (wiggle) on the suction surface compared to the mid-span profile. This was at approximately 0.6Cx and could be associated with an effect of the blade support rod however as will be shown later this was still evident without the rod. The actual experimental loading would be slightly higher without this rod and closer to the CFD prediction.

A significant change with increased clearance on the blade pressure profile was observed. Of note was the change in blade loading towards the tip of the blade with increasing tip clearance values (Figure 4.7(d)). Reasonable agreement between experimental and computational results was observed. In general with increasing TC value there was a decrease in loading at the leading edge and an increase in loading towards the trailing edge. At mid-span a change in loading at the leading edge indicated a change in inlet yaw angle, which was attributed to a redistribution of mass flow towards mid-span and therefore a decrease in incidence as seen in Figures 4.6(a) and 4.6(c). Furthermore this pattern was also predicted computationally. At the tip the change in loading was associated with the interaction of the vortex on the suction surface.

4.3 CFD Results

CFD results are now presented; this allows for additional comparison of experimental and the previously presented computational results and also the study of clearance sizes not experimentally studied and further exploration of the clearance flow physics. Downstream loss contours and downstream pitch averaged plots of loss, yaw and axial velocity are shown for clearance values up to and including 10% span. The blade loading along the blade will be shown and the effect of clearance size on loss increase through the cascade.

4.3.1 Downstream Traverses at 1.2Cx

Figure 4.8 shows contour plots downstream of the blade row (at 1.2Cx) which correspond to the previously given experimental plots in Figure 4.5. When compared

to the experimental data the agreement was reasonable but in general the CFD was more dissipative. Therefore the extent of loss due to the endwall flows and wake was larger but the peak values were lower for the CFD. This explains the CFD's loss over prediction.

Pitch averaging of the downstream traverse gave the following plots; Figure 4.9 shows the Yaw (4.9(a)), Cp_0 (4.9(b)) and Axial (4.9(c)) velocity. The yaw angle for the 0%TC case showed the classic under-turning over-turning detailed within much literature. An increase in loss towards the casing due to the secondary flow and corner stall occurred; in fact the loss on the casing for the zero percent case showed the highest loss peak. The 1%TC case had less over-turning on the casing because the TC flow suppressed the corner stall. For the large tip clearances, 2-10%TC, the flow underwent a significant over-turning and under-turning towards the casing caused by the tip clearance vortex. The loss peak at the leakage vortex core decreased in magnitude with increased TC but the area of loss increased in size. The leakage vortex moved away from the casing with increased clearance.

The effect of the blockage on the stage mass flow is shown in Figure 4.10. A linear relationship existed between blockage and tip clearance value above 2%TC, as seen when examining the mass flow tip clearance relationship (Figure 4.10 on Page 101). A 4.8% reduction in mass flow from 0% to 10% was found. Therefore for the computational results the mass flow reduction was approximately 0.5% per 1% increase in tip clearance size.

Figure 4.11 shows the increase in loss from inlet to exit for the outer 50% span. It can be seen that the overall loss increased until 6%TC above which no further increase occurred. These results were similar to the previously shown results in Section 4.1 without an inlet boundary layer profile, suggesting that the inlet angle within the TC region had limited effect on the loss and exit angle. The effect of the inlet boundary layer will be further investigated in Chapter 5.

The experimental mass weighted area averaged Cp_0 loss is also shown in Figure 4.11 and was observed to follow the same pattern as the CFD results. As expected from the pitch averaged plots the experimental area mass averaged loss was slightly lower than the CFD's prediction.

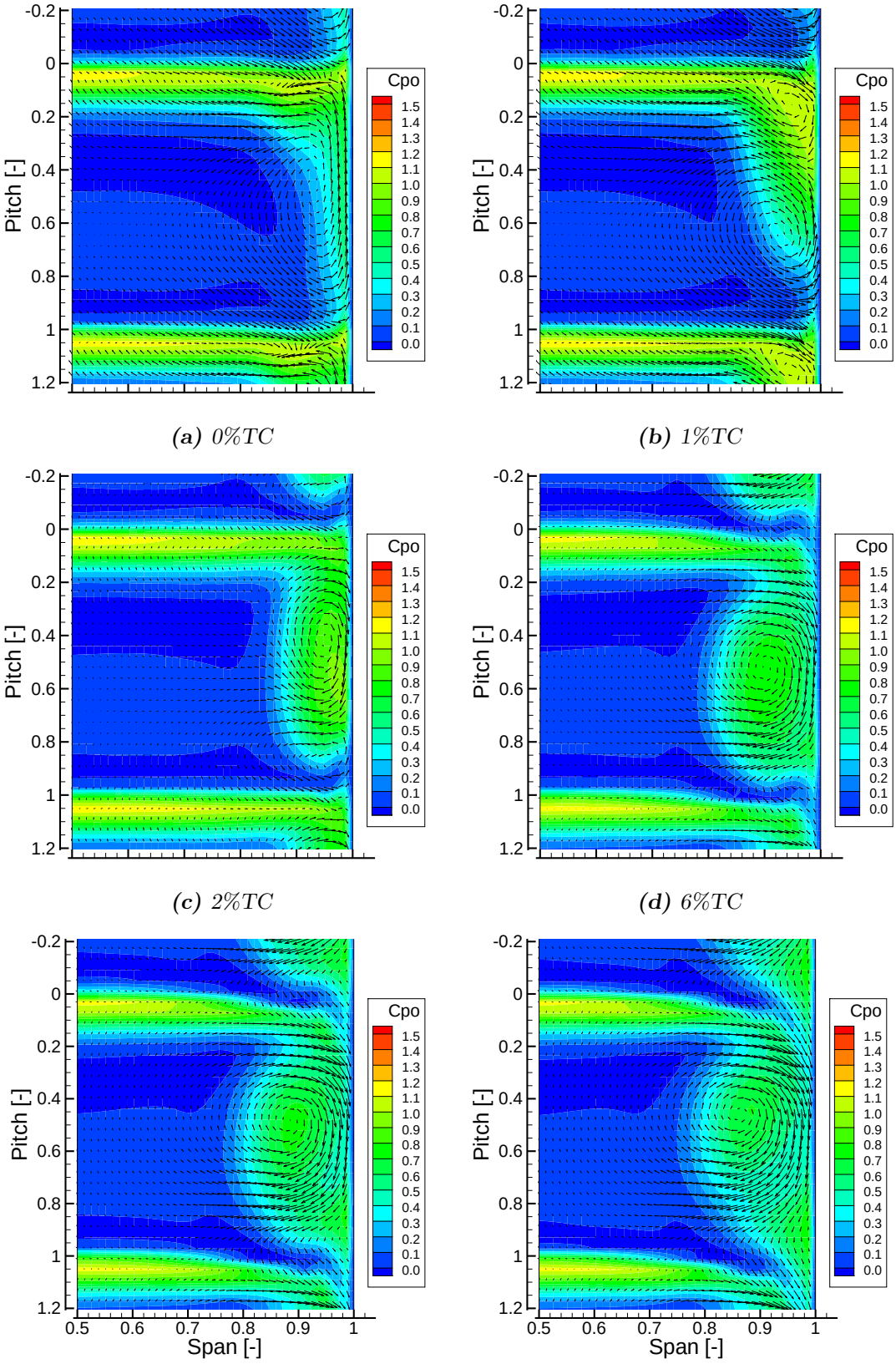

(a) *0%TC* ***(b)*** *1%TC*

(c) *2%TC* ***(d)*** *6%TC*

(e) *8%TC* ***(f)*** *10%TC*

Figure 4.8: *CFD Cp_0 Contour Plots*

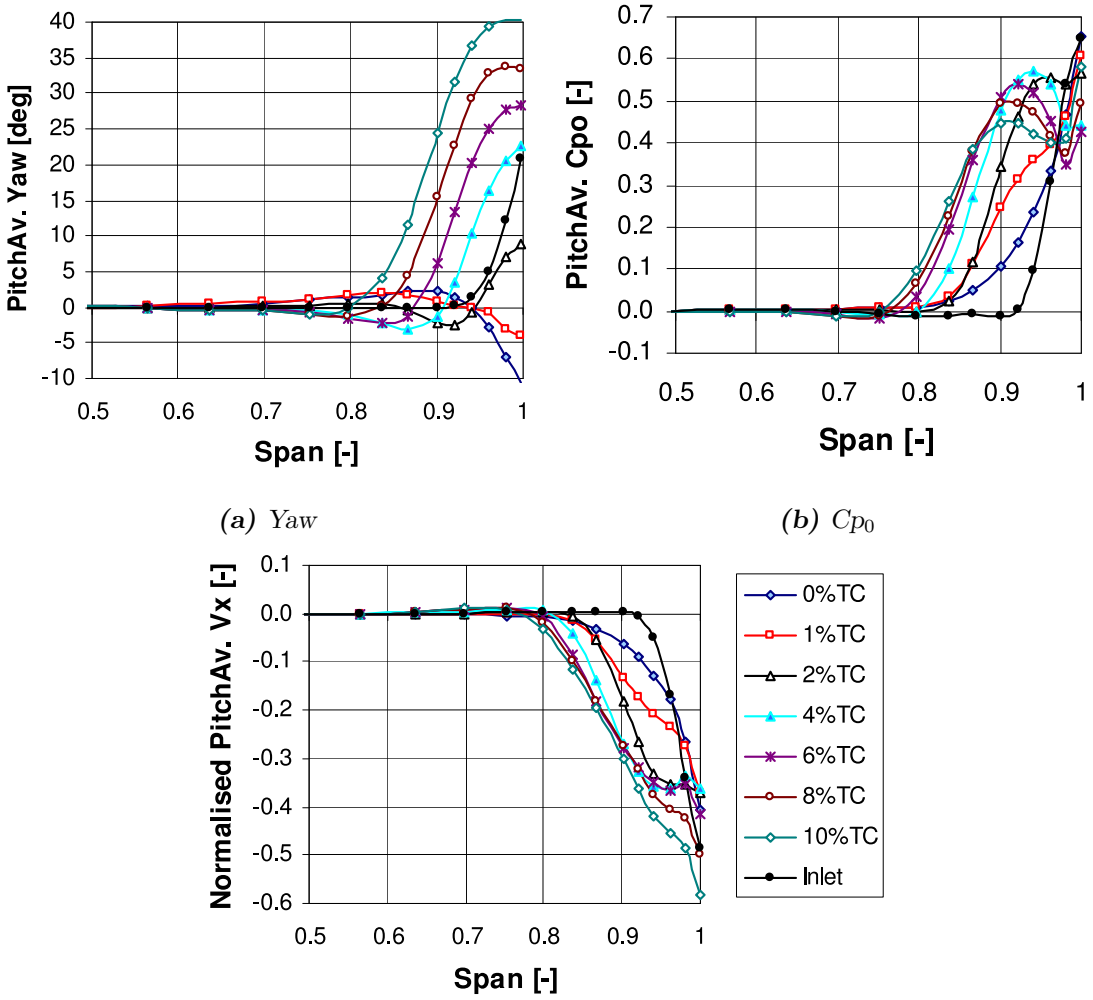

(a) *Yaw* *(b)* Cp_0

(c) $V_{x,Norm}$ *(Normalised with* $V_{Isentropic}$*)*

Figure 4.9: *CFD Pitch Mass Averaged Results*

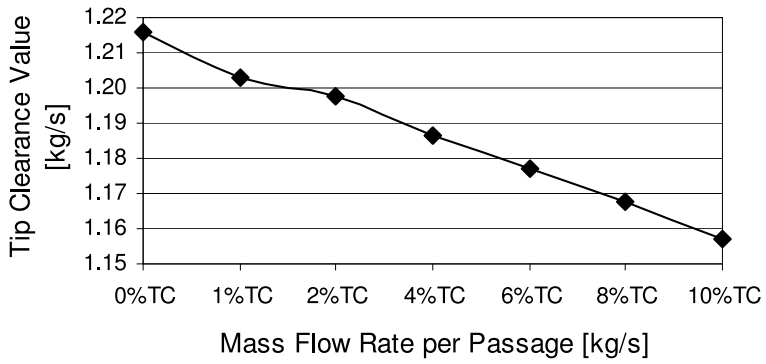

Figure 4.10: *CFD Mass Flow Rate per Passage*

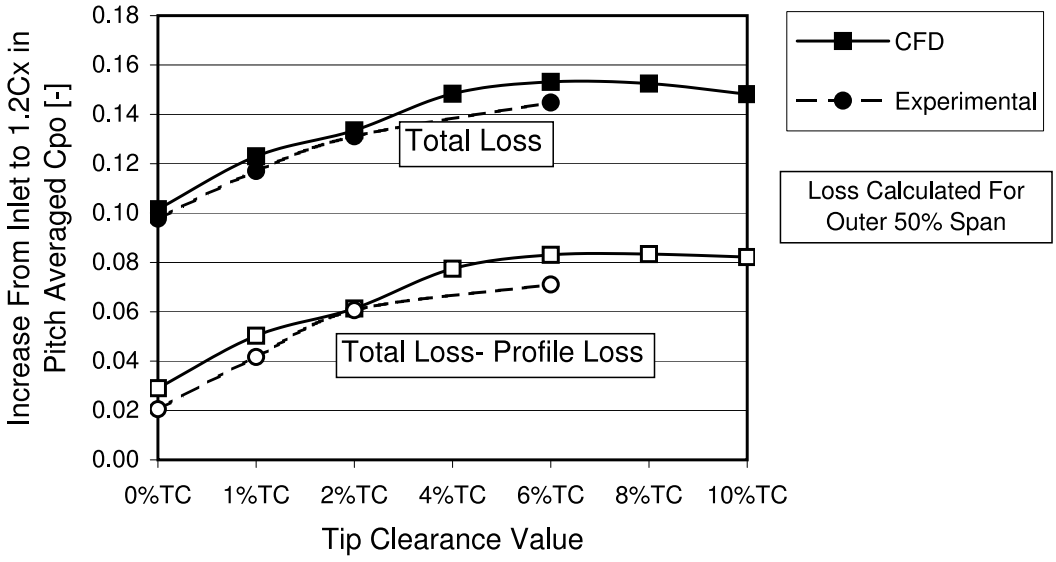

Figure 4.11: *CFD Area Averaged Cp_0 (Outer 50% span)*

Removing the profile loss from the overall loss for the outer 50% span gave the loss attributed to the endwall secondary flows including the tip clearance flows, this is also shown in Figure 4.11 by the white symbols. The endwall flow loss accounted for approximately 45% of the total loss for the smaller TC values (including the 0%TC case) and increased to approximately 62% of the total loss for the 10%TC case. Although not shown, the same pattern was observed at the computational domain exit at 3.0Cx (2 axial chords downstream).

The blade loading integrated become the tangential blade force (Figure 4.12) and then the blade force integrated along the blade gives the overall tangential blade force per unit length (Figure 4.13 on Page 103); these were all shown relative to the mid-span value. The overall blade force per unit length was plotted relative to the 0%TC value. Importantly, as will be discussed later, this shows an increase in tangential blade loading towards the tip of the blade with 6% tip clearance. A reasonably similar pattern was observed between the experimental and CFD data.

Figure 4.13 shows the overall blade force coefficient per unit span for each measured tip clearance, which is shown relative to the 0%TC case. This total blade force was the integration of Figure 4.7(d) and therefore was integrated from the the tapping row at the tip of the blade (2% span or 3.8mm from the blade tip) to a distance of half the annulus height (50% span or 95mm from the blade tip) from the

blade tip. Therefore with changing clearance the integrated area did not change but it did move away from the casing, this was a reasonable method as the blade loading was zeroed at mid-span and therefore the loading at mid-span was negligible. The 1%TC and 0%TC had similar blade force but with a tip clearance above 2%TC there was an increase in blade force and this increased with increasing tip clearance.

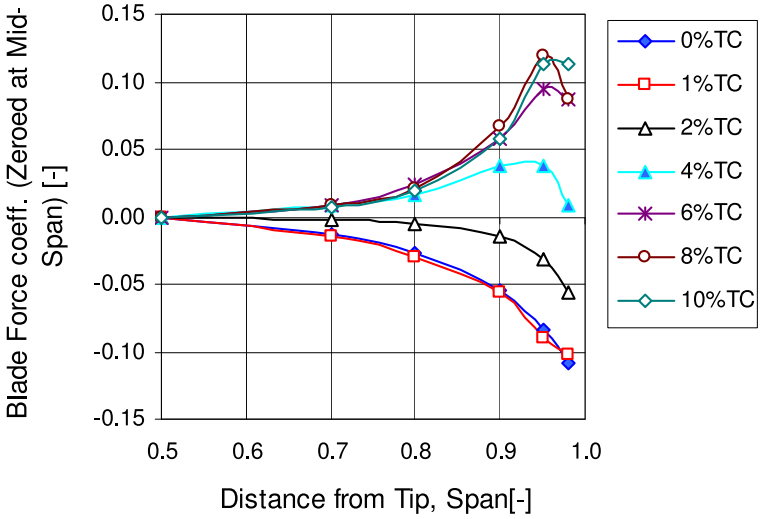

Figure 4.12: *CFD Blade Force Coefficient Results*

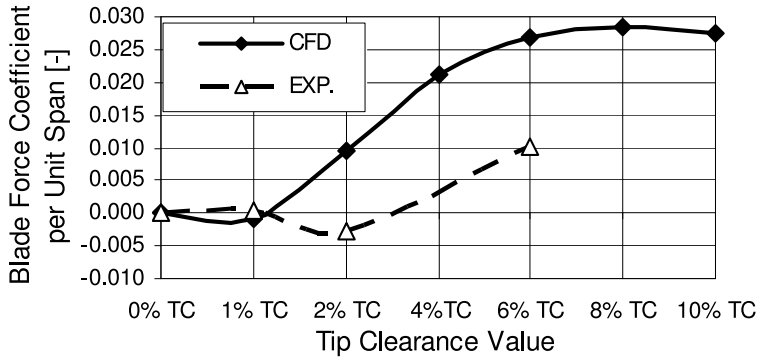

Figure 4.13: *Total Blade Force vs. TC for CFD & Exp. Data*

The blade loading (Figure 4.12), as with the experimental data, increased for the larger tip clearances towards the tip of the blade. This showed that the total blade force for the outer half of the cascade increased with TC value above 1%TC as also seen in Figure 4.13. This increase in blade loading further increased until 6% TC where the total blade force plateaued and appeared to start to decrease. This diminishing blade force was attributed to the decrease in blade loading at the

tip (0.2% span from the tip) due to the blade moving out of the skewed boundary layer. The experimental data also had a total blade loading increase, which although having a lower magnitude than the CFD showed an increase with 6%TC, thus it can be assumed that this was a valid result.

No experimental data was taken above 6%TC so the decline in blade force above 6%TC was not experimentally investigated. The differences between the CFD and experimental blade force was clear when examining the blade pressure coefficient profile plots (Figure 4.7 on Page 97). In general on the suction surface CFD results are overloaded especially at the blade leading edge and so the calculated blade force was higher than the experimental force. This was as a result of the CFD and experimental boundary conditions not matching exactly. The reason for this offset was investigated further for Build-B in Section 5.1.6 on Page 138.

4.3.2 6%TC Examined

6%TC is now explored to further study large clearance flows for the first geometry and to reveal the origin of the increase in loading. 6%TC was chosen as it is engine representative. Loss contours and velocity vectors through the cascade are shown in Figure 4.14, and the blade surface pressure profiles are shown in Figure 4.15. The flow features are described through the cascade:

0.0Cx: At inlet to the blade row the inlet boundary layer was skewed and loss due to the friction on the casing existed.

0.20Cx: In the forward section of the cascade row the the blade loading developed and the TC flow accelerated through the clearance. A small separation bubble became evident on the blade tip. The blade loading close to the tip decreased due to the tip leakage flow increasing the pressure on the suction surface and lowering it on the pressure surface.

0.4Cx: Approaching mid-chord the blade loading approached its maximum and the tip leakage flow significantly accelerated approximately in the tangential direction. The start of a tip clearance vortex roll up was evident, although small and positioned close to the suction surface.

0.6Cx: After the peak loading the tip leakage flow increased further and the

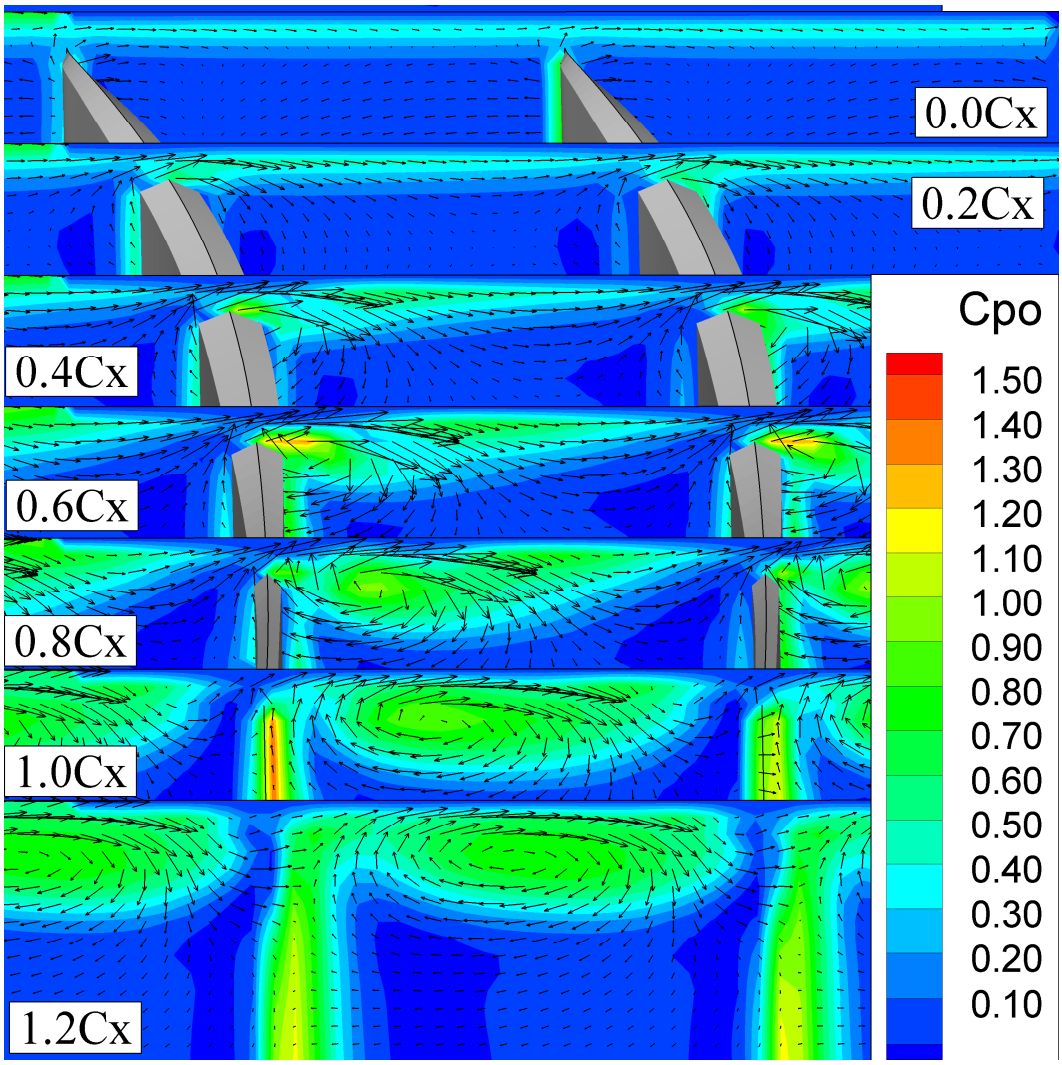

Figure 4.14: *CFD 6%TC Cp_0 Contours Through Blade Row*

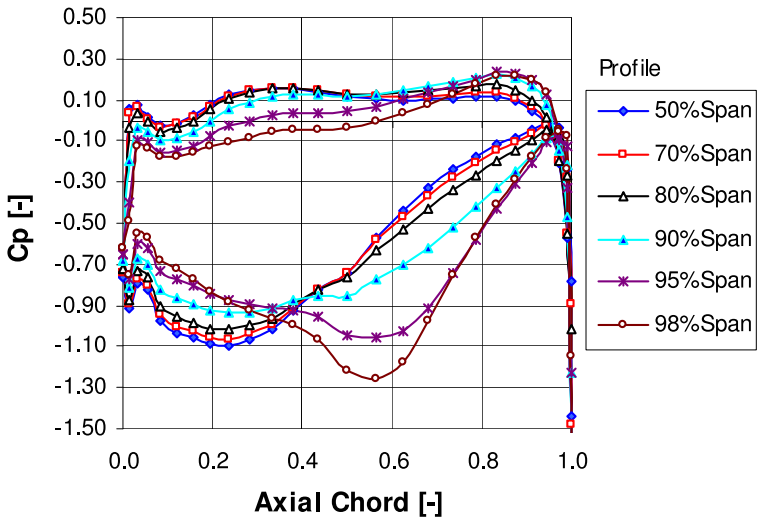

Figure 4.15: *CFD 6%TC Cp Blade Pressure Profile Along Blades*

vortex started to move away from the suction surface. At mid-passage a lower momentum region existed but unlike smaller TC values no counter rotating vortex was evident. The incoming flow was pushed against the pressure surface and down into the cascade due to the significant blockage created by the tip leakage flows. The tip leakage vortex induced lower pressure fluid on to the blade SS and towards the tip thus lowering the SS pressure creating a higher blade force. The blade force reached a maximum at approximately 0.6Cx of two thirds higher than the mid-span value.

0.8Cx: Approaching the rear end of the cascade the TC vortex moved further away from the suction surface of the blade. Still however some interaction between the blade and clearance vortex was evident but the blade loading was reduced to approximately twice that at mid-span for the same axial location. Lower loss fluid could be seen to be pulled through the tip clearance reducing the loss on the casing.

1.0Cx: At the exit of the cascade the TC vortex moved away from the SS and filled the majority of the passage of the outer 20% span. A counter rotating vortex was apparent in the passage. This was due to an interaction of the cross passage and boundary layer flows interacting. As found by in Section 4.1 a rotating casing would suppress the counter rotating vortex and push the vortex trajectory slightly further across the passage.

4.4 Results Discussion

This chapter shows that for the higher values of tip clearance an increase in blade loading towards the tip of the blade was found and that although the loss through the cascade increased with increased tip clearance up to approximately 4%TC, above this the loss plateaued and there was no further increase in loss. This discussion aims to relate these phenomena to the flow physics of large clearance flows for the geometry of Build-A and how the flows would change within the engine environment.

For the computations the tip clearance was modelled using a simple pinch tip method which allowed for investigation of several tip clearances without use of extensive computer resources. Experimental measurements were used to show the

computational work's accuracy. It was found that at 0% and 6% tip clearance, the computation gave good agreement with experiments. The yaw angle was predicted well, but the loss was over predicted. The 1%TC and 2%TC results were not so good, but this was to be expected with the pinch tip model and the mesh used. However as the thrust of this work was to the larger clearances, the choice of the pinch tip appears justified. As the tip clearance increases the solutions grid dependency diminishes, in particular the detailed pinch tip model; this was because the end-wall had a smaller effect on the tip leakage flow for the higher clearances. For this reason it should be assumed that the 8%TC and 10%TC solutions were valid. The observation from the numerical work suggested that if an improved solution to the smaller tip clearance value was required then the use of another tip clearance modelling method would be essential.

The detailed study for 6%TC showed that at entry to the blade row the blade loading was significantly reduced for the first 35% chord within 20% span of the casing. This was because the high pressure flow moved across the blade tip from the PS to the SS, resulting in an increase in pressure on the SS and reduction in pressure on the PS blade tip. At mid chord the TC vortex started to roll up close to the SS of the blade. This flow feature created a blockage reducing the row's mass flow rate and forcing the incoming flow towards mid span. The TC vortex induced low pressure fluid up the SS of the blade for 20% span reducing the SS pressure and so increasing the blade force. At approximately 60% chord the TC vortex left the suction surface of the blade and moved across the passage which coincided with the blade's peak tip force. The TC vortex continued to induce low loss fluid along the blade SS into the tip clearance region. Low loss fluid was found to move through the TC gap from the PS and this served to reduce the loss close to the casing.

An important feature here was that the TC vortex stayed relatively close to the suction surface, moving to about mid passage by blade exit. This meant that with a high tip clearance, the strong vortex close to the suction surface induced the high velocities on to the suction surface as noted above and therefore increasing the suction surface loading. Also the pressure on the pressure surface was increased by the cross passage leakage jet stagnating near the tip of the adjacent blades pressure

surface. These two features both raised the blade tip loading.

This lack of cross passage movement was in contrast to the movement right across the passage to near the pressure surface usually observed in most of the studies in the literature. It did not appear that the high tip clearance was the reason for the lack of movement of the TC vortex, as the lower TC values studied here show that the vortex was also at about mid passage at exit. The significant feature of this blading was probably the low stagger so that the tip jet was nearly perpendicular to the axial direction. The loading of the stage would clearly have an effect on the trajectory of the leakage vortex but at the operating point this was valid. The effect of the geometry will be further investigated in the next chapter.

After 6%TC there was found to be no significant change in blade loading and this therefore suggested that the casing had a decreased effect on the blade loading. With a further increase in TC value, the flow around the blade behaved with reduced influence from the casing. This may help to explain the plateau of loss with increased tip clearance; since the flow across the tip was a pressure driven jet there was limited increase in the loss producing mechanisms on the endwall or tip. In effect the flow became more like that of a wing tip trailing vortex.

It should be noted that the blade force values shown here (Figure 4.13) were dimensionless values and therefore are the blade force per unit length. As the TC increases, of course the blade gets shorter and this was reflected in the large amount of under-turning seen in Figure 4.9(a) at higher TC values. Thus the work done by the blade (if it were a rotor) would be reduced, but not by as much as might be expected. This coupled with the overall loss becoming independent of the TC value, meant that the penalties associated with TC values around 4%TC and above were not as great as might be expected with typical LPC blading. Unfortunately an increase in blockage still occurred so that the mass flow reduced by 0.5% per 1% increase in tip clearance.

With the significant blockage effect, the axial velocity would not have been constant at blade inlet, even though the upstream boundary was the same for the different tip clearances. To try and separate the tip leakage flow effects from the blockage effect, the results for angle, loss and blade force distributions along the

span were referenced to the mid-span value. This was perhaps debatable, but it was felt to be most helpful for this study.

It is important to remember that this study was for a linear cascade and that in a rotating machine there would be a number of differences. For instance in a multi-row environment the inlet boundary layer would be thick and possibly further skewed; relative motion of the end-wall and radial effects would also be a factor. However the results from the earlier section showed that the moving end-wall did not have a large effect with large tip clearances. The effect of the end-wall motion was shown to move the vortex trajectory further away from the suction surface and close to the end-wall. The end-wall motion increased the skew on the end-wall at inlet and therefore exit. Within this chapter the inlet skew angle was reasonable at $\approx 10^{\circ}$ however the thickness was too small and therefore not engine representative.

The aerodynamic designer may find these results interesting; if a design with similar HPC blades requires a large tip clearance then the designer who has always strived to reduce the tip clearance value may find that in fact the aerodynamic penalty is not as large as previously thought. Therefore cost savings may be made in the mechanical design of the HP stages. The overall blade loading also increased for the larger clearances allowing for slightly higher stage loading. From this study however this was difficult to conclude as the geometry and boundary conditions were not particularly engine representative and their effect on the clearance flows unknown.

4.5 Conclusions

Tip leakage flows within a compressor cascade of low stagger and relatively high turning have been studied experimentally and computationally. The experimental results were used to validate the CFD. Tip clearances of up to 10% span (12.67% chord) have been studied with application to the HPC compressor of an industrial gas turbine. A pinch tip clearance model for the computation was used, and this was found to give satisfactory results for the larger tip clearances but for the smaller clearances another model would be essential to establish quantitatively accurate

results. The following conclusions may be drawn:

- Increasing the tip clearance above 4%TC incurred no further increase in loss and at the same time there was an unexpected increase in blade force towards the tip due to the tip clearance flows.
- The plateau in blade force was due to the effect of the strong tip clearance vortex which remained close to the blade suction surface. Unlike as often observed for high stagger blading, where the leakage vortex moved across the blade passage to the adjacent blades pressure surface.
- In general it was found that the CFD over-predicted the loss in the casing region although at mid-span there was a very good agreement. The flow angle prediction was very good for the higher tip clearance values although it was not accurate for the smaller clearances.

This chapter has explored the end-wall flows with large clearances and low stagger blading and the main conclusions have been outlined above. Two significant questions still remain: what was the effect of the boundary layer skew and thickness; and what was the effect of the geometry? The CFD and experimental results within the later part of this chapter had a reasonably high inlet skew on the casing but the thickness was unrepresentatively thin at only $\approx 10\%$ span. The geometry of this cascade was not particularly engine representative as the stagger was too low. This may explain the trajectory of the leakage vortex, but may also be due to the low loading of the cascades operating point.

For these reasons the next chapter will present data for a second cascade with more engine representative stagger and inlet boundary layer skew/thickness.

Chapter 5

Build-B, Results and Discussion

This chapter presents and explores a selection of the results obtained from the second cascade as described in Chapter 3.4. This cascade consisted of engine realistic geometry with relatively high stager (46.5°) and relatively low turning (10°) compared to the cascade explored in Chapter 4. The effect of inlet skew and clearance size were investigated and the conclusions compared to the previous cascade. This cascade enabled the control of the inlet boundary layers skew and thickness. Experimental results were conducted for two inlet boundary conditions: 'high skew' (realistic inlet conditions) and 'natural skew' (natural cascade boundary layer, non realistic inlet conditions with low skew and low thickness) with tip clearance values from 0%TC to 12%TC. The results presented include downstream traversing, internal passage traversing and blade loading. Computational results are briefly presented and compared to the experimental data, this was to evaluate the code and further investigate the clearance flows where experimentation was not undertaken.

5.1 Experimental Results

5.1.1 Exit Traverse Results

Traversing at the exit of the cascade was undertaken at 1.2Cx and 1.5Cx across the exit of 3 passages as shown in Figure 3.17 on page 73. Little difference between the results at both downstream axial locations was found, therefore the results at 1.5Cx

are not included here but given in appendix A.

Within this work the tip clearance size was defined as the percentage of cascade span. Table 5.1 shows the tip clearance size conversion to absolute values and percentage chord.

% Cascade Span	0	1	2	4	6	8	10	12
Tip Clearance (mm)	0.0	1.8	3.6	7.2	10.8	14.4	18	21.6
% Blade Chord	0.00	0.88	1.76	3.51	5.27	7.02	8.78	10.54

Table 5.1: *Build-B Tip Clearance Size Definition*

Exit pitch averaged results of yaw angle, axial velocity and stagnation pressure loss are shown with the natural and high skew inlet conditions at 1.2Cx for different tip clearance values in Figure 5.1. The inlet value is included for comparison. Initially the natural skew results are considered and then the effect of the high skew examined.

Effect of Clearance Size

With the natural skew and without tip clearance the yaw angle (Figure 5.1(a)) followed a classic, under-turning (at $\approx 0.85span$) and over-turning (at $\approx> 0.9span$) pattern towards the casing; this was a consequence of the passage vortex corner separation as discussed in the literature survey and found for the previous cascade in Chapter 4 Section 4.2.

As expected, introducing tip clearance altered the exit flow and resulted in a reversal of end-wall flow turning. As with Build-A over-turning occurred away from the casing and under-turning towards the casing wall for the larger clearances; the clearance value at which this switched is well known, less than 1%TC and therefore not investigated. The under-turning on the wall increased up to 6%TC. Above this clearance the yaw angle on the casing was constant with an outlet flow angle of approximately 70° and therefore under-turning of 26°. This was 14° higher than the casing inlet angle and therefore the exit skew angle was higher than at inlet to the row. Above 10%TC the flow turning pattern was different and the under-turning was reduced on the casing. In general (except for the extreme 12%TC case) an increase

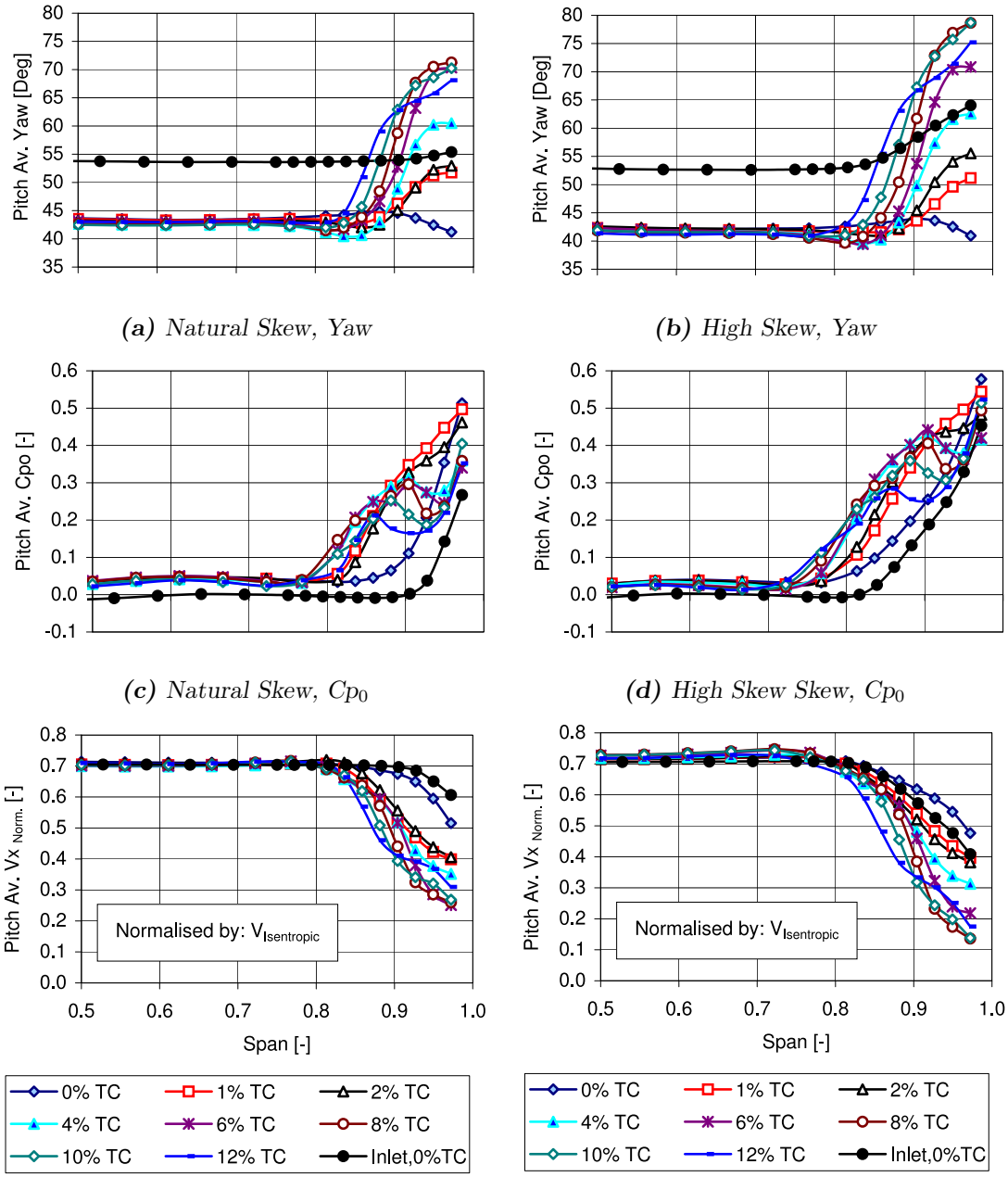

(a) Natural Skew, Yaw *(b) High Skew, Yaw*

(c) Natural Skew, Cp_0 *(d) High Skew Skew, Cp_0*

(e) Natural Skew, $V_{X,Norm.}$ *(f) High Skew, $V_{X,Norm.}$*

Figure 5.1: *Pitch Averaged Exit Traverse at 1.2Cx*

in tip clearance made the under-turned area thicker and therefore consumed more of the span.

Figure 5.1 also shows the pitch averaged loss. Without clearance the loss profile followed a similar but thicker and higher profile to the inlet; the highest loss was on the casing. Increasing the TC up to 2% created a much larger loss area over

approximately 20% span, and slightly reduced the magnitude of the peak loss on the casing. Above 2%TC a bump (increase) in loss occurred representing the TC vortex core. The position of which moved away from the casing and reduced in magnitude with increased TC from 0.9 span with 2%TC to 0.85% span with 12%TC. Above 2%TC the loss on the casing (at 5mm from the casing) was constant and only slightly higher than at inlet. Previously, Section 4.1 showed computationally that the loss increase on the casing was reduced with relative casing motion, therefore in a real machine the loss on the casing would be lower.

The blockage within the end-wall region of the row was found to instigate a redistribution of the cascades mass flow towards mid-span. This resulted in an increase in axial velocity at mid-span (Figure 5.1(e)) of the inlet and exit. As a consequence, because the blockage increased with clearance size, a small increase in mid-span axial velocity occurred with increased clearance. The end-wall blockage was displayed by a reduction in axial velocity towards the casing and increase in low axial velocity region away from the casing. The difference on the casing between inlet and outlet was approximately 2ms^{-1} without clearance, and increased to 5ms^{-1} for the higher clearances.

Effect of skew

The high skew inlet altered the exit flow marginally and in general followed a similar pattern to that with the natural (low skew) inlet. One effect was to thicken the region affected by the end-wall flows creating a larger under-turned and higher blockage region; the thickening from the casing was by approximately 5% of the span. This was coupled with an increase in under-turning and reduction in axial velocity on the casing. For the smaller clearances of 4%TC and below, this reduction was small. However for the larger clearances ($>$ 6%TC) there was a significant increase in under-turning on the casing from 70° to 80° which was similar to the 10° increase at inlet. Therefore the turning within the end-wall region for the higher clearances was independent of the inlet skew. The exit angle change was accompanied by an increase in loss and reduction in axial velocity (increase in blockage), again the difference in these values was similar to the change at inlet.

Increasing the inlet boundary layer thickness in general increased the blockage and under-turning of the cascade within the casing region. The change in exit casing flow magnitude was similar to the inlet change and therefore linked. However the thickness increase was smaller than the thickness increase by less than one half. Therefore the skew at inlet had a higher impact on the exit than the increased skew thickness.

5.1.2 Loss and Turning Through Cascade

Figure 5.2(a) shows the total mass averaged Cp_0 at 1.2Cx (from 50% to 0.972% span) for both inlet conditions and all tip clearances. With natural skew the maximum loss was found to occur with 1%TC, and then a reduction occurred to 2%TC, a slight reduction to 5%TC and then a further increase in clearance size resulted in a marked reduction in loss. At 12%TC the loss was similar to the 0%TC case. With increased skew the maximum loss was at 4%TC and a reduction in loss occurred above 6%TC.

Figure 5.2(a) shows the total mass averaged Cp_0 at 1.2Cx (from 50% to 0.972% span) for both inlet conditions and all tip clearances. With natural skew the maximum loss was found to occur with 1%TC, and then a reduction occurred to 2%TC, a slight reduction to 5%TC and then a further increase in clearance size resulted in a marked reduction in loss. At 12%TC the loss was similar to the 0%TC case. With increased skew the maximum loss was at 4%TC and a reduction in loss occurred above 6%TC.

The not loss, or increase in loss, was calculated by subtracting the inlet loss (-0.5Cx) from the exit loss. As expected from the pitch averaged plots (Figure 5.1(c) & Figure 5.1(d)) the total loss at 1.2Cx was higher with increased skew. However the net loss was lower than for the natural skew and therefore the loss increase through the cascade was lower with the high skew inlet. The secondary loss increase through the cascade due to the end-wall flows is also shown in Figure 5.2(a); this was calculated by subtracting the mid-span loss across the entire span at exit and then subtracting the inlet loss. This secondary loss increase was found to be effectively the same for both inlet conditions. Therefore the difference in loss between the inlet

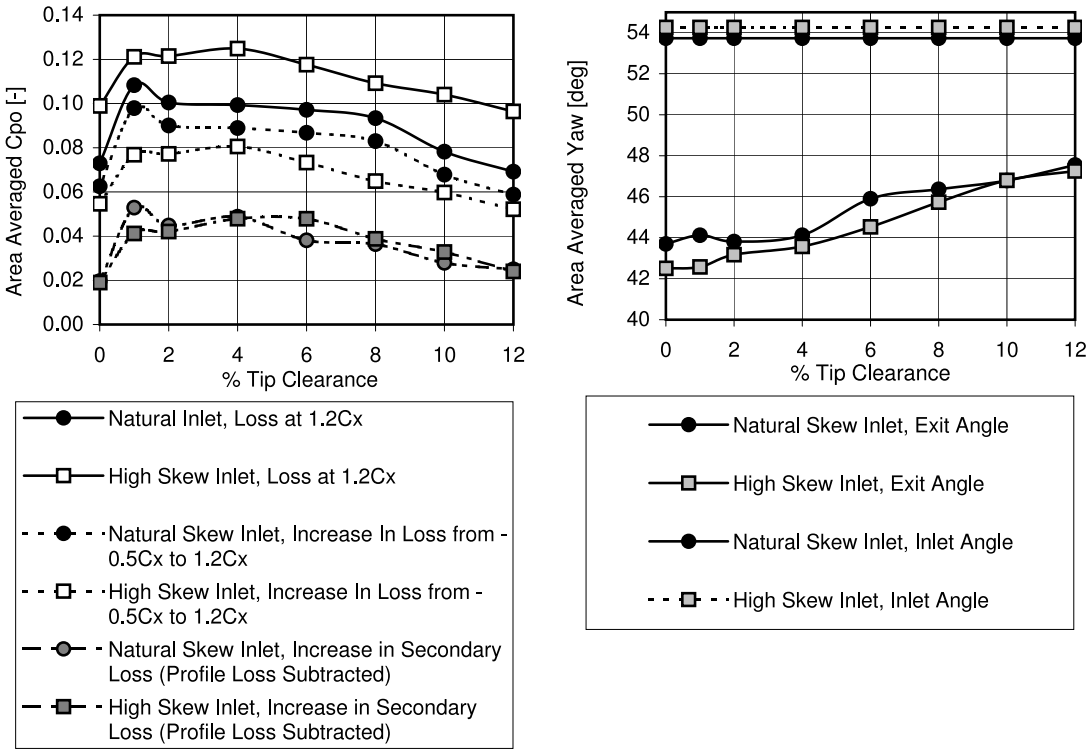

(a) Cp_0 ***(b)*** *Yaw*

Figure 5.2: *Area Mass Weighted Averaged Loss and Turning at 1.2Cx*

skew conditions was due to the change in mid-span flow, and so change in mid-span loss, and not a change in the endwall flow features. This partly explains the decrease in loss with increased clearance.

This reduction in peak loss at higher tip clearances was coupled with a large reduction in turning (Figure 5.2(b)). The decrease in turning was virtually linear with increased clearance and at 12%TC halved for the outer 50% span. For the lower clearances the natural inlet showed slightly less turning ($< 1°$) than for the high skew. With a higher clearance the exit angle was shown to be similar for both inlet conditions and therefore essentially independent of inlet skew.

Cp_0 Contour Plots

Figure 5.3 (natural skew inlet) and Figure 5.4 (high skew inlet) show contour plots of Cp_0 at 1.2Cx for the full range clearance measured; this was the data used for the pitch and area averaged results. For 0%TC the full span is shown and therefore

indicates the quality of the achieved cascade symmetry and periodicity. At the hub, as with the first cascade, there was found to be a decrease in total pressure compared to the casing, this however was deemed to be unimportant due to its negligible effect on the TC flow.

With clearance a similar flow structure was observed as with the previous cascade. Several features of the leakage vortex with the low skew inlet were observed. The position of the leakage vortex can be seen in the contour plots or more quantitatively in Figure 5.7 which shows the position of the central blades vortex core for each of the measured clearances. With increased TC values a small shift in leakage vortex core location was found in the radial direction away from the casing, which can also be seen in the pitch averaged plots (Figure 5.1). In the pitch-wise direction there was a significant change (0.2 pitch variation) in vortex core location between clearance size. Up to 6%TC the vortex moved across the passage away from the SS towards the PS of the adjacent blade. Above 6%TC the tip leakage vortex core returned closer to the suction surface of the blade. Above 10%TC the vortex was closer to the SS than for the 1%TC case.

The same trend was observed with the increased inlet skew. With the high skew and thicker inlet boundary layer, the vortex core location in the span-wise direction was indistinguishable from the natural skew inlet (as seen in Figure 5.7(b). The movement across the passage varied with TC with a shift from the suction surface of $\geq$ 2% & $\leq$ 15% pitch occurred.

These results showed that the leakage vortex had a reduced interaction with the casing with increased clearance size. For the higher TC values of 10%TC and 12%TC there was little interaction. This was evident in Figure 5.3 and explains the different flow patterns observed with the highest clearances in the pitch averaged plots. With 10%TC, increasing the boundary layer skew increased the end-wall flows interaction with the casing and therefore had a similar pattern to the lower clearances. For the large clearances low loss fluid passed through the tip clearance and re-energising the end-wall flow.

A counter-rotating vortex was observed and this was formed by the interaction of the passage vortex with the flow passing over the leakage vortex and the shear on

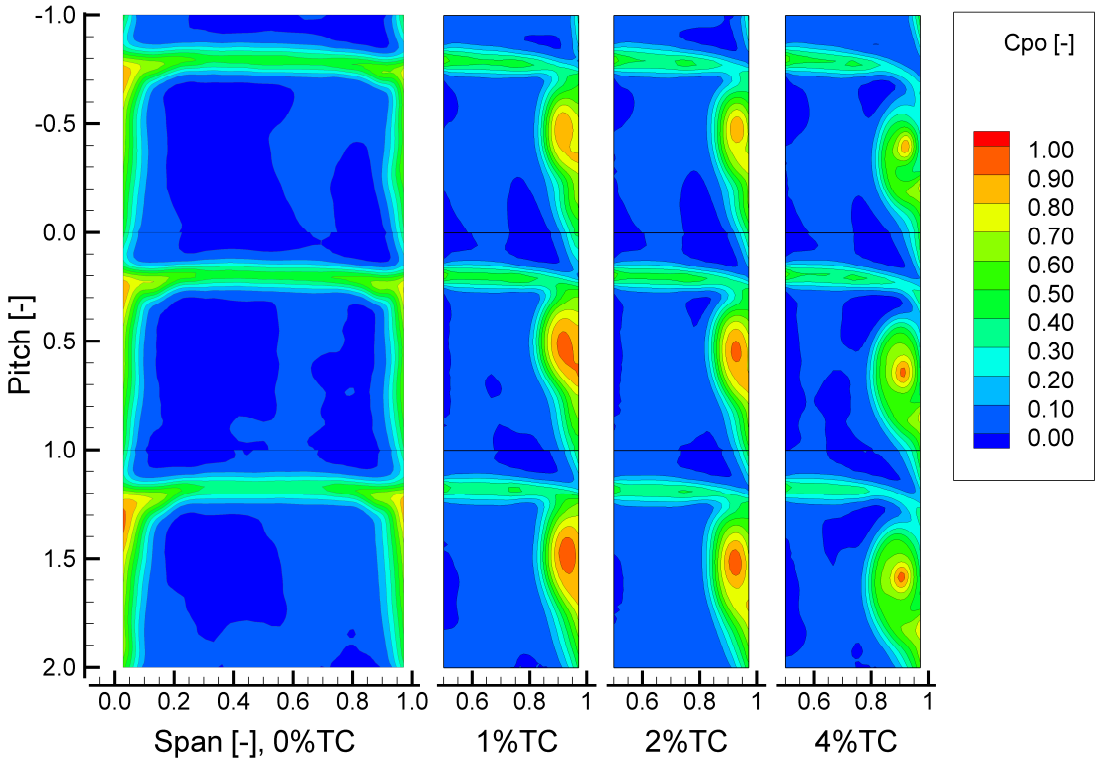

(a) Clearances 0%TC to 4%TC

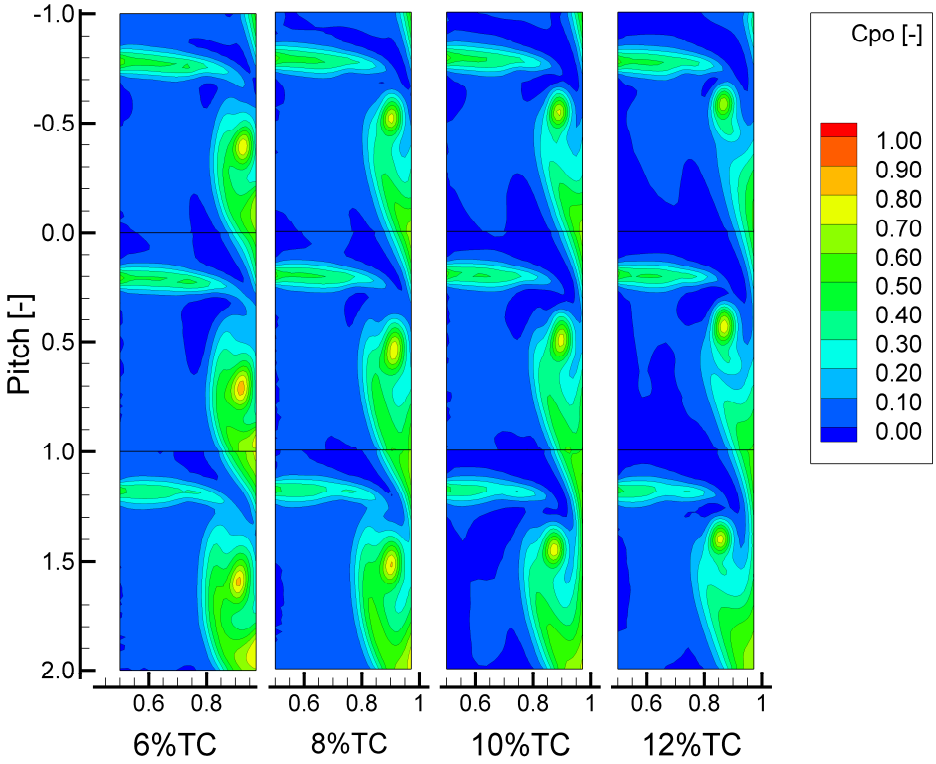

(b) Clearances 6%TC to 12%TC

Figure 5.3: *Natural Skew Inlet Cp_0 Contour Plots at 1.2Cx*

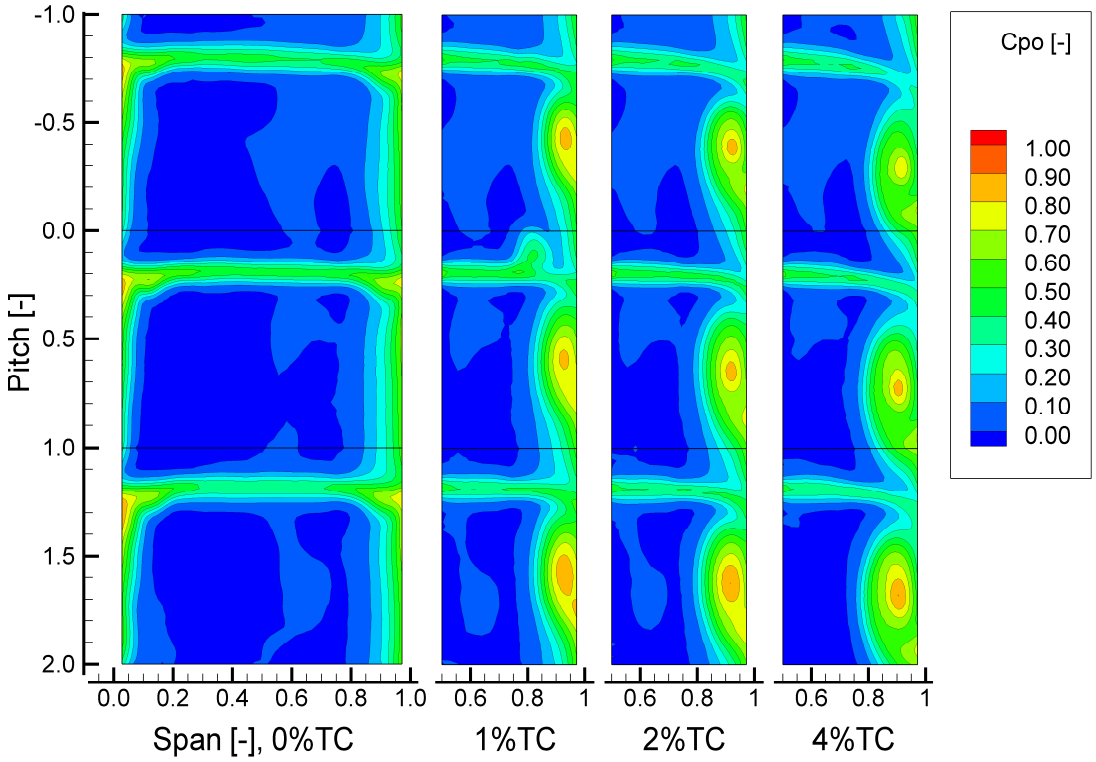

(a) Clearances 0%TC to 4%TC

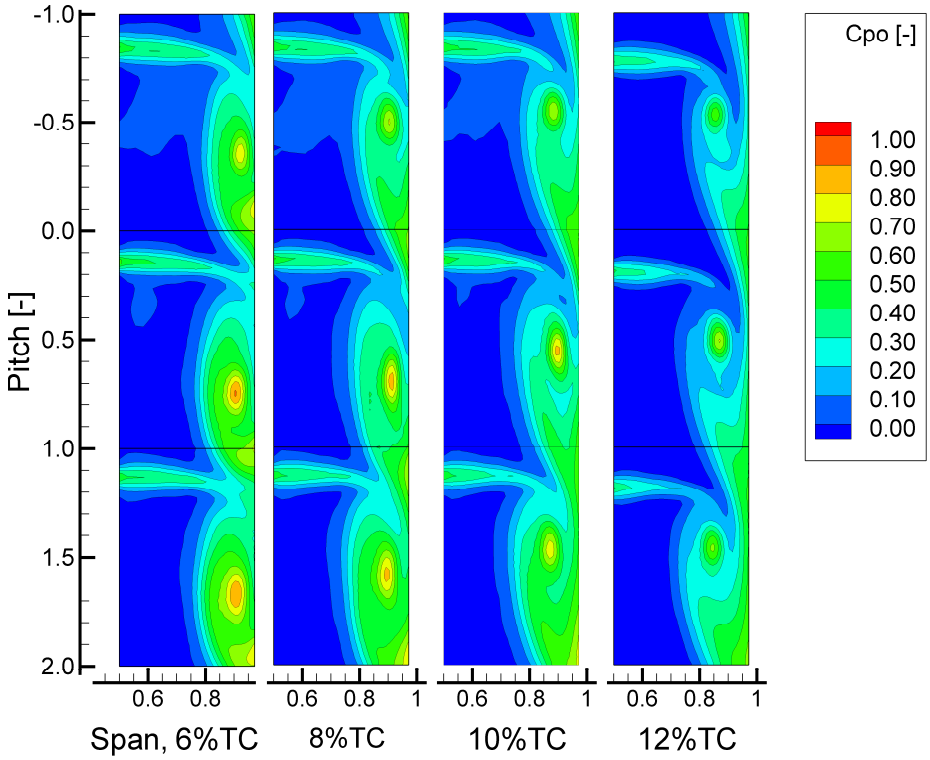

(b) Clearances 6%TC to 12%TC

Figure 5.4: *High Skew Inlet Cp_0 Contour Plots at 1.2Cx*

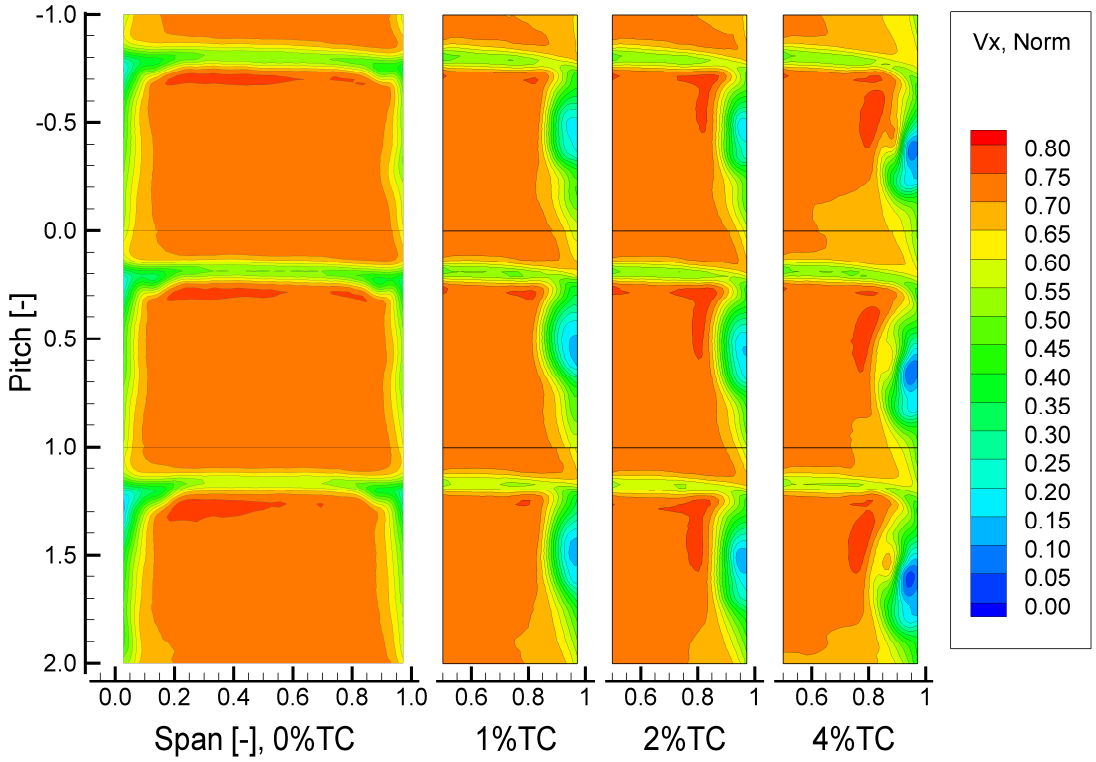

(a) Clearances 0%TC to 4%TC

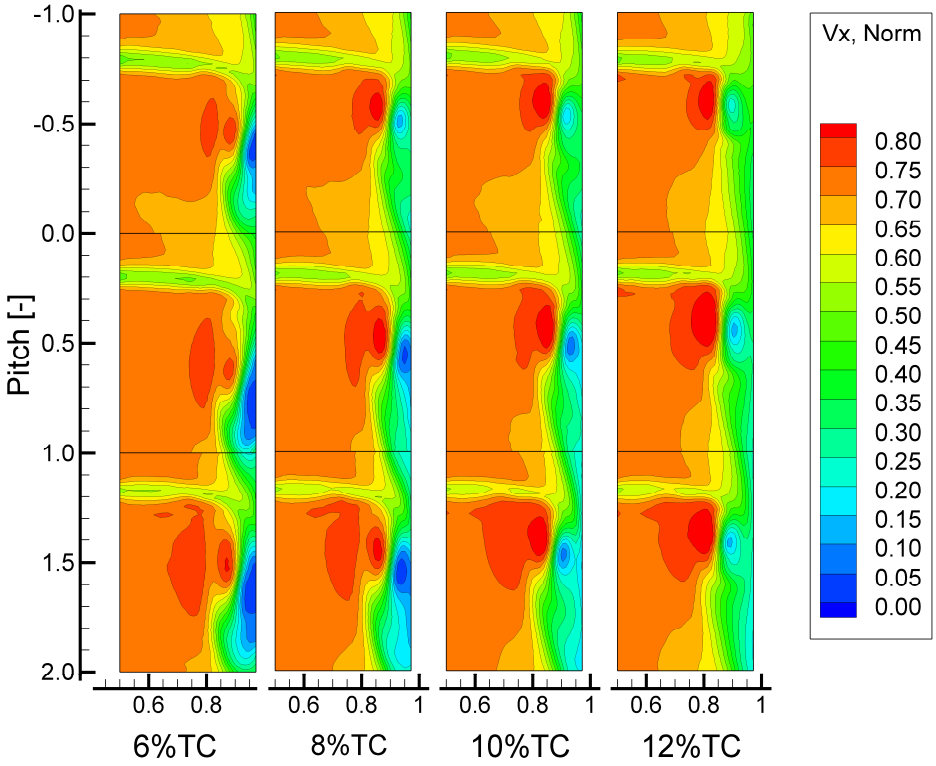

(b) Clearances 6%TC to 12%TC

Figure 5.5: *Natural Skew Inlet $V_{x,Norm}$ Contour Plots at 1.2Cx*

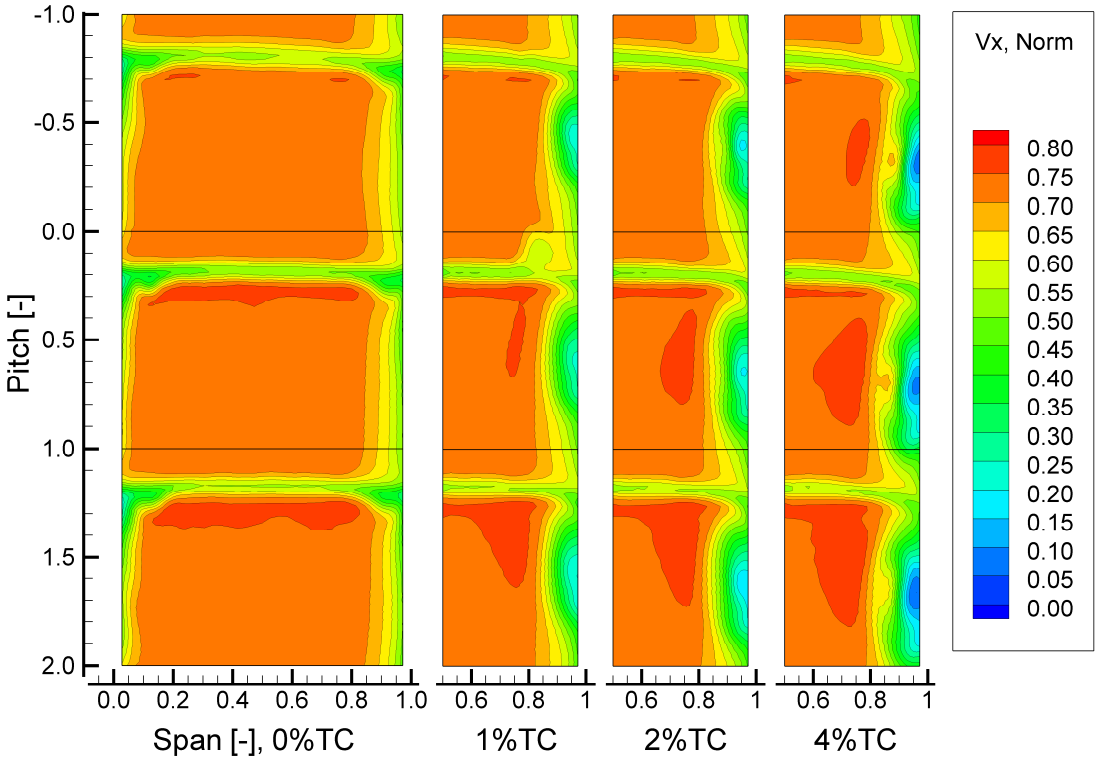

(a) Clearances 0%TC to 4%TC

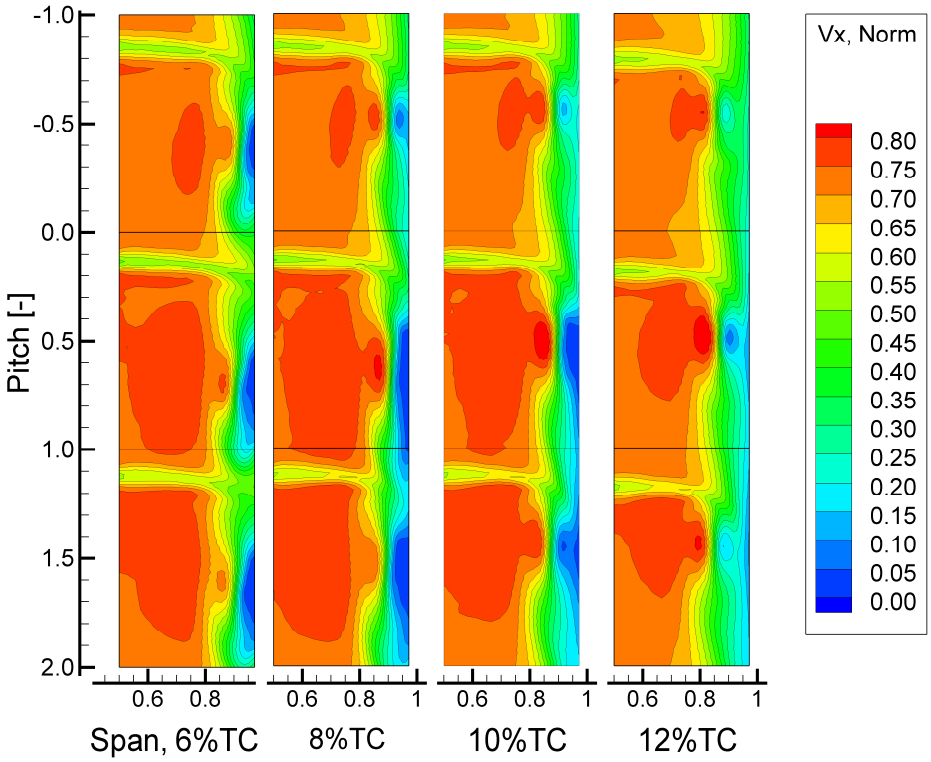

(b) Clearances 6%TC to 12%TC

Figure 5.6: *High Skew Inlet $V_{x,Norm}$ Contour Plots at 1.2Cx*

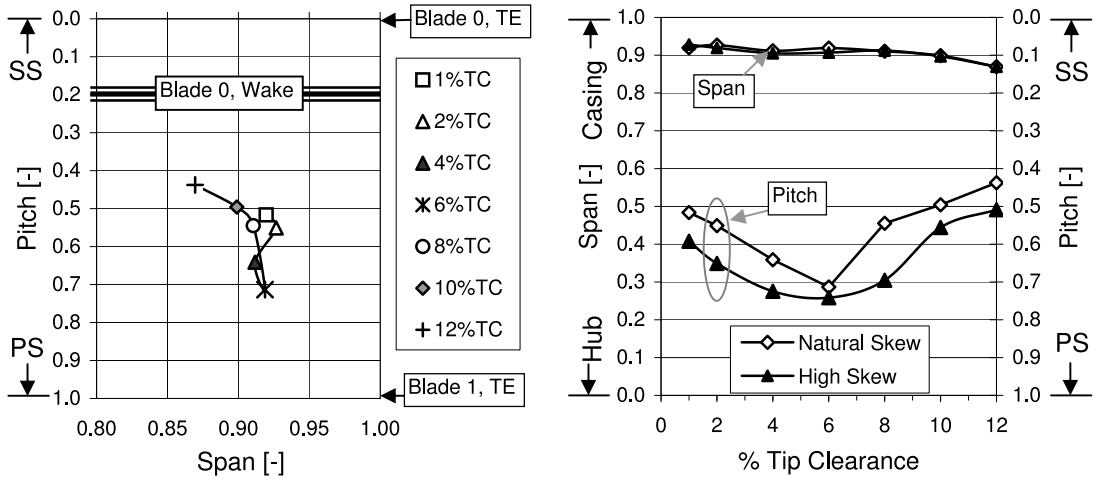

(a) *Span v.s. Pitch, Natural Skew Only* ***(b)*** *Clearance v.s. Span & Pitch*

Figure 5.7: *Effect of Clearance Size on Leakage Vortex Location*

the end-wall. The increased loss region associated with this peaked at ≈ 6%TC and was suppressed at the higher clearances. Although the contour plots (Figure 5.3 & 5.4) do not show vectors this feature was clearly present. For a real machine (as seen in Section 4.1) with relative end-wall motion the casing shear and the leakage flow would be increased therefore suppressing the counter-rotating vortex formation and reducing the loss in the end-wall region as previously discussed.

Figure 5.5 and Figure 5.6 show the axial velocity and therefore the associated blockage as a result of the end-wall flows. It is clear from these plots that the largest blockage was associated with the leakage vortex. Note that the lowest axial velocity area did not correspond to the centre of the vortex core but this was a consequence of the flow angle not being perpendicular to the measurement plane. If the absolute velocity were plotted then there would be alignment of the minimum velocity with the leakage vortex core.

5.1.3 Internal Traverse Results

Internal passage traversing results are now presented. Cp_0 loss contours are shown in Figures 5.8, 5.10 and 5.12 for 2, 6 and 10%TC for both natural and high skew boundary layer configurations. Figures 5.9, 5.11 and 5.13 show axial velocity contours for the same clearances. Clearances values of 4%, 8% & 12% are shown in

Appendix A Figures A.7 to A.12 starting at Page 207.

At 2%TC with the natural boundary layer (low skew), a much stronger loss core existed than with the high skew inlet. However with the high skew, the vortex was more elongated in the pitch-wise direction consuming a larger proportion of the passage. The counter rotating vortex loss region was also much larger with increased skew and therefore together filling much more of the passage than the natural skew. As with the downstream plots the trajectory of the TC vortex was moved across the passage with increased TC up to 6%TC and then moved back towards the SS for the largest clearance values. The axial location at which the TC vortex separated from the blades suction surface was found to move downstream with increased TC. The higher skew advanced this vortex movement, therefore leaving the suction surface earlier by approximately 10% axial chord.

The axial velocity plots indicate the extent of the blockage within the passage. With a small clearance (2% Figure 5.9) the majority of the low velocity fluid was associated with the clearance vortex core and the skew was found to elongate the blockage along the casing. At the higher clearances (8%TC & 10%TC Figures 5.11 & 5.13) the low axial velocity region was much more elongated and increased in magnitude across the majority of the passage. A change in vortex trajectory occurred with increased clearance as shown by Cp_0 and V_x contours. At 2%TC there was a clear low velocity region associated with the leakage vortex core, but for the higher clearances a low V_x region was accompanied by a high V_x region on the central passage side. This suggested that the vortex trajectory shifted and passed from the left to right on the plots. The increased skew decreased the axial velocity on the casing and within the counter rotating passage vortex region.

Figure 5.14 shows tangential velocity contours through the cascade with 6%TC. The high tangentially velocity flow over the tip of the blade can be clearly seen. This continued across the passage to form the casing side of the leakage vortex and the reduced tangential velocity associated with the other side of the leakage vortex was evident. This was still positive because of the high tangential velocity due to the high stager angle. The lowest tangential velocity was associated with the loss region further across the passage. As this was positive there was no cross passage

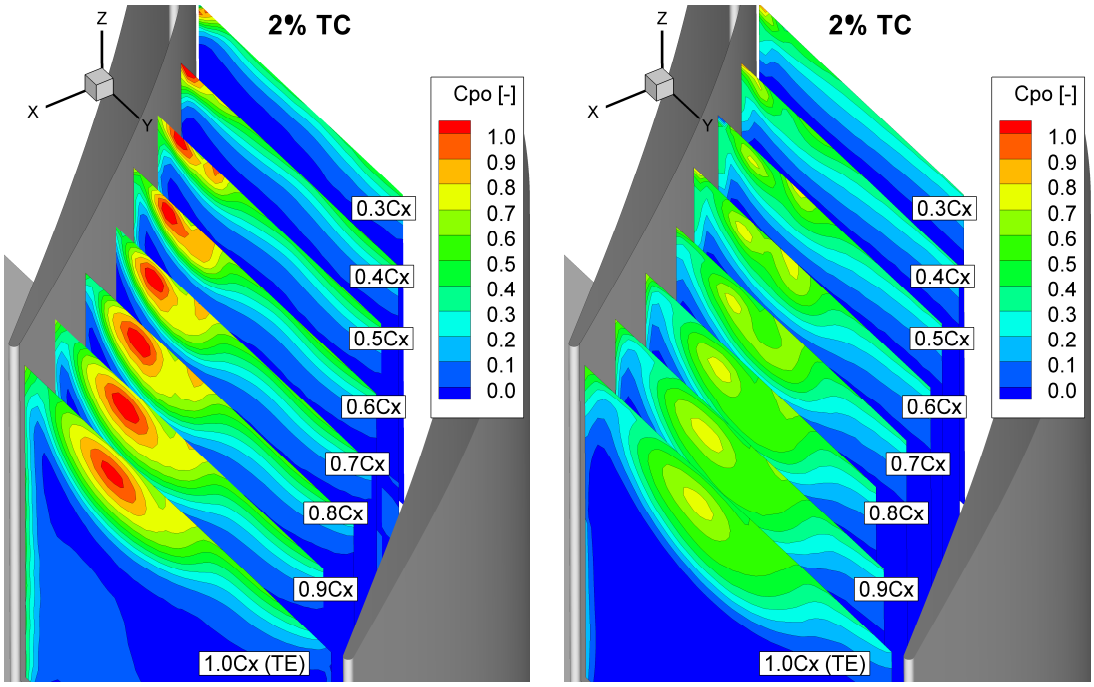

(a) Natural Skew *(b) High Skew*

Figure 5.8: *2%TC Internal Traverse Cpo Contour Plots*

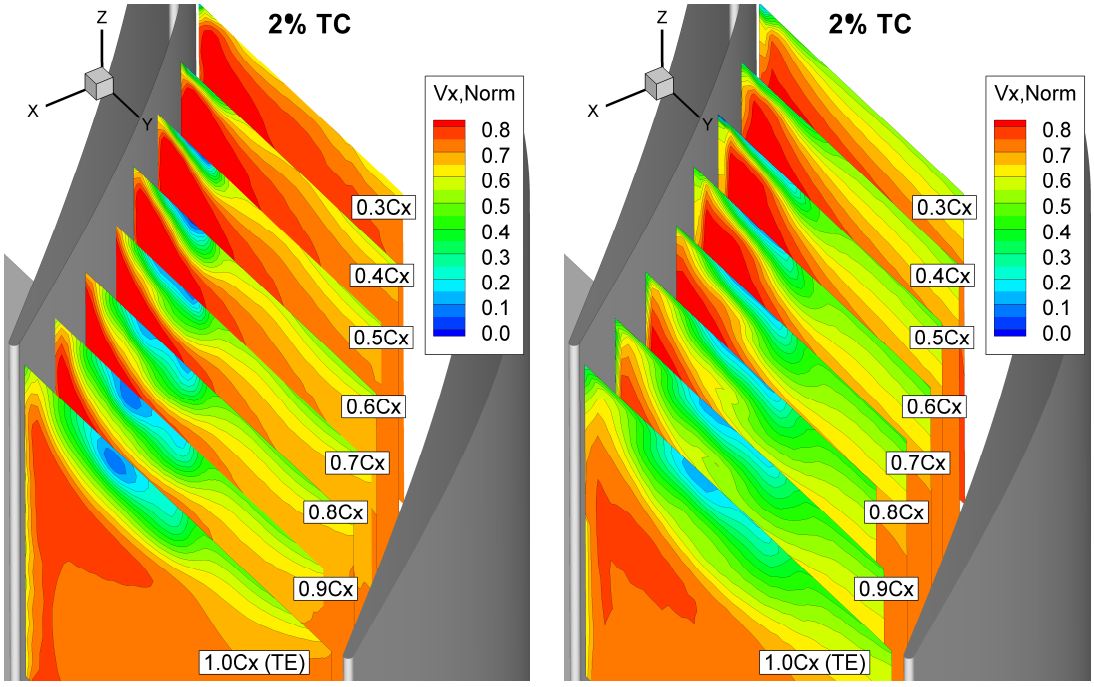

(a) Natural Skew *(b) High Skew*

Figure 5.9: *2%TC Internal Traverse $V_{x,Normalised}$ Contour Plots (Normailsed With $V_{Isentropic}$)*

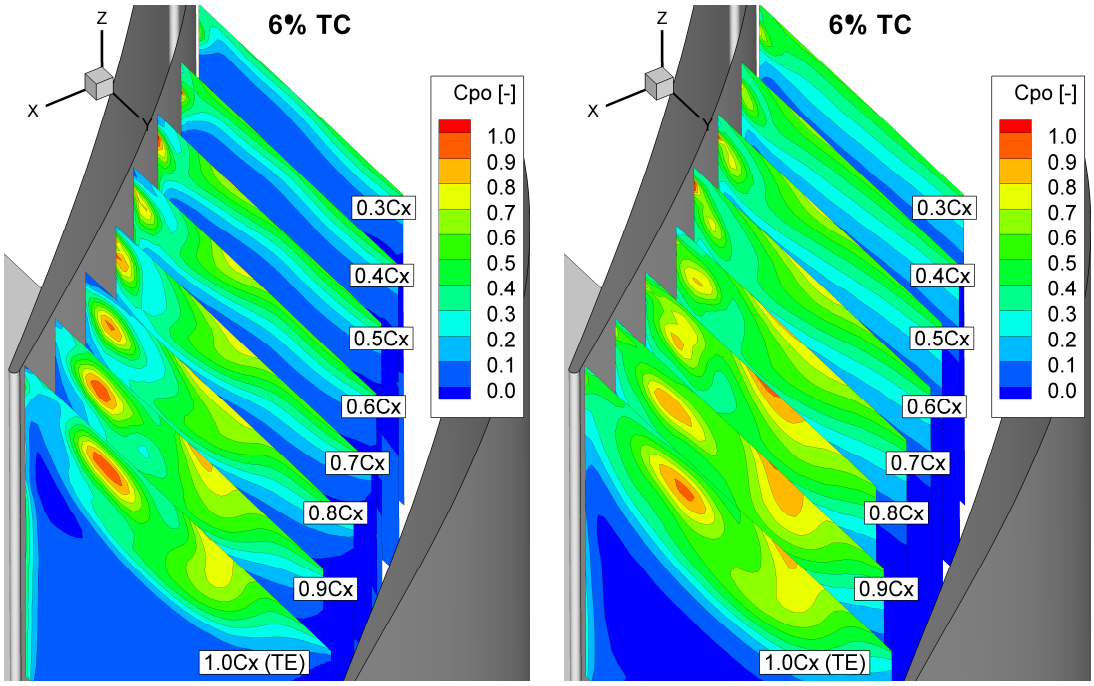

(a) Natural Skew *(b) High Skew*

Figure 5.10: *6%TC Internal Traverse Cp_0 Contour Plots*

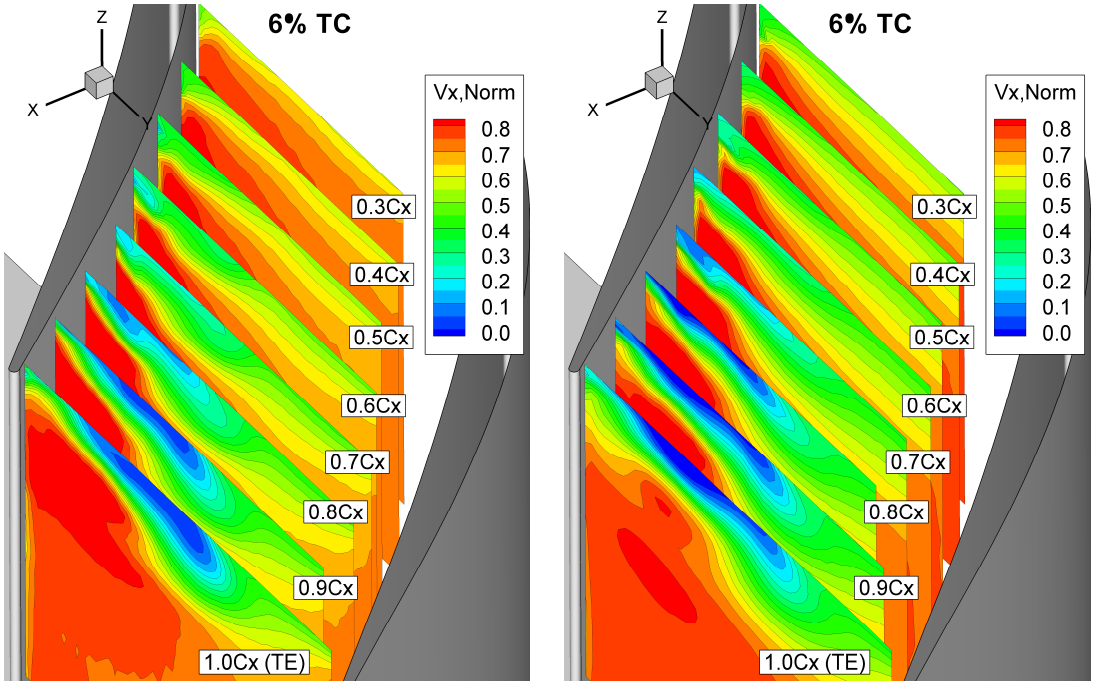

(a) Natural Skew *(b) High Skew*

Figure 5.11: *6%TC Internal Traverse $V_{x,Norm}$ Contour Plots*

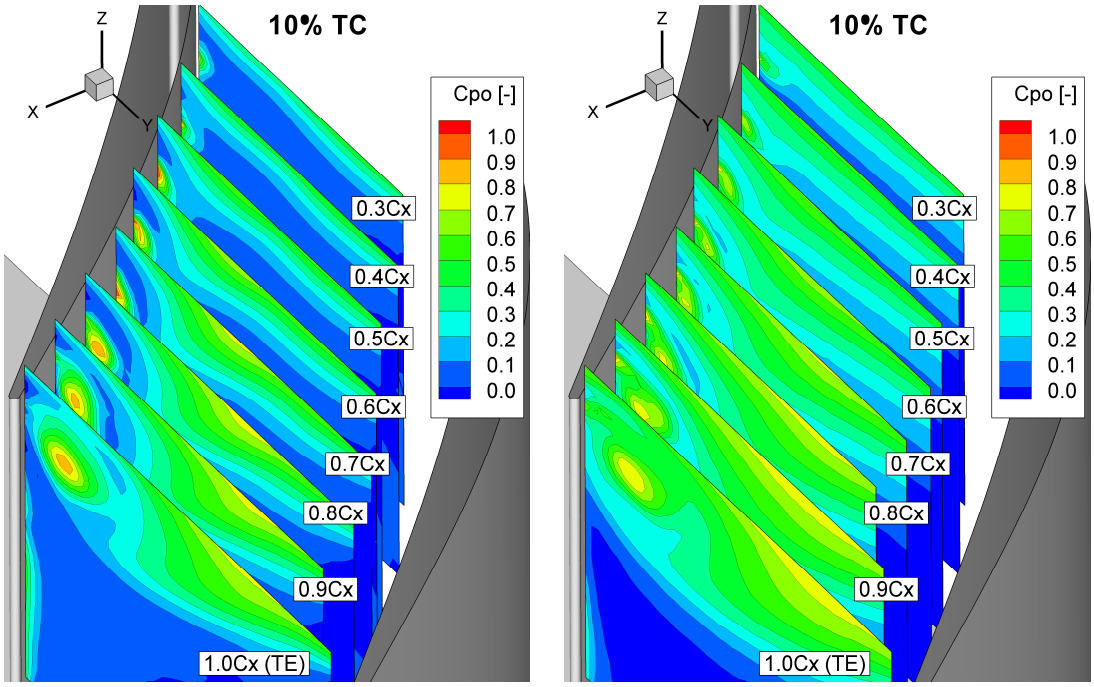

(a) Natural Skew *(b) High Skew*

Figure 5.12: *10%TC Internal Traverse Cp_0 Contour Plots*

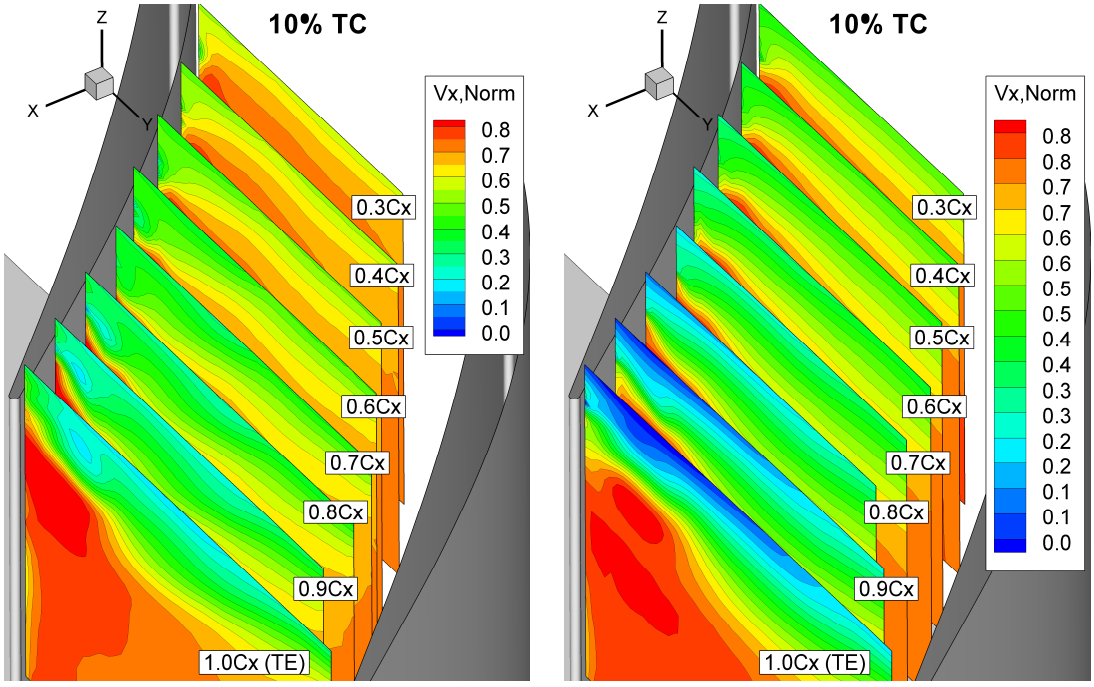

(a) Natural Skew *(b) High Skew*

Figure 5.13: *10%TC Internal Traverse $V_{x,Normalised}$ Contour Plots (Normailsed With $V_{Isentropic}$)*

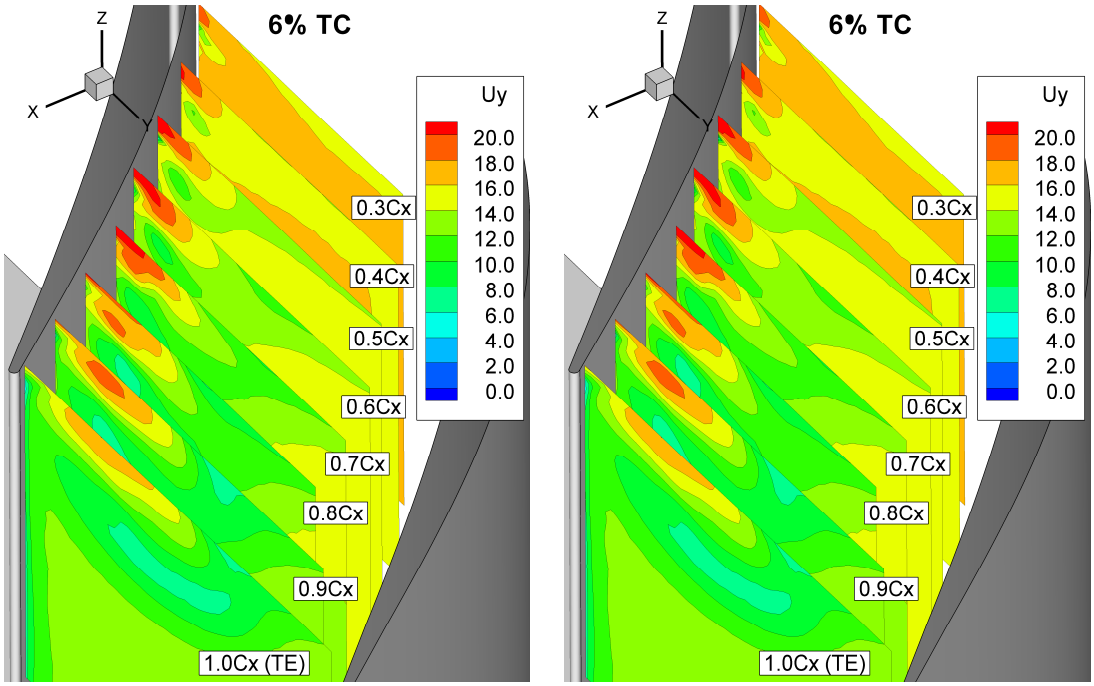

(a) Natural Skew *(b) High Skew*

Figure 5.14: *6%TC Internal Traverse Tangential Velocity (V_y in ms^{-1}) Contour Plots*

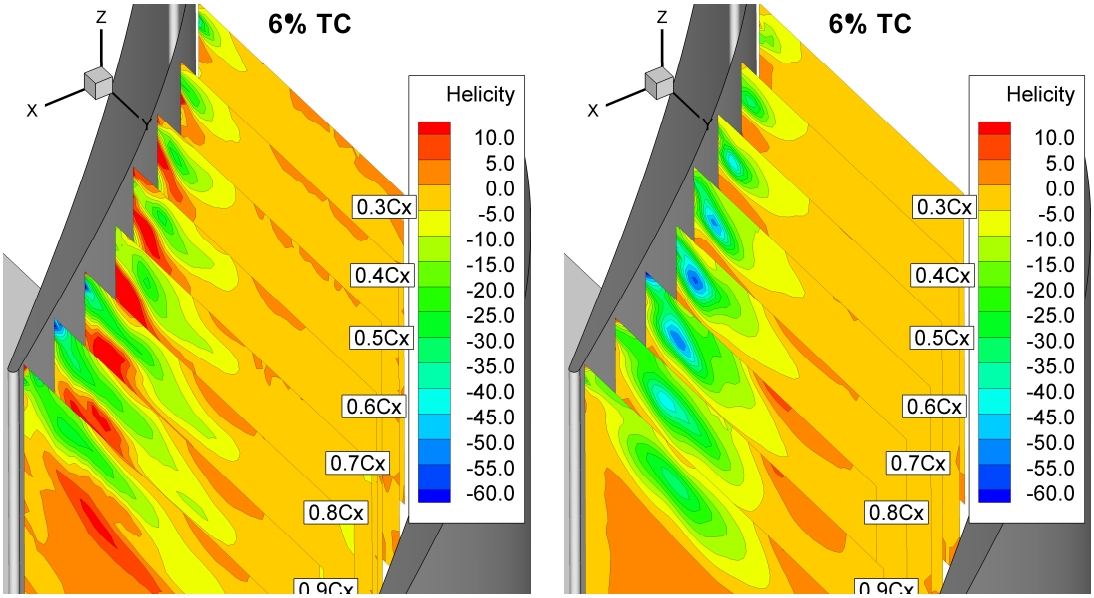

(a) Natural Skew *(b) High Skew*

Figure 5.15: *6%TC Internal Traverse Helicity Contour Plots*

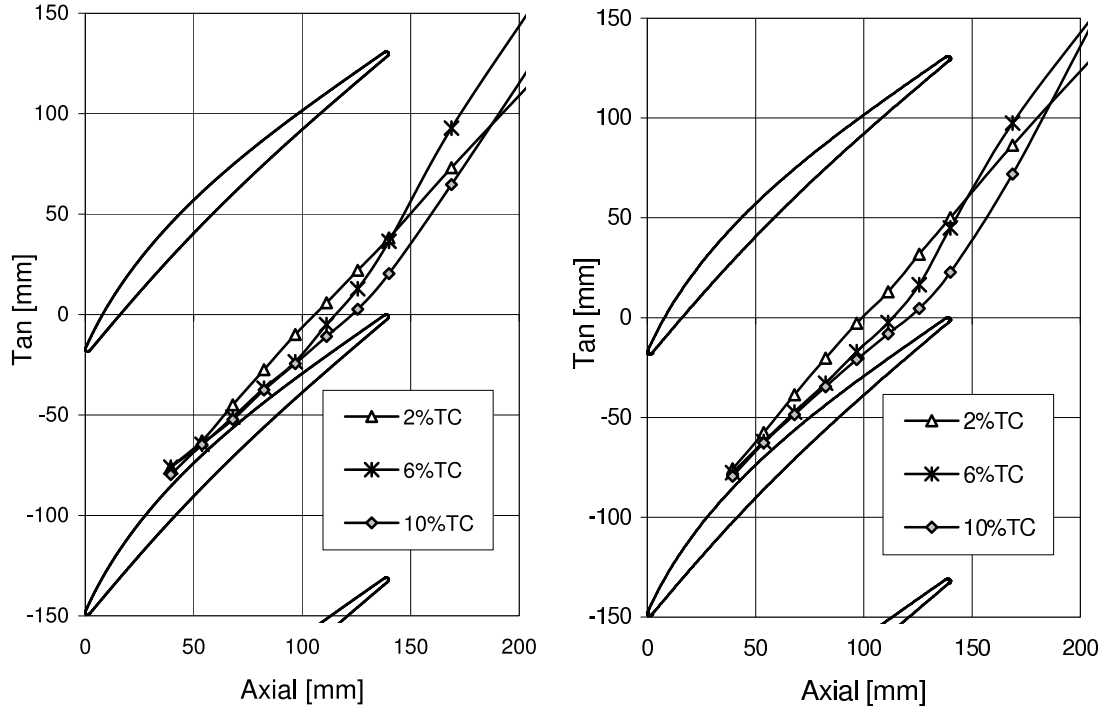

(a) Natural Skew *(b) High Skew*

Figure 5.16: *Leakage Vortex Location*

flow associated with the passage vortex. Increasing the skew had little effect on the tangential velocity associated with the over tip leakage or the leakage vortex. However the tangential velocity further across the passage was reduced slightly.

Helicity contours in Figure 5.15 indicate the rotational direction of the flow through the cascade with 6%TC. The leakage vortex, as expected, rotated clockwise and the induced vortex rotated anti-clockwise as looking from down-upstream. Therefore the formation of the induced counter rotating vortex was proven. Also of note was the higher magnitude of the leakage vortex and counter rotating vortex with the higher skew.

Figure 5.16 shows the vortex core location for 2%, 6% and 10% tip clearances. With 2%TC the vortex core moved away from the suction surface at approximately 40% axial chord. For the larger clearances the vortex core trajectory was similar for the majority of the passage. The 6%TC vortex core moved away from the SS at approximately 0.7% axial chord and the 10%TC remained closer to the SS. At the trailing edge the vortex core location was similar for the 2% and 10% tip clearance

cases. After the blade row the clearance vortex trajectory was similar to the pitch averaged exit angle shown in Figure 5.1 on Page 113 and so the higher clearance had a higher vortex trajectory exit angle. The traverse planes were therefore at a higher angle to the vortex trajectory therefore explaining the elongated nature of the vortex within the contour plots. The effect of the skew was small and resulted in a slight movement of the vortex trajectory across the passage.

The vortex core pitch-wise location at the trailing edge was similar for the 2% and 6% tip clearance cases, for both inlet conditions (Figure 5.16). The mass averaged blockage and loss was however significantly higher with 6%TC downstream of the cascade (Figure 5.1). This was mostly as a result of the increased counter rotating vortex blockage region rather than the shift in leakage vortex position. Furthermore the increased inlet skew further increased the blockage and loss within this region.

5.1.4 Blade Loading

The blade loading is now shown, firstly pressure coefficient blade surface contour plots are presented for clearance values of 0%TC, 2%TC, 6%TC & 10%TC in Figures 5.17 to 5.20 for both inlet conditions. Then the same data is presented in 1-D to assess the change in blade pressure profile along the blade (Figures 5.21 & 5.22).

The following contour plots allow for a quick assessment of the effect of the clearance on the blade pressure distribution. Without clearance there was an increase in the SS pressure towards the casing. With the small clearance (Figure 5.17): an increase in pressure occurred on the PS close to the tip; and a pressure eduction occurred on the SS close to the tip caused by the leakage vortex interaction. The effect of the skew was to reduce the SS low pressure region at the tip. Increasing the clearance further reduced the SS pressure associated with the leakage vortex interaction and moved this region axially further along the blade. The PS pressure was reduced towards the tip with increased clearance.

The effect of inlet skew on the blade pressure profile without tip clearance was shown in Figure 5.21. A decrease in peak SS loading within 10% chord of the tip of the blade existed, as seen by the increase in the SS minimum pressure. This was coupled with an increase in pressure on the PS LE and was a consequence

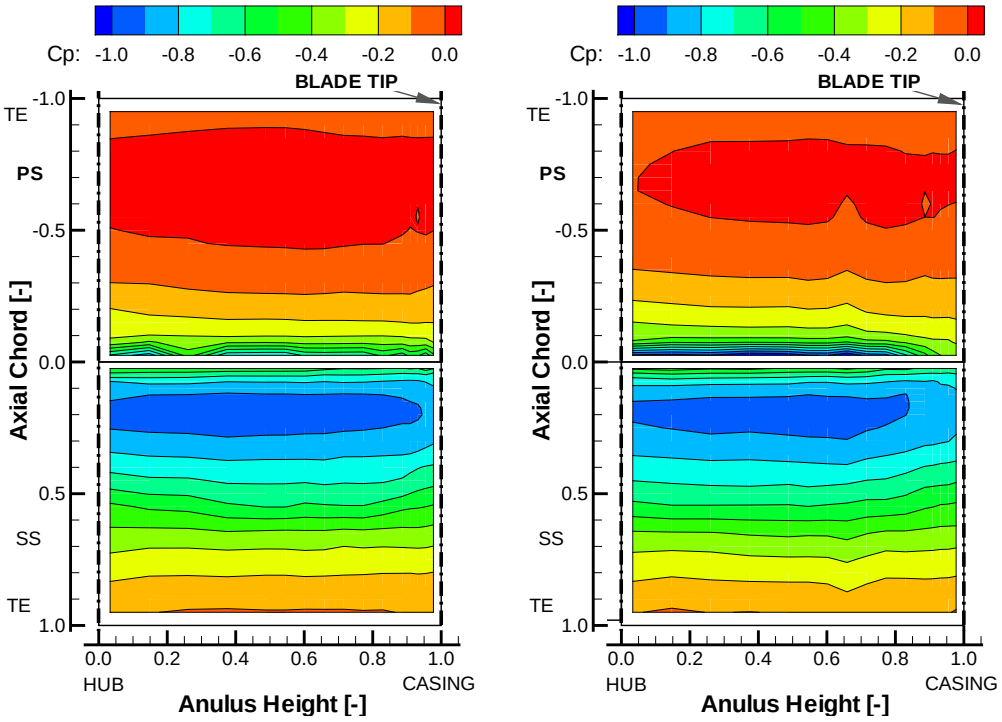

(a) Natural Skew *(b) High Skew*

Figure 5.17: *Blade Pressure Cp Contour Plots 0%TC*

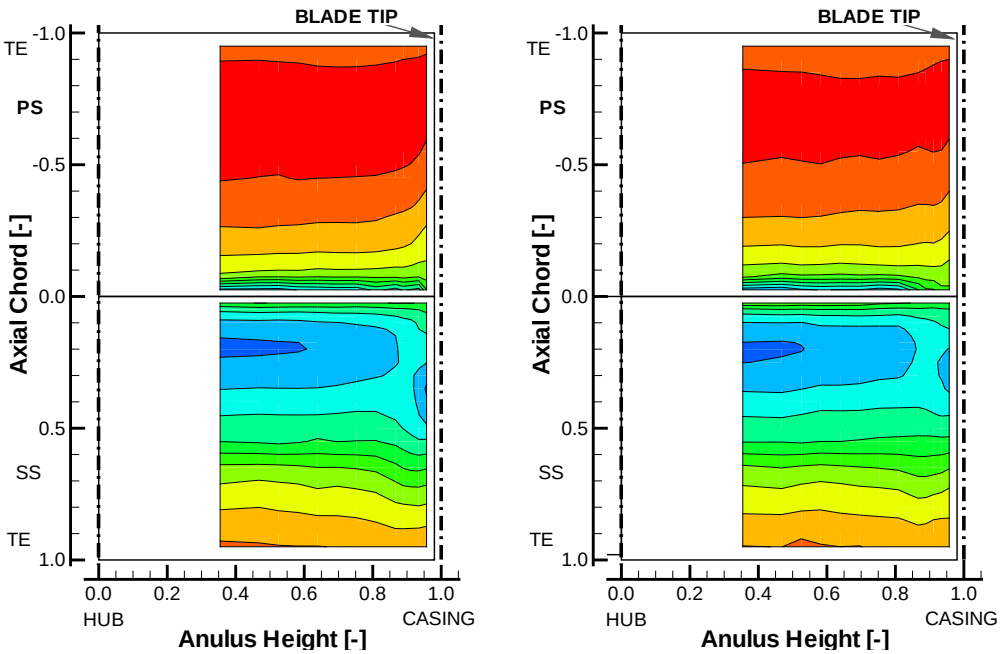

(a) Natural Skew *(b) High Skew*

Figure 5.18: *Blade Pressure C_p Contour Plots 2%TC*

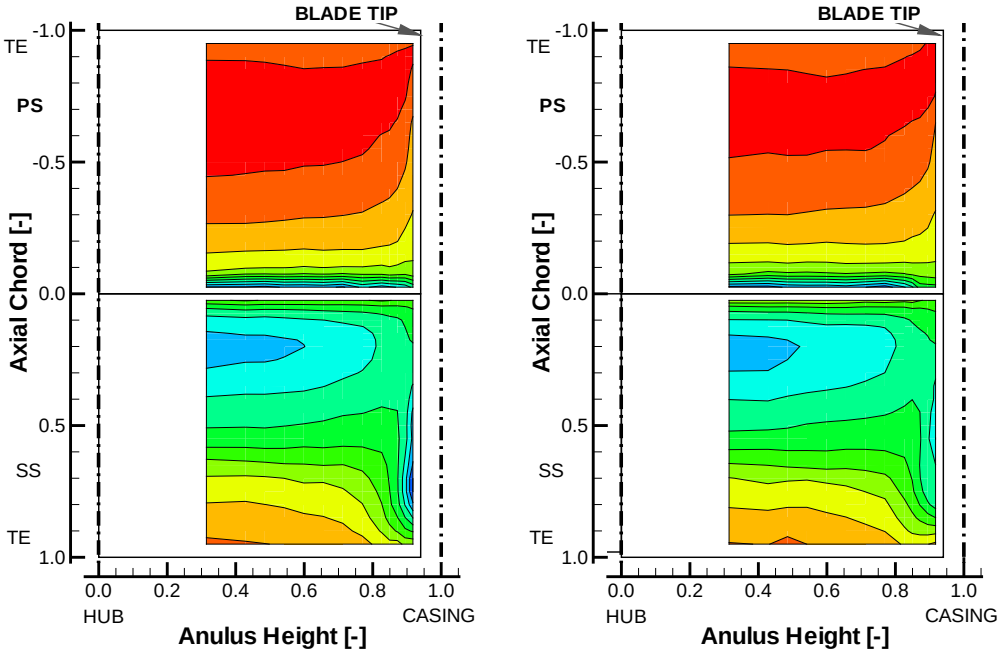

(a) Natural Skew *(b) High Skew*

Figure 5.19: *Blade Pressure C_p Contour Plots 6%TC*

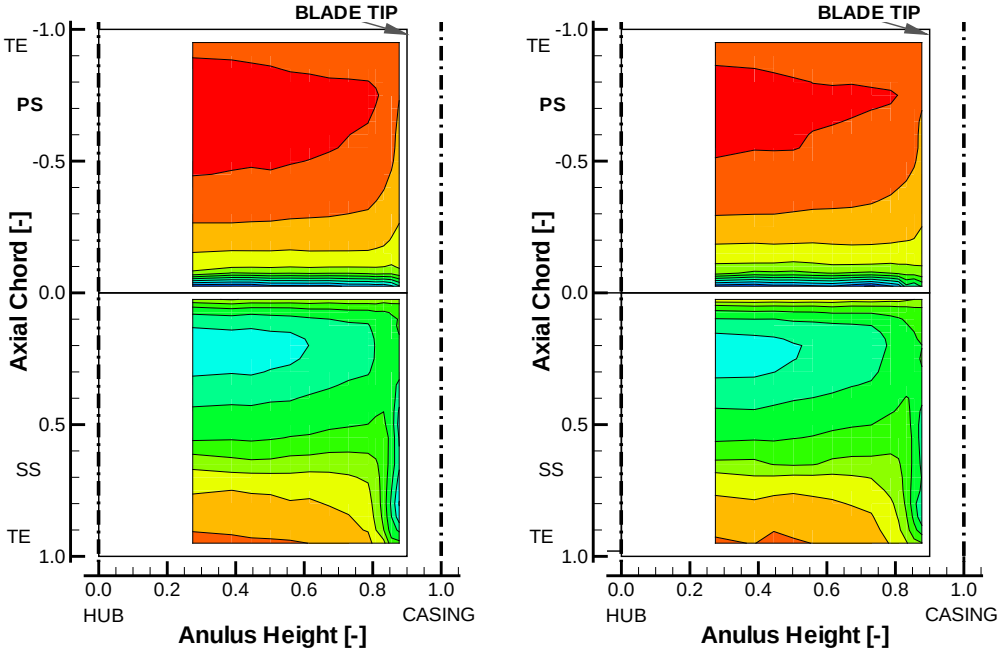

(a) Natural Skew *(b) High Skew*

Figure 5.20: *Blade Pressure C_p Contour Plots 10%TC*

of the increased inlet skew at the casing. Increasing the skew (Figure 5.21(b)) moved this effect further away from the casing to 20% chord as might be expected with the thicker inlet boundary layer. A significant change in loading along the

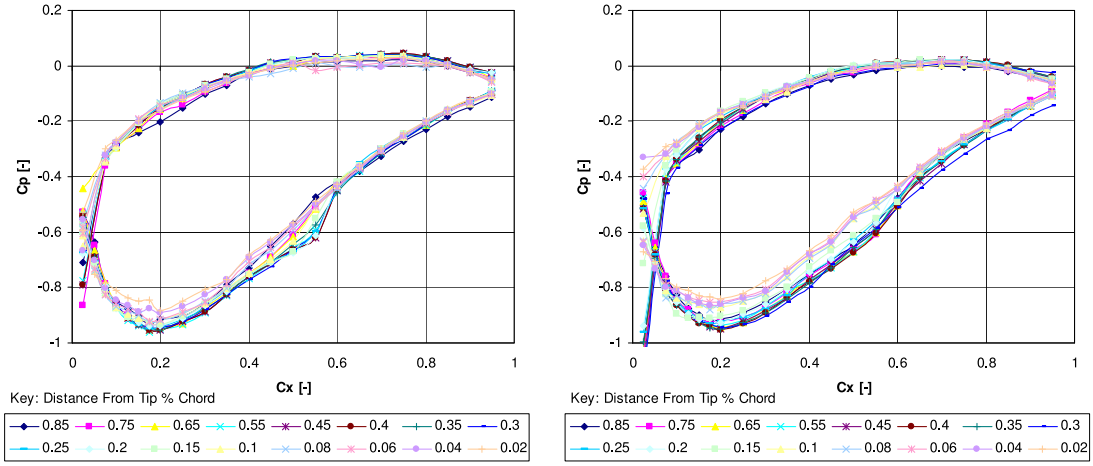

(a) *Natural Skew* ***(b)*** *High Skew*

Figure 5.21: *0%TC, Blade Cp Profile Along Blade Length*

length of the blade occurred for all tip clearances (Figure 5.22). Towards the tip of the blade there was a reduction in loading at the LE and an increase towards the TE. At the front of the blade both surfaces experienced reduced loading. For the last half of the blade the PS again underwent under-loading but the SS pressure was reduced and therefore increases the SS loading. The reason for the change in pressure on the PS was increased flow passing along and over the tip of the blade and on the SS was the leakage vortex interaction pulling low pressure fluid on to the SS. This was similarly observed with Build-A. For the small clearances (e.g. 2%TC, Figure 5.22(a)) this effect was insignificant but for the larger clearance of 6%TC (Figure 5.22(c)) the change in tip loading was significant. Increasing the clearance further to 10%TC (Figure 5.22(e)) again incurred a significant increase in tip loading but the SS pressure was slightly higher and therefore the loading not as large.

Increasing the skew lowered the reduction in SS pressure towards the tip of the blade. In fact for the 2%TC case (Figure 5.22(b)) the effect of the skew was to remove the SS increase in loading at the rear of the blade and therefore the blade tip loading was similar to the loading without clearance (Figure 5.21(b)). This effect

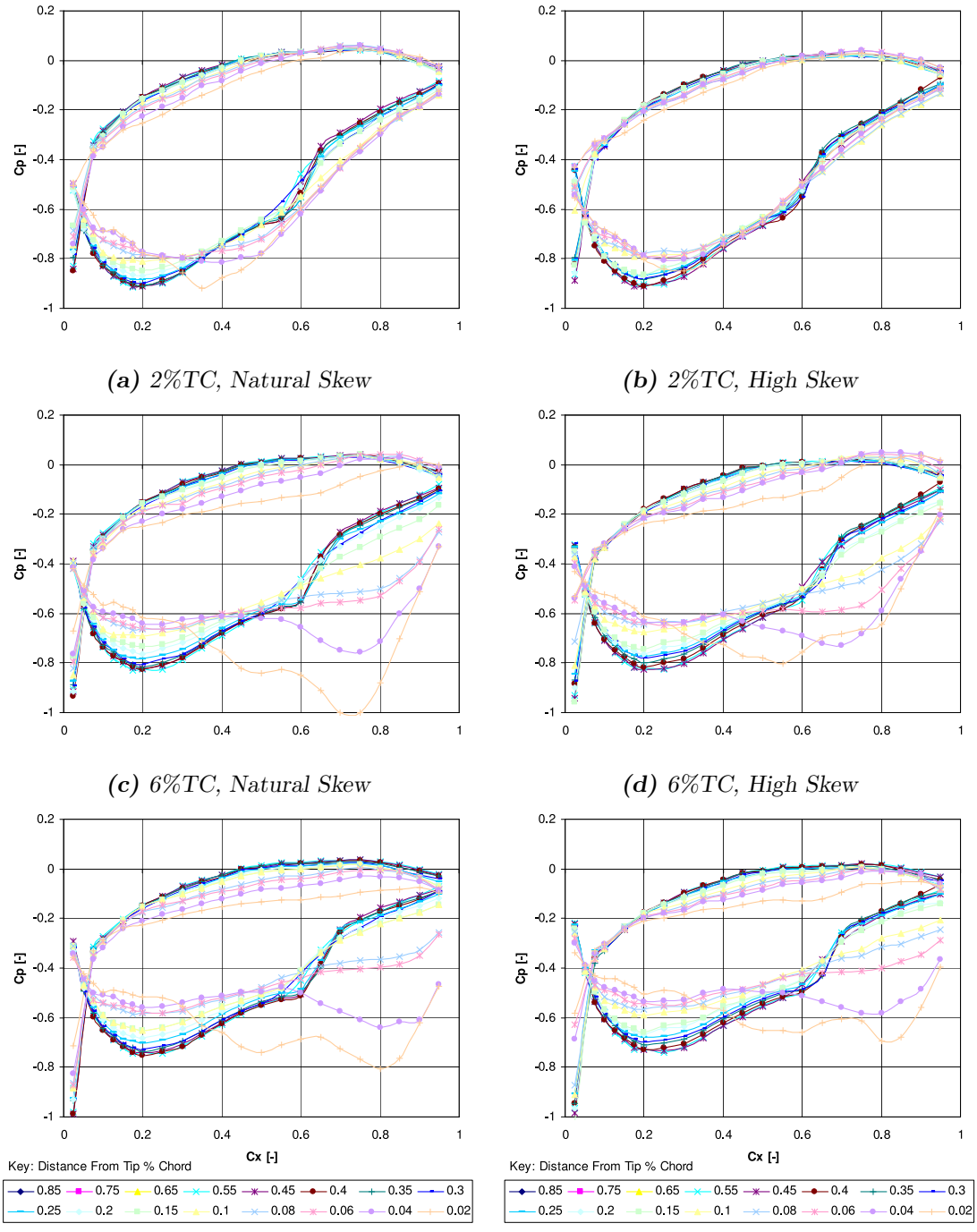

(a) 2%TC, Natural Skew

(b) 2%TC, High Skew

(c) 6%TC, Natural Skew

(d) 6%TC, High Skew

(e) 10%TC, Natural Skew

(f) 10%TC, High Skew

Figure 5.22: *With Clearance, Blade Cp Profile Along Blade Length*

was more apparent in Figure 5.23(a) where the pressure profile was plotted at the tip of the blade for all the measured clearances.

As previously mentioned an increase in tip clearance significantly affected the cascade loading. The blade pressure profiles at mid-span are shown in Figure 5.23(c). On the PS there was little change in pressure with the clearance size but on the SS there was a significant increase in pressure or decrease in loading. The reason for this was a change in inlet flow angle brought about by the increase in cascade blockage, the effect of which is investigated in Section 5.1.6.

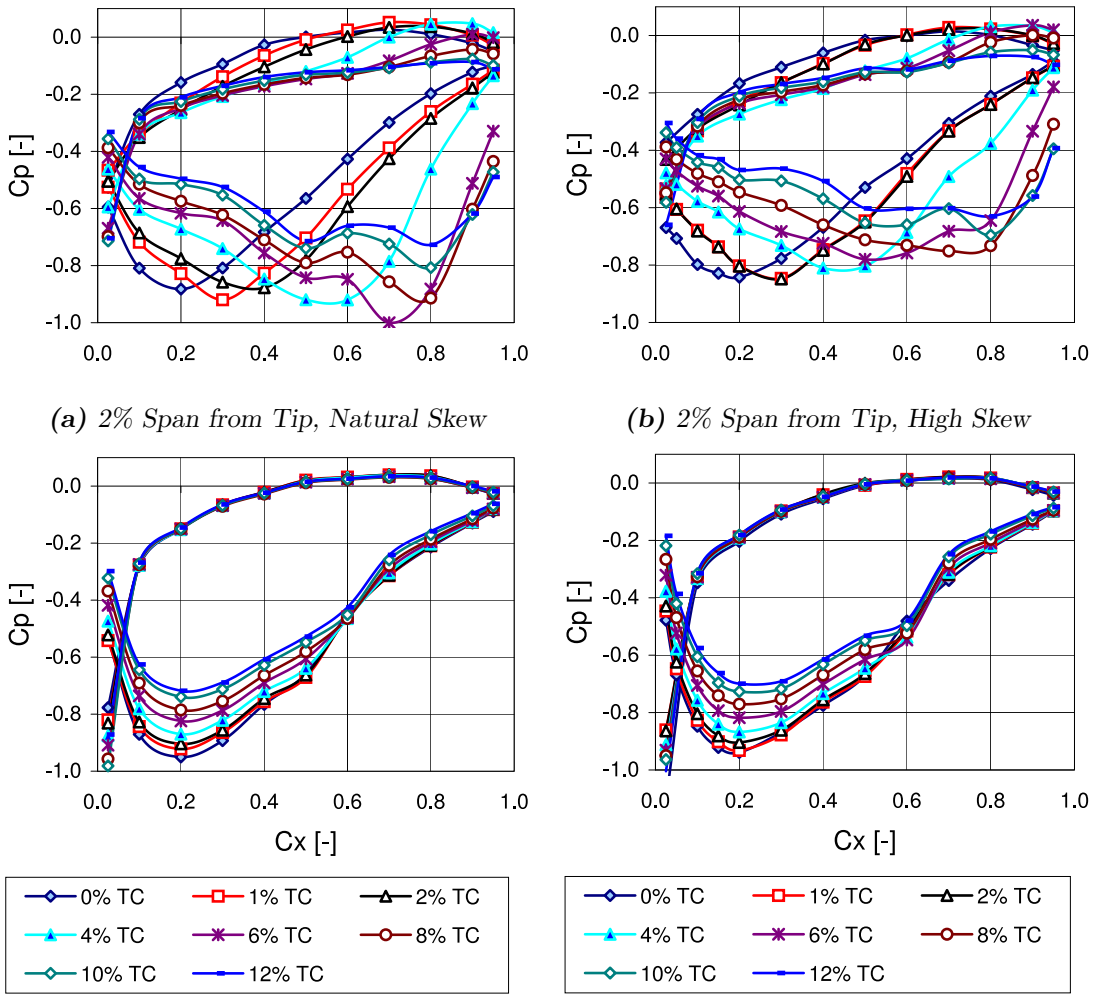

(a) 2% Span from Tip, Natural Skew

(b) 2% Span from Tip, High Skew

(c) 45% Span from Tip, Natural Skew

(d) 45% Span from Tip, High Skew

Figure 5.23: *Blade C_p Profile at 45% and 2% Span From Blade Tip with Varying TC*

Figure 5.25 showed the blade force along the length of the blade for both inlet

conditions and varying clearance. Figures 5.25(a) and 5.25(b) show the absolute blade force coefficient values and Figures 5.25(c) and 5.25(d) show the loading relative to mid-span which removed the mid-span loading offset. This method of zeroing the data to the mid-span value was debatable as it was unclear if the effect offset was the same towards the casing but it enabled the clearances to be more easily compared without the mid-span offset.

Without clearance an approximately linear reduction in loading occurred towards the casing up to 90% span. Closer to the casing within the boundary layer the loading further decreased. However with the higher skew the decreased loading at the tip did not occur. Above 2%TC the reduction in loading still existed along the length of the blade but the loading increased at the tip to a value similar to mid-span. For the larger clearances the tip loading was larger than at mid-span and the higher inlet skew decreased this increased loading.

Integrating the blade loading (Figure 5.25) produced the overall blade loading shown in Figure 5.24 which was undertaken for the outer 50% span only. The absolute total blade loading (Figure 5.24(a)) and the blade loading with the mid-span value subtracted (secondary blade loading change) is shown in Figure 5.24(b). An overall reduction in blade loading with increased inlet skew occurred. This reduction was however a consequence of the reduction in mid-span loading coupled with the end-wall secondary flows. Removing the mid-span variation (Figure 5.24(b)) showed that the total blade force was increased up to 4%TC and then decreases with increased clearance and at 6%TC the blade loading was approximately the same as without clearance. Increasing the skew had little effect at 6%TC and above, but for the smaller clearances the effect was to significantly reduce the loading compared to the same clearance for the low skew case.

5.1.5 Blade Tip Pressure

The pressure coefficient on the blade tip end with natural skew is shown in Figure 5.26. The pressure tapings were located on the tip of the blade at approximately 2mm from the blade surfaces as shown in Figure 3.16 on Page 71. On the PS edge a decrease in pressure occurred from the LE until the minimum pressure was reached

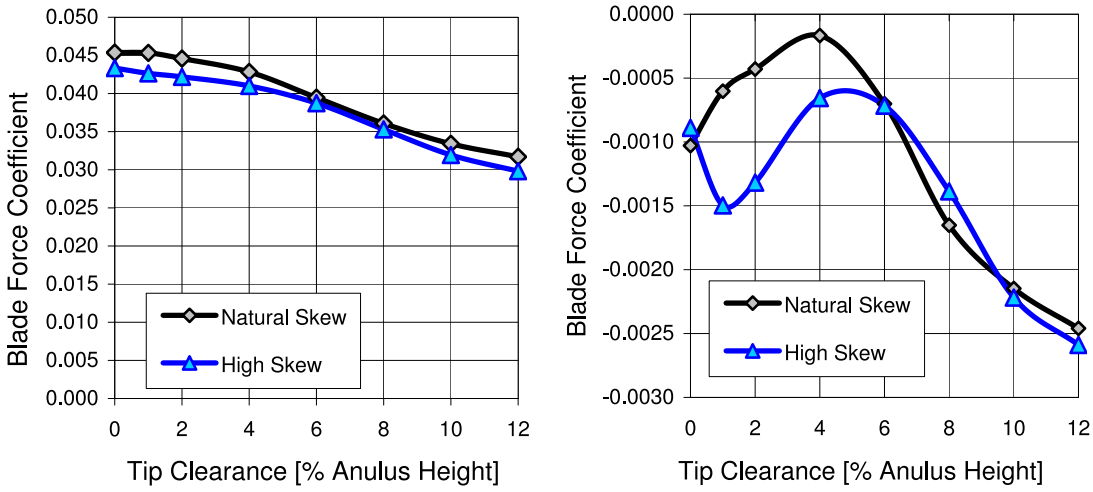

(a) *Absolute* ***(b)*** *Zeroed at Mid-Span*

Figure 5.24: *Blade Force for Outer 50 %Span*

between 0.5Cx and 0.7Cx. The minimum pressure peak moved downstream and increased in pressure with increased clearance. On the SS edge with a high clearance of $\geq 6\%TC$ the pressure was similar to the PS edge, and so showing that the flow over the tip of the blade was separated across the full blade tip and suggesting a vina-contractor like flow feature existed.

With a smaller clearance $< 4\%TC$ the minimum pressure, high velocity fluid, occurred closer to the LE than on the PS side and then had a higher pressure for the remainder of the chord. This therefore showed that a separation bubble was formed around the PS edge and then reattachment occurred. The axial location of the minimum SS pressure corresponded to the roll up of the leakage vortex as found in the internal contour plots (Figures 5.8 to 5.12). Storer and Cumpsty [1991] found that the ratio of clearance height divided by maximum blade thickness must be less than 0.4 for reattachment. Therefore for Build-B with maximum blade thickness of 11 mm reattachment would occur above 2.4%TC. Therefore these results appear to agree with Figure 2.3 by Glanville [2001] and Storer's reattachment criteria (Storer and Cumpsty [1991]).

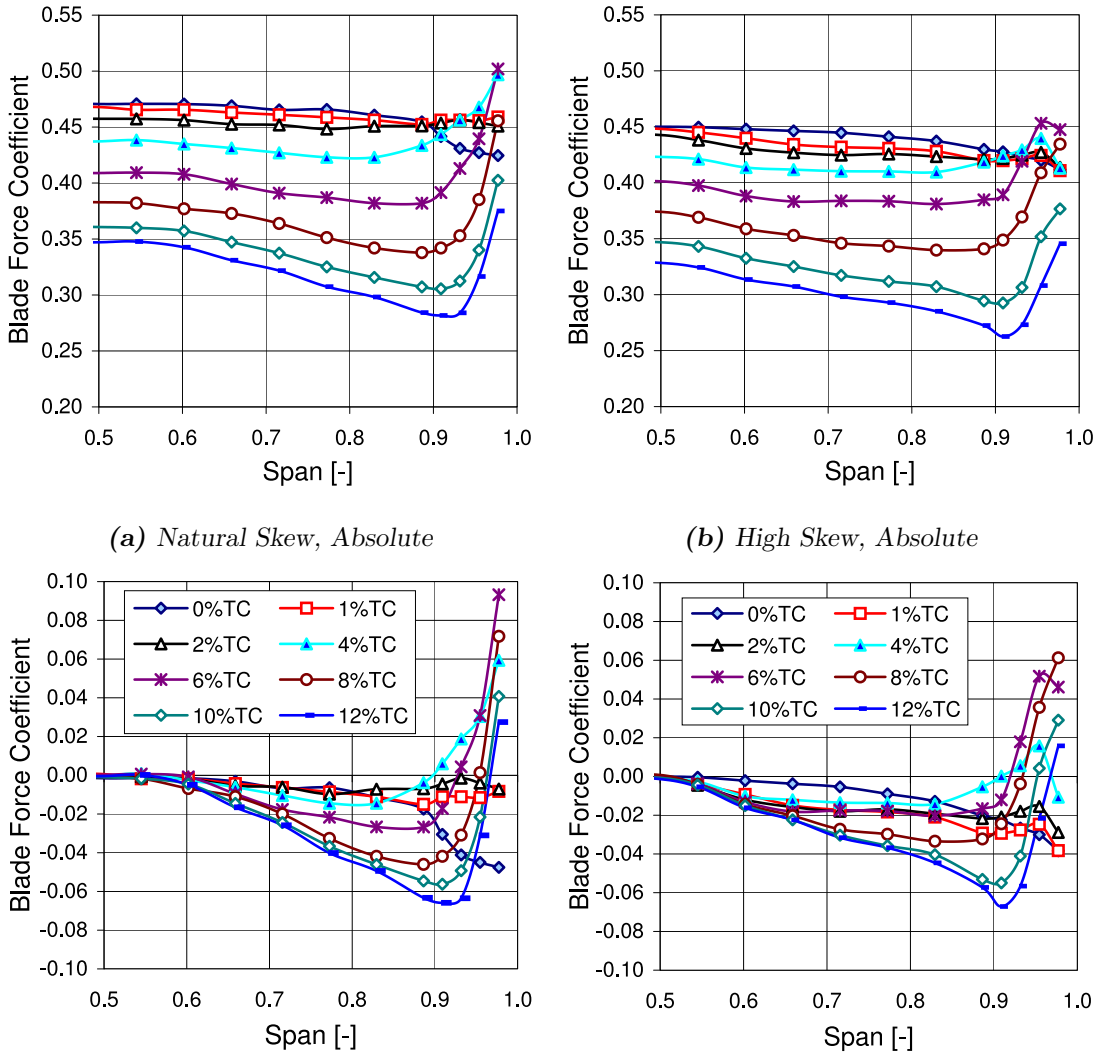

(a) Natural Skew, Absolute

(b) High Skew, Absolute

(c) Natural Skew, Zeroed at Mid-Span

(d) High Skew, Zeroed at Mid-Span

Figure 5.25: *Blade Force Coefficient*

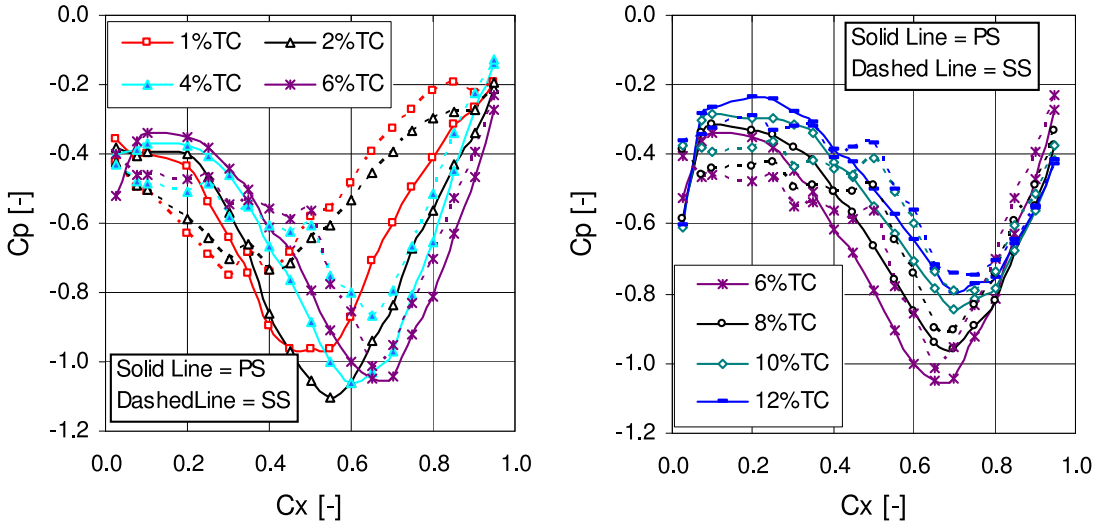

(a) Clearances 1%TC to 6%TC *(b) Clearances 6%TC to 12%TC*

Figure 5.26: *Pressure Coefficient on Blade Tip*

5.1.6 Inlet Conditions

Influence of Cascade Blockage on Inlet Flow

The experimental results show a reduction in mid-span loading with increased tip clearance and increased skew. The reason for this was a change in the upstream boundary conditions due to the change in cascade blockage. Figure 5.27 shows pitch averaged data taken upstream of the central measured passage ('pass1') without clearance and with 10%TC for both inlet skew conditions. A significant change in axial velocity and yaw angle with increased clearance and inlet skew occurred. The low skew inlet shows a mid-span reduction of $\approx 0.6m/s$ and reduction of $\approx 0.6°$ in axial velocity and yaw angle respectively. With the high inlet skew the inlet axial velocity and yaw angle were further decreased. Within the boundary layer the clearance size had little effect on the inlet flow angle or velocity. Although not shown, there was no change of inlet total or dynamic pressure with change in clearance. An explanation of this feature follows.

The reduction in inlet angle with increased clearance and skew was a result of increased blockage. This increase in blockage, as seen in Figure 5.28 resulted in a redistribution of the incoming stream lines towards the centre of the cascade and redistributing the mass flow and therefore increasing the mid-span axial velocity.

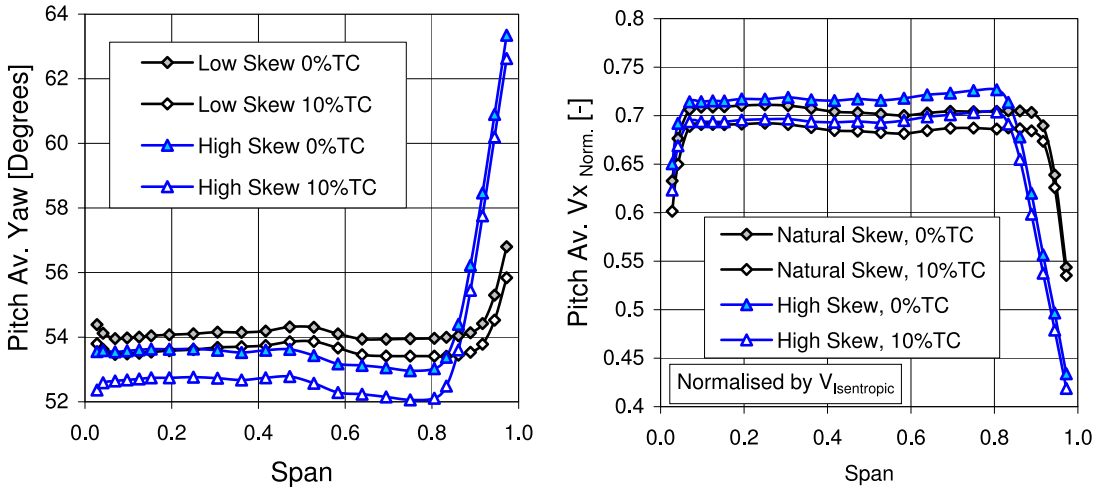

(a) Yaw Angle *(b) Axial Velocity*

Figure 5.27: *Inlet Flow Conditions at 0.5Cx Upstream*

An increase in axial velocity, with constant inlet velocity, would therefore account for the reduction in inlet angle as seen in Figure 5.27(b). However as clearly seen in Figure 5.27(b) the actual axial velocity decreased and therefore a reduction in inlet velocity and therefore mass flow occurred with increased clearance. Neglecting the effect of the cascades upstream end-wall bleed and top and bottom bypass this must have been due to an increase in the wind tunnels supply fan loading and therefore decrease in volumetric flow rate.

Inlet Flow Geometrical Offset

For both cascades, the geometrical inlet angle and the measured inlet angle were different. For Build-B the geometrical angle was set to 58° but the inlet flow angle was measured at ≈ 54°. The reason for this was unclear, but to give some insight Figure 5.29 shows the inlet conditions for 'pass1' for several axial locations upstream of the LE, without clearance. Note that this was only a partial traverse at the 0Cx location because of the probe thickness. Approaching the LE the axial velocity was reduced and the yaw angle increased which resulted in a higher than expected loading on the cascade. This outcome will be important when considering the computational results in Section 5.3.

The reason for this geometrical offset was not fully understood, previously it was

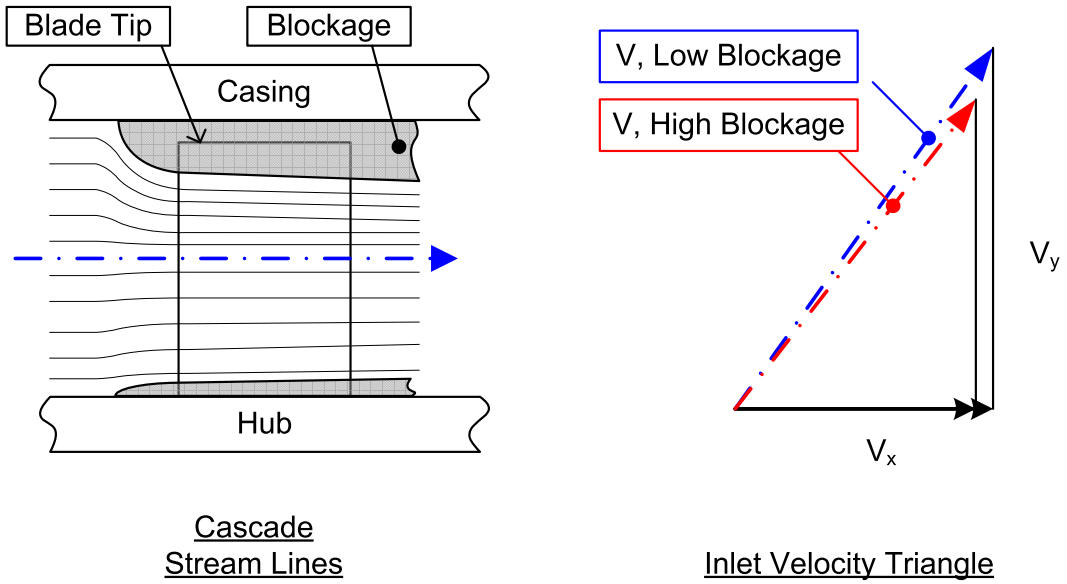

Figure 5.28: *Influence of Blockage on Inlet Velocity Triangle*

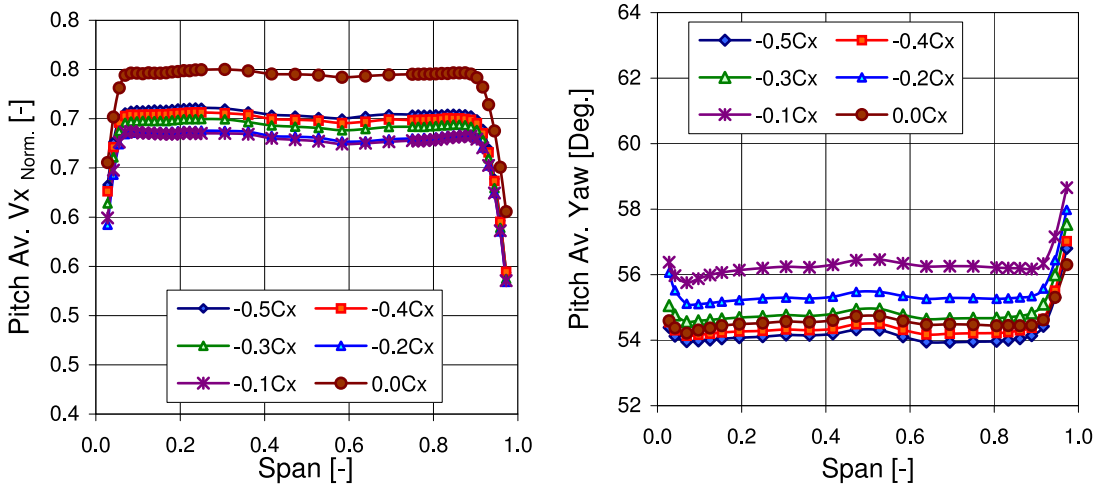

(a) *Normalised Axial Velocity* ***(b)*** *Yaw Angle*

Figure 5.29: *Natural Skew, Inlet Flow Conditions at Various Upstream Axial Locations*

shown that an inlet angle decrease occurred with increased blockage on the casing due to a redistribution of the streamlines. This may indeed be a contributing factor however another explanation was that the cascade was to short and therefore the upstream and downstream splitter plates and exit diffusers had an influence on the inlet angle. Certainly the top and bottom exit diffusers were found to effect the incoming flow, by altering the diffusion in the top and bottom passages, and this was the method used to ensure reasonable periodicity. This geometrical to flow angle offset was therefore attributed to the cascade being too short.

5.2 Experimental Results Discussion

The new cascade (Build-B) developed for this work had the capability to study large tip clearances with engine representative geometry and inlet conditions. The geometry had a much higher stagger angle and lower turning than previously investigated with Build-A in Chapter 4. Previously for Build-A it was observed that the tip clearance vortex behaved differently from low or intermediate pressure stages. It was shown that the tip clearance vortex remained within the SS side of the passage at nominal operating conditions. This vortex interacted with the blade and reduced the pressure on the SS, increasing the blade loading towards the tip of the blade. Increasing the clearance above 4%TC incurred no further increase in loss.

Measurements from the new cascade have shown similar results with more realistic HPC inlet conditions and geometry, with a more comprehensive data set. Traversing within the cascade passage gave a clear insight in to the progression of the end-wall flows and in particular the tip leakage vortex and counter rotating vortex. For this geometry the tip leakage vortex appeared to have a much higher elongation in the pitch-wise direction. This was caused by the higher angle of the traverse plane with the vortex trajectory than with the previous low stagger aerofoil. The loss increase through the cascade varied with tip clearance and peaked between 1%TC and 4%TC depending on the inlet boundary layer. Above this peak a reduction in loss occurred with increased clearance until at 12%TC the loss was approximately the same as without clearance.

5.2.1 Effect of Tip Clearance Size

The effect of the tip clearance size was similar to previously reported results in Chapter 4. The patterns of the variations due to the tip clearance size were the same for both inlet conditions with slightly different magnitudes. Compared to the previous cascade the pitch averaged exit yaw angle was higher than at inlet close to the casing. This was most likely the result of the over tip leakage flow direction which although not measured was expected to have a negative axial velocity. The axial velocity within the casing region was almost zero creating a large blockage.

The trajectory of the tip clearance vortex was shown to move away from the casing with increased tip clearance value which was to be expected because the blade tip moves from the casing; interestingly the trajectory across the passage differs with tip clearance as seen in the internal plots (Figures 5.8 to 5.13).

At the lower value of 2%TC (Figure 5.8 & 5.9) the tip clearance vortex core moved away from the suction surface at approximately 0.4Cx and then proceeded to move across the passage to approximately 0.3 pitch at the TE. With a 6%TC the vortex core moved from the SS much later at approximately 0.6Cx and then moved across the passage exiting at approximately 0.28 pitch from the SS. The vortex core was weaker and smaller in size than for 2%TC. Increasing the gap further to 10%TC prolonged the detachment of the tip clearance vortex from the SS further to 0.8Cx. At the TE with 10%TC the vortex core was approximately 15% pitch from the SS and therefore only filled approximately 30% of the pitch-wise passage. The magnitude of the tip clearance vortex core was reduced with increased tip clearance.

As previously found, for Build-A, a secondary counter rotating vortex was evident on the casing wall adjacent to the tip clearance vortex; this was a result of the incoming casing flow, passing over the blade and tip clearance vortex, separating from the wall due to the adverse pressure gradient (deceleration of the flow) and the casing shear separating the flow. This in turn was found to create a counter rotating vortex and therefore a blockage. A larger blockage was created with the larger tip clearances as a result of the increased flow passing over the tip clearance vortex.

The area averaged loss for the outer 50% cascade annulus height showed that increasing the tip clearance from 1%TC to 10%TC incurred an increase in loss

though the cascade compared to the 0% case. Above this (12%TC) there was a reduction in loss with increased TC. This was similar to Build-A (Chapter 4) where the loss levelled of above 6%TC. However area averaged yaw showed a significant reduction in turning through the cascade with increased TC.

5.2.2 Effect of Inlet Boundary Layer

Build-A reported results with a realistically skewed inlet of 10° relative to mid-span but the boundary layer was unrealistically thin (within 10% span of the casing). Build-B allowed for a realistic inlet boundary layer to be implemented and to be compared to the cascade with a small, natural, boundary layer.

The pitch averaged exit plots at 1.2Cx (Figure 5.1) showed that with 6%TC or less, only a small change in yaw angle with the increased skew was found. There was an increase in yaw of less than 2° close to the casing and no significant radial shift with the high skew inlet boundary. Above 6%TC an increase in exit angle of 10° close to the casing occurred and a radial shift (although small) away from the casing was apparent. The area averaged exit angle (Figure 5.2(b)) indicated that for the smaller tip clearance values the higher skew decreased the exit angle. Some of this can be accounted for by a reduced mid-span inlet angle and therefore a reduced blade loading and exit angle. Note however, that the total inlet angle with high skew was higher (because of the higher boundary layer skew) than for the natural skew boundary layer, therefore with the high skew inlet the turning through the cascade was higher.

The inlet boundary layer had a significant impact on the stagnation pressure loss at exit. The pitch averaged plots (Figure 5.1) show a significant thickening of the exit loss regions and increase in the loss attributed to the TC vortex. However this increase in loss was not a result of an increased TC vortex core loss as the contour plots (Figures 5.8 to 5.13) clearly showed that the loss core was lower in magnitude with the increased skew. The origin was an overall thickening of the loss area in the casing region including the counter rotating vortex loss increase. Area averaging the loss at 1.2Cx (exit) showed that there was an overall increase in loss at exit with increased inlet skew. Subtracting the inlet loss profile from the exit profile,

resulted in a reduction in loss with the highly skewed inlet compared to the natural inlet. Therefore the net loss increase through the cascade was reduced slightly by the increased inlet skew.

It is not yet clear as to whether this reduction in loss was due to the increase in a thickness of the inlet boundary layer or its skew. The increased skew opposed the passage vortex but the increased thickness created a larger blockage and therefore redistribution of the cascade mass flow which reduced the exit angle and therefore the mid-span loss. This will be discussed further in Chapter 7 and comparison with Build-A made to further the understanding of the effect of the skew.

5.3 Computational Investigation

Computational results are now presented for the Build-B. The boundary conditions, CFD code and details of the grid used within this section were presented in Section 3.5.4 on Page 85. The purpose of this section is to give explanation and insight in to some of the the issues surrounding the experimental results. Firstly the CFD results are validated against the experimental data. The effect of rotation with this geometry is briefly investigated and then cascade results given.

5.3.1 Computational Results Validation

A validation exercise showed that the CFD predicted the flow trends correctly but the magnitudes were not so good. Figure 5.30 compares exit (1.2Cx) pitch averaged CFD results for the low skew against the experimental data previously given. Due to the large amount of data the results have been split in to two plots; small clearances $\leq 4\%TC$, and large clearances $\geq 6\%TC$.

In general the CFD qualitatively predicted the pattern of the experimental data well, but as with the previous cascade, quantitatively it failed to predict the low clearance magnitudes correctly. At mid-span the CFD over predicted the loss which was caused by the negative incidence angle and therefore a thicker PS boundary layer. This was an effect of the low inlet angle which was also evident in the CFD's higher mid-span exit yaw angle. Within the end-wall region, again the 1%TC case

showed the worst comparison; the CFD under predicted the thickness and magnitude of yaw therefore under predicting the blockage and over predicting the loss. Above and including 4%TC the agreement was much better; a slight over prediction in the secondary flow thickness existed in the yaw and axial velocity. The loss however was significantly over predicted but again qualitatively followed the trends. The blade

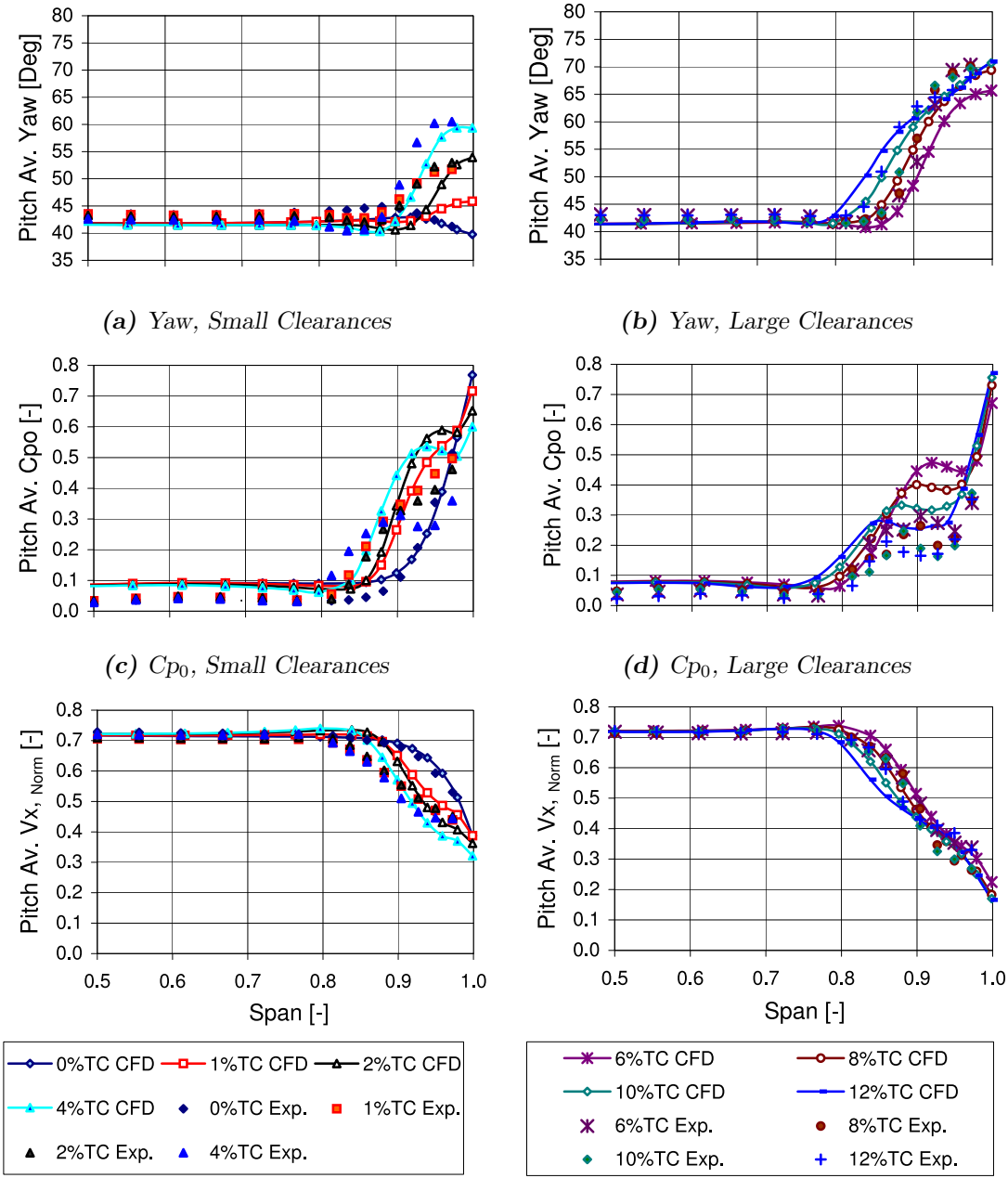

(a) Yaw, *Small Clearances*

(b) Yaw, *Large Clearances*

(c) Cp_0, *Small Clearances*

(d) Cp_0, *Large Clearances*

(e) $V_{x,Norm}$, *Small Clearances*

(f) $V_{x,Norm}$, *Large Clearances*

Figure 5.30: *Pitch Averaged CFD & Experimental Results Comparison at 1.2Cx*

loading was significantly under predicted compared to the experimental data. The reason for this was the increasing inlet yaw angle towards the leading edge of the cascade as found in Section 5.1.6. Therefore because within the CFD prediction the measured inlet angle at -0.5Cx was specified the computational prediction was under loaded compared to the experimental cascade. Figure 5.31 shows this under loading within C_p plots. With no clearance (Figure 5.31(a)) the leading edge pressure surface and the suction surface had a significantly different pressure profile for all span-wise locations shown.

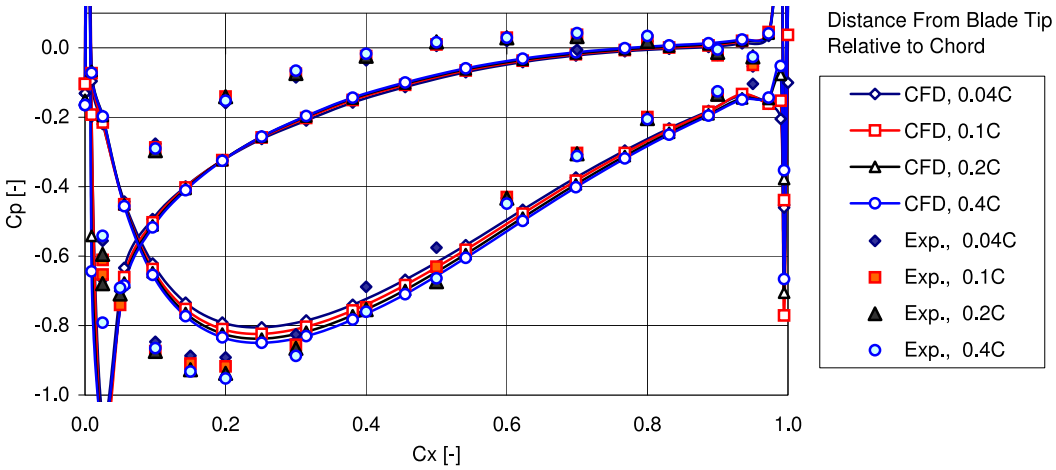

(a) *0%TC*

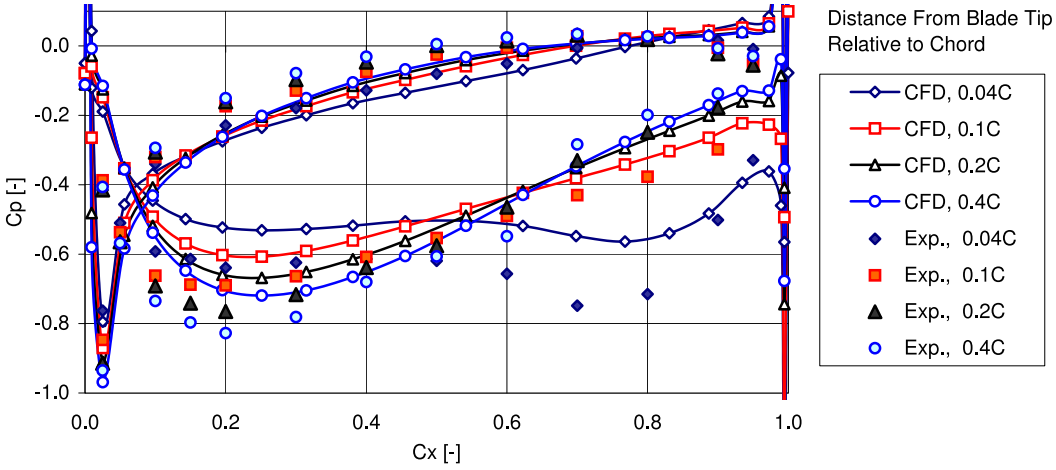

(b) *6%TC*

Figure 5.31: *Blade Pressure Profile CFD & Experimental Results Comparison*

The CFD blade loading profile suggested a negative incidence angle on to the blade leading edge, and this explained the requirement for the boundary layer trip

on the pressure surface to ensure convergence. Despite the under loading, the CFD showed good agreement with the experimental data and similarly a reduction in peak loading on the SS towards the tip was predicted. With a clearance of 6%TC (Figure 5.31(b) again the CFD was under loaded but did show the experimental patterns as discussed previously in Section 5.1.4.

5.3.2 Computational Results

The following are a selection of computational results which allow for comparison with the experimental data and further understanding of the clearance flows. The downstream contour plots (Figure 5.32) and pitch averaged results (Figure 5.33) compliment the experimental data well. As with Build-A the CFD was over diffusive, as seen in Figure 5.32, and therefore over predicted the loss. The loss again increased in thickness from the casing but decreased in magnitude with increased clearance. The same flow structures were evident with the CFD as with the experiment.

The area averaged exit loss and yaw for the outer 50% span are shown in Figure 5.34 and can be compared to the experimental data in Figure 5.2 on Page 150. The exit yaw generally agreed well with the experimental data but the loss was over predicted. Due to the over predication there was only a small reduction in loss above the maximum loss which peaked between 4%TC & 6%TC. For the experimental data it was found that the high skew inlet had a smaller net loss increased across the cascade than for the low skew inlet. This was not the case with the CFD and can be assumed as a result of the loss over prediction. Although the total loss magnitude was different it does show that increasing the clearance had no significant impact on the loss above a certain value but there was a penalty of an overall reduction in turning.

The secondary loss increase through the cascade, shown by the grey symbols with the dot-dash line in Figure 5.2, was found to differ from the experimental data. With the experimental data the secondary loss was the same for both inlet conditions far all clearances. The CFD however showed a higher increase in secondary loss for the high skew inlet and the reason for this again is probably due to the CFD's over prediction in loss and the inaccurate specification of the inlet flow conditions within

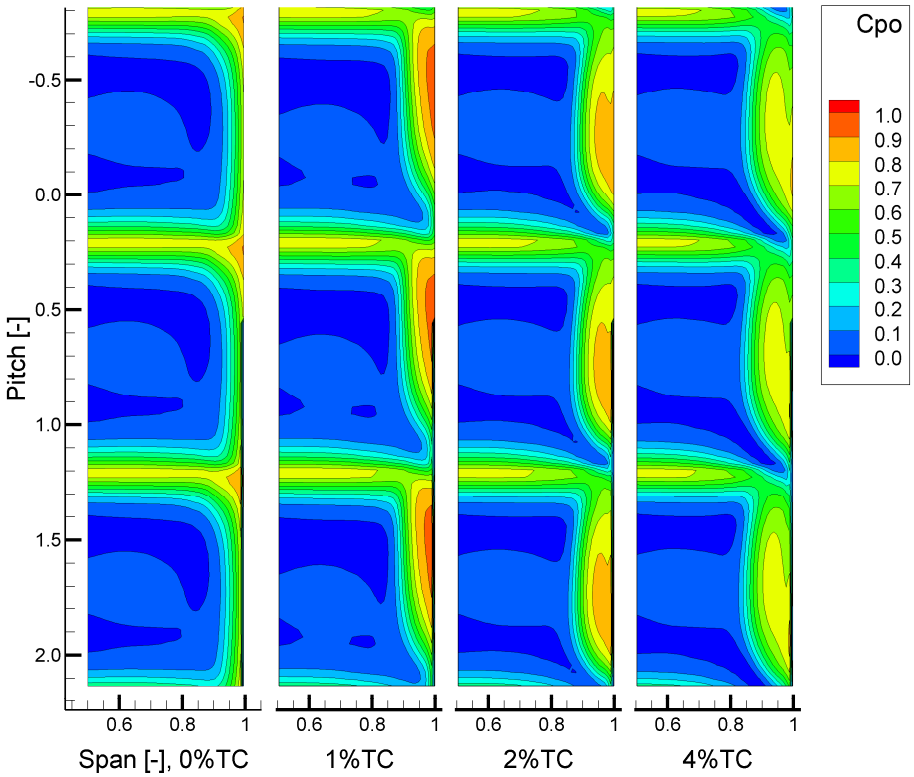

(a) Tip Clearances from 0%TC to 4%TC

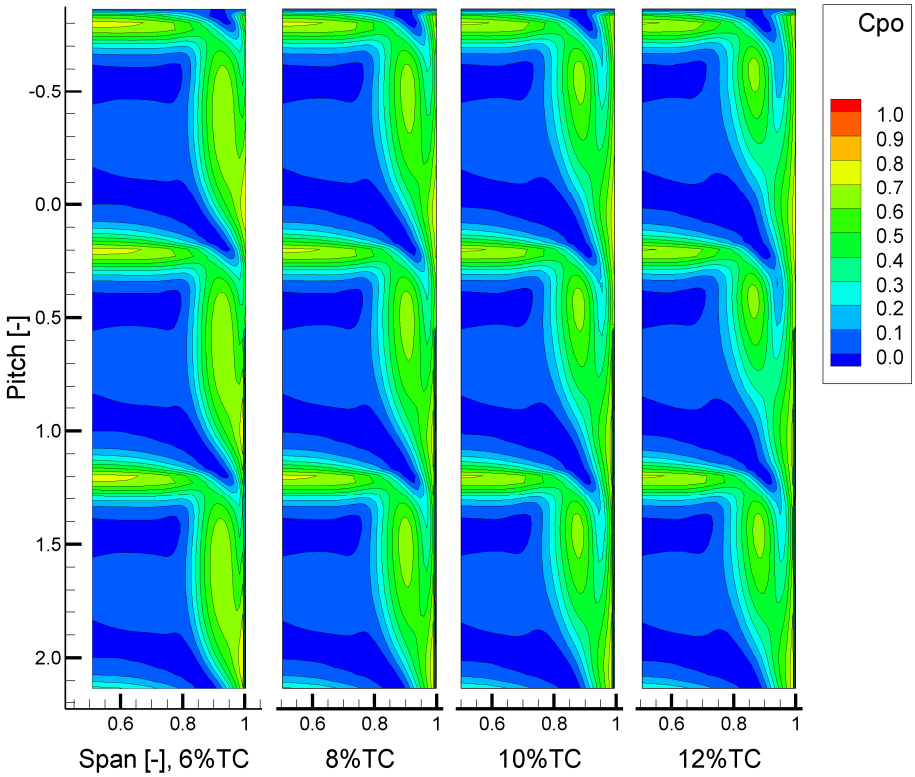

(b) Tip Clearances from 6%TC to 12%TC

Figure 5.32: *Natural Skew Inlet, CFD Cp_0 Contour Plots at 1.2Cx*

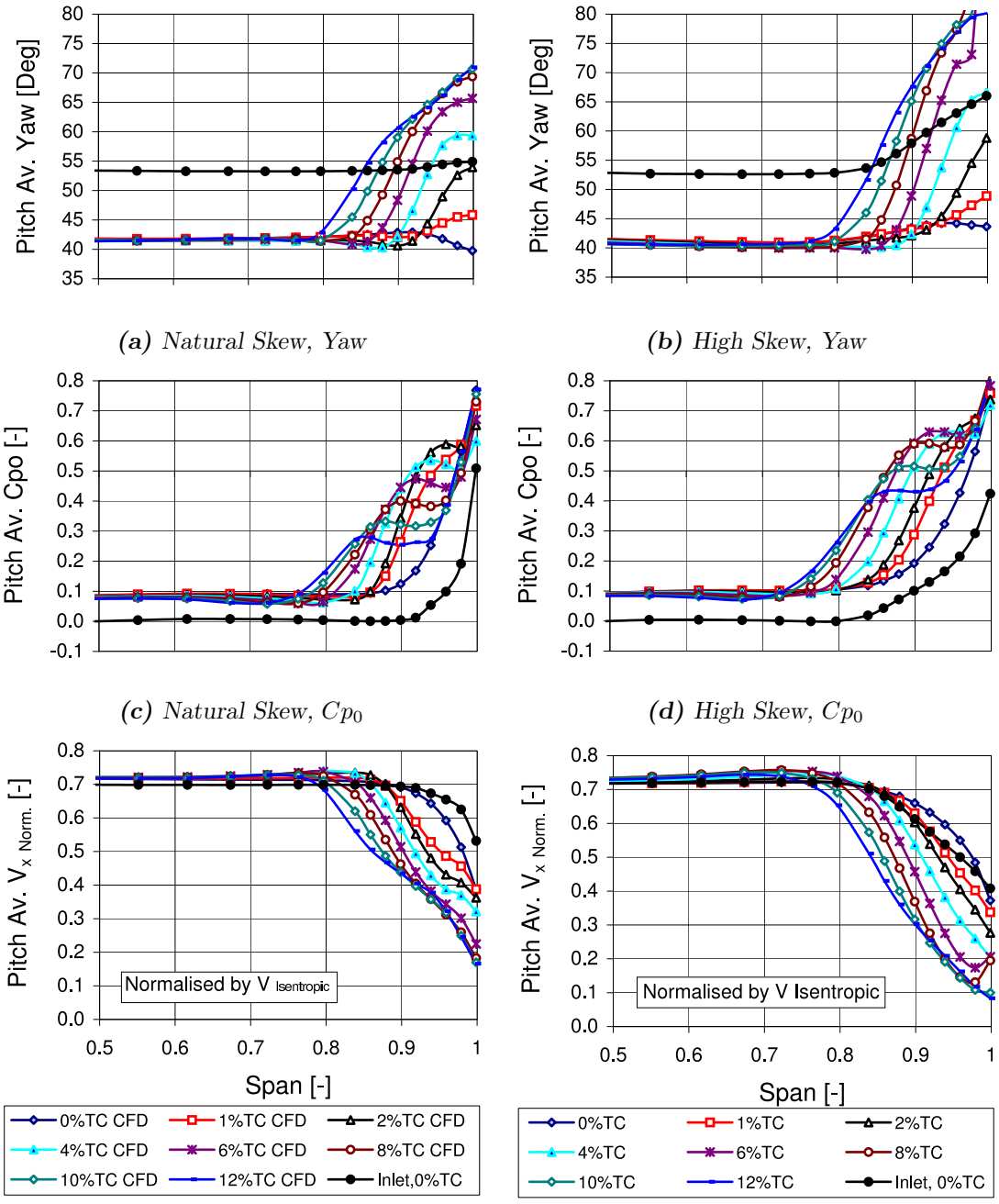

(a) Natural Skew, Yaw

(b) High Skew, Yaw

(c) Natural Skew, Cp_0

(d) High Skew, Cp_0

(e) Natural Skew, $V_{x,Norm}$

(f) High Skew, $V_{x,Norm}$

Figure 5.33: *CFD Results Pitch Averaged at 1.2Cx*

the CFD.

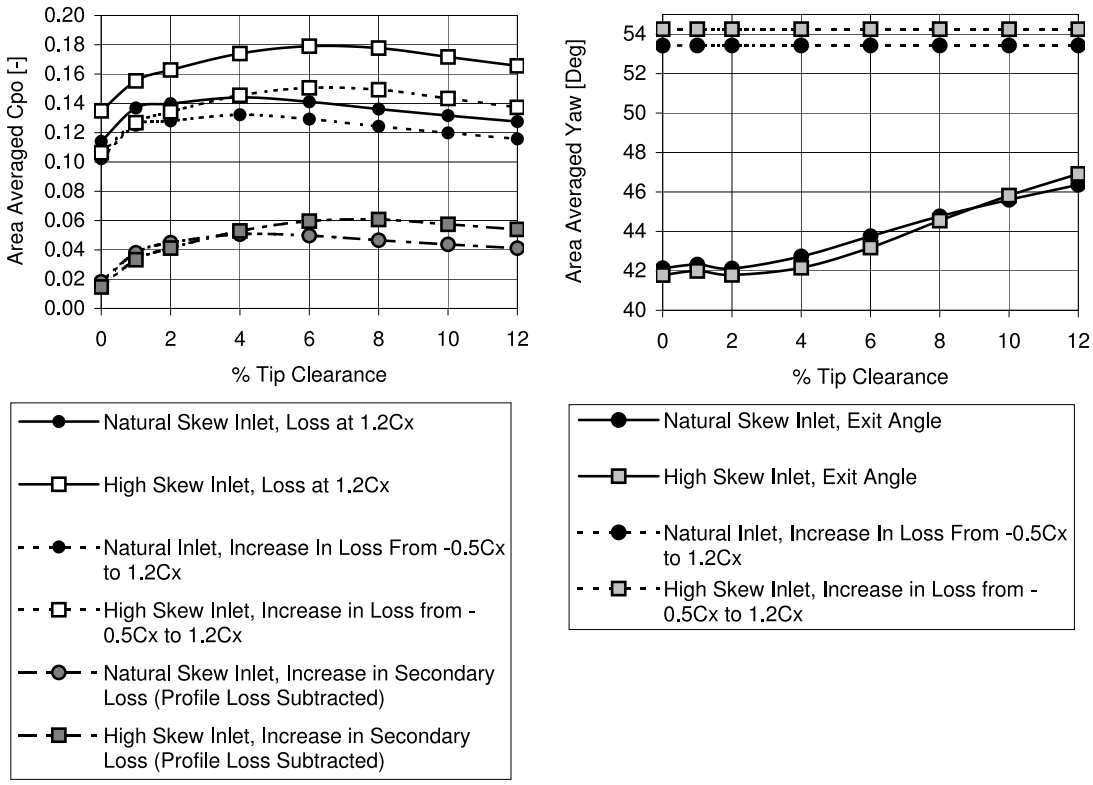

(a) Cp_0 *(b)* *Yaw*

Figure 5.34: *CFD, Area Mass Weighted Averaged Loss and Turning at 1.2Cx*

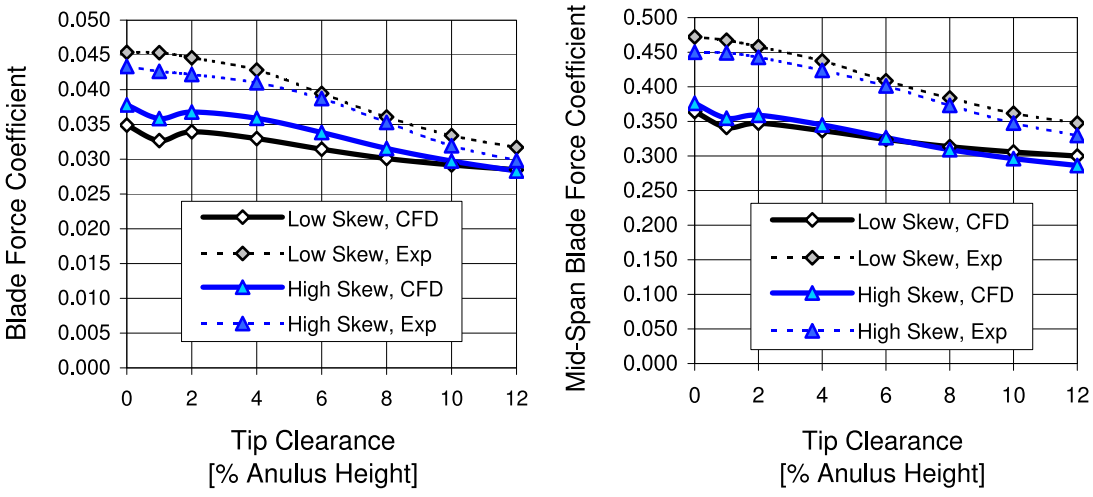

(a) *Total Blade Loading For Outer 50%Span* *(b)* *Blade Loading at Mid-Span*

Figure 5.35: *CFD, Total Blade Force Coefficient*

The computational blade loading along the length of the blade is shown in Fig-

ure 5.36. Although the magnitude of loading was lower, the patterns were again similar. At mid-span there was a reduction in loading with increased clearance. Towards the tip of the blade the increase in loading was larger for the low skew case. Importantly for the low skew case there was also a reduction in loading from mid-span to 0.9 span, this was important as it supported the experimental data.

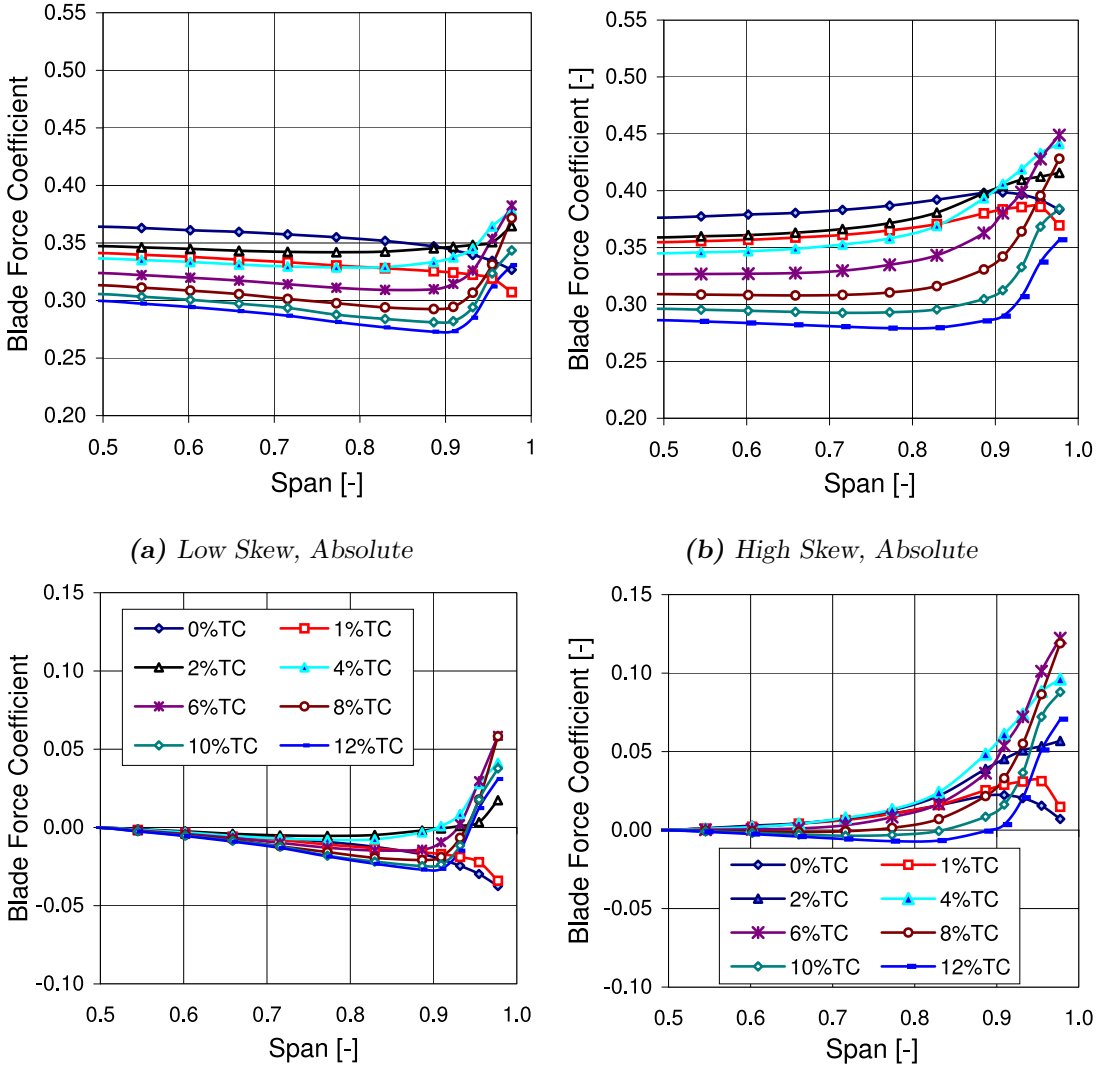

(a) Low Skew, Absolute

(b) High Skew, Absolute

(c) Low Skew, Zeroed at Mid-Span

(d) High Skew, Zeroed at Mid-Span

Figure 5.36: *CFD, Blade Force Coefficient*

5.3.3 Effect of Rotation

Computationally it was found for Build-A that the effect of relative casing motion was limited and predictable. This section explores the effect of motion with Build-B geometry, having higher stagger and lower loading. Figure 5.37 shows pitch averaged plots at 20% axial chord downstream of the cascade of yaw angle, axial velocity and loss, with and without relative casing motion with 6%TC and 10%TC.

The under-turning with 6%TC (Figure 5.37(a)) was significantly increased close to the casing with motion but this was not observed in the axial velocity plots. This was due to negative axial velocity fluid within the casing region resulting in the CFD code giving non realistic values. The more realistic pitch averaged value with 6%TC should be close to 80°. With rotation the pitch averaged loss profile was only changed marginally with motion. There was a decrease in loss on the casing and a peak loss increase associated with the leakage vortex for the 6%TC case but decrease with 10%TC occurred. A small reduction in the end-wall flow loss thickness occurred. With the larger clearance compared to the smaller clearance there was a smaller effect on the yaw and velocity but an increased effect on loss. An increase in yaw of 9° occurred for 10%TC on the casing with motion, which was much smaller than the smaller clearance yaw increase, but the loss increased by ≈ 0.25 as opposed to ≈ 0.15 for 6%TC. The value of yaw with rotation for the small clearance was however a questionable result and may have been due to an incorrect value from the code. Certainly the axial velocity was negative within this region for the 6%TC with rotation but not for the 10%TC clearance or the 6%TC without motion.

The pitch averaged plots (Figure 5.37) were undertaken at 20% axial chord downstream of the blade (1.2Cx). To further the understanding the pitch averaged changes Figure 5.38 shows loss contours through the cascade, from the leading edge to the 1.2Cx plane, with and without rotation for 6%TC. It is clear from these plots that the effect of motion was the same as for the low stagger cascade. The motion enhanced the over tip leakage flow, effectively dragging the fluid through the gap. This reduced the loss on the casing and the high loss counter rotating region. A small shift in vortex trajectory was observed away from the suction surface and closer to the casing, coupled with a lower pressure vortex core. The reduction of

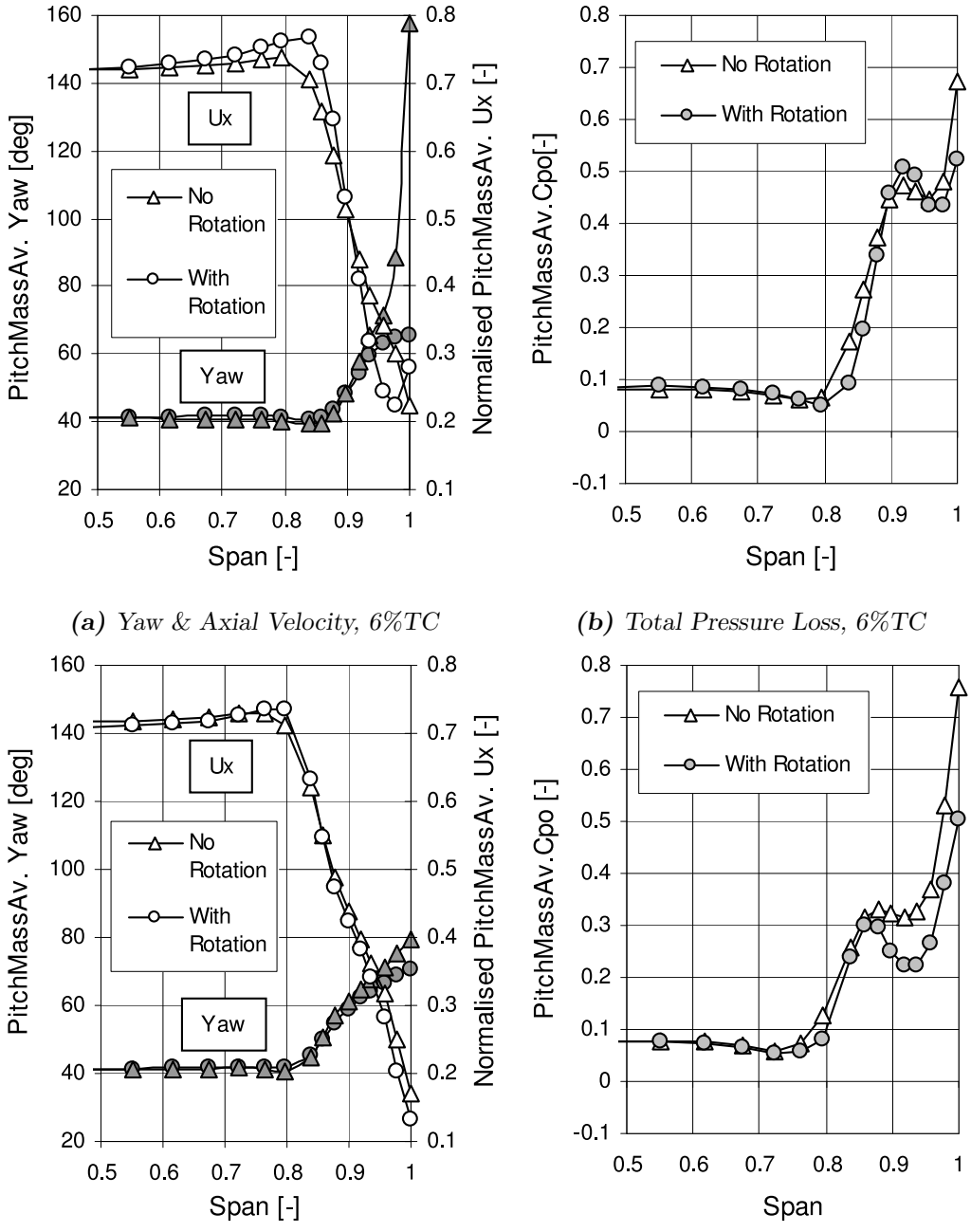

(a) Yaw & Axial Velocity, 6%TC

(b) Total Pressure Loss, 6%TC

(c) Yaw & Axial Velocity, 10%TC

(d) Total Pressure Loss, 10%TC

Figure 5.37: *Pitch Average Plots Showing Effect of Relative Casing Motion at 1.2Cx*

loss on the casing also reduced the loss within the clearance region. This therefore reduced the blockage within the clearance effectively increasing the clearance size and therefore moving the roll-up of leakage vortex slightly down stream.

Figure 5.38 shows the internal Cp_0 flow field with and without casing rotation. A slight shift in leakage vortex location across the passage and towards the casing occurs. This was similar to Build-A, the downstream plots were shown in Figure 4.1 on page 89. More low loss fluid was also seen to pass through the clearance at 0.6Cx and 0.8Cx.

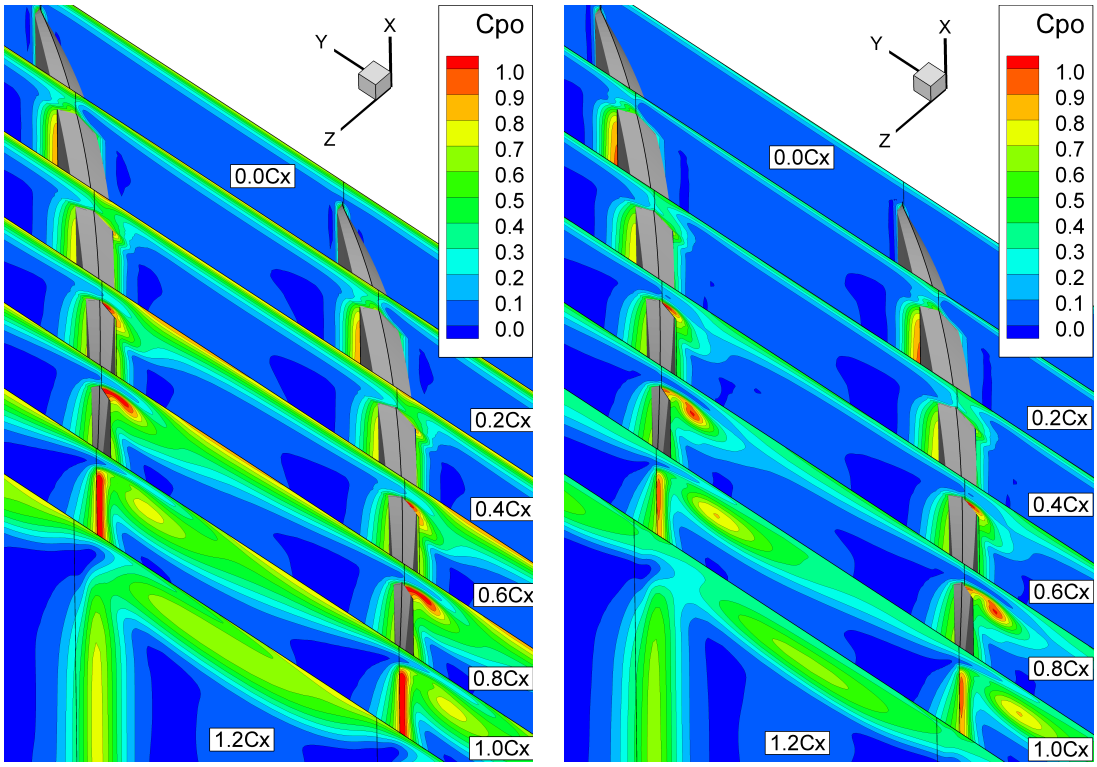

(a) *No Rotation* ***(b)*** *With Rotation*

Figure 5.38: *Cp_0 Contour Plots, Effect of Relative Casing Motion with 6%TC*

This study showed that, as with Build-A, the casing motion had a small and qualitatively predictable effect on the end-wall flows and that with increased clearance the effect was reduced. Therefore the linear cascade results were valid for tip leakage study.

5.4 Discussion and Conclusions

5.4.1 Discussion

This chapter has utilized both experimental and computational techniques to investigate the tip leakage flows within a cascade of high stagger (46.5°) and low turning ($\approx 10°$ turning) HPC engine representative geometry. This was in contrast to Chapter 4 where the cascade had low stagger (14.2° and higher turning ($\approx 30°$). Remarkably similar results have been found for both cascades leading to the conclusion that the stagger and blade turning are not dominating factors influencing HPC tip leakage flows. Rather the clearance size and stage turning had an impact on the leakage vortex and blockage. The skew also had a small influence.

It has been shown that the leakage vortex rolls up at a position within the blade passage of the highest peak loading and therefore the geometry can control this, but also increasing the clearance postpones this. Of significant interest was the leakage vortex trajectory dependence on clearance. For the larger clearances investigated the leakage vortex remained close to the suction surface and passed out of the rear of the cascade. This suggested that the vortex became independent of the casing for the high clearances behaving more like a wing tip vortex and therefore should be expected to create reduced blockage. Unfortunately a large blockage was still created by the flow which passed over the tip of the blade, interacted with the passage vortex and through the fluids shear on the casing formed a high loss region adjacent to the leakage vortex.

Due to the large passage, low momentum, high loss region it is still unclear how the clearance size affects the onset of stall. This high loss region blocked the movement of the clearance vortex across the passage. Stall generally occurs when the leakage flow moves around the front of the adjacent blade and therefore increasing the clearance to a high value would suggest that stall could be postponed by increasing the clearance. This potential was however thwarted by the fact that increasing the clearance also reduced the turning in the row, and therefore the work done, even if the blade loading was not significantly affected. Increasing the inlet skew incurred a larger blockage area but reduced leakage vortex core strength. This

would suggest that increasing the inlet skew would advance the onset of stall due to the higher flow angle and leakage vortex trajectory shift.

Increasing the clearance increased the blockage within the cascade and this was coupled with a decrease in turning. The CFD's turning prediction was close to the experimental data but the CFD predicted exit angle was offset from the experimental data. The reason for this offset was the CFD's inlet specification. The inlet angle to the CFD was set as for the measurement plane -0.5Cx, however as shown the angle on the blade was higher, therefore the CFD inlet angle was too low. The loss was computationally over predicted due to excessive computational diffusion; this was similarly found with the previous cascade. Despite the differences the CFD was useful and found to complement the experimental data.

Experimentally an almost linear reduction in blade loading was observed from mid-span to approximately 20% span from the tip of the blade. The reason for this was initially unclear but because it was observed within the CFD this was a real feature and not experimental error. Upstream traversing of the cascade showed no significant change in inlet angle apart from within the boundary layer and therefore the cause was an increase in pressure on the suction surface. This high pressure region was clearly evident in the experimental Cp_0 contour plots through the cascade. The mechanism was incoming low loss and high pressure fluid being moved against the suction surface of the blade via interaction with the leakage or secondary flows. This was also observed in the blade loading plots along the length of the blade; at mid-span a low pressure bump occurred suggesting separation which although not seen in the CFD (possibly because of the lower loading) then appeared to form a higher loss suction surface region at the trailing edge (again evident in the experimental contour plots, Figure 5.8 to 5.12 on Page 124 to 126). Closer to the casing this separation was suppressed by the leakage vortex moving high energy (high pressure) fluid on to the suction surface resulting in a thinner and in some cases almost non existent blade wake towards the blade tip. This thinning of the blade wake was not as evident within the CFD. An explanation was found in the blade loading variation along the blade which was not as large as for the experimentation. The reason was the under loading of the blade within the CFD prevented the suction

surface separation.

For the higher clearances an increase in blade loading occurred towards the tip of the blade; this counteracted the reduction in blade loading associated with the end-wall flows as found with no clearance and the smaller clearances. Increasing the inlet skew reduced this increase in blade tip loading because the leakage vortex moved further from the suction surface of the blade. The CFD showed the opposite affect to the experimental data, with increased skew the blade tip loading was decreased, and therefore questioned the validity of using a pinch tip model to mesh the clearance. Although for the higher clearances the pinch model appeared a valid method for obtaining an acceptable downstream pitch averaged prediction, it was not an appropriate option for obtaining an accurate prediction of the blade tip loading.

The flow over the tip of the blade was shown to remain unattached over the end of the blade for the larger clearance values but for the smaller clearances reattachment occurred. This followed the predictions from literature. The lowest pressure on the suction surface blade tip edge was found to be associated with the leakage vortex role up and this moved downstream from approximately 0.3Cx with 1%TC to 0.8Cx with 12%TC. The minimum pressure on the blade tip was reduced with increased clearance suggesting lower velocity fluid as would be expected within a separated region.

5.4.2 Conclusions

Tip clearance values between 0% and 12% span have been measured experimentally with a naturally thin low skew inlet and a highly skewed thick inlet boundary layer more representative of a real machine. The key findings are:

- Increasing the tip clearance above 1%TC incurs no further increase in loss through the cascade. The loss reduces with increased tip clearance until 10%TC where the loss was similar to the 0%TC case.

- A reduction in mass averaged turning occurred with increased TC gap. With 12%TC the turning was halved compared to 0%TC.

- Increasing the inlet boundary layer skew and thickness increased the exit gross loss. However the net loss increase through the cascade was reduced.
- The tip clearance vortex remained close to the suction surface of the blade rather than moving across the passage.
- This had the effect of increasing the loading on the blade and suppressing suction surface separation.
- Overall similar results were obtained for both inlet skew configurations investigated.

These conclusions are derived from results at the design condition and may change at off-design conditions.

Two different cascades, with different geometry and inlet conditions, have been computationally and experimentally investigated. For both cascade the end-wall flows were as expected, found to increase loss and reduce the turning within the cascade. As explored in the literature many attempts have been made to reduce the negative influence of such flows and circumferential grooves appeared a reasonable method. The next chapter investigates leakage flows with circumferential casing treatment implemented within Build-B. As changes were made to the cascade for the following chapter the altered cascade was termed Build-B1.

Chapter 6

Build-B1, Casing Treatment

As discussed in Chapter 2 there are many reported methods for the reduction of the blockage associated with over tip leakage flows. This chapter investigates the use of circumferential groves as a method for reducing the blockage. The casing treatment design chosen was that of Müller et al. [2007], which showed promising results in a rotating transonic compressor test rig. Within this chapter the design, experimental implementation, results and conclusions will be presented.

Circumferential casing treatment grooves were implemented on Build-B to form Build-B1, this was undertaken using interchangeable casing modules to allow for rapid alterations to the design to be made. These modules could be inserted from the outside of the cascade through the casing. Two modules were constructed and tested: firstly a smooth wall to represent the flat no casing teatment case; and secondly the grooved design. The cascades casing wall modifications are shown in Figure 6.1 where the casing module can be clearly seen. A significant re-build of the cascade was required and therefore upstream traversing was undertaken to ensure the correct inlet conditions and downstream traversing with the smooth module ensured there was no unwanted effects on the compressor through flow from the module. The natural and high skew inlets were investigated with a clearance value of 6%TC with the smooth and grooved wall.

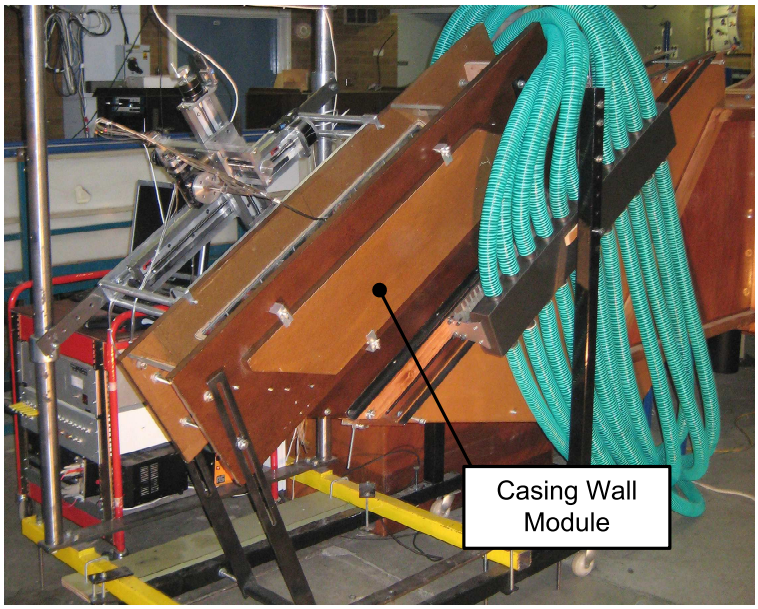

Figure 6.1: *Picture of Build-B After Casing Treatment Implementation*

6.1 Casing Treatment Design & Implementation

The casing treatment design was similar to Müller et al. [2007] but altered slightly for ease of manufacture. The groove design is shown in Figure 6.2, firstly Müller's design is shown and then the design used. There were 6 grooves that, for the used design, commenced at 10%Cx and finished at 0.95%Cx with a groove width of 10%Cx and distance between grooves of 5%Cx. The groove width to depth ratio was 1/3 therefore the groove depth was 42mm deep which corresponded to 20.6%C, 30%Cx or 23.3% cascade span.

As already stated the grooves were implemented onto the cascade through exchangeable modules located in the casing. Figure 6.3 is a sketch of the modules and Figure 6.4 shows a photograph of the grooves in the cascade. The modules extended the full tangential length of the cascade and the grooves extended to approximately half a pitch of the top and bottom passages of the cascade. 6 passages out of 8 were therefore fully covered by the grooves. The modules were made from the same material (Medium-density Fibreboard) as the cascade wall.

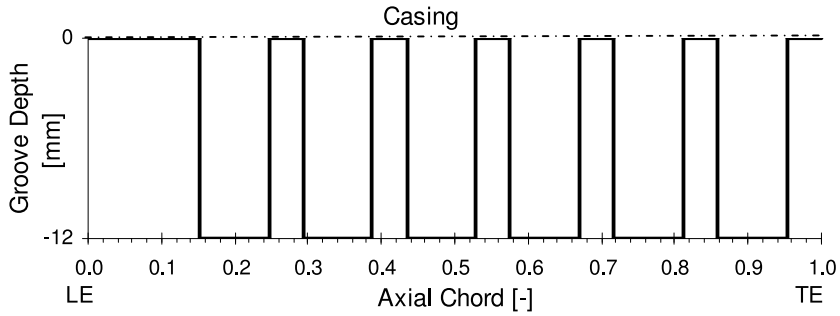

(a) *Müller et al. design*

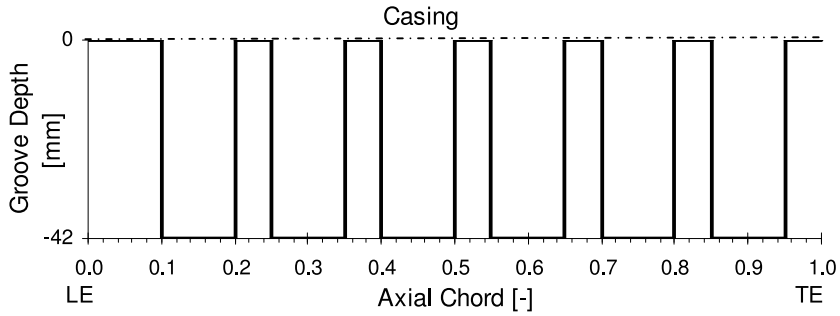

(b) *Used Design*

Figure 6.2: *Casing Treatment Groove Location*

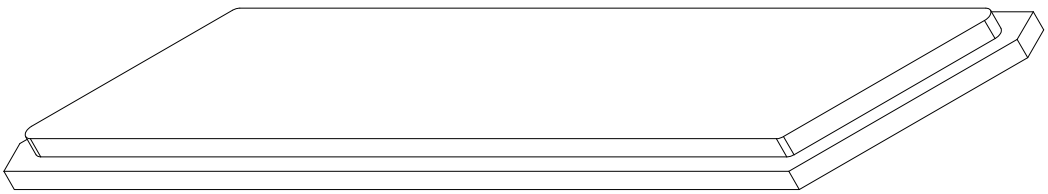

(a) *Smooth Wall*

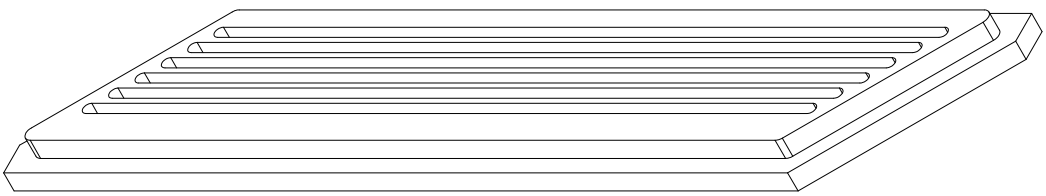

(b) *Grooved Wall*

Figure 6.3: *Casing Modules*

(a) View From Downstream *(b) View From Hub*

Figure 6.4: *Pictures of Grooves in Location*

6.2 Experimental Results

6.2.1 Cascade Inlet Conditions

Disassembly and reassembly of the cascade was required to implement the casing treatment and this process might have altered the inlet boundary conditions. Upstream traversing was therefore undertaken at the inlet traverse plane (-0.5Cx) as previously used and shown in Figure 3.17, on Page 73. A comparison between the inlet conditions before and after the modification for both inlet conditions with 0%TC are shown in Figure 6.5, showing pitch averaged results at inlet to the passages of interest (Pass-1 to Pass2).

The inlet total pressure, shown as loss in Figure 6.5(a), was practically the same after the changes as before; for both inlet conditions a slight decrease in loss at mid-span and increase on the end-wall's existed. The yaw (Figure 6.5(b)) increased by $\approx 1^\circ$ along the the majority of the span for the low skew. With the higher skew there was a 1° increased offset at mid-span but the angle on the casing was decreased by $\approx 2^\circ$ compared with before the changes. The axial velocity (Figure 6.5(c))was decreased at mid-span by $\approx 1ms^{-1}$ for both inlets, which complemented the yaw angle shift. On the casing the low skew had a similar offset but with the high skew the axial velocity was the same as before the changes. The difference in yaw angle was similar to the estimated error in measurement at $\pm 1^\circ$

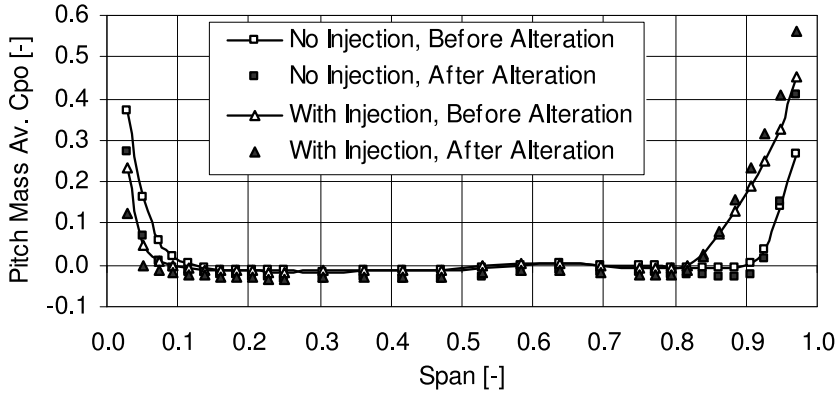

(a) Pitch Averaged Cp_0

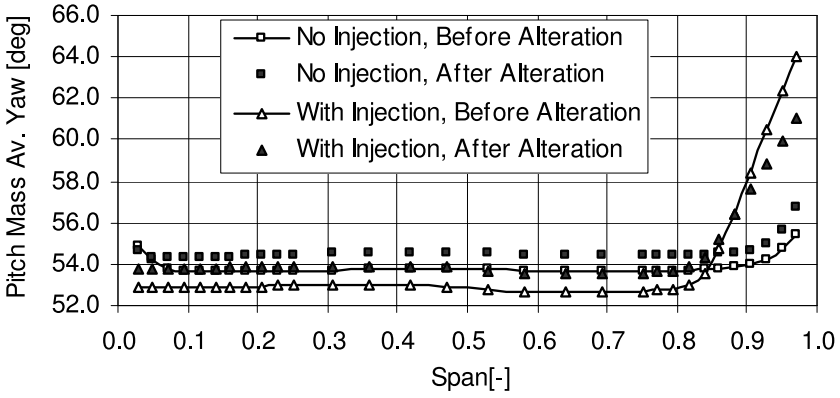

(b) Pitch Averaged Yaw

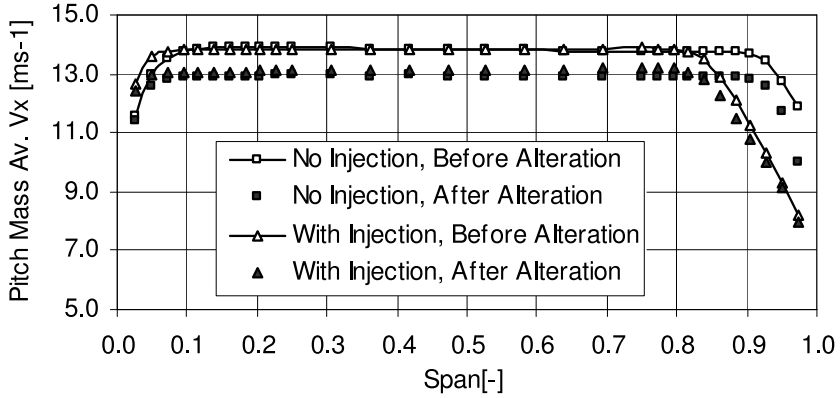

(c) Pitch Averaged V_x

Figure 6.5: *Inlet Conditions (-0.5Cx) Before and After Changes*

The reason for the changes in inlet condition were unclear but because the changes were small this was accepted. To ensure a direct comparison between the smooth and grooved casing downstream traversing was therefore undertaken with the smooth wall after reconstruction and those results are used for comparison in this section.

6.2.2 Exit Results

The flow structure downstream of the cascade is now shown and comparison made between the smooth and grooved casing. The exit traverses location and grid file was the same as for the previous results and was shown in Figure 3.17 on Page 73.

Comparison between the exit conditions before and after the rebuild can be found by Williams et al. [2008c]. A brief description of the changes follow. With 0%TC at mid-span the exit yaw angle was the same but there was a small reduction in loss after the rebuild for both inlet conditions. Closer to the casing there was however a reduction in over-turning of $\approx 3°$. This was coupled with a small reduction in blockage on the casing. These changes followed for both the 1.2Cx and 1.5cx axial traverse plane locations.

Figure 6.6 shows Cp_0 contour plots at exit (1.2Cx) for both inlet conditions and the smooth and grooved wall of Build-B1. With the smooth wall the contours closely match those before the changes of Build-B shown in Figure 5.4 on Page 119. For the smooth wall the contour plots (Figure 6.6) showed a small increase in leakage vortex magnitude and increase in loss area along the cascade from top to bottom. This flow structure indicated that the cascade was not truly periodic, however as this change was small and because the difference between clearances was the important factor this did not effect the results. With the circumferentially grooved casing treatment the periodicity was greatly reduced. For the top passage measured there was little change between casing modules but for the bottom cascade there was a significant change. This suggested that the effect of of the grooves was established over several passages and therefore the cascade was to short.

The pitch averaged (Figure 6.7) and area averaged (Figure 6.8) plots show a doubling of the loss with the casing treatment. A change in flow direction in the

bottom passage was also observed by the secondary velocity vectors indicating a lower tangential velocity within the end-wall flows than within the other two passages measured. As previously shown for 6%TC the effect of skew was small.

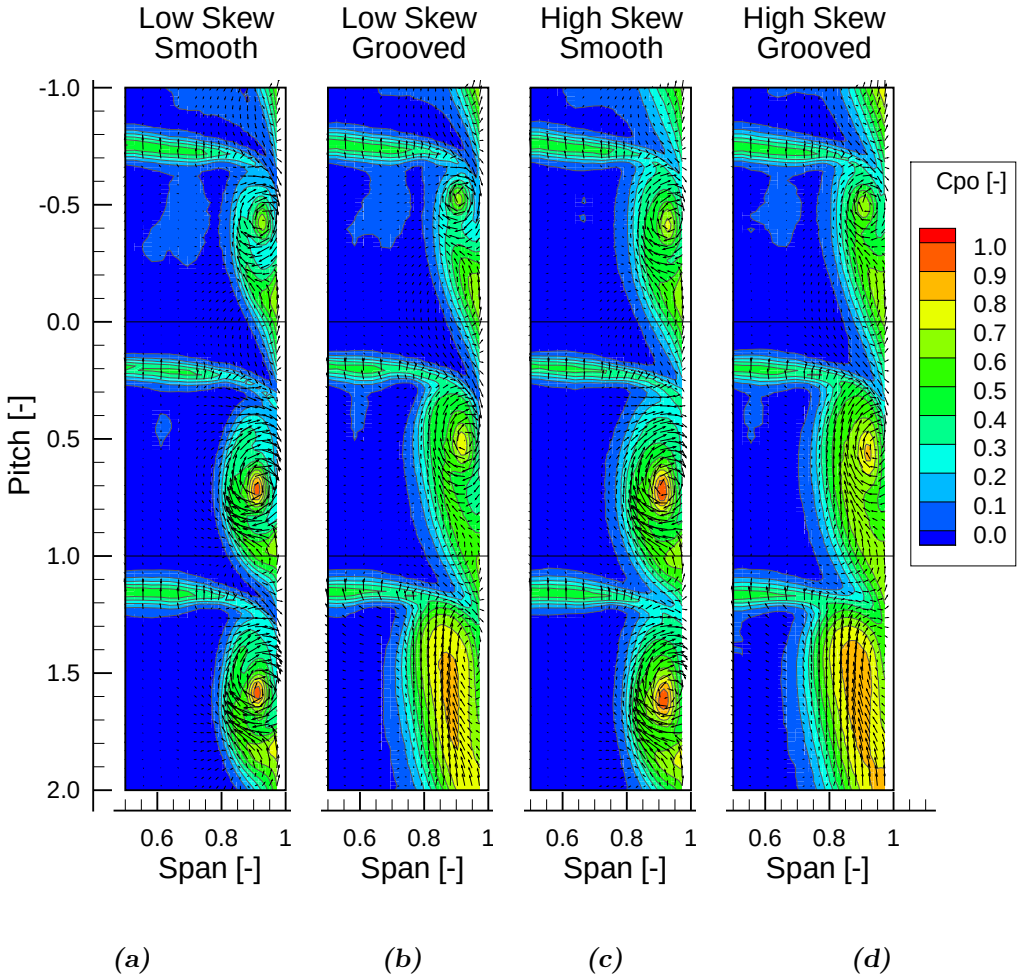

Figure 6.6: *Smooth vs. Grooved Casing, Cp_0 Contour Plots, 6%TC at 1.2Cx*

The effect of the grooved casing is shown in Figure 6.7, where pitch averaged yaw, Cp_0 and $V_{x,norm}$ are plotted at 1.2Cx and 1.5Cx. This was for 6%TC and therefore as previously found the effect of rotation was small compared to some of the other clearances; the skew increased the loss by ≈ 0.1 in the end-wall region and the Yaw and blockage were also marginally increased. With the grooved casing treatment the effect of increased skew was the same as for the smooth casing.

The effect of the grooves was to: slightly reduce the angle at mid-span (increase turning); significantly increase the yaw (decrease the turning) between 0.7 and 0.9

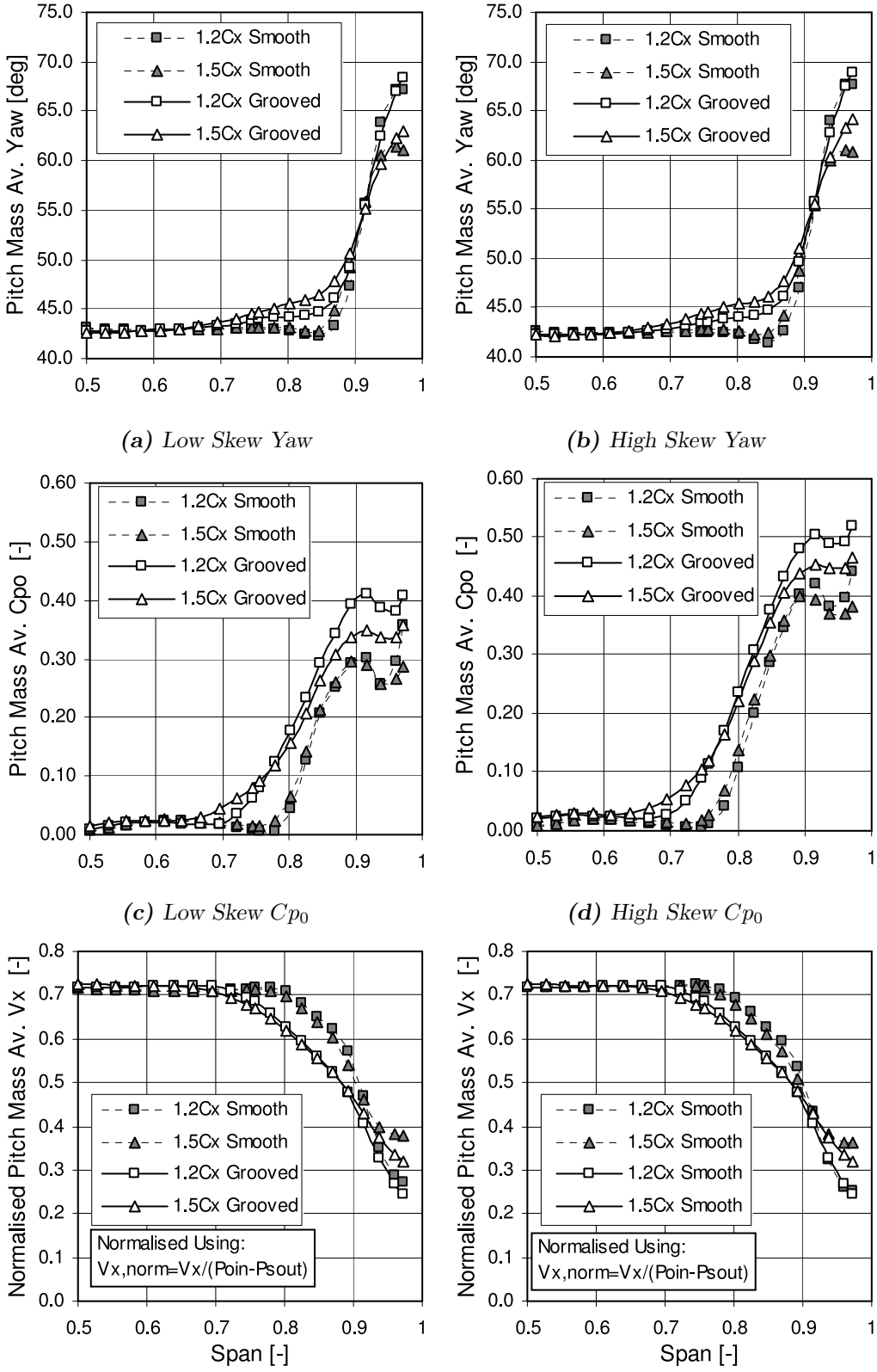

(a) Low Skew Yaw *(b) High Skew Yaw*

(c) Low Skew Cp_0 *(d) High Skew Cp_0*

(e) Low Skew $V_{x,norm}$ *(f) High Skew $V_{x,norm}$*

Figure 6.7: *Smooth vs. Grooved Casing, Pitch Averaged Exit Plots, 6%TC*

span; and further reduce the turning on the casing. This was paralleled by a significant reduction (0.1 of the dynamic head) in axial velocity between 0.7 and 0.9 span. A further reduction in turning and axial velocity with grooves was measured at 1.5Cx which was more so than for the smooth wall. There was a significant increase (≈ 0.1) in loss above 0.7 span with the grooved casing. It would also appear that there was a decrease in loss between 1.2 and 1.5Cx this however was clearly non-physical and was caused by a combination of the poor cascade periodicity and pitch averaging boundaries capturing different flow features.

The loss was further investigated in Figure 6.8; Figure 6.8(a) shows the total loss and Figure 6.8(b) shows the loss with the mid-span value deducted (Secondary Loss). The negative loss at input for the low skew was caused by the position of the pitot-probe and the poor total pressure periodicity. Both plots show the exit loss with the inlet loss deducted i.e. net loss. Again some of the loss with the grooved wall appeared to decreases from 1.2Cx to 1.5Cx but this was due to the pitch averaging boundaries capturing different flow features. These plots clearly show that an increase in overall loss of approximately 50% occurred with the circumferential groove casing treatment compared to the smooth wall.

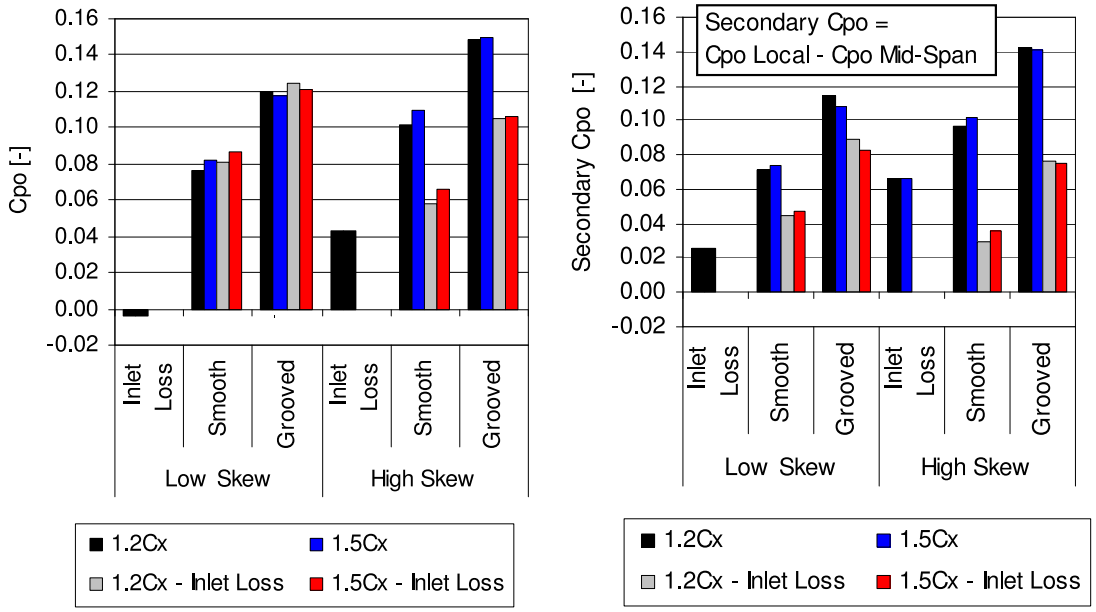

(a) *Cp_0* **(b)** *Secondary Cp_0 (Mid-span Subtracted)*

Figure 6.8: *Smooth vs. Grooved Casing, Area Averaged $Cp0$*

6.3 Discussion and Conclusions

Within this chapter circumferential grooves were investigated in a linear cascade. The aim of circumferential grooves was to reduce the end-wall blockage and underturning without reducing efficiency or increasing loss. Within this work this was undertaken at design condition. The circumferential grooves were implemented on to Build-B by adding interchangeable casing modules to the cascade. Traversing was undertaken to ensure a similar inlet to the previous measurement campaign reported in Chapter 5, acceptably similar agreement was found to the previously measured result.

The circumferential grooves were investigated through downstream traversing at 1.2Cx and 1.5Cx with a tip clearance of 6%, which was chosen because of its engine applicability. Comparison was then made against the cascade with the smooth casing module. The casing treatment was found to increase the loss and blockage and decrease the turning, therefore opposite to the desired effect. The reason for this was not entirely clear but was probably as a result of the poor periodicity of the cascade and so linear cascades are not an appropriate method for investigating this. The flow at exit of the cascade with the casing treatment had poor periodicity. At the highest passage exit measured the grooves had little influence on the normal cascade end-wall flows, but further down the cascade (Pass2 exit) there was a significant change in the flow patterns. This suggested that the grooved effect required several passages to develop and a 9 passage cascade was not long enough to investigate this.

Although it appears, from these results, that the grooves increase the loss and blockage and decrease the turning at the operating condition the lack of periodic flow means these results have to be viewed with caution. Therefore from these results the author cannot stipulate if circumferential grooved casing treatment is beneficial or not within high pressure compressor stages. Furthermore only one clearance value, one operating condition with one casing treatment design were investigated. Circumferential grooves have been proved to work for transonic flow where the flow is affected by shocks and this may be a fundamental mechanism towards a positive outcome. Further work is required to explore the practicalities and the flow physics within the end-wall region with circumferential grooves. Unfortunately the appli-

cation of a linear cascade, of the type used within this thesis, appears not to be appropriate for such work.

This chapter failed to conclude if circumferential casing treatments are an appropriate method for HPC stall margin increase. The use of linear cascade testing was not appropriate for such investigations and a rotating method of investigation should be used. The next chapter will explore and discuss the findings from this thesis, link them to the literature and the industrial context.

Chapter 7

Overview and Discussion

Tip clearances representative of high pressure industrial axial compressors have been investigated using experimental and computational techniques. Within literature little work has been undertaken examining such clearances and the influence on the compressor's performance. This chapter will further the discussion undertaken within the results chapters, pull together the findings of this thesis and relate them to the literature.

The aim of this thesis was to: investigate the influence of large clearances on compressor blade row loss and performance; investigate the influence of geometry; investigate the influence of inlet conditions and inlet boundary layer skew on clearance flows; and investigate methods for reducing the loss and blockage associated within the endwall flows of such compressor rows.

This thesis used two different linear cascades with different geometry and inlet flow conditions. The first cascade had low stagger and fairly high turning and the second cascade had higher stagger with lower turning. Both cascades were moderately loaded with a diffusion factor of approximately 0.3. The comparison between the results of the two cascades will allow for the influence of the geometry, inlet boundary layer, stagger and blade turning on the over tip leakage flow and its effect on row performance.

Build-A (from Chapter 4) had low stagger (14.2°) and high turning ($\approx 30°$) unlike Build-B (from Chapter 5) which was more engine representative with a high stagger (46.5°) and lower turning ($\approx 10°$). Therefore the two geometries had a marked

difference in mainstream (mid-span) flow. Despite their differences in flow angle the diffusion factors of the cascades were similar. Build-A had a design diffusion factor of 0.32 and Build-B's was 0.29, both of which are low compared to a general design value of 0.45 (as stated by Cumpsty [1989]).

7.1 Experimental and Computational Methods

The CFD within this thesis allowed for further investigation that was either not possible or too time consuming if undertaken experimentally. All experimental and computational investigations within this work concerned linear cascades. This allowed for detailed measurement within the passage. The difference between the real machine and the linear cascade was discussed and the influence of the relatively moving casing investigated. Qualitatively the CFD over predicted the loss and over diffused the flow structures. The simulations however predicted the endwall flow structures well and the changes with increased clearance followed the experimental pattern. For the small clearances in the region of 2%TC or less the prediction was poor and this was found to be caused by the pinch meshing model. The outcome was similar for both cascades.

7.1.1 Pinch Tip Model

The reason for this was because the pinch model predicts a vena-contracta over the tip of the blade (e.g. Storer and Cumpsty [1991], Van Zante et al. [2000] & Gupta et al. [2003]). However as explained in the literature if the flow reattaches on to the tip of the blade then a vena-contracta cannot be assumed and fully meshing the region is the better option. Glanville [2001] showed that if the aspect ratio of clearance size to blade thickness was less than 0.4 then reattachment on to the blade tip would occur. This was valid for this work where an aspect ratio of 0.4 equates to a clearance size of $\approx$ 2.4%TC. Build-A's downstream pitch averaged results for 0%TC and 6%TC showed good agreement between CFD and experimental results but for the small clearances the agreement was poor suggesting that this criteria held and the CFD was capable of modelling the flows. For Build-B the downstream

pitch averaged CFD and experimental agreement (Figure 5.30) was poor at 2%TC and below and also the blade tip pressure on the SS and PS edge was significantly different. Above these values the agreement was better and the pressure on the tip of the blade was similar on the SS and PS edge (Figure 5.26).

The use of a pinch tip was justified for the modelling of large clearances. If the subject of this thesis had been small clearances then full meshing of the clearances region would be required. The CFD aided with these investigations as it filled in the gaps where experimentation was not undertaken.

7.1.2 Use of a linear Cascade

The choice of a linear cascade allowed for measurements surrounding the blades and within the passage; the total pressure could also be measured. This would not have been easy or practical within the rotating environment measurement which would have been extremely complicated, expensive and difficult so beyond the scope of the available resources. For both cascades, simulations were undertaken with a stationary and moving casing to assess the differences. The result justified the use of the linear cascade for this application.

The casing motion was found to pull the fluid on the casing through the clearance and in doing so move the roll up point of the leakage vortex slightly upstream and shift its trajectory slightly across the passage. A reduction in the relative shear on the casing reduced the induced vortex and the cross passage flow and so reduced their associated loss region. The relatively moving casing reduced the shear work on the casing and because of its motion added energy to the passage in the relative frame reduced the end-wall loss. The outcome of the motion was therefore found to move the vortex slightly and decrease the loss within the end-wall region. A linear cascade with a stationary wall therefore over predicts the loss and slightly under predicts the leakage vortex's trajectory.

A rotating test rig would further aid with these investigations in proving that these findings are correct. The CFD modelling of a rotating machine would be advantageous to decide if such experimentation were required.

7.1.3 Upstream Skew Experimentation

Build-B included an upstream injection method to control the inlet boundary layer skew and thickness; this was successful. The inlet boundary layer was found to move the leakage vortex roll-up further upstream and move the leakage vortex slightly further across the passage with an overall increase in blockage and loss. The change on the casing in pitch averaged exit yaw angle and loss was found to be similar to the change at inlet. For this work the conclusions for both inlet findings were similar and so for future work it may not be necessary to simulate the correct upstream conditions closely.

7.2 Tip Leakage Flow Discussion

7.2.1 Without Clearance

Without clearance both cascades showed the classic under-turning and then over-turning of the flow towards the casing. The over-turning on the casing for Build-A was much higher at $\approx 10^\circ$ than for Build-B at $\approx 3^\circ$. This over-turning on the casing was therefore approximately three times higher for Build-A than Build-B, similar to the mid-span percentage turning decrease. As Cumpsty [1989] explained this was due to the higher camber and therefore turning of the blade in Build-A generating a stronger passage vortex. The increased inlet skew for Build-B had little effect on the over-turning.

Without clearance the end-wall loss increase through the cascade was small for Build-A and Build-B with the high skew but Build-B with natural (low) skew had a larger loss increase. Therefore the increase in skew on the casing appeared to decrease the loss increase through the cascade. A credible explanation for this was that the increased skew opposed the cross passage secondary vortex and therefore reduced the suction surface corner separation. This appears to be a feasible explanation when comparing the exit contour plots of Build-B (Figure 5.3 on Page 118 & Figure 5.4 on 119). Without clearance a more uniform loss area on the end-wall across the full pitch was evident with the higher skew than the natural skew. Also

the blade wake and end-wall interaction region showed the possibility of a small separation with the natural (low) skew.

The CFD modelled the cascade without clearance well for both cascades. For Build-A a clear passage vortex and corner separation was evident. An increased loss area on the SS corner existed for Build-B showing that low momentum fluid had gathered there. This fits with the increased camber of the blading with Build-A setting up a stronger cross passage flow than for Build-B and therefore having a stronger passage vortex and corner separation.

7.2.2 Small Clearance

With the small clearance of 1%TC, from the experimental data, Build-A still exhibited over-tuning on the casing but Build-B had under-turning. The reason for this was due to the higher camber of the blade increasing the cross passage flow. This was evident in the experimental (Figure 4.5 on Page 95) and computational (Figure 4.8 on Page 100) contour plots for Build-A with a clearly evident cross passage flow and induced counter rotating vortex adjacent to the leakage vortex. For Build-B there was no cross flow associated with the passage vortex, but there was a reduced tangential velocity and a loss region in place of the counter rotating vortex suggesting that a weak feature may have existed there. The inlet skew had little effect on Build-B's exit angle. The CFD at low clearances showed reasonable flow structure but the qualitatively results were poor.

With 2%TC both cascades had under-turning on the casing, of approximately 10°. Again the skew had little effect (with 2%TC) on Build-B's exit angle and because the first cascade also had 10° of skew the geometries turning appeared to have little influence on the under-turning at exit but rather the end-wall flow structure.

For Build-A the passage vortex was clearly evident at 1%TC and reduced at 2%TC. For Build-B the CFD leakage vortex propagation was much larger and did not match the experimental prediction. Therefore these results were not used.

7.2.3 Large Clearance

With 6%TC both cascades (Build-A and Build-B with high skew) had a similar under-turning of 30° on the casing. Therefore the exit under-turned angle was not dependent on the geometry but instead the amount of skew on the casing at inlet. This was further supported by the lower under-turning with natural skew for Build-B; but also when comparing the CFD results of Build-A with no inlet skew in Section 4.1.1 and Build-A with inlet skew in Section 4.3, the later had an increased exit under-turning with the increased inlet boundary layer.

The roll-up point of the leakage vortex, for both cascades, was found to move downstream with increased clearance as shown by Storer and Cumpsty [1991]. This occurred for both inlet skew conditions of Build-B. Increasing the skew moved the roll up point upstream which was also shown by Storer and Cumpsty [1991] and also Brandt et al. [2002]. As well as the the roll-up of the leakage vortex moving downstream with increased clearance the leakage vortex trajectory also remained closer to the suction surface and was reduced in size for the larger clearances. The leakage vortex therefore had reduced dependency on the end-wall, behaving more like a wing tip vortex. This reduction in vortex size and strength reduced the overall loss for Build-B compared to the small clearances and had no further increase in loss for Build-A. This was however accompanied by a decrease in turning and increase in blockage. The change in turning was due partly to the end-wall flows and also to a mid-span change in blade loading. This result was of interest as if the compressor could be designed to accommodate the blockage, then the loss increase would not be as large as previously thought while having similar stage loading characteristics. This would require the mid-span design to accommodate the redistribution in mass flow caused by the clearance flows. Within the multi row environment, the next row must also accommodate this redistribution and the end-wall flows.

Although the loss does not increase with increased clearance and for the higher clearances, the yaw angle and blade length are reduced. Through an increase in the blade loading at the tip, with increased clearance, the blade loading decrease was not as significant as might be expected. The efficiency is however, still reduced with increased clearance although no further increase in loss occurs. This is because of

the reduced turning and shortened blade meaning that the work done by the row is lower than with a small clearance with a longer blade and higher overall turning.

7.2.4 Loss Through Cascade

Figure 7.1 compares the experimental mass weighted averaged Cp_0 loss increase, for the outer 50% Span, of both cascades and both inlet conditions of Build-B. Without tip clearance the loss increase for Build-B was approximately sixty percent of that of Build-A. Removing the mid-span profile loss showed that the secondary loss increase was similar for both cascades. A small clearance increased the loss for both cascades and again at 1%TC the secondary loss increase was similar for both cascades and inlet conditions. Between 2%TC and 6%TC Build-B's loss plateaued but Build-A's secondary loss increased further until 6%TC. Above 6%TC Build-A's secondary loss CFD prediction plateaued and Build-B's (for both inlet conditions) was reduced. This reduction in loss for Build-B may have been partly due to the reduction in cascade loading.

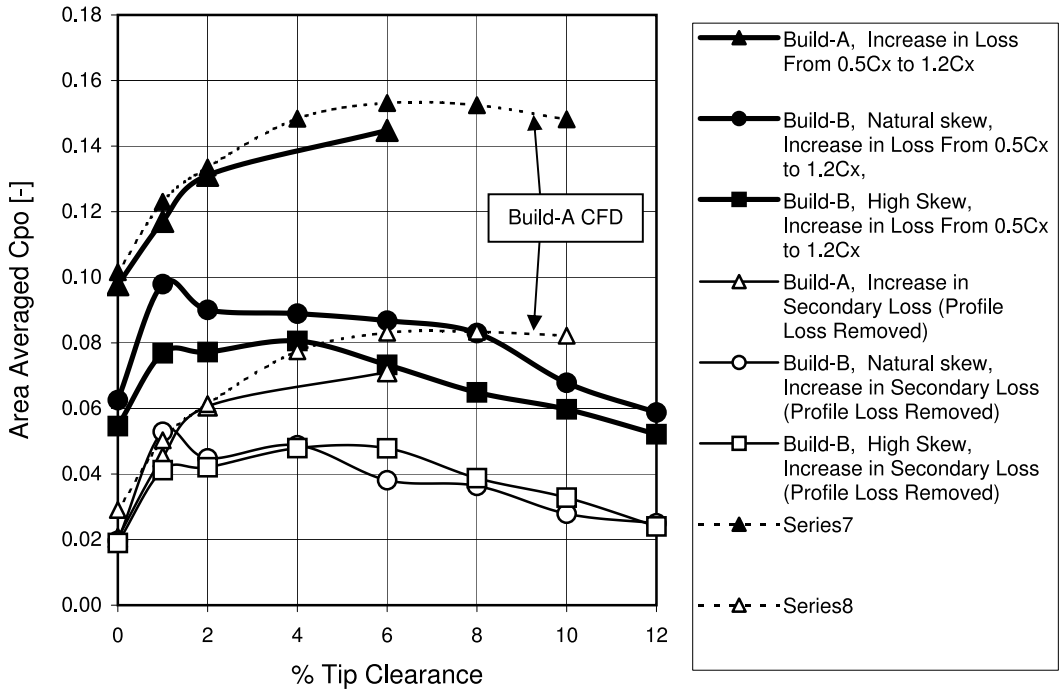

Figure 7.1: *Area Mass Weighted Averaged Experimental Cascade Loss Comparison*

At small clearances the difference between secondary loss of both cascades was small. The difference in secondary loss increased until at 6%TC Build-A's secondary loss increase was approximately twice that of Build-B. The geometries influence on the secondary loss was therefore small with a small clearance, in the region of 1%TC; and the geometries influence increased with increased clearance. This may be as a result of the blade tip loading which with 6%TC was 0.15 for Build-A and 0.1 for Build-B compared to mid-span. Suggesting that the blade tip leakage driving force may have an influence on the loss increase through the cascade. This is perhaps unfortunate as the increased tip loading also improved the overall blade loading of the compressor. For this reason if large clearances are unavoidable, as within the context of this thesis, then the geometry of the blade tip is essential to minimise the secondary loss which is dominated by the leakage flows.

As the secondary loss increase was found to be the same for both inlet conditions of Build-B then the effect of the inlet skew was found not to affect the loss increase through the cascade but rather the blockage and leakage vortex trajectory. Any further loss increase with increased skew in the machine must therefore be due to the increased blockage and its effect on the downstream stator root corner separation.

7.2.5 Flow Coefficient

All testing and computations were undertaken reasonably close to design conditions and therefore the blade row loading has not been considered within the testing of both cascades. For a higher loading condition close to stall the features will be somewhat different. Brandt et al. [2002] and Saathoff and Stark [1999] are two examples of work within the literature which investigated the increase in row loading. Both showed that with an increased inlet angle or higher loading, the vortex moved across the passage and then eventually passed around the front of the adjacent blade. When this occurred the compressor end-wall region stalled and the total pressure increase was diminished from the operating point. No investigations have been undertaken at higher loading, close to stall, within this thesis. However it is the author's view, that because increasing the clearance resulted in the flow becoming less dependent on the casing, and therefore remaining closer to the blade suction

surface, then this would delay the onset of stall.

Both Brandt et al. [2002] and Saathoff and Stark [1999] used a clearance of 3% of the chord and therefore not representative of the HPC. However, interestingly Brandt related the clearance to the incoming boundary layer thickness. He found that increasing the inlet boundary layer thickness forced the roll up of the clearance vortex to move upstream, similarly to increasing the clearance. This was also found within this thesis for Build-B, for all the clearances measured the higher skew moved the vortex roll-up upstream. Therefore increasing the boundary layer thickness will have a detrimental influence on the stall mass flow, but as found for Build-B increasing the clearance to a large value above 6%TC reduced the movement of the leakage vortex across the cascade. As Hunter and Cumpsty [1982] and Saathoff and Stark [2001] showed, one mode of stall which can occur in such compressor rows is when the leakage vortex moves around the front of the adjacent blade. Therefore it follows that postponing the movement of the vortex across the passage may postpone the onset of stall. So increasing the tip clearance size may increase the stall margin but this requires further work to assess this hypothesis.

7.2.6 Blade loading

For both cascades an increase in blade loading occurred at the tip of the blade with the highest clearances. This feature was also reported by Storer and Cumpsty [1991] who varied the clearance up to 4% of the chord. For their largest 4% clearance a small increase in blade load at the tip was found, but for one and two percent they had a decline in loading towards the tip. Both cascades, within this thesis, also underwent an increase in loading above 4%TC and this was seen to increase further up to approximately 8%TC where no further increase in blade tip loading occurred. The mechanism behind this was found to be the interaction of the leakage vortex with the SS of the blade. High velocity fluid within the vortex lowered the pressure on the suction surface. This was also coupled with a reduction in PS pressure at the tip of the blade which decreased in pressure with increased clearance. The mechanism behind this was flow accelerating, and so undergoing a reduction in pressure, around the tip of the blade.

This again suggested that for these large clearances the clearance vortex became independent of the casing. With Build-A the blade loading coefficient was increased with clearance value until a plateau at 8%TC, however for Build-B there was a reduction above 4%TC which was attributed to the blockage increase decreasing the blade loading along the full length of the cascade. In Storer's (Storer and Cumpsty [1991]) case and with Build-A the blockage had less influence on the blade loading away from the casing than with Build-B. The reason for this was due to the larger blockage found with build-B than Build-A.

7.2.7 General Discussion

The choice of clearance within the engine is usually set for mechanical reasons. This clearance is generally kept to a minimum as it significantly affects the operation of the engine and this is indeed still the case within the HPC. The problem within the HPC is that the clearance is larger than the optimum and cannot be reduced. It is shown from these results that increasing the clearance is not as bad as previously thought for HPC geometry. For Build-A a levelling and for Build-B a reduction of loss was found with increased clearance. This was coupled with an increase in blade loading towards the tip of the blade and therefore a smaller reduction in blade loading than expected. This reduction in blade loading was partly due to the reduction in blade length but also due to a reduction in the mid-span inlet angle. A change in the operating condition of the inlet fan due to the increased cascade blockage caused this; a change which may also occur within the real machine. A significant reduction in turning was also found to occur with increased clearance; which was a result of the increased exit skew area.

Above 6%TC the leakage vortex was found to move closer to suction surface. This was however coupled with an increase in thickening of the end-wall loss and low momentum fluid from the casing, so the overall blockage still increased. This is an important result as it means that the stall of that stage may be reduced by increasing the clearance. That is as long as the leakage vortex trajectory and the velocity on the casing are the dominant factors which lead to stall. Therefore if the engine stalls within that stage then increasing the clearance may be beneficial

to increase the stall margin of the engine. This hypothesis would require further investigation to assess it.

7.3 Casing Treatment

Casing treatment is generally used to decrease the blockage within a compressor and therefore increase the operating range. Many forms of casing treatment have been proposed within the literature and some of these have shown promising results without reducing the efficiency. This thesis investigated the use of circumferential slots within Build-B, termed Build-B1. The design chosen in conjunction with Alstom was the same as used by Müller et al. [2007]. This design, as discussed in Section 2.7.4 on Page 40, had previously been reported to show potential within a rotating transonic compressor test rig.

As the working mechanism of circumferential grooves can operate at low speed and does not rely on the relative motion of the rotor and casing, it was thought that the linear cascade may have been an appropriate testing method. Unfortunately the periodicity of the cascade within the end-wall region was reduced to an unacceptable level with the grooved casing. For the top passage exit measured (Pass-1) the effect of the grooves was negligible. At the bottom measured passage exit (Pass-2) a significant change occurred. This suggested that the casing treatment mechanisms were formed over several passages. For this reason it was concluded that Build-B1 was not capable of such casing treatment investigations. The author speculates that a longer cascade with more blades may have helped but cannot conclude if the linear cascade is an appropriate method to use.

This casing treatment was found to incur a small decrease in turning, increase in loss and increase in blockage at the cascades design point. However it was not clear if this was a real result or due to the cascades poor periodicity. Furthermore because this was undertaken at design condition it is not clear if this method would aid the stall margin.

The working mechanism of circumferential grooves was investigated in the literature (e.g. Lu et al. [2006b], Müller et al. [2007], Perrot et al. [2007] and Yu [2004])

and found to be the removal of the high pressure flow on the PS blade tip in to the slots, thus reducing the immediate cross blade tip flow and the blade tip loading. This removed flow then emerged within the passage low pressure region. A reduction in the over tip clearance flow momentum therefore reduced the clearance vortex roll up keeping the leakage vortex closer to the suction surface of the blade. This change in leakage vortex trajectory towards the blade suction surface and reduction in core strength was evident within these results. Therefore the casing treatment may reduce the onset of stall. The increase in total loss was associated with an increase in the mid-pitch loss, which without casing treatment was associated with the passage vortex and leakage vortex interaction. With the casing treatment this was further complicated by the flow exiting the grooves. Further investigations would be required to ascertain the internal passage flow physics.

Although these casing treatment results did not allow for any conclusions to be made, it has shown that there is potential with this method. The leakage vortex was moved closer to the blade's suction surface which at higher row loading would postpone stall. Therefore circumferential casing treatments could be used to increase the operating range of high pressure compressors.

From the evidence it is unclear how the tip clearance size affects the use of casing treatment. For the larger clearances investigated (smooth casing), it was found that the clearance vortex became independent of the casing and the leakage vortex remained close to the suction surface of the blade. This outcome is similar to how circumferential grooves work and therefore increasing the clearance may be a more appropriate method of controlling the stall margin rather than using circumferential grooves. Increasing the clearance was shown in Chapter 5 to reduced the loss but casing treatment generally increases the loss. The preferred method may therefore be to increase the clearance.

Other groove designs within the literature may be an improvement. Perrot et al. [2007] investigated the influence of each groove on a five equally spaced design. He found that the first grooves in the row were of benefit at high throttling, but at design conditions the later grooves were of benefit. Therefore if the HPC stages are not the driving force behind engine stall, and the vortex always remains within

the passage, then the first grooves may not be required and the later grooves could reduce the blockage.

The next chapter will conclude this thesis. Some recommendations on potential future work will also be given.

Chapter 8

Conclusions

This thesis aimed to further the understanding of relatively large tip clearance flows such as those found within the high pressure stages of industrial gas turbines. A measurement campaign on two compressor cascades was undertaken. Build-A consisted of low stagger and reasonably loaded geometry and Build-B had greater engine representative geometry with higher stagger and lower loading. The measurement techniques used were 5-hole pressure probe measurements at inlet, within the passage and at exit, and blade surface static pressure measurements. Clearances up to 6% of the span were investigated experimentally for Build-A and 12% span for Build-B. Computational investigations on both cascades were also conducted and a pinch tip meshing method was used to model the tip clearance region. The computational results were validated against the experimental data and used for further investigation of the clearance flows. The computations allowed for additional clearances to be examined ranging up to 10% of the span for Build-A and 12% span for Build-B. Finally a circumferential grooved casing treatment was implemented on Build-B to become Build-B1. This chapter draws together the key points from the previous seven chapters and provides recommendations for future work.

In the introduction (Chapter 1 on Page 2) it was stated that the aim of this thesis was to:

A - Investigate the influence of large clearances on compressor blade row loss and performance.

B - Investigate the influence of geometry.

C - Investigate the influence of inlet conditions and inlet boundary layer skew on clearance flows.

D - Investigate methods for reducing the loss and blockage associated within the endwall flows of such compressor rows.

The following conclusions fulfil these aims.

8.1 A - Influence of Large Clearances

- Increasing the tip clearance above 4% span incurred no further increase in loss. For Build-A a small loss decrease occurred above this. With Build-B the loss reduction was significant and at 12%TC the loss was similar to the no clearance cascade.

- A reduction in cascade turning was found with increased tip clearance. For Build-B the turning was reduced by 50% with 12%TC. This reduction in turning was caused by the leakage flows and the reduction in blade length.

- Increasing the clearance moved the vortex trajectory across the passage up to 6%TC. Above this the vortex returned closer to the SS of the blade and became independent of the casing.

- Increasing the clearance moved the roll-up point downstream.

- For the larger clearances the leakage flows became independent of the casing. This was observed through no further increase in loss, turning, or axial velocity on the casing itself. Further change with increased clearance in the exit pitch averaged profile was associated with a thickening of endwall flow region and a move away from the casing. Increasing the skew reduced the angle when this occurred. With Build-B and low inlet skew this occurred at approximately 6%TC but for the higher skew of Build-A and Build-B (high skew) it was postponed until 8%TC.

- An increase in blade loading occurred close to the blade tip for both cascades for larger clearances. This was due to the leakage vortex moving low pressure fluid against the SS of the blade.

- With Build-A an increase in total blade loading per unit length occurred above 2%TC but for Build-B there was a reduction. This difference was due to Build-A's leakage vortex remaining closer to the suction surface of the blade, and Build-B having a higher blockage indicated by the lower axial velocity within the casing region. This higher blockage caused a reduction in mid-span loading due to the consequent change in inlet angle.

8.2 B - Influence of Geometry

- Similar conclusions for both cascades were found. The flow features of large tip clearance flows are therefore not significantly influenced by the geometry within reason. This confirmed that the results for Build-A were relevant for the HPC.

- The influence of the geometry on the loss increase through the cascade was however significant as Build-A had a loss of almost twice that of Build-B. For a small clearance the effect of the geometry on the loss was small.

8.3 C - Influence of Inlet conditions

- The inlet boundary layer skew and thickness had little influence on the reduction in turning with increased clearance.

- Increasing the clearance moved the leakage vortex roll-up point upstream.

- A greater skew lead to a reduction in the total loss increase through the cascade, moved the leakage vortex roll-up upstream, and moved the vortex trajectory further across the passage. The turning on the casing was influenced by the increased skew and the difference in exit yaw angle was the same as the difference in inlet skew. Increased skew had little or no influence on the

secondary loss and so the decreased total loss was due to the mid-span loss reduction. Which was a consequence of the increased blockage and therefore reduced mid-span inlet flow angle.

- Increasing the clearance and the skew incurred a larger blockage in the casing region. Because of this a change in mid-span blade loading was incurred and reduction in mass flow rate through the cascade. This therefore explains the change in mid-span blade loading with increased tip clearance and skew. This was more evident with Build-B, and more so with the higher inlet skew, because of its larger blockage.

8.4 General Conclusions

- Both cascades had an approximate plateau of loss with increased clearance. A small reduction in loss occurred for both builds above 6%TC however this may have been a result of the change in loading of the cascade brought about by the higher blockage rather than a reduction in secondary loss generation. The inlet skew and boundary layer thickness had little influence on the secondary loss increase but it did have an effect on the blockage and vortex trajectory. Therefore the increased skew reduced the overall loss increase because of the reduced mid-span loss. The effect of the skew was therefore to reduce the turning of the row and so the work done and pressure rise of the cascade. This would have a significant influence on the downstream stator.

- The geometry had the largest influence on the loss increase through the cascade and so it is the authors' recommendation that this is the primary concern for the designer. Build-A with low stagger and high turning had a much larger secondary loss increase for the larger clearances than Build-B with high stagger and low turning. Although with 1%TC the loss increase of both cascades was similar. As the under-turning increased with skew but the loss did not, the difference would appear to be the stagger angle of the blades and so this should be of concurn to the designer.

- A pinch tip CFD meshing model was reasonable for the investigation of large tip clearances as it predicted the flow features well. For small clearances this method was not appropriate and therefore struggled to predict the flows correctly. This was because the pinch tip failed to model the physics of the flow over the blade correctly. For small clearances the flow reattached on to the end of the blade rather than remaining separated.

- The computational studies showed that a moving endwall enhanced the tip leakage flows. A reduction in the cross passage flow also occurred and therefore the passage vortex was suppressed. This strengthening of the flow and the reduction in the passage vortex moved the leakage vortex slightly across the passage and closer to the casing. The relative motion also reduced the loss on the casing (in the relative frame) and the secondary induced vortex loss area; and so the total loss was reduced. Increasing the clearance reduced the influence of the casing motion on the end-wall flows.

8.5 D - Loss and Blockage Reduction Techniques

- The use of linear cascades to investigate circumferential casing treatment is not appropriate as the periodicity of the cascade became unacceptable. Lengthening the cascade may have helped, but this is only speculation.

- Circumferential casing treatment should be feasible within these stages but would require significant effort to find a design that will be appropriate. This method unlike many other casing treatments does not rely on transient and compressible effects so it is the author's view that circumferential casing treatment is one of the more promising methods within the literature.

8.6 Recommendations for Future Work

- This thesis has aided in the understanding of the effect of the clearance flow within a single rotor row. No investigations in the rotating row, stage or multi-

row context were undertaken and this is therefore an obvious extension of the research.

- This thesis has clearly shown that the increase in loss for the large clearances is not as bad as may have been expected. In fact for Build-B the loss was reduced from the 1% tip clearance case, and not dissimilar to that of the stage without clearance. Unfortunately the increase in clearance also reduced the turning and therefore the row loading and ultimately the work done by the row.

  The under-turning in the multi-stage environment has the effect of reducing the angle at entry to the stator resulting in a negative angle of attack on to the following stator blade. This may create a large separation on the stator blade casing corner creating loss. The multi-stage environment is of significant importance and so further investigation to understand the multi-row influence on the overall stage loss is required.

- All work within this thesis has been undertaken at design conditions. If the compressor was operated at higher loading and so closer to stall, it is unclear from these results how the clearance size would influence this. It was found that for the highest clearances the vortex became independent of the casing and remained close to the suction surface of the blade. The blockage was increased with clearance this was due to a thickening of the end-wall flows with increased clearance rather than a reduction in velocity on the casing. Therefore from this it is possible to hypothesize that large clearances may increase the stall margin. This is therefore a further area of research.

  Further testing at the off design condition is required to investigate if increasing the clearance would increase the stall margin. The cascade's periodicity was found to be poor at higher loading (increased inlet angle) and so this investigation would need to be undertaken using a rotating machine, computationally or perhaps within a longer cascade.

- A pinch tip method to model the clearance was justified for this work because of the large clearances involved. For small clearances this method is not ap-

propriate as it fails to model the leakage flows realistically. Full meshing of the clearance region is essential with smaller clearances.

- As has been shown in this thesis the influence of a large clearance is detrimental to stage performance compared to a very small clearance. It was hoped that the deployment of circumferential grooves would have demonstrated a reduction in these adverse effects, but this was not established with these experiments. A method of controlling these flows, decreasing the under-tuning through the cascade and increasing the operating range would be advantageous and is a further area of research.

- The circumferential casing treatment design used was found to increase the loss and blockage through the cascade. These results were unreliable as the cascades periodicity was poor. This was thought to be due to the cascade being too short for such tests but it is unclear if a longer cascade would improve these results. The author therefore suggests that the testing of casing treatment is not possible within linear cascades. Rotating machine CFD or experimentation would be required.

- The casing treatment was tested only at design condition and not at increased row loading where it may be expected to be of benefit. Therefore varying the row loading is important to fully understand the effects of casing treatment.

- The design chosen for this work was taken from Müller et al. [2007] and was a design for a transonic machine. For this reason this design may not have been appropriate for the low speed compressor. Although it requires substantial computational effort a design tailored to the needs of the HPC should be used in future work.

- It was beyond the scope of the time available for this thesis to investigate large tip clearances in the multi-row environment and this is therefore a further area of interest. With the reduction in loss, reduction in turning and possible increase in stall margin associated with such large clearances it may be possible for the compressor to be adapted to work with these flows rather than trying

to suppress them. It was clearly shown that there was a significant change in mid-span flow with the end-wall blockage and this therefore must be accounted for in the design of the compressor.

This thesis has given some insight, through numerical and experimental investigations, into the flows at large tip clearances within the HPC. The work undertaken significantly increased the understanding of these flows and it is hoped will be useful for the compressor designer.

Bibliography

Baldwin, B. and Lomax, H. (1978). Thin-layer approximation and algebraic model for separated turbulent flows. *AIAA Paper 78-257*.

Beheshti, B. H., Teixeira, J. A., Ivey, P. C., Ghorbanian, K., and Farhanieh, B. (2004). Parametric study of tip clearance casing treatment on performance and stability of a transonic axial compressor. *Transactions of the ASME, Journal of Turbomachinery*, 126(4):527–535.

Boos, P., Möckel, H., Henne, J. M., and Selmeier, R. (1998). Flow measurement in a multistage large scale low speed axial flow research compressor. *ASME Paper 98GT-432*.

Booth, T. C., Dodge, P. R., and Hepworth, H. K. (1982). Rotor-tip leakage part 1basic methodology. *Transactions of the ASME, Journal of Engineering for Gas Turbines and Power*, 104:154–161.

Brandt, H., Fottner, L., Saathoff, H., and Stark, U. (2002). Effects of the inlet flow conditions on the tip clearance flow of an isolated compressor rotor. *ASME Paper GT2002-30639*.

Came, P. and Marsh, H. (1974). Secondary flow in cascades: Two simple derivations for the components of velocity. *Proc. I. Mech. E., Part C, J. Mechanical Engineering Science*, 16:391–401.

Chen, G. T., Greitzer, E. M., Tan, C. S., and Marble, F. E. (1991). Similarity analysis of compressor tip clearance flow structure. *Transactions of the ASME, Journal of Turbomachinery*, 113(2):260–269.

Chen, H. and Fu, S. (2005). CFD investigation on tip leakage flow and casing treatment of a transonic compressor. *ISABE-2005-1098*.

Corsini, A. and Rispoli, F. (2003). The role of forward sweep in subsonic axial fan rotor aerodynamics at design and off-design operating conditions. *ASME Paper GT2003-38671*.

Crook, A. J., Greitzer, E. M., Tan, C. S., and Adamczyk, J. J. (1993). Numerical simulation of compressor endwall and casing treatment flow phenomena. *Transactions of the ASME, Journal of Turbomachinery*, 115(3):501–512.

Cumpsty, N. A. (1989). *Compressor Aerodynamics*. Krieger Publishing Company.

Denton, J. D. (1993). The 1993 igti scholar lecture: Loss mechanisms in turbomachines. *Transactions of the ASME, Journal of Turbomachinery*, 115(4):621–656.

Dong, Y., Gallimore, S. J., and Hodson, H. P. (1987). 3-dimensional flows and loss reduction in axial compressors. *Transactions of the ASME, Journal of Turbomachinery*, 109(3):354–361.

Eckerle, W. and Langston, L. (1987). Horseshoe vortex formation around a cylinder. *Transactions of the ASME, Journal of Turbomachinery*, 118:613–621.

Emmrich, R., Honen, H., and Niehuis, R. (2007). Time resolved investigations of an axial compressor with casing treatment: Part 1 — experiment. *ASME Paper GT2007-27581*.

Fischer, A., Riess, W., and Seume, J. R. (2004). Performance of strongly bowed stators in a four-stage high-speed compressor. *Transactions of the ASME, Journal of Turbomachinery*, 126(3):333–338.

Foley, A. C. and Ivey, P. C. (1996). Measurement of tip-clearance flow in a multistage, axial flow compressor. *Transactions of the ASME, Journal of Turbomachinery*, 118(2):211–217.

Freeman, C. (1985). Effect of tip clearance on compressor stability and engine performance. *Tip Clearance Effects in Axial Turbomachines, von Karman Institute for Fluid Mechanics Lecture Series. 1985-05.*

Gallimore, S. (1999). Axial flow compressor design. *Proc. I. Mech. E., Part C, J. Mechanical Engineering Science*, 213(5):437.

Gallimore, S. J., Bolger, J. J., Cumpsty, N. A., Taylor, M. J., Wright, P. I., and Place, J. M. M. (2002). The use of sweep and dihedral in multistage axial flow compressor blading—part i: University research and methods development. *Transactions of the ASME, Journal of Turbomachinery*, 124(4):521–532.

Gbadebo, A. S., Nicholas, A. C., and Tom, P. H. (2007). Interaction of tip clearance flow and three-dimensional separations in axial compressors. *Transactions of the ASME, Journal of Turbomachinery*, 129(4):679–685.

Gerolymos, G. A. and Vallet, I. (1999). Tip-clearance and secondary flows in a transonic compressor rotor. *Transactions of the ASME, Journal of Turbomachinery*, 121(4):751–762.

Glanville, J. (2001). Investigation into core compressor tip leakage modelling techniques using a 3d viscous solver. *ASME Paper 2001-GT-0336.*

Gostelow, J. P. (1984). *Cascade aerodynamics.* Pergman Press Ltd.

Gregory-Smith, D. (2003). A review of end wall flows in axial compressors; report for alstom power. baden. Technical report, University of Durham.

Gupta, A., Arif Khalid, S., Scott McNulty, G., and Dailey, L. (2003). Prediction of low speed compressor rotor flowfields with large tip clearances. *ASME Paper GT2003-38637.*

Hah, C. and Loellbach, L. (1999). Development of hub corner stall and its influence on the performance of axial compressor blade rows. *Transactions of the ASME, Journal of Turbomachinery*, 121:67–77.

Harvey, N. W. (2008). Some effects of non-axisymmetric end wall profiling on axial flow compressor aerodynamics. part i: Linear cascade investigation. *ASME Paper No GT2008-50990*.

Harvey, N. W. and Offord, T. P. (2008). Some effects of non-axisymmetric end wall profiling on axial flow compressor aerodynamics. part ii: Multi-stage hpc cfd study. *ASME Paper No GT2008-50991*.

He, L. (2000). Three-dimensional unsteady navier-stokes analysis of stator-rotor interaction in axial-flow turbines. *Proc. I. Mech. E., Part A, J. Power and Energy*, 214:13–22.

Hoeger, M., Cardamone, P., and Fottner, L. (2002). Influence of endwall contouring on the transonic flow in a compressor blade. *ASME Paper GT2002-30440*, 2002.

Horlock, J. (1995). Secondary flow in repeating stages of axial turbomachines. *Proc. I. Mech. E., Part A, J. Power and Energy*, 209:101–110.

Huang, X. D., Chen, H. X., and Fu, S. (2008). Cfd investigation on the circumferential grooves casing treatment of transonic compressor. *ASME Paper No GT2008-50047*.

Hunter, I. H. and Cumpsty, N. A. (1982). Casing wall boundary-layer development through an isolated compressor rotor. *Transactions of the ASME, Journal of Engineering For Power*, 104(4):805–818.

Ingram, G. (2003). *Endwall Profiling for the Reduction of Secondary Flow in turbines*. PhD thesis, School of Engineering, University of Durham.

Ingram, G. and Gregory-Smith, D. (2006). An automated instrumentation system for flow and loss measurements in a cascade. *Flow Measurement and Instrumentation*, 17(1):23–28.

Inoue, M. and Kuroumaru, M. (1989). Structure of tip clearance flow in an isolated axial compressor rotor. *Transactions of the ASME, Journal Of Engineering For Gas Turbines And Power*, 107(2):374–386.

Inoue, M., Kuroumaru, M., and Furukawa, M. (1986). Behavior of tip leakage flow behind an axial compressor rotor. *Transactions of the ASME, Journal of Engineering for Gas Turbines and Power*, 108(7).

Jia, X., Wang, Z., and Cai, R. (2001). Numerical investigation of different tip gap shape effects on aerodynamic performance of an axial-flow compressor stator. *ASME Paper No 2001-GT-0337*.

Johnson, M. C. and Greitzer, E. M. (1987). Effects of slotted hub and casing treatments on compressor endwall flow-fields. *Transactions of the ASME, Journal of Turbomachinery*, 109(3):380–387.

Kang, S. and Hirsch, C. (1995). Tip clearance flows and loss in axial compressor cascades. *AGARD PEP 85th Symposium in Derby, UK*.

Koch, O. and Smith, L. (1976). Loss sources and magnitudes in axial flow compressors. *Transactions of the ASME, Journal of Engineering For Power*, 98:411–424.

Lakshminarayana, B., Pougare, M., and Davino, R. (1982). Three-dimensional flow field in the tip region of a compressor rotor passage - part i: Mean velocity profiles and annulus wall boundary layer. *Transactions of the ASME, Journal of Engineering For Power*, 104:760–771.

Layachi, M. and Bölcs, A. (2002). Effect of tip clearance on the characteristics of a 1.5 compressor stage with regard to the indexation. *9th. Symposium on Transport Phenomena and Dynamics of Rotating Machinery, Hawaii*.

Lin, F., Ning, F., and Liu, H. (2008). Aerodynamics of compressor casing treatment part i: Experiment and time-accurate numerical simulation. In *ASME Paper GT2008-51541*, volume 2008, Barcelona. ASME.

Lu, X., Chu, W., Zhu, J., and Wu, Y. (2006a). Experimental and numerical investigation of a subsonic compressor with bend skewed slot casing treatment. *ASME Paper GT2006-90026*.

Lu, X., Chu, W., Zhu, J., and Wu, Y. (2006b). Mechanism of the interaction between casing treatment and tip leakage flow in a subsonic axial compressor. *ASME Paper GT2006-90077*.

Lu, X., Zhu, J., Nie, C., and Huang, W. (2008). The stability-limiting flow mechanisms in a subsonic axial-flow compressor and its passive control with casing treatment. In *ASME Paper GT2008-50006*, volume 2008, Berlin, germany. ASME.

Mailach, R., Sauer, H., and Vogeler, K. (2001). The periodical interaction of the tip clearance flow in the blade rows of axial compressors. *ASME Paper 2001-GT-0299*.

Marsh, H. (1974). Secondary flow in cascades: The effect of axial velocity ratio. *Proc. I. Mech. E., Part C, J. Mechanical Engineering Science*, 16:402–407.

Massey, B. S. and Ward-Smith, J. (1998). *Mechanics of fluids*. Taylor and Francis.

Müller, M. W., Biela, C., Schiffer, H. P., and Hah, C. (2008). Interaction of rotor and casing treatment flow in an axial single-stage transonic compressor with circumferential grooves. *ASME Paper No GT2008-50135*.

Müller, M. W., Schiffer, H. P., and Hah, C. (2007). Effect of circumferential grooves on the aerodynamic performance of an axial single-stage transonic compressor. *ASME Paper No GT2007-27365*, pages 115–124.

Müller, R., Sauer, H., Vogeler, K., and Hoeger, M. (2003). Influencing the secondary losses in compressor cascades by a leading edge bulb modification at the endwall. *Proc. 5th. European Conference on Turbomachinery Fluid Dynamics and Thermodynamics*.

Müller, R. and Vogeler, K. (2007). Effects of 3d aerofoil tip clearance variation on a 4-stage low speed compressor. *Proceedings of the 8th International Symposium on Experimental and Computational Aerothermodynamics of Internal Flows*.

Ning, F. and Xu, L. (2008). Aerodynamics of compressor casing treatrment part ii: A quasi-steady model for casing treatment flows. In *ASME Paper GT2008-51542*. ASME.

Pandya, A. and Lakshminarayana, B. (1983). Investigation of the tip clearance flow inside and at the exit of a compressor rotor passage.1. mean velocity-field. *Transactions of the ASME, Journal of Engineering For Power*, 105(1):1–12.

Peacock, R. E. (1982). A review of turbomachinery tip gap effects: Part 1: Cascades. *International Journal of Heat and Fluid Flow*, 3(4):185.

Peacock, R. E. (1983). A review of turbomachinery tip gap effects: Part 2: Rotating machinery. *International Journal of Heat and Fluid Flow*, 4(1):3–16.

Perrot, V., Touyeras, A., and Lucien, G. (2007). Detailed cfd analysis of a grooved casing treatment on an axial subsonic compressor. In *Proc. 7th. European Conference on Turbomachinery Fluid Dynamics and Thermodynamics*.

Rabe, D. C. and Hah, C. (2002). Application of casing circumferential grooves for improved stall margin in a transonic axial compressor. *ASME Paper GT2002-30641*.

Saathoff, H., Deppe, A., Stark, U., Rohdenburg, M., Rohkamm, H., Wulff, D., and Kosyna, G. (2003). Steady and unsteady casingwall flow phenomena in a single-stage low-speed compressor at part-load conditions. *International Journal of Rotating Machinery*, 9(5):327–335.

Saathoff, H. and Stark, U. (1999). Endwall boundary layer separation in a single-stage axial-flow low-speed compressor and a high-stagger compressor cascade. *Forschung im Ingenieurwesen*, 65(7):217.

Saathoff, H. and Stark, U. (2001). Tip clearance flow in a low-speed compressor and cascade. *Proc. 4th. European Conference on Turbomachinery Fluid Dynamics and Thermodynamics*.

Sanger, N. (1983). The use of optimization techiques to design-controlled diffusion compressor blading. *Transactions of the ASME, Journal of Engineering For Power*, 105:256–264.

Sanger, N. and Shreeve, R. (1986). Comparison of calculated and experimental cascade performance for controlled-diffusion compressor stator blading. *Transactions of the ASME, Journal of Turbomachinery*, 108(1):42–50.

Schlechtriem, S. and Lotzerich, M. (1997). Breakdown of tip leakage vortices in compressors at flow conditions close to stall. *ASME Paper 97-GT-41*.

Smith, G. and Cumpsty, N. A. (1984). Flow phenomena in compressor casing treatment. *Transactions of the ASME, Journal of Engineering for Gas Turbines and Power*, 106:532–541.

Songtao, W. and Zhongqi, W. (2002). The tip and hub leakage flow of a repeated two stage compressor. *ASME Paper GT2002-30437*.

Spalart, P. R. and Allmaras, S. R. (1992). A one-equation turbulence model for aerodynamic flows. *AIAA Paper 92-0439*.

Storer, J. A. and Cumpsty, N. A. (1991). Tip leakage flow in axial compressors. *Transactions of the ASME, Journal of Turbomachinery*, 113(2):252–259.

Suder, K. (1998). Blockage development in a transonic, axial compressor rotor. *Transactions of the ASME, Journal of Turbomachinery*, 120:465–476.

Suder, K. L. and Celestina, M. L. (1996). Experimental and computational investigation of the tip clearance flow in a transonic axial compressor rotor. *Transactions of the ASME, Journal of Turbomachinery*, 118(2):218–229.

Takata, H. and Tsukuda, Y. (1977). Stall margin improvement by casing treatment - its mechanism and effectiveness. *Transactions of the ASME, Journal of Engineering For Power*, 99(1):121–133.

Tang, G., Simpson, R. L., and Tian, Q. (2006). Experimental study of tip-gap turbulent flow structure. *ASME Paper GT2006-90359*.

Tschirner, T., Johann, E., Muller, R., and Konrad, V. (2006). Effects of 3d aerofoil tip clearance variation on a 4-stage low speed compressor. *ASME Paper GT2006-90902*.

Van Zante, D. E., Strazisar, A. J., Wood, J. R., Hathaway, M. D., and Okiishi, T. H. (2000). Recommendations for achieving accurate numerical simulation of tip clearance flows in transonic compressor rotors. *Transactions of the ASME, Journal of Turbomachinery*, 122(4):733–742.

Wagner, J. H., Dring, R. P., and Joslyn, H. D. (1985a). Inlet boundary-layer effects in an axial compressor rotor.1. blade-to-blade effects. *Transactions of the ASME, Journal Of Engineering For Gas Turbines And Power*, 107(2):374–380.

Wagner, J. H., Dring, R. P., and Joslyn, H. D. (1985b). Inlet boundary-layer effects in an axial compressor rotor.2. throughflow effects. *Transactions of the ASME, Journal Of Engineering For Gas Turbines And Power*, 107(2):381–386.

Walker, M. (2004). Tip clearance flow in compressors. *Final Year Project, School of Engineering, Durham University.*

Walker, M., Gregory-Smith, D., and He, L. (2005). A study of large tip clearance flows in an axial compressor blade row. *Proc. 6th. European Conference on Turbomachinery Fluid Dynamics and Thermodynamics.*

Wilke, I. and Kau, H. P. (2002). A numerical investigation of the influence of casing treatments on the tip leakage flow in a hpc front stage. *ASME Paper GT2002-30642.*

Williams, R., Greggory-Smith, D., and Ingram, G. (2008a). Progress report 3 for alstom power (switzerland), linear prismatic cascade results, no inlet wall injection. Technical Report 3, School of Engineering, Durham University.

Williams, R., Greggory-Smith, D., and Ingram, G. (2008b). Progress report 4 for alstom power (switzerland), linear prismatic cascade results, with inlet wall injection. Technical Report 4, School of Engineering, Durham University.

Williams, R., Greggory-Smith, D., and Ingram, G. (2008c). Progress report 5 for alstom power (switzerland), linear prismatic cascade results, circumferential groove casing treatment. Technical Report 5, School of Engineering, Durham University.

Williams, R., Gregory-Smith, D., and He, L. (2006). A study of large tip clearance flows in an axial compressor blade row. *ASME Paper No GT2006-90463*.

Williams, R., Gregory-Smith, D., He, L., and Ingram, G. (2008d). Experiments and computations on large tip clearance effects in a linear cascade. *ASME Paper No GT2008-50557*.

Williams, R., Gregory-Smith, D., and Ingram, G. (2009). Large tip clearances and highly skewed inlet conditions. *Proc. 8th. European Conference on Turbomachinery Fluid Dynamics and Thermodynamics*.

Williams, R., He, L., and Greggory-Smith, D. (2007a). Preliminary progress report for alstom power (switzerland). Technical Report 1, School of Engineering, Durham University.

Williams, R., He, L., Greggory-Smith, D., and Ingram, G. (2007b). Progress report 2 for alstom power (switzerland), cascade design. Technical Report 2, School of Engineering, Durham University.

Wisler, D. C. (1985). Loss reduction in axial-flow compressors through low-speed model testing. *Transactions of the ASME, Journal Of Engineering For Gas Turbines And Power*, 107(2):354–363.

Yang, H. (2004). *3D Unsteady Flow In Oscillating Compressor Cascade*. PhD thesis, School of Engineering, University of Durham.

Yu, V. (2004). Development of new casing treatment configuration. *JSME International Journal Series B Fluids and Thermal Engineering*, 47(4):804–812.

Appendix A

Build-B Supplementary Results

The following results are those taken at 1.5Cx for Build-B. These results complement those presented in Chapter 5.

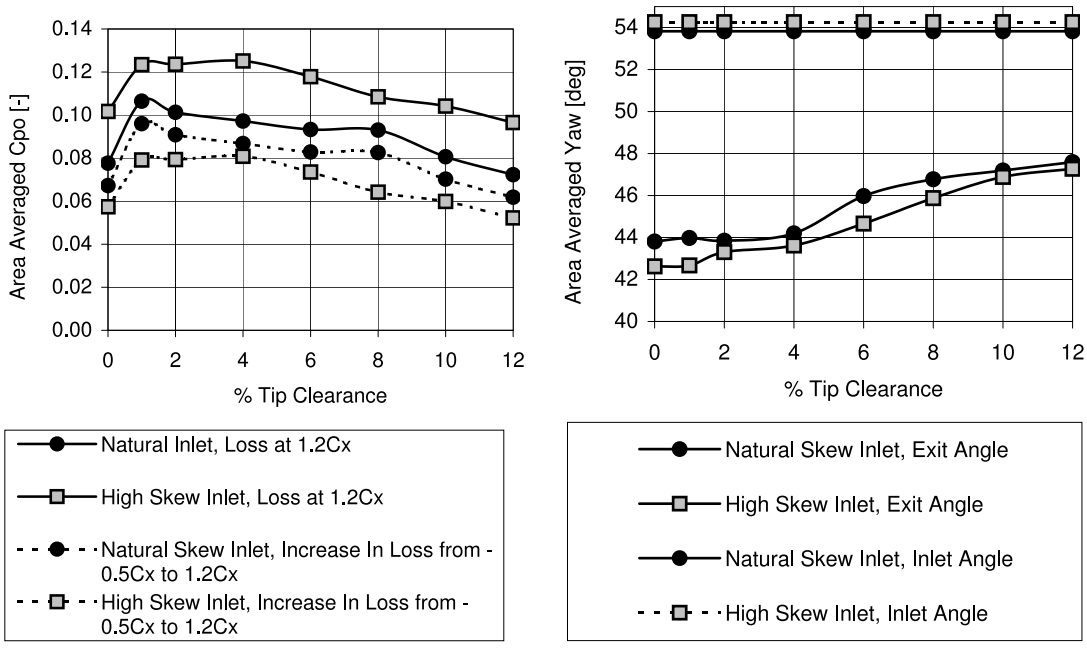

(a) Cp_0 ***(b)*** *Yaw*

Figure A.1: *Area Mass Weighted Averaged Loss and Turning at 1.5Cx*

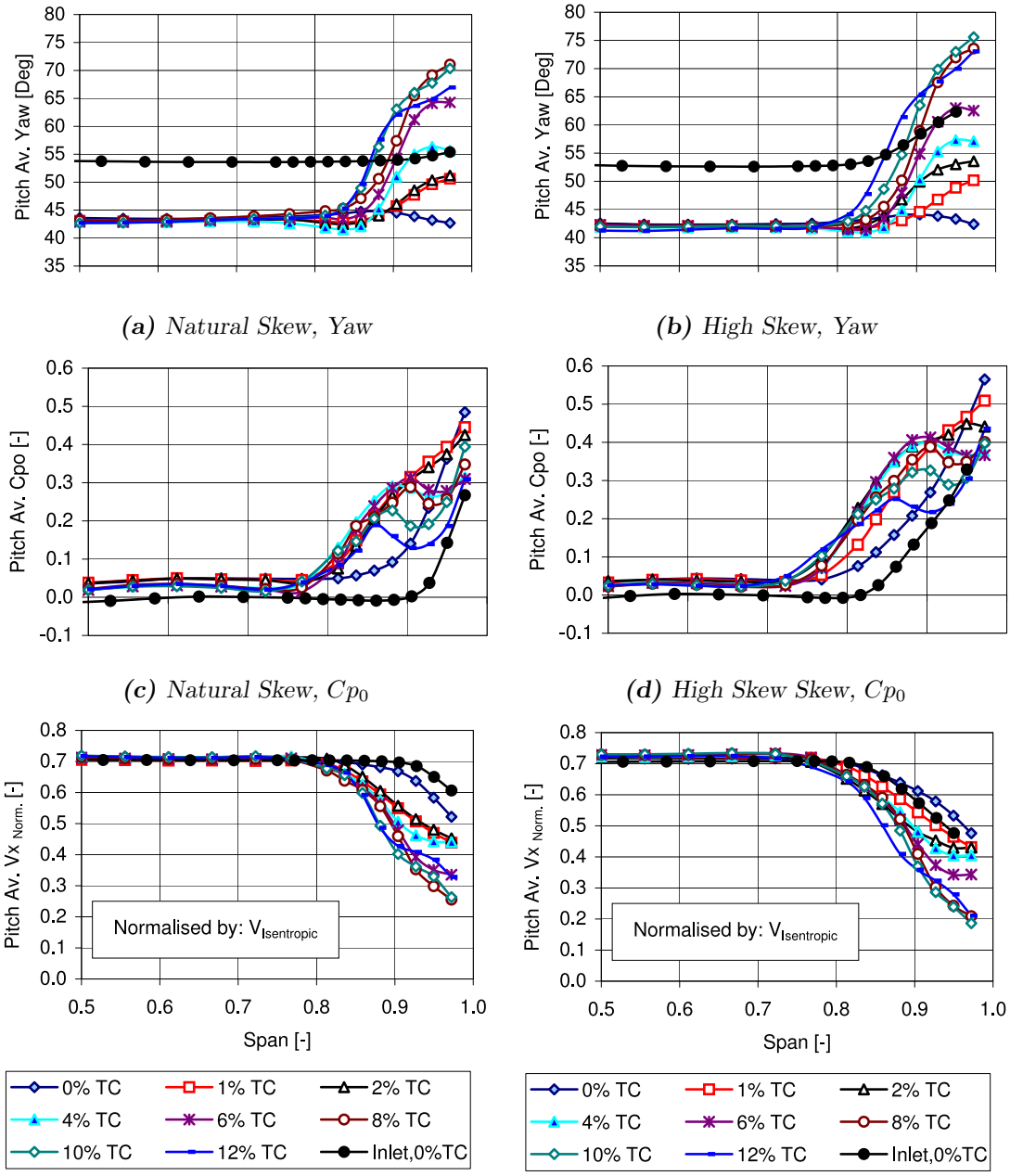

(a) Natural Skew, Yaw *(b) High Skew, Yaw*

(c) Natural Skew, Cp_0 *(d) High Skew Skew, Cp_0*

(e) Natural Skew, $V_{X,norm.}$ *(f) High Skew, $V_{X,norm.}$*

Figure A.2: *Pitch Averaged Exit Traverse at 1.5Cx*

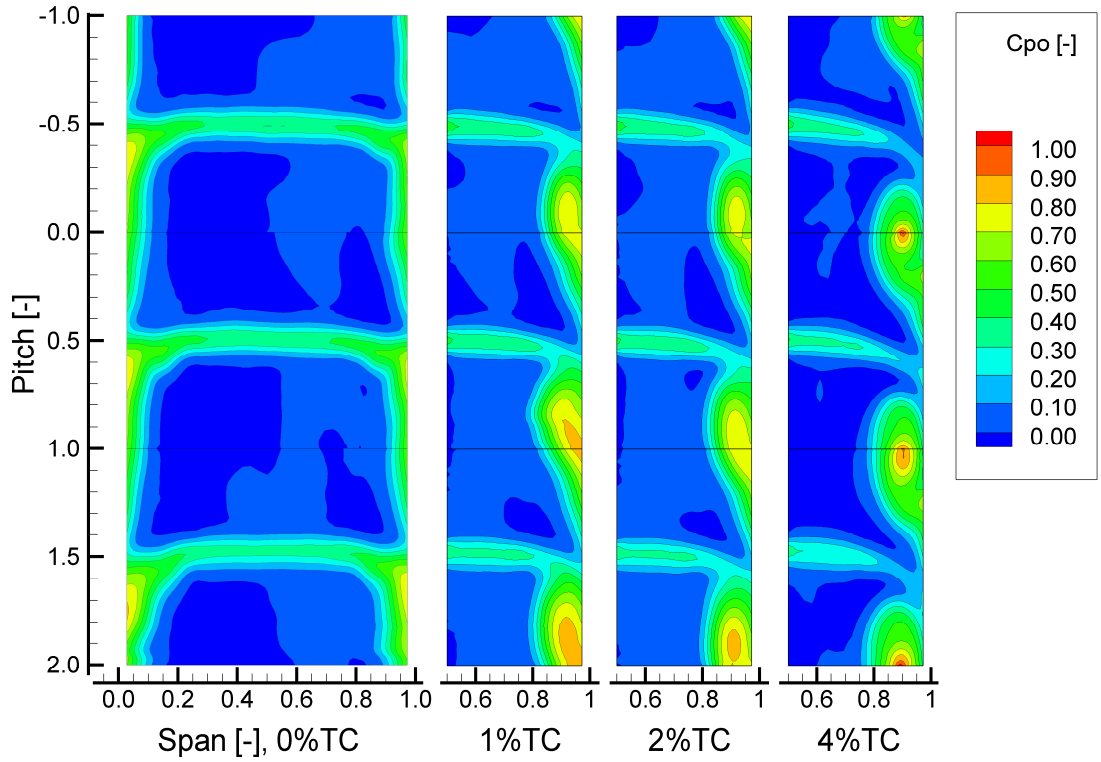

(a) Clearances 0%TC to 4%TC

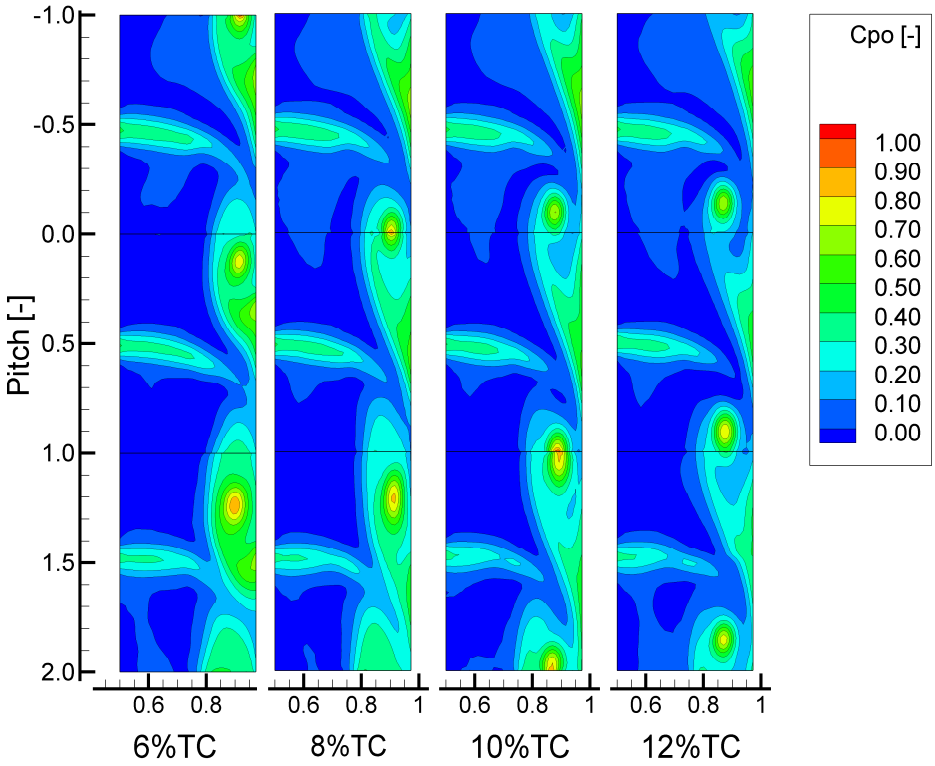

(b) Clearances 6%TC to 12%TC

Figure A.3: *Natural Skew Inlet Cp_0 Contour Plots at 1.5Cx*

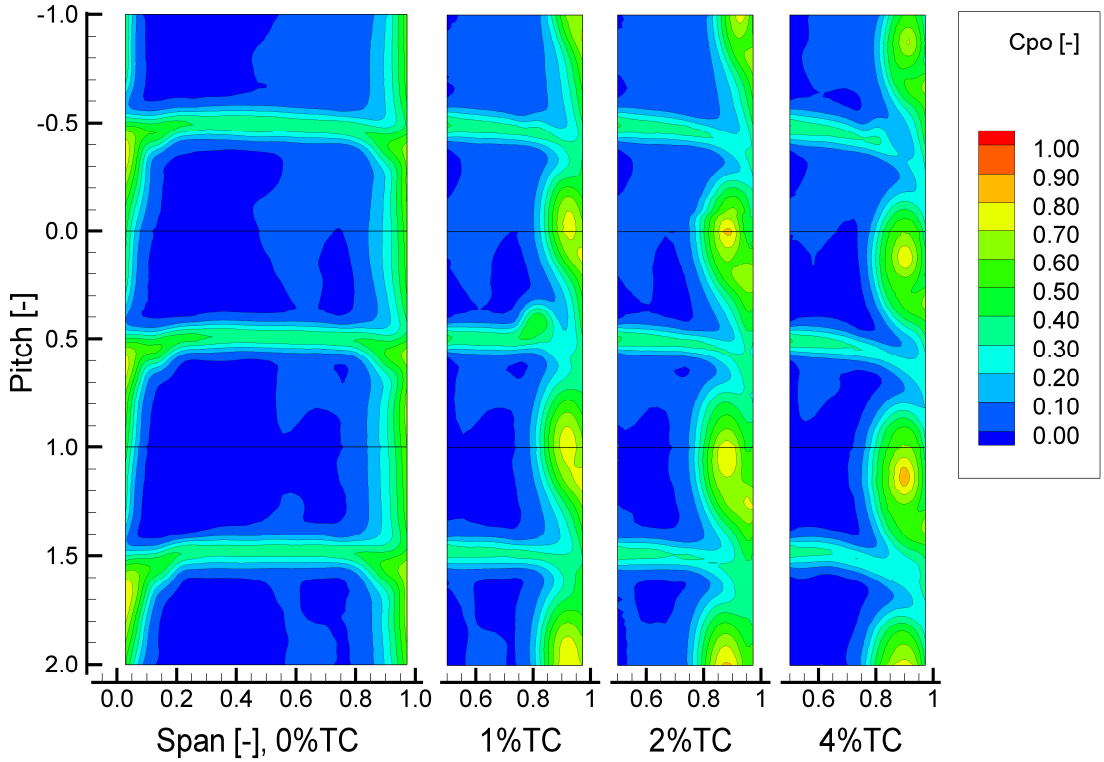

(a) Clearances 0%TC to 4%TC

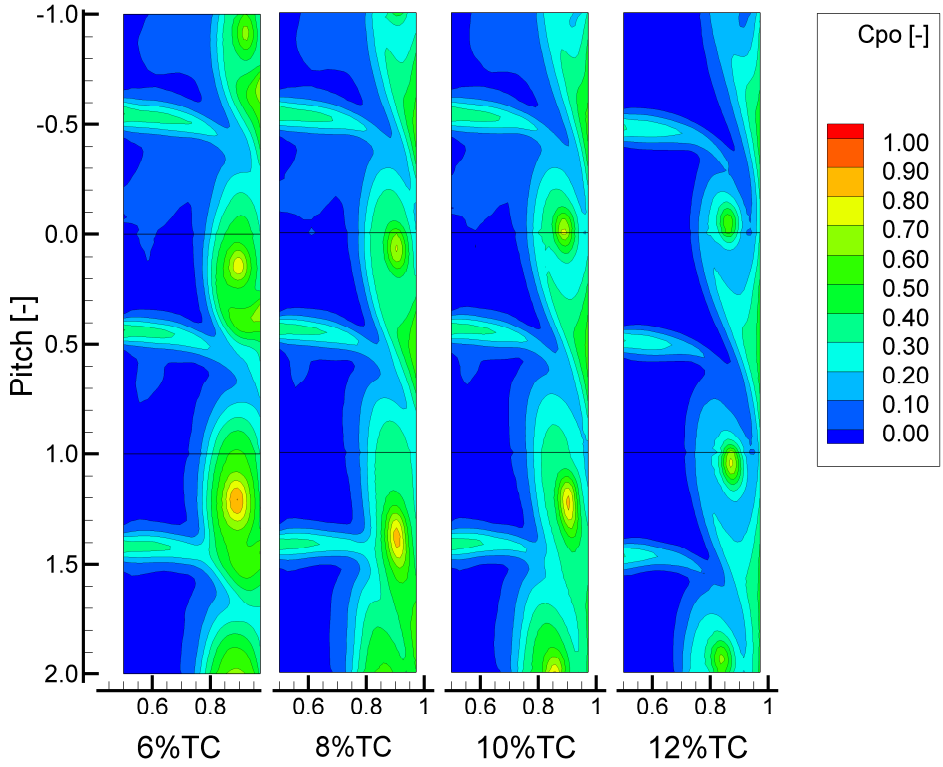

(b) Clearances 6%TC to 12%TC

Figure A.4: *High Skew Inlet Cp_0 Contour Plots at 1.5Cx*

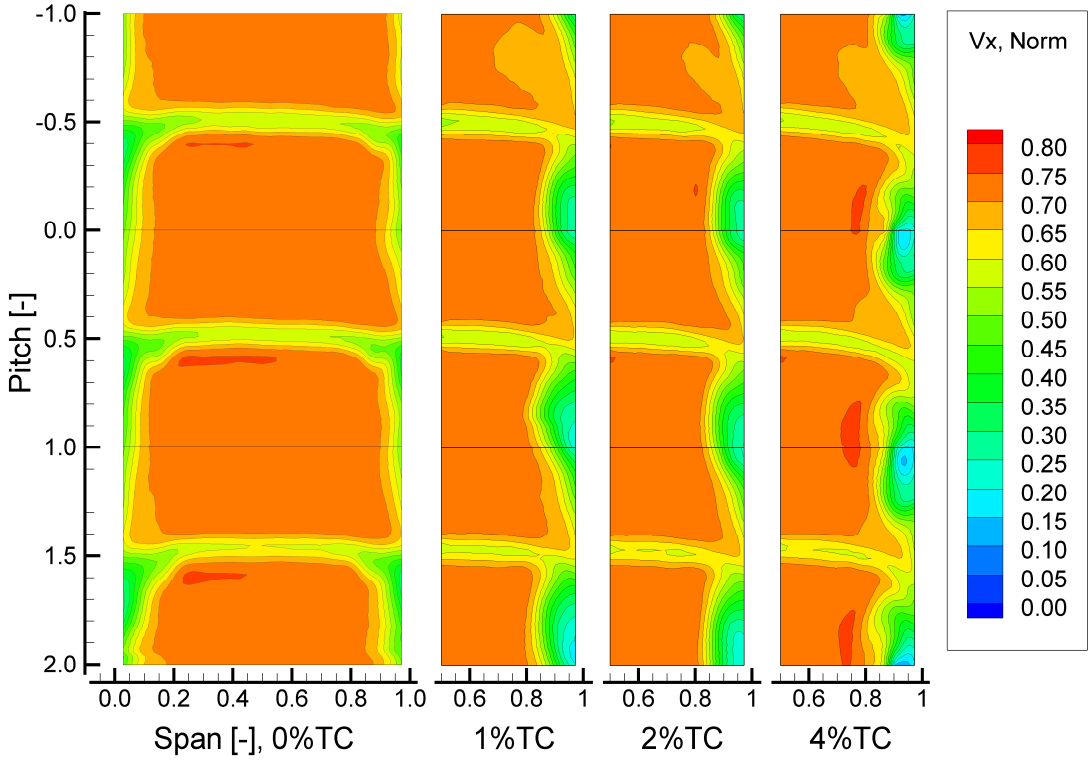

(a) Clearances 0%TC to 4%TC

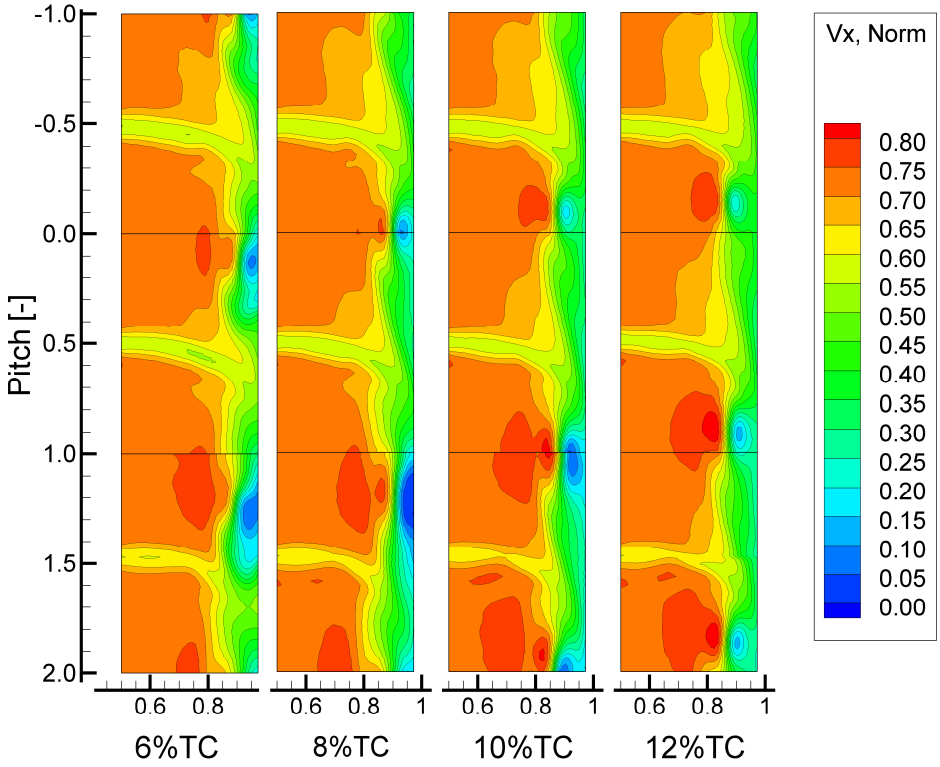

(b) Clearances 6%TC to 12%TC

Figure A.5: *Natural Skew Inlet $V_{x,norm}$ Contour Plots at 1.5Cx*

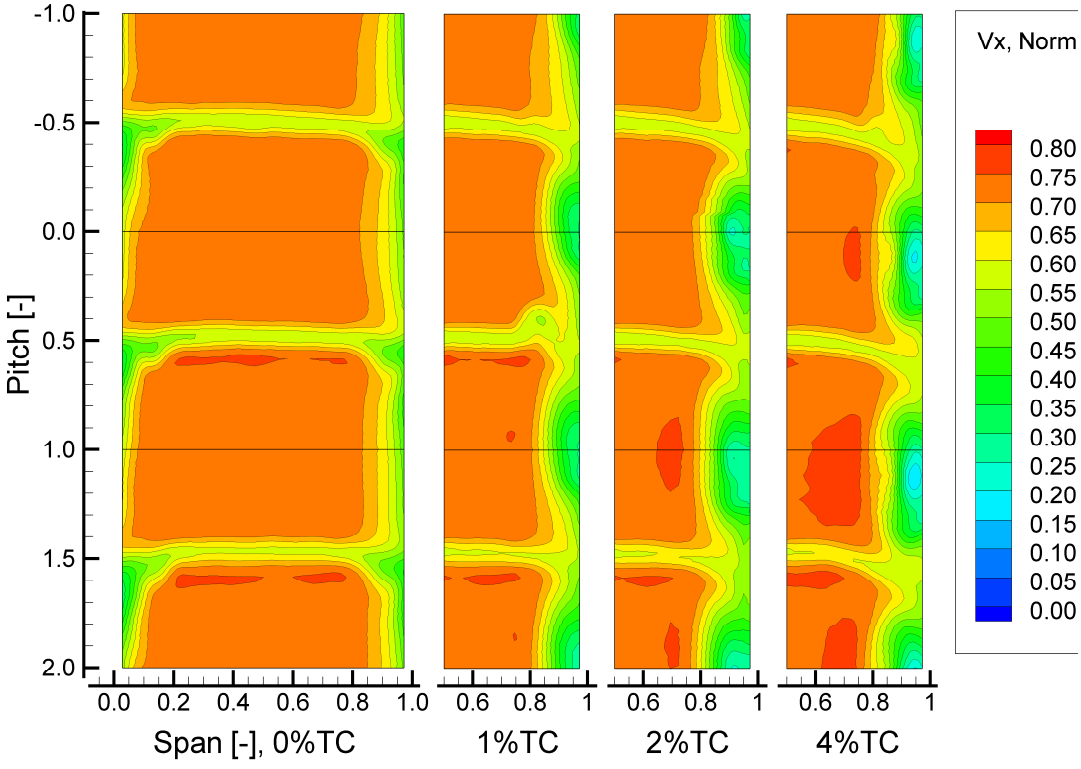

(a) Clearances 0%TC to 4%TC

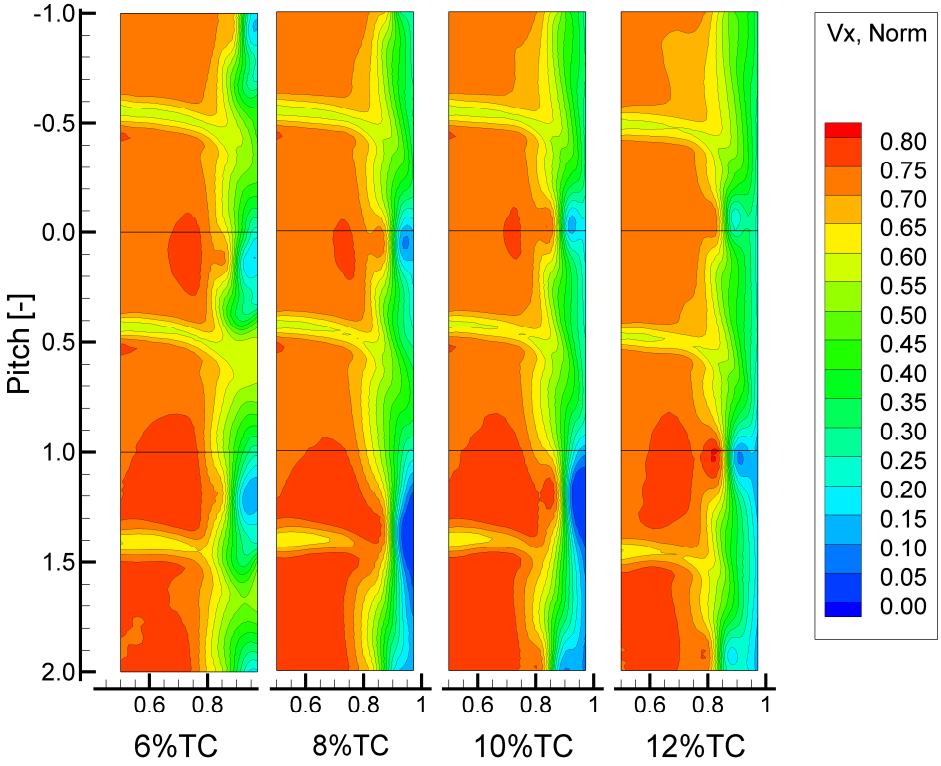

(b) Clearances 6%TC to 12%TC

Figure A.6: *High Skew Inlet $V_{x,norm}$ Contour Plots at 1.5Cx*

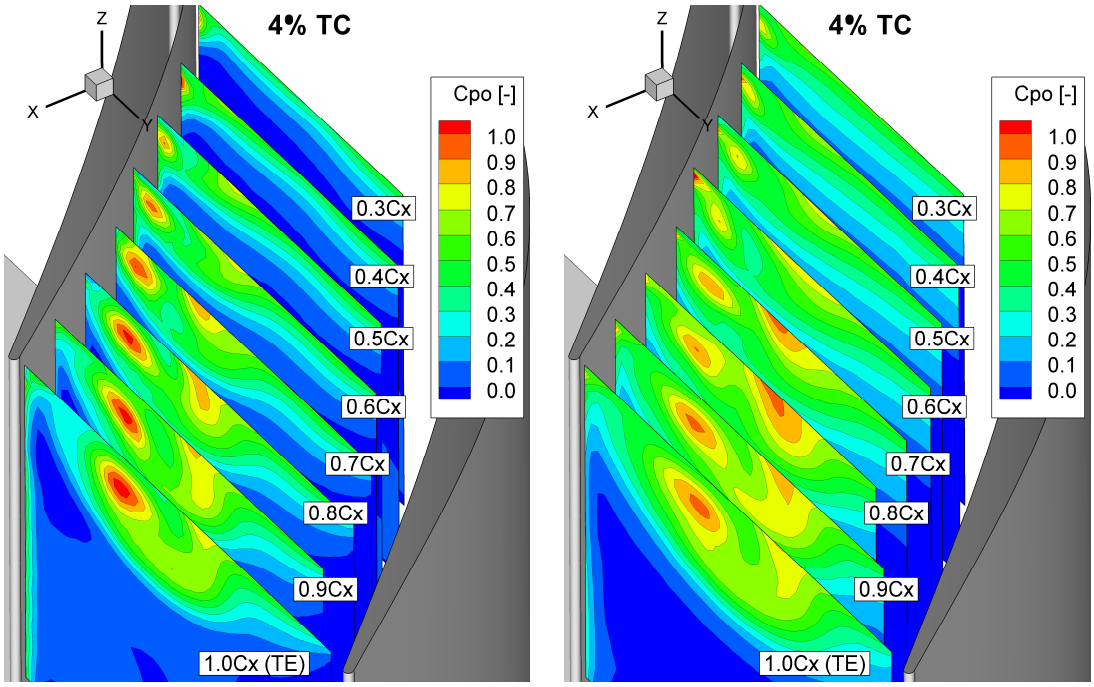

(a) Natural Skew *(b) High Skew*

Figure A.7: *4%TC Internal Traverse Cp_0 Contour Plots*

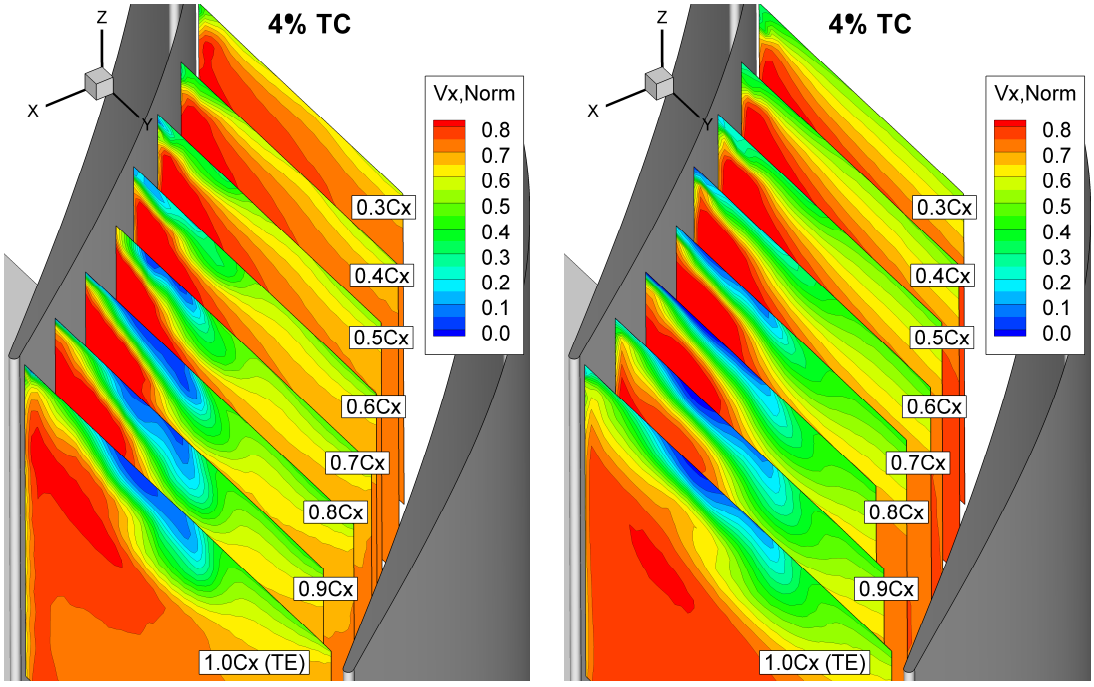

(a) Natural Skew *(b) High Skew*

Figure A.8: *4%TC Internal Traverse $V_{x,norm}$ Contour Plots (Normailsed With $V_{Isentropic}$)*

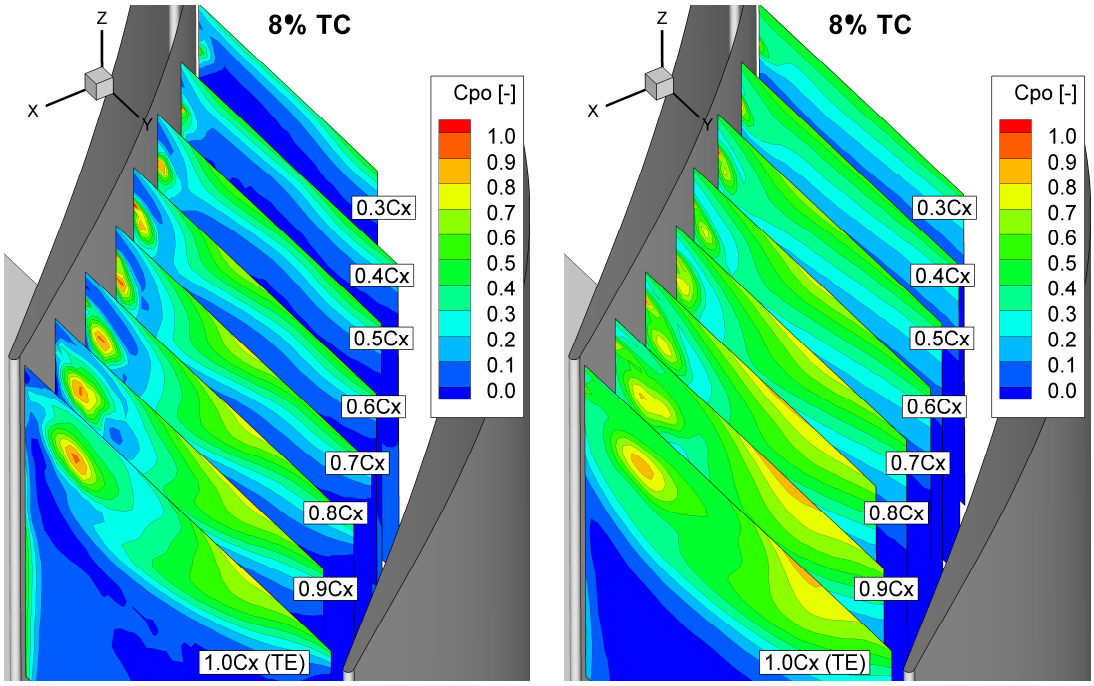

(a) Natural Skew *(b) High Skew*

Figure A.9: *8%TC Internal Traverse Cp0 Contour Plots*

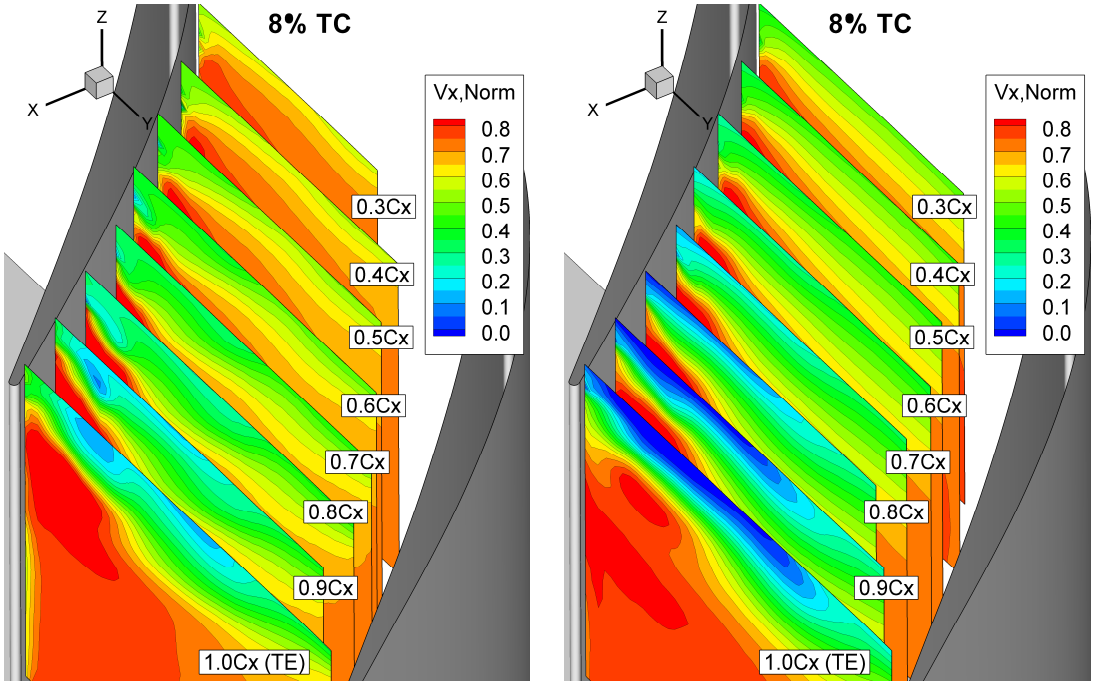

(a) Natural Skew *(b) High Skew*

Figure A.10: *8%TC Internal Traverse V_x Contour Plots*

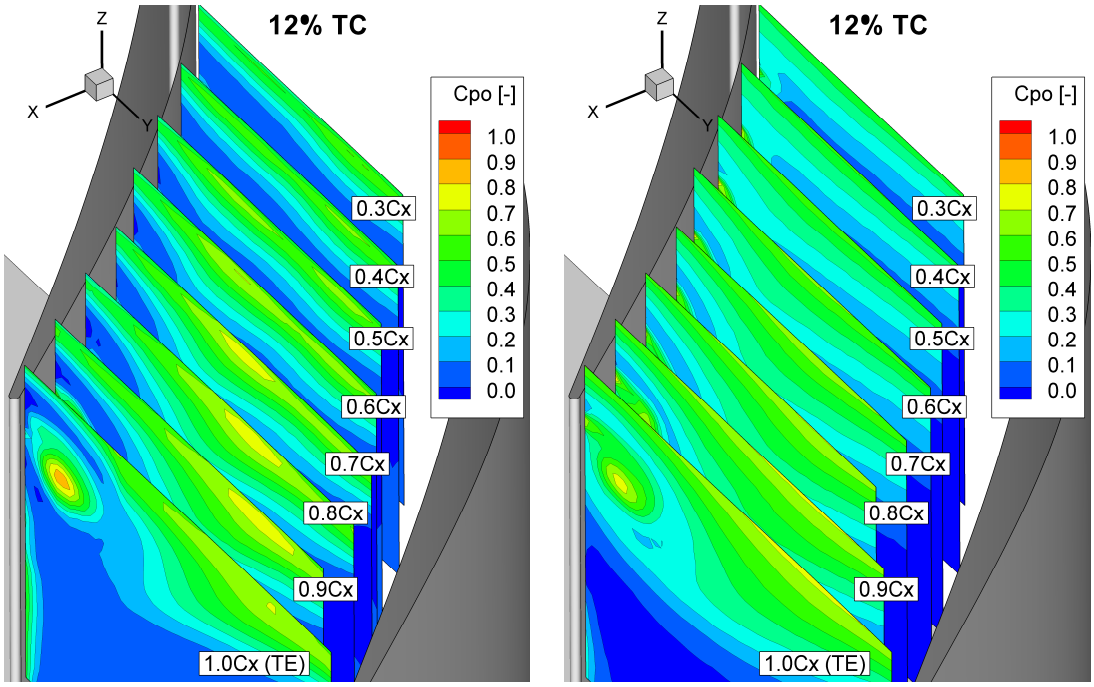

(a) Natural Skew *(b) High Skew*

Figure A.11: *12%TC Internal Traverse Cp_0 Contour Plots*

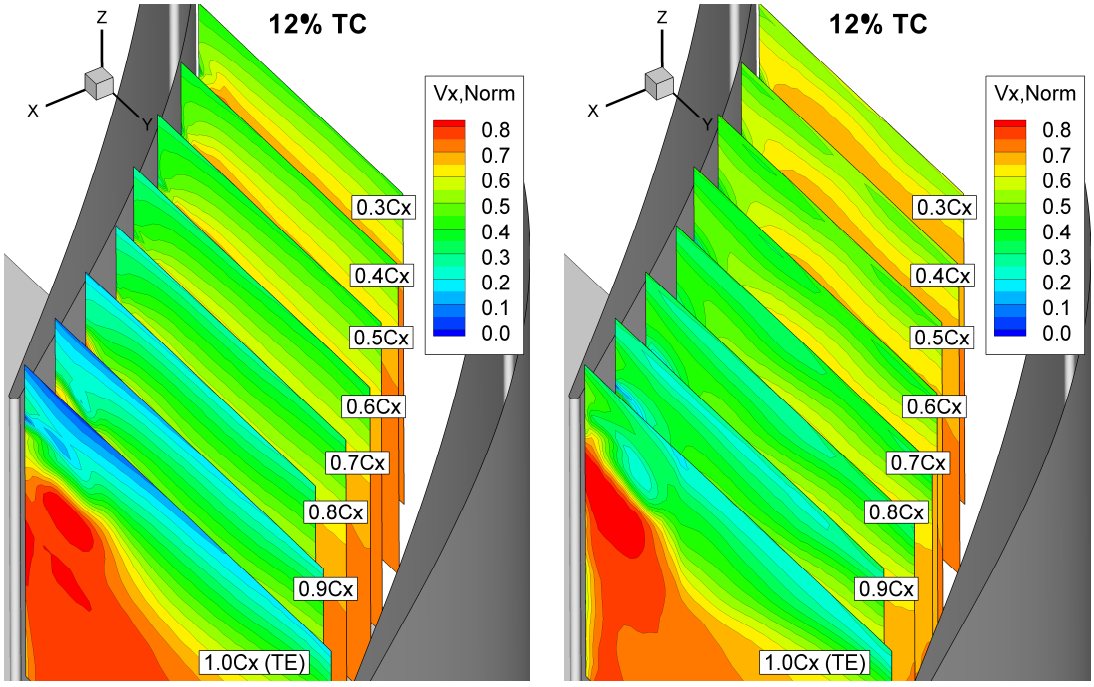

(a) Natural Skew *(b) High Skew*

Figure A.12: *12%TC Internal Traverse $V_{x,Normalised}$ Contour Plots (Normailsed With $V_{Isentropic}$)*

Appendix B

Supporting Papers

This appendix contains the 3 conference papers that were produced for the work within this thesis.

These papers include Williams et al. [2006], Williams et al. [2008d] and Williams et al. [2009]. Williams et al. [2008d] was also converted to a journal of turbomachinery paper.

B.1 Paper 1. Williams et al. [2006]

Proceedings of ASME Turbo Expo 2006:
Power for Land, Sea, and Air
May, 8-11, 2006, Barcelona, Spain

GT2006-90463

A STUDY OF LARGE TIP CLEARANCE FLOWS IN AN AXIAL COMPRESSOR BLADE ROW

Richard Williams, David Gregory-Smith, Li He
University of Durham, U.K.

ABSTRACT

The tip clearance flow of industrial axial compressor rotors has a significant impact on compressor performance. Most tip clearance flow research work has been undertaken in the earlier low-pressure transonic stages of compressors. The main differences between the earlier (low-pressure) and later (high-pressure) stages include blade profile, stagger angle, Mach number, blade length and tip clearance. The tip clearance in the later stages of an industrial axial compressor is relatively large due to mechanical constraints and short blading. The stagger angle is much lower and so the tip clearance flow is at a higher angle to the (negative) axial direction. In the present work, a computational method has been employed to investigate tip clearance flow from 1% span to 10% span for blading such as that found in the later stages. A pinch tip model is used to model the blade tip in a cascade with a stationary and moving end-wall. It has been found that the tip clearance flow rolls up into a vortex much later than in the earlier stages. The migration of the tip clearance vortex across the passage is much less than for the earlier stages and also the induced vortex is much weaker. Comparisons between a cascade with fixed and moving end-walls are made, the main difference being that the tip clearance flow is stronger with a moving end-wall. The 1% tip clearance flow structure with stationary end-wall is shown to be different from all other cases investigated.

NOMENCLATURE

C	Chord (m)
$Cp = \frac{Ps - Ps_1}{Po_1 - Ps_1}$	Static pressure coefficient
$Cpo = \frac{Po_1 - Po}{Po_1 - Ps_1}$	Pitch averaged total pressure loss coefficient
$C_L = \int_0^C (Cp_{pressure} - Cp_{Suction})dx$	Blade loading coefficient
M	Mach Number
P_0	Total Pressure (Pa)
P_{01}	Inlet Total Pressure (1 chord upstream) (Pa)
P_S	Static Pressure (Pa)
P_{S1}	Inlet Static Pressure (Pa)
PS	Pressure Surface
R	Gas Constant
Re	Reynolds Number based on blade chord and inlet velocity
S	Entropy
SS	Suction Surface
TC	Tip Clearance; this is given as a percentage of duct height, i.e. casing radius – hub radius
x	Radial Coordinate
y	Circumferential Coordinate
z	Axial Coordinate
β	Relative flow angle (° to the axial direction)

INTRODUCTION

Tip clearance is required in a non-shrouded compressor rotor due to the relative motion of the moving blades with the stationary casing. This tip clearance allows for passage of air from the pressure surface to the suction surface of the blade, which is termed tip leakage flow. Loss is generated by the interaction between the clearance and mainstream flows through viscous shearing due to the velocity gradients. As the resulting relatively low stagnation pressure fluid moves downstream, an effective blockage is generated. This results in a reduction in flow area and a decrease in pressure rise across

the stage. Suder [1] found that the blockage in the end-wall region is 2-3 times that of the core flow where only blade wakes cause blockage.

Tip clearance flows in axial compressors have been widely investigated. However most of the studies have been undertaken with reasonably small tip clearances of the order of 1.5% span (e.g. Layachi and Blocs [2]) or 2%-4% chord (e.g. Storer and Cumpsty [3]). These tip clearance values are typical of aero engines or the earlier low-pressure stages of industrial gas turbines. The tip clearances in the later stages of industrial compressors are much larger as a percentage of the span, for example values of 6% span are not uncommon. The later high-pressure stages are usually loaded much less. This low loading is to allow for a reasonable surge margin. Other differences include the blade profile (e.g. low stagger) and a lower fluid velocity, i.e. the early stages exceed a Mach number of unity but the later stages can have a mach number in the region of 0.3-0.5.

Walker [4] numerically investigated tip clearances up to 8% span. Of particular interest was an increase in section loading close to the tip of the blade for larger tip clearances. This current work expands on Walker's work and develops the computational model further to investigate the flow physics in greater detail.

Secondary Flow

Secondary flows result from the turning of the shear layer on the end-wall. With no tip clearance, the flow is over-turned near the end-wall and under-turned further out. This main feature of secondary flow, termed the passage vortex, may produce corner stall. In a compressor the relative motion of the blade rows produces skewed flow at inlet on the end-wall due to the boundary layer and opposes the secondary flows and may give under-turning close to the end-wall. With tip clearance the tip leakage vortex also results in under-turning near the end-wall and may completely dominate the flow near the end-wall.

Tip Clearance Flow Physics

The main feature of the tip clearance is a pressure driven jet approximately normal to the chord. This jet rolls up into a tip clearance vortex located close to the end-wall and the suction surface. The main source of loss is the mixing between the tip clearance flow and the mainstream flow.

The flow in the tip clearance depends on the aspect ratio, i.e. the gap height divided by the maximum blade thickness. Glanville [5] quotes Storer (1991) who found that for reattachment the aspect ratio must be less than 0.4. Generally for a compressor with thin blades the flow will separate from the tip creating a vena contracta. For lower aspect ratio tip gaps, reattachment of the flow on the blade tip occurs. The larger tip clearances in the later stages of HP compressors are likely to prevent reattachment.

Storer and Cumpsty [3] investigated the tip clearance flow in a cascade, both numerically and experimentally. They demonstrated that the static pressure field close to the tip controls the chord-wise distribution of the flow across the tip. This means that the tip clearance flow is strongest where the blade loading is at a maximum. Although the tip clearance vortex affects the local pressure field, the overall magnitude of the clearance flow remains strongly related to the aerodynamic loading of the blade. They also found that as the tip clearance was increased the roll-up of the clearance vortex moved downstream and the blade force near the tip increased with tip clearance. As the tip clearance is increased the tip clearance vortex increases in magnitude altering the blade pressure distribution. This change moves the minimum pressure downstream along the chord. Several authors have observed a second weaker tip clearance vortex. The main vortex emanates from the front part of the blade with the largest PS to SS pressure difference. The second vortex has been observed to grow from further along the chord.

As the tip leakage jet meets the mainstream flow it rolls up into a vortex close to the suction surface. The tip leakage vortex opposes the secondary flow and has been shown in some cases to suppress completely the passage vortex. One benefit of the tip clearance vortex is that it prevents the formation of a corner stall. Another feature of the tip clearance flow is an induced counter vortex on the casing; this is developed by the wall shear layer and its strength depends on the difference between the tip clearance flow velocity and the end-wall velocity. Transonic rotors lead to a much stronger counter vortex than a subsonic rotor. Van Zante, et al [6] showed that the induced vortex has the effect of inhibiting the migration of the tip clearance vortex across the passage to the pressure surface of the adjacent blade. Walker [4] found that for a stationary subsonic rotor and large tip clearances of 8% span an induced counter vortex was observed. However with a moving end-wall no induced vortex was observed for the same tip clearance.

For a rotating machine the end-wall moves relative to the blades. This means that in the relative frame of motion the flow on the end-wall does not fall to zero but to the speed of the end-wall. For a compressor this motion is in the same direction as the pressure drop leading to an increase in the tip clearance flow. The end-wall movement also pushes the tip leakage vortex away from the suction surface as observed by Lakshminarayana, et al [7].

As has been previously stated one of the main differences in the later stages as opposed to the early stages is the lower stagger angle. Relative to the blade, the tip clearance flow is at a higher angle to the upstream axial direction and the relative end-wall motion is nearly normal to the relative mainstream flow. Whereas in the earlier stages with high stagger angle the tip clearance flow has a significant component in the upstream direction and the end-wall motion is at a much shallower angle to the relative mainstream flow.

Several authors have investigated the effect of tip clearance value. Hunter and Cumpsty [9] varied the tip clearance significantly from 1% chord to 9.2% chord. They found that the under-turning and loss are significantly increased by the tip clearance flow. This increase in loss also increased the blockage significantly as might be expected. The trajectory of the vortex was found to be independent of the tip clearance gap by Storer and Cumpsty [3].

For the real context a compressor has several stages of rotors and stators. The wake and secondary flows that leave one stage are passed into the next. The under-turning created by the rotor tip clearance persists into the stator producing larger

secondary flow and possibly, depending on the design, corner separation of the stator leading to a large blockage, as found by Horlock [8]. The stator hub tip leakage results in stator row under-turning that is passed into the rotor. The unsteady interactions of tip leakage and secondary flows between rows have been investigated by some authors, for example Layachi and Bölcs [2].

Tip clearance modeling

Accurate modeling of the tip clearance flow is difficult; there are three common methods employed: assuming flow periodicity across the tip of the blade, rounding an H grid to fill the gap over the blade (a pinch tip), and fully gridding the clearance with a separate grid block. The methods above are listed in order of complexity and thus computational solution time required.

Van Zante et al [6] compared these three methods and concluded that no significant advantage was found from gridding the tip gap, and that the fine gridding of the casing boundary layer (in order to capture the induced vortex) is the key to an accurate result. Glanville [5] has also compared these methods. Unlike Van Zante et al [6] the compressor was low speed. He found that the pinch tip model leads to an over prediction of loss. The multi-block scheme was found to improve the results greatly, although the grid was more time consuming to make and solve. The first type of modeling technique was also tried and good results were obtained. Although not as good as the other two methods, the simplicity and reduced computational time means that it has some utility.

Walker [4] used the first two methods and found that the pinch tip model generally gave a better result. For this reason this work also uses a pinch tip model. One disadvantage is that it is impossible to know exactly what percentage tip clearance is being modeled. However, as this work is qualitative due to the lack of experimental data at the present time, this is not a significant problem.

COMPUTATIONAL CODE

This work uses a CFD code developed by He at the University of Durham. He [10] gives a good explanation of some of the codes features. A brief description follows. The code iteratively solves the Reynolds averaged 3D unsteady compressible Navier-Stokes equations. Turbulence closure is undertaken using the Baldwin and Lomax model. Alternatively the Spalart-Allmaras model can be used, although the work undertaken in this report uses the Baldwin-Lomax. The governing equations are discretized in space using the cell-centered finite volume scheme. These discretized equations are integrated in time using the explicit four-step Runge-Kutta method. The multi-grid technique and the local time stepping are used to accelerate the solution convergence.

For this problem the solver using multi-grid was run for approximately 3000 time steps to give good convergence.

Modeled Blade Row

The blade used in this work is the same as that of Walker [4] and attempts to model an experimental cascade at the School of Engineering, University of Durham. Walker made some comparisons of static pressure distributions and found a good correlation between results, thus providing some validation for this work. Further comparisons will be possible with future traverse results.

The blade profile is a Controlled-Diffusion Blade which was designed by Sanger [1983] and has been intensively investigated at the Naval Postgraduate School, USA. It was chosen to allow for comparison with the large amount of open literature. The blade profile is shown in Figure 1 and the blade section properties are summarized in Table 1.

Number of airfoils	7
Aerofoil Type	Controlled-Diffusion Blade
Maximum thickness	0.07C
Leading Edge Radius	0.00132m
Trailing Edge Radius	0.00186m
Chord length, C	0.15m
Pitch	0.09m
Blade Span	0.19m
Aspect ratio	1.27
Solidity	1.67
Stagger angle	-14.2°
Inlet flow angle	-37.5°
Isentropic exit velocity	19.5m/s
Reynolds number based on chord	195000

Table 1: Cascade Blade Details

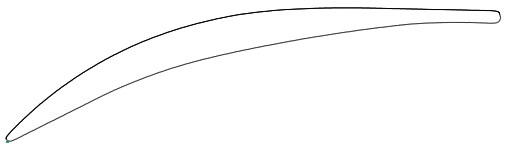

Figure 1 Blade Profile

CFD Mesh

An H-mesh is used in this work, as it is simple to construct. The mesh extends one axial chord length upstream and two axial chord lengths downstream of the blade. The long mesh downstream is to allow for mixing of the tip clearance vortex before reaching the computational domain exit. There are 156 axial, 60 span-wise and 41 pitch-wise mesh cells, giving a total of 383760 mesh cells. The mesh extends at an angle of -37.5º upstream and 0º downstream with reference to the axis. This is to match the inlet and outlet flow angles, although the outlet flow angle is not exactly axial. The blade profile is based on the measured cascade geometry (rather than the nominal coordinates).

The span-wise mesh spacing is such that it captures the tip clearance flow for up to a tip clearance of 10% span. The mesh with a 6% tip clearance at 90% axial chord can be seen in Figure 2. Each cell is 0.5% of the span, so for 6% tip clearance there are 12 cells in the gap. The pinch is two percent of the span i.e. over 4 cells. The fine mesh extends to 12% tip clearance, i.e. 26 cells. Beyond this the mesh spacing becomes larger towards mid-span before becoming finer again close to

the hub. To simulate the linear cascade, the hub radius was set to 100 m, giving a casing radius of 100.19 m.

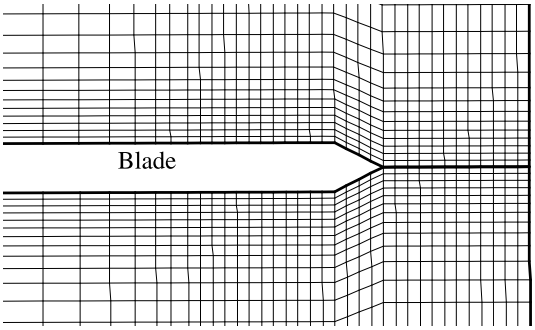

Figure 2, Pinch tip mesh for 6%span tip clearance

Boundary Conditions

The inlet boundary conditions for the stationary case are as follows: a flow angle (β_1) of -37.5°, stagnation pressure of 1.01575 bar and total temperature of 293 K. The specific heat capacity at constant pressure is 1005.0 kJ/kgK and the specific heat capacity ratio is 1.4. The exit boundary condition is a static pressure of 0.99 bar.

For the rotating case the stagnation pressure at inlet is 1.0031 bar with an inlet (absolute) flow angle of zero. To ensure the same velocity triangle as for the stationary case, the rotor rotates at 4.355 revolutions per minute.

RESULTS

No Rotation

Figure 3 and Figure 4 show the yaw angle and pressure loss coefficient at 0.9C. With 0% and 1% tip clearance, over-turning of the flow on the end-wall is due to the secondary flow passage vortex. At all clearances above 2% the flow is under-turned as the tip clearance flow dominates the much weaker secondary flow. Figure 5 shows the entropy contours and velocity vectors with 1% tip clearance where it appears that a flow structure similar to a corner stall occurs. As indicated three vortices are observed; firstly the secondary flow passage vortex (vortex 1), secondly the tip clearance vortex (vortex 2) that is located close to the blade tip on the suction surface and a third vortex (vortex 3) further along the blade surface towards the hub. Downstream of the blade the third vortex largely mixes out. Figure 6 shows the entropy contours and velocity vectors with 2% tip clearance, which shows the elimination of the corner stall region seen in Figure 5. The passage vortex is swamped by the stronger tip clearance vortex.

In Figure 4 with 0% tip clearance the pressure loss coefficient has a typical pattern as reported by Walker [4] and other literature. Noticeable features include loss at mid-span created by the blade boundary layers, a reduction in loss at 0.9span and increased loss at the end-wall due to secondary flow interaction with the mainstream flow. Of particular interest is the 1% tip clearance case. Two distinct areas of increased loss can be seen. The two vortices in the corner region, seen in Figure 5, can be seen in Figure 4 by the two bumps at approximately 0.8 and 0.89 spanwise position. With 2% tip clearance there is a reduction in the loss between 0.5span and 0.8span. Closer to the casing at approximately 0.9span there is an increase in loss due to the tip clearance vortex. 4% tip clearance has a similar pattern to that of 2% with higher loss at 0.9span. It can be seen that 6-10% tip clearance then follows a steady trend of increased loss moving towards mid-span and a reduction in peak loss suggesting a more diffused tip clearance vortex.

The position of the tip clearances central core is similar with varying tip clearance as seen when comparing figures 6 and 13. This backs up Storer and Cumpsty's [3] findings that the tip clearance vortex trajectory is independent of tip clearance size.

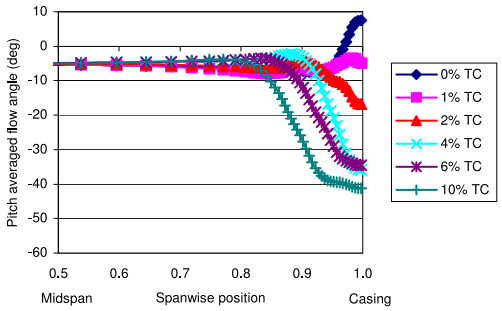

Figure 3, Yaw angle 0.9C, No Rotation

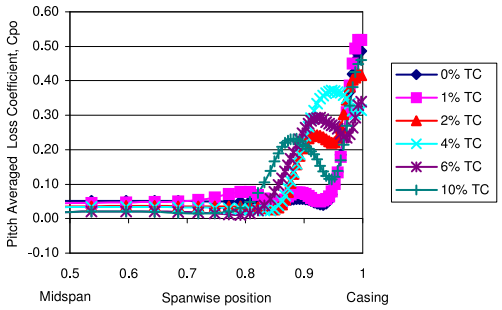

Figure 4, Cpo, 0.9C, No Rotation

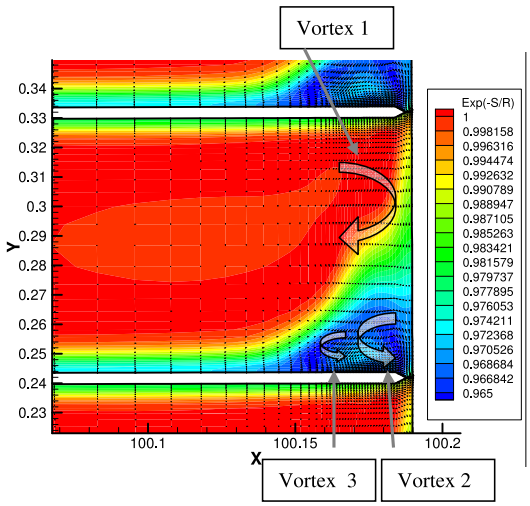

Figure 5, Entropy Contours & Velocity Vectors, 0.9C, 1%TC, no Rotation

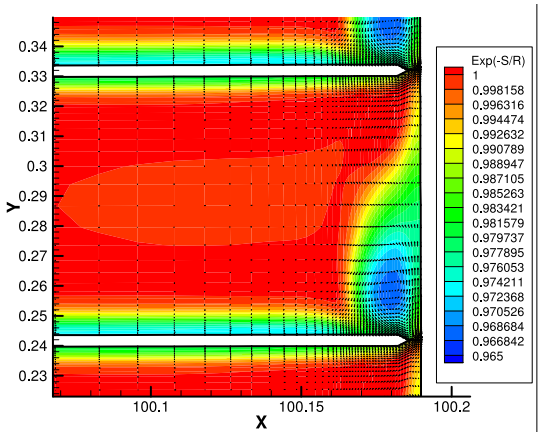

Figure 6, Entropy Contours & Velocity Vectors, 0.9C, 2%TC, no Rotation

Static Pressure Profiles

At 3% span from the blade tip the static pressure distribution is significantly affected by the tip clearance flow as seen in Figures 7 and 8, for the smaller and larger tip clearance ranges, respectively. 1% tip clearance has a lower pressure at mid chord and higher pressure at the trailing edge on the suction surface when compared to the case without tip clearance. For larger tip clearances a general pattern is observed; on the pressure surface there is an increase in pressure at the leading edge and a slight increase at the trailing edge. The suction surface has an increase in pressure at the leading edge and a large decrease from about 0.4C towards the trailing edge. This decrease is due to the tip clearance vortex interacting on the suction surface of the blade resulting in higher velocity fluid close to the surface. The decrease in pressure on the pressure surface is due to the flow accelerating radially along the blade and around the tip. This can be seen in Figure 6, both by the velocity vectors and the entropy contours, which suggest a smaller boundary layer close to the tip.

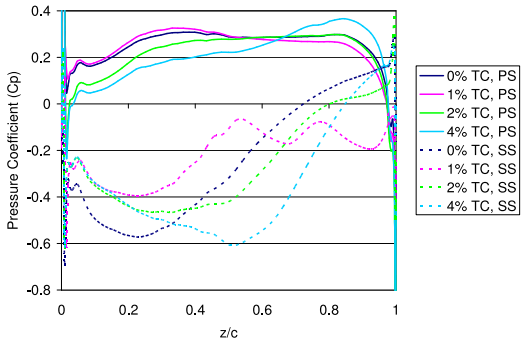

Figure 7, Cp at 3%-span From Tip No rotation

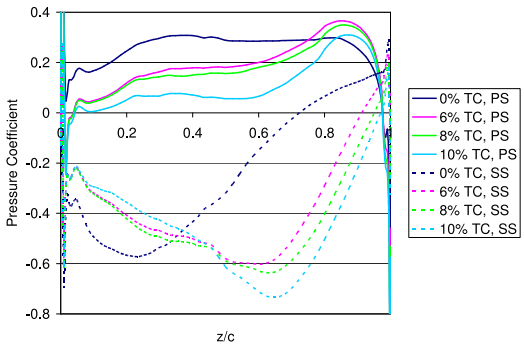

Figure 8, Cp at 3%-span From Tip No rotation

The blade loading is shown in Figure 9. The blade with no tip clearance has a small decline in blade loading towards the end of the blade. This decrease in loading is due to the interaction of the mainstream flow with the boundary layer and the passage vortex, creating an increased pressure on the suction surface. All of the tip clearances have a decrease in loading on the pressure surface within ten percent of the tip. The 1% case has reduced loading further away from the tip, spanwise along the pressure surface. Particularly the 1% and also the 2% tip clearances have a decrease in blade loading towards the tip due to an increase in pressure on the suction surface. For 4% tip clearance and larger there is a reduction in pressure on the suction surface close to the tip as well as the reduction in pressure surface static pressure. The reduction in suction surface pressure is larger than that of the reduction in pressure surface pressure and so overall there is an increase in blade loading. However it should be noted that the reduction in blade length generally offsets any increase in blade tip loading. At mid span a change in loading is observed. Because the

computations are performed with fixed pressure boundary conditions, there is a slight change in mass flow rate at mid span due to the change in tip clearance flow blockage. The changed mass flow rate changes the angle of attack and the loading.

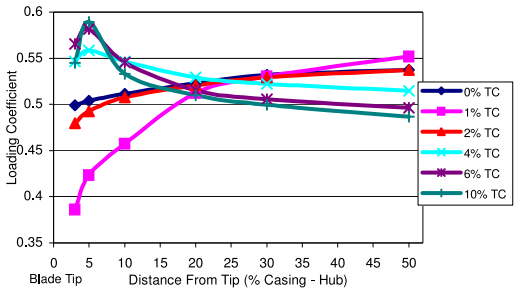

Figure 9, Blade Loading No Rotation

Flow through the cascade passage

This section looks in more detail at the tip clearance flow physics through the passage. An arbitrary 6% tip clearance is used. Figures 10 to 13 show the entropy contours and velocity vectors through the passage from the leading to the trailing edge of the cascade without rotation.

Between 0C and 0.4C there is no roll up of the tip clearance flow, but at 0.6C the tip clearance flow starts to roll up into a tip clearance vortex. At 0.1C (Figure 10) there is some loss on the end-wall. The boundary layer on the blade surface has grown, with more loss on the pressure surface than the suction surface. There is no evidence of a passage vortex and little tip clearance flow. At 0.4C (Figure 11) significant tip clearance flow is seen, causing a thickening of the end-wall loss near the SS and a reduction near the PS. Some indication of a counter vortex can be observed. At 0.6C, (Figure 12) the tip clearance flow rolls up into a tip clearance vortex, positioned on the tip of the suction surface. This corresponds with the blade pressure coefficient plots, where the position of maximum blade loading (difference between PS and SS pressure coefficient) is close to 0.6C. The maximum pressure difference moves along the chord with increasing tip clearance, suggesting that the roll up point will move downstream with increasing tip clearance. Also of note is the increase in suction surface boundary layer thickness due to the adverse pressure gradient. The loss created on the suction surface of the pinch tip has increased. A general trend is observed from 0.6C up to the trailing edge. Firstly the tip clearance vortex becomes stronger with increasing axial position. Secondly the tip clearance vortex moves pitch-wise away from the suction surface, until at the trailing edge the center is approximately at 0.25pitch. This is less than that seen in much of the literature with high stagger blading where the vortex moves across most of the passage.

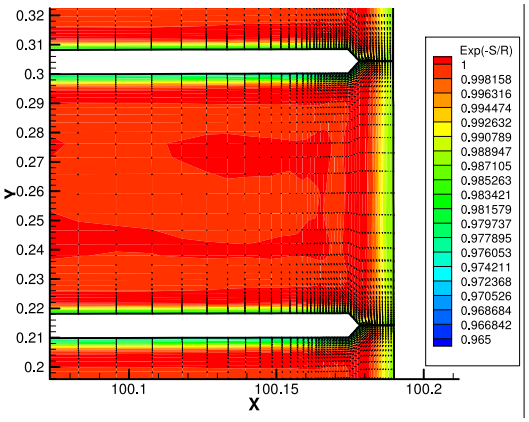

Figure 10, Entropy Contours & Velocity Vectors, 6%TC, 0.1C

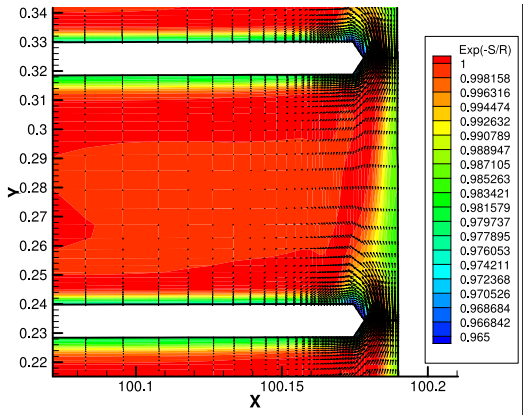

Figure 11, Entropy Contours & Velocity Vectors, 6%, 0.4C

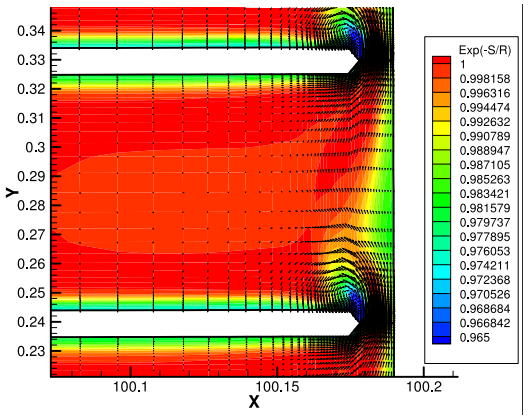

Figure12, Entropy Contours & Velocity Vectors, 6%, 0.6C

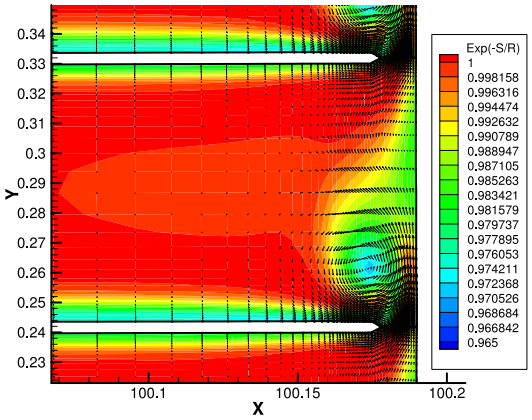

Figure13, Entropy Contours & Velocity Vectors, 6%, 0.9C

Cascade with moving end-wall

Noticeable changes from the non-rotating cases include a decrease in loss at the casing because in the relative frame of motion the end-wall is doing work on the fluid. It should be noted that if the fluid was inviscid then the casing would not affect the tip clearance flow as it would be a purely pressure driven jet. The secondary flow is no longer identifiable with a moving end-wall.

Figure 14 shows the entropy contours & velocity vectors for 6%TC and 0.9C with a moving end-wall, this can be compared to Figure 13 without rotation. As well as the differences discussed above, another difference is the lack of an induced vortex that is present without rotation. This is because the velocity gradient is lower with a moving end-wall.

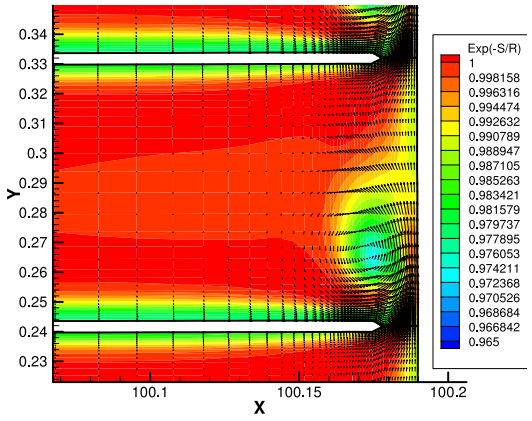

Figure 14, Entropy Contours & Velocity Vectors, 6%TC, 0.9C, with Rotation

Figure 15 shows 1%TC at 0.9C with rotation. When compared to Figure 5 without rotation it can be seen that the corner stall no longer occurs. This is because of the low energy fluid in the corner stall being energized by the increased tip clearance flow due to the effect of the end-wall motion. There is a smaller tip clearance vortex and the third vortex that was observed on the blades suction surface is not present.

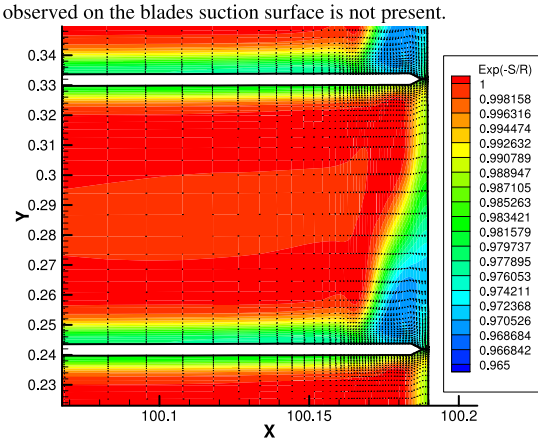

Figure 15, Entropy Contours & Velocity Vectors, 1%TC, 0.9C, with Rotation

Flow development with and without rotation

The pitch-wise mass averaged pressure loss coefficient for the non-rotating and rotating blades are shown in Figure 16 and Figure 17 respectively for 6% TC with varying axial chord positions. To allow for comparison the upstream data has also been included.

There are several differences between the rotating and non-rotating cases. It can clearly be seen in Figures 16 and 17 that when comparing the pressure loss coefficient, the loss is larger close to the end-wall for the non-rotating case. As mentioned above the moving end-wall does work on the fluid. The peak loss due to the tip clearance vortex is very similar both in span-wise position and magnitude for all axial sections shown. The magnitude quickly diminishes towards mid-span at 1.0C (i.e. the trailing edge) so that the loss has reached its mid-span value by 0.84span with rotation; without rotation the higher loss region extends to 0.8span. This is clearer when considering the loss at 2.0C (i.e. one chord length downstream of the trailing edge). With rotation the loss has settled to the mid-span value by 0.8span but without rotation it extends to 0.7span.

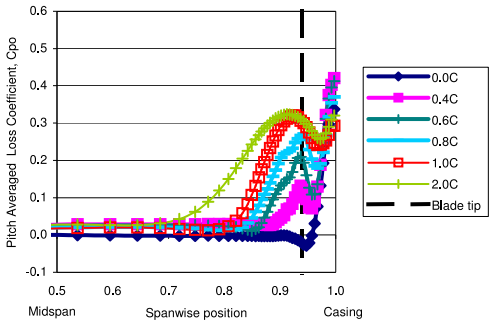

Figure 16, Pressure Loss Coefficient through Stage, 6%TC, No Rotation

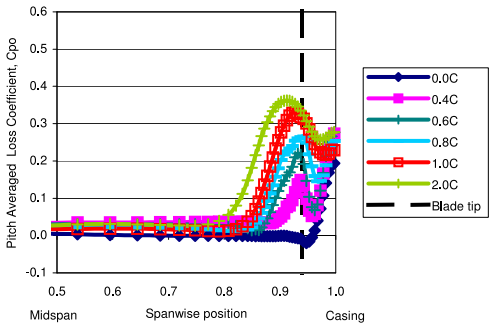

Figure 17, Pressure Loss Coefficient through Stage, 6%TC, With Rotation

Figures 18 and 19 show the yaw angle for varying axial chord position with 6% tip clearance. It can be seen that upstream the angle is approximately minus -37º until the leading edge. As the flow moves through the stage it is turned until exiting at approximately -5º at mid-span. Until approximately 0.8 span there is no under-turning close to the tip of the blade; beyond this under-turning is present. The magnitude of the under-turning increases as the span-wise position increases, so that in the tip clearance region the flow is barely turned at all. After the trailing edge there is some turning due to span-wise mixing.

With rotation, (Figure 19) there is more under-turning due to the shear layer on the end-wall dragging the fluid toward the pressure surface. Unlike the non-rotating case the level of under-turning further increases downstream of the trailing edge. This is because of the relative motion between the blade and end-wall which continues downstream of the trailing edge.

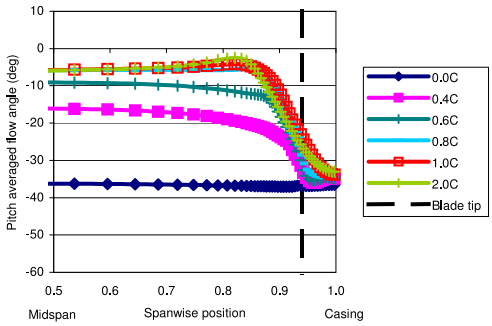

Figure 18, Yaw Angle through Stage, 6% TC, No Rotation

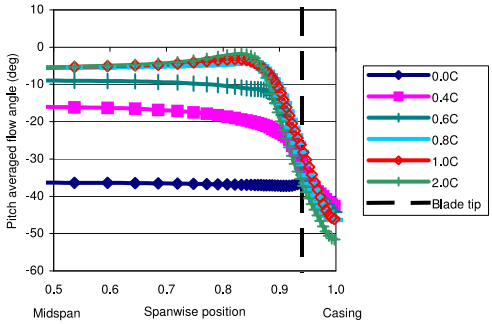

Figure 19, Yaw Angle through Stage, 6% TC, With Rotation

CONCLUSIONS

The work undertaken in this paper has attempted to develop the understanding of large tip clearance flow in axial compressors. Unlike most published literature the tip clearances are relatively large and the blade geometry is that of the later stages. This means that the blade has relatively low loading and stagger angle compared to the geometry of the low-pressure stages. It is important to note that the study is performed using a linear cascade of airfoils. The following conclusions may be drawn:

- With this linear cascade it was found that the tip clearance flow has no effect on the blade pressure distribution at 50% span but causes significant changes close to the tip. The effect of the tip clearance flow on the pressure distribution close to the tip is dependent on the tip clearance size. Generally, decreased loading occurs for the first 40% of the chord and increased loading for the last 60% of the chord. Overall the change in pressure distribution results in a reduction in loading coefficient towards the tip of the blade below 2% tip clearance.

Above 2% tip clearance there is an increase in blade loading towards the blade tip.

- For 6% tip clearance the tip clearance vortex rolls up at approximately 60% chord. This is much later than most literature describes. From the blade pressure distribution this is at approximately the position for the highest blade loading. Literature suggests that the maximum blade loading moves further along the chord with increasing tip clearance. This suggests that the roll-up point will move further towards the trailing edge with increasing tip clearance.

- As the clearance vortex grows through the passage it moves from the suction surface towards mid pitch near the trailing edge. In this study this movement is much less than what most of the previous work on smaller tip clearances suggests. The size of the tip clearance vortex alters with varying tip clearance.

- Rotation also results in notable changes to the tip clearance vortex. Without rotation there is over-turning close to the tip of the blade for 1% tip clearance. All other tip clearances, with and without rotation, under-turn the flow in the tip gap region. With rotation the tip clearance vortex moves further across the passage away from the suction surface. The tip clearance vortex stays closer to the end-wall with rotation than without.

- Without rotation a counter vortex is observed on the end-wall, but this is not observed with rotation. This is because with rotation the relative motion of the end-wall is in the direction of the tip leakage.

- There is reduced loss on the end-wall with rotation due to the work done by the moving end-wall on the fluid in the rotating frame.

- A corner stall is present with 1% tip clearance with no rotation. Rotation or larger values of tip clearance prevent this corner stall, as the stronger tip clearance vortex induces lower loss fluid along the suction surface.

REFERENCES

1. Suder, K. L., 1998, "Blockage Development in a Transonic, Axial Compressor Rotor." J. Turbomachinery, **120**, pp.465-476.

2. Layachi, M. Y. and A. Bölcs., 2002, "Effect of Tip Clearance on the Characteristics of a 1.5 Compressor Stage with regard to the Indexation." 9th. Symposium on Transport Phenomena and Dynamics of Rotating Machinery, Hawaii, February.

3. Storer, J. A. and N. A. Cumpsty., 1991, "Tip Leakage Flow In Axial Compressors." J. Turbomachinery **113**(2): 252-259.

4. Walker M., Gregory-Smith D.G., He L. 2005. "A Study of Large Tip Clearance in a Row of Low Speed Compressor Blades." Proc. 6th. European Conference on Turbomachinery, Lille, **1**, 122-134. March 2005

5. Glanville, J. P., 2001, "Investigation Into Core Compressor Tip Leakage Modelling Techniques Using a 3D Viscous Solver." ASME Paper 2001-GT-0336.

6. Van Zante, D. E., A. J. Strazisar, et al.. 2000, "Recommendations for achieving accurate numerical simulation of tip clearance flows in transonic compressor rotors." J. Turbomachinery **122**(4): 733-742.

7. Hunter, I. H. and N. A. Cumpsty., 1982, "Casing Wall Boundary-Layer Development Through An Isolated Compressor Rotor." Journal of Engineering for Gas Turbines and Power **104**(4): 805-818.

8. Lakshminarayana, B., M. Pougare, et al., 1982, "Three-Dimensional Flow Field in the Tip Region of a Compressor Rotor Passage - Part I: Mean Velocity Profiles and Annulus Wall Boundary Layer." J. Engineering for Gas Turbines and Power, **104**, pp.760-771.

9. Horlock, J. H, 1995, "Secondary Flow in Repeating Stages of Axial Turbomachines." Proc. I. Mech. E., Part A, Journal of Power and Energy, **209**, pp. 101-110.

10. He, L., 2000, "Three-Dimensional unsteady Navier-Stokes analysis of stator-rotor interaction in axial-flow turbines." Proc. I. Mech. E., Part A, Journal of Power and Energy, **214**, pp13-22.

11. Sanger, N. L., 1983, "The Use of Optimization Techniques to Design Controlled-Diffusion Compressor Blading." Journal of Gas Turbines and Engineering For Power **105**: 256-264.

B.2 Paper 2. Williams et al. [2008]

Proceedings of ASME Turbo Expo 2008: Power for Land, Sea and Air
GT2008
June 9-13, 2008, Berlin, Germany

GT2008-50557

EXPERIMENTS AND COMPUTATIONS ON LARGE TIP CLEARANCE EFFECTS IN A LINEAR CASCADE

Richard Williams, David Gregory-Smith, Li He*, Grant Ingram
University of Durham, South Road, Durham, DH1 3LE, UK
(*currently Oxford University, Dept of Engineering Science)

ABSTRACT

Large tip clearances typically in the region of six percent exist in the high pressure stages of compressors of industrial gas turbines. Due to the relatively short annulus height and significant blockage, the tip clearance flow accounts for the largest proportion of loss in the HP. Therefore increasing the understanding of such flows will allow for improvements in design of such compressors, increasing efficiency, stability and the operating range. Experimental and computational techniques have been used to increase the physical understanding of the tip clearance flows through varying clearances in a linear cascade of controlled-diffusion blades.

This paper shows two unexpected results. Firstly the loss does not increase with clearances greater than 4% and secondly there is an increase of blade loading towards the tip above 2% clearance. It appears that the loss production mechanisms of the pressure driven tip clearance jet do not increase as the clearance is increased to large values. The increase in blade force is attributed to the effect of the strong tip clearance vortex which does not move across the blade passage to the pressure surface, as is often observed for high stagger blading.

These results may be significant for the design of HP compressors for industrial gas turbines.

NOMENCLATURE

C	Chord	m
Cx	Axial Chord	m
	Static Pressure Coefficient	-
	Total Pressure Loss Coefficient	-
	Blade Loading Coefficient	-
Po	Total Pressure	Pa
Po_1	Inlet Total Pressure	Pa
Ps	Static Pressure	Pa
Ps_2	Exit Static Pressure	Pa
PS	Pressure Surface	-
$\mathrm{Re} = \frac{VC}{\nu}$	Reynolds Number	-
SS	Suction Surface	-
TC	Tip Clearance. % Duct Height	-
X	Axial	-
β	Yaw angle Rel. Axial	-

INTRODUCTION

Industrial axial compressors usually have blade rows at low pressure (LP), intermediate pressure (IP) and high pressure (HP) stages. Within the stages there are numerous sources of loss, traditionally “profile loss”, “end wall loss” and “leakage loss”. The percentage that each source contributes towards the total loss varies from stage to stage. One such loss source (“leakage loss”) is the pressure driven tip clearance (TC) flow which passes from pressure to suction surface over the end of the blades in non shrouded rows. Within LP stages the TC is usually within one percent of the annulus height and there is a limited effect on the overall loss of the stage at the normal operating condition. However within the LP stages the TC flow is widely understood to act as a trip towards stage stall. Due to this and the applicability within aero engines most TC work has been undertaken for small TC values where the loss is approximately proportional to the TC gap.

In the later stages the TC flow has a larger influence on the overall stage loss, mostly because of the increased relative TC value (typically about six percent span) due to the reduced length of blades. Note that the absolute TC value is not necessarily larger but relative to span it is. The rotor and stator TC flow can create a blockage up to approximately twenty percent span from the casing and hub respectively, creating a

significant blockage. This blockage affects the mass flow rate that can travel through the HP thus significantly affecting the operating and stability range of the compressor.

As argued by Denton [1] loss sources in turbomachinery are difficult to quantify, therefore it is important to have a physical understanding of the flow and origins of loss. The motivation for this work is further to understand and model the flow physics with large tip clearance flows; this progresses work previously undertaken by Williams [2] and Walker [3]. Previously most literature suggests that increasing the TC value has a diminishing effect on stage efficiency above an optimum. However this paper shows an increasing tip clearance can have a beneficial effect on the stage loading. This will allow for improved designs aimed at reducing losses and increasing the operating range of the HP compressor, therefore increasing efficiency and the surge/stall limits.

Tip Clearance Flow Physics

As is widely known, the tip clearance flow consists of a pressure driven jet which moves from the pressure surface to the suction surface across the tip of the blade. As discussed by Peacock [4] the strength of the TC jet depends on the blade pressure field close to the tip of the blade. This tip clearance flow rolls up into a tip clearance vortex along the suction surface of the blade which then moves across the passage towards the pressure surface of the adjacent blade. Storer and Cumpsty [5] found that the point at which this happens is usually at the maximum loading of the blade. They also concluded that the axial position of the highest blade force varies with TC value; a higher TC value moves the position of highest loading further downstream thus delaying the roll up of the TC vortex. In HP blades, the vortex remains closer to the SS (Suction Surface) and so is different to that in LP blades. Although the TC gap size affects the strength of the TC vortex Hunter and Cumpsty [6] found that the trajectory is unaffected.

Gbadebo [7] considers the interaction between tip clearance flows and 3-D flows close to the endwall. He found that the tip clearance flow largely removes the 3-D secondary flows. This was attributed to the suppression of the LE horseshoe vortex and the interaction of the tip clearance rolling up into a TC vortex. Clearly then an optimum tip clearance will increase the operating range of the stage. The flow within the tip clearance depends on the thickness of the blade. In the case of a compressor with thin blades the flow separates from the tip forming a vena contracta. This separates the flow from the blade tip reducing the effective tip clearance. Work undertaken by Tang [8] measured the flow through the tip clearance within a cascade for 2 different tip gaps. They found a tip separation vortex formed on the tip due to the sudden turning undertaken by the flow entering the TC. Sjolander [9] dedicates a section on large tip clearance flows up to 15% chord and he presents measurements by De Cecco [10] for a turbine. He suggests that for larger clearances the blade loading is not entirely responsible for the tip clearance flow because of the huge under turning undertaken in the end wall region.

The trajectory of the TC vortex is clearly dependent on the interaction with the mainstream flow. Saathoff and Stark [11] investigated the trajectory of the TC vortex with varying inlet angle they found that as the inlet angle/loading is increased the TC trajectory moves further across the passage thus creating a larger blockage. At stall the TC vortex moves across the LE of the adjacent blade. Therefore for higher loading the TC flows can have a negative axial velocity.

The TC vortex counteracts the secondary/passage vortex and for the larger TC values completely suppresses it. However it has been found by Van Zante, et al [12] and Williams [2] that for some tip clearance values a counter rotating vortex is found which lies on the casing/hub and prevents the movement of the TC vortex across the passage. This applies for smaller TC values while the for larger TC values the counter rotating vortex is completely suppressed by the tangential TC flow.

One of the main differences between the LP and HP geometry is that HP geometries typically have lower blade loading i.e. lower stager angle and turning. Therefore the TC flow in the later stages is almost tangential as opposed to the earlier stages where it often has an upstream component due to the high stager angle. The relative Mach numbers (typically 0.4-0.6) are much lower than the LP (typically larger than 1)

Clearly the stage geometry significantly affects the TC vortex therefore control of the trajectory and loss should be possible.

This work investigates the TC flow within a linear cascade. There are significant well known differences between cascade testing and rotating machines. Namely rotating machines have a skewed inlet, twisted blades, radial effects, moving end walls and for the real machine are in a multi row/stage environment. Therefore the real case is far more complicated than the idealized linear cascade but the results are still valid and useful. Peacock [4] discussed the differences between cascades and rotating machines and found that the casing motion has a significant effect on the tip clearance flow due to the viscosity of the fluid. The walls relative motion pulls the fluid through the TC gap. Previously Williams [2] undertook a study which investigated the difference between moving end walls and the stationery cascade. He concluded that with the same inlet conditions the moving end wall skews the flow within the TC region which increases the loading on the tip of the blade. Also in the relative frame of the blade the end wall drags the TC flow through the clearance region increasing the flow. This makes the TC vortex stronger and pushes the TC vortex core away from the SS of the blade further across the passage while keeping it closer to the casing thus reducing blockage. In the relative frame the end wall effectively does work on the flow adding energy to the fluid and therefore the overall loss with a moving end wall is reduced.

Real machines are multistage and in the HP the low Mach number means the TC flow has an effect on the adjacent rows. This is mostly the case for the downstream row where the casing/hub section of the Stator/Rotor will see overturned

flow, thus increasing the loading and almost certainly producing a corner stall.

This work shows that large TC values have a beneficial effect on the blade loading of the cascade. This paper strives to further the understanding of large tip clearance flows and so explain the reason behind the beneficial effects with loading. To do this experimental data from a linear cascade is presented and consequently used to assess the capability of a computational code to predict the large TC flows. The CFD code is then used to advance the understanding of the TC physics.

EXPERIMENTAL WORK

This section of the paper shows some of the linear cascade experimental work which will later be used to assess the CFD code. However firstly there is a brief explanation of the wind tunnel, cascade and measuring equipment.

Experimental apparatus

The linear cascade compressor test facility based at the Durham University uses an open flow wind tunnel arrangement, as described by Yang [13]. This consists of a fan, diffuser, settling chamber, gauze screen, 7.5:1 contraction, honey comb and test section. The flow exits the tunnel through a 0.25x0.8m section into the cascade.

The cascade located at the wind tunnel exit exhausts to atmosphere one axial chord after the trailing edge. As shown in Figure 1, seven aerofoil including profiled upper and lower walls give eight passages in total; allowing for reasonably periodic flow. Hinges at the top of the cascade enables the geometric inlet angle to be altered. A bottom splitter plate allows for the vertical change in inlet due to the change in angle; below the splitter plate a bypass exhausts to atmosphere. The bypass is controlled using a moveable plate to control the diffusion. A side wall boundary layer bleed is located one axial chord length upstream of the leading edge. The bleed plate is 3mm thick ensuring a high quality bleed.

The controlled diffusion aerofoil used is that as designed by Sanger [14] and intensely tested in open literature including Sanger and Shreeve [15] and Williams [2]. Blade properties are shown in Table 1 and the profile is shown in Figure 2. Two of the blades are instrumented, these being the central one and one other which can be moved in to any blade location. There are tappings at various locations along the blade on both surfaces. Passing the blades radially through the hub enables the TC value to be altered. The blades are supported using a 3mm threaded bar at the tip and supported by the hole in hub at the other end. This tip suspension bar has some effect on the blade loading close to the tip but due to its relatively small size this is a limited effect.

Instrumentation

Both 5-hole probe and blade static pressure measurement instrumentation is available. Two 5-hole probe measurement plains were used 0.5Cx (50% axial chord) upstream and 0.2Cx downstream of the blade row. The probe is moved and held using traverse gear located downstream of the cascade. The upstream plane is traversed using a kinked probe projected through the blade. A straight probe was used for the downstream traverse. Both probes used had a diameter of 4.5mm limiting the measurements close to the wall to approximately 3% span.

Number of aerofoil	7
Pitch	0.09m
Blade Span	0.19m
Stager angle	14.2°
Inlet flow angle (Nominal)	37.5°
Isentropic exit velocity	19.5m/s
Reynolds number based on chord	195000
Side wall Bleed Location	1 Axial Chord Upstream
Pitot-Probe Location	1 Cx Upstream

Aerofoil Type	Controlled-Diffusion Blade
Chord length, C	0.15m
Aspect ratio, h/C	1.27
Maximum thickness	0.07C
Leading Edge Radius	0.00132m
Trailing Edge radius	0.00186m
Solidity, C/S	1.67

Table 1, Cascade Properties

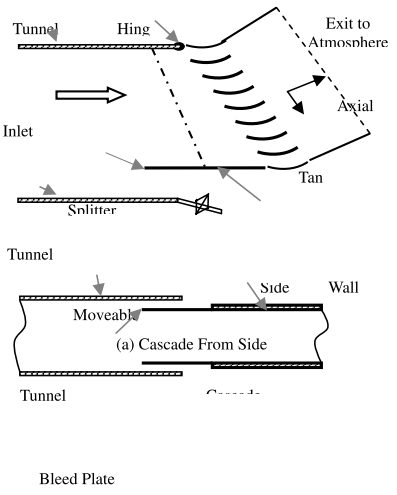

Figure 1, Cascade Details

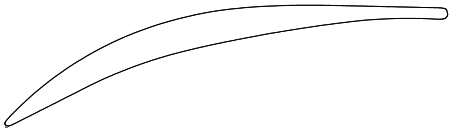

Figure 2, Blade Profile

The probe pressures are measured relative to the upstream total pressure via a pitot-probe positioned 1.0Cx upstream of the cascade. The upstream total to atmospheric pressure is measured as the isentropic dynamic pressure. The traverse gear is operated and the pressures recorded using software developed at Durham University. Calibration of the pressure transducers and probes is accounted for within the software. Probe calibration is undertaken using a calibration rig at Durham University; this process is described by Ingram [16]. The software post processes the data including pitch mass averaging thus allowing for a traverse grid of varying density.

The same software system was used to measure the blade static pressures. By controlling a scani-valve connected to the blade pressure tapings only one transducer was required. The upstream total to downstream static (atmospheric) dynamic pressure was also recorded to enable the values to be made non-dimensional.

Inlet Conditions

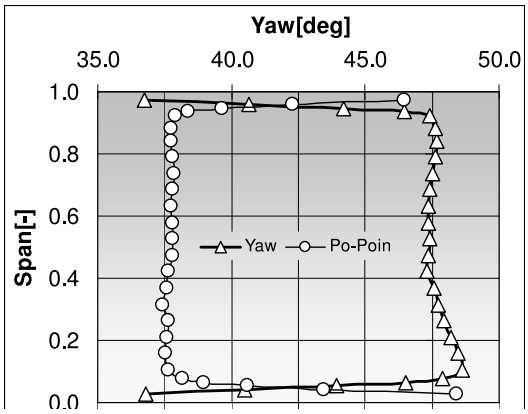

Figure 3, Cascade Inlet conditions

The inlet flow to the cascade was conditioned to ensure uniform periodicity and an inlet flow angle of 37.5°. The downstream results (Figure 4) suggest that acceptable periodicity has been obtained. The inlet flow angle however was still approximately 5° different to the geometrical angle. Good practice was found to include the angle of the bottom plate the bottom diffuser and the diffusion of the side-wall bleeding being accurately set. The inlet pitch mass averaged yaw and total pressure can be seen in Figure 3. It can be seen that there is a significant boundary layer with low total pressure and high skew on the walls, which can be attributed to the sidewall bleed pushing the flow down. Considering the multi-row case with highly skewed flow at the wall these inlet conditions were deemed acceptable.

Also of note is the increase in total pressure and decrease in yaw towards the hub. However because only the outer 50% span is of interest this is acceptable.

Downstream Flow Results

Initially to ensure good periodicity and a base to compare result 0% TC was analysed across the central two passages for the full span of the cascade. The stagnation pressure loss coefficient is shown in Figure 4 for the 0% TC case across the full passage.

Four tip clearance values were then evaluated (0%, 1%, 2% and 6% span) for both central passages of the cascade but only covering the outer 50% span. Cpo loss contour plots are shown in Figure 4 to Figure 7. Pitch mass averaged results of yaw and Cpo loss can be seen in Figure 8 and Figure 9 denoted "Meas". These are referenced to mid-span thus highlighting the effects due to the end-wall region secondary flows. Of note are the increase in size of the tip clearance vortex and blockage. The counter rotating vortex is clearly present and indicated in Figure 6. For the 6% case it can be seen that higher momentum flow is pulled onto the wall decreasing the Cpo loss close to the wall.

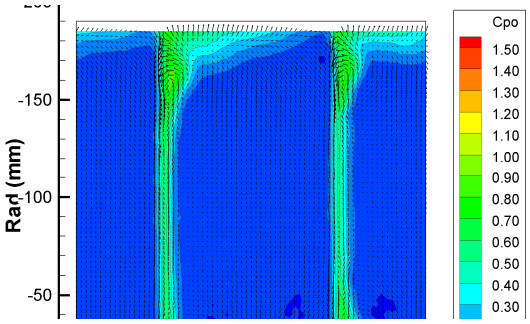

Figure 4, 0%TC, 1.2Cx, Experimental Loss (Cpo)

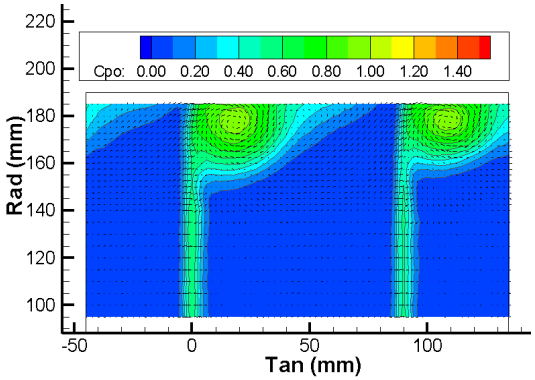

Figure 5, 1%TC 1.2Cx, Experimental Loss (Cpo)

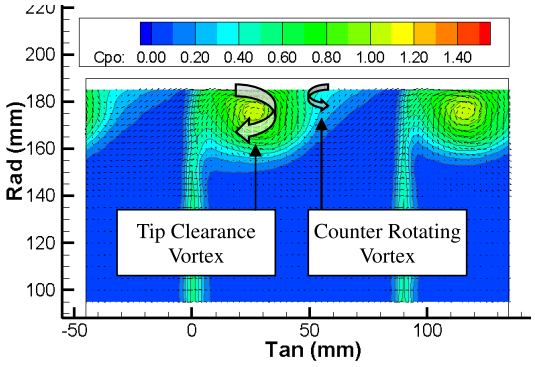

Figure 6, 2%TC 1.2Cx, Experimental Loss (Cpo)l

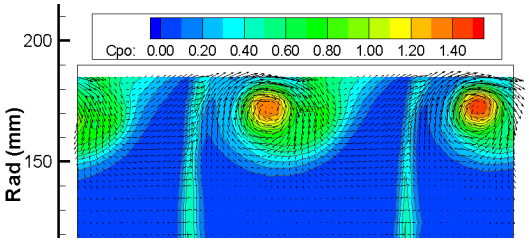

Figure 7, 6%TC 1.2Cx, Experimental Loss (Cpo)

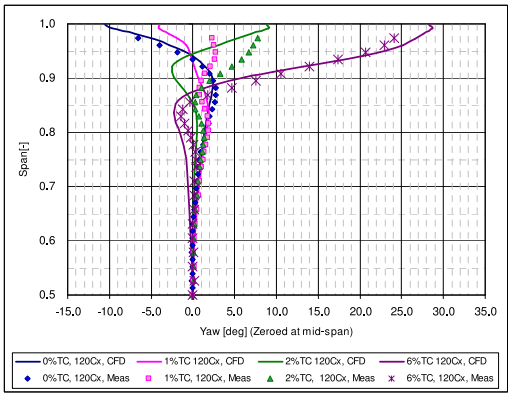

Figure 8, Pitch Mass Averaged Yaw 1.2Cx

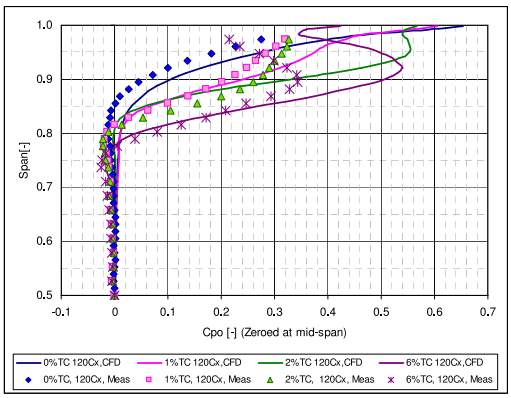

Figure 9, Pitch Mass Averaged Cpo 1.2Cx

Blade Static Pressure Results

The blade pressure coefficient profiles are shown in Figure 10, Figure 11 and Figure 12 for 50%, 90% and 98% span-wise locations respectively. Of note is the change in blade loading towards the tip of the blade with increasing tip clearance values. In general with increasing TC value there is a reduction in loading at the leading edge and an increase in loading towards the trailing edge. At 98% span and 6% TC the experimental data shows what appears to be a high pressure region on the suction surface at approximately 0.6Cx, this is almost certainly an effect of the blade support rod. Integrating the pressure coefficient plots creates a blade force; this can be seen in Figure 13where blade force is plotted against distance in blade span from the tip of the blade. Figure 14 shows the overall blade force for each measured TC, and this is shown relative to the zero clearance case. Importantly as will be discussed later this shows an increase in tangential blade loading towards the tip of the blade for the six percent tip clearance.

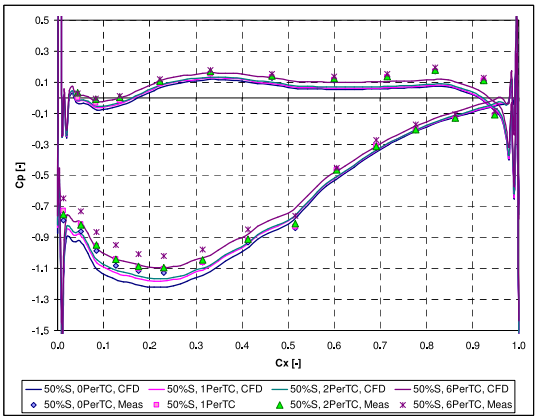

Figure 10, Blade Pressure Coefficient (Cp) at 50% Span

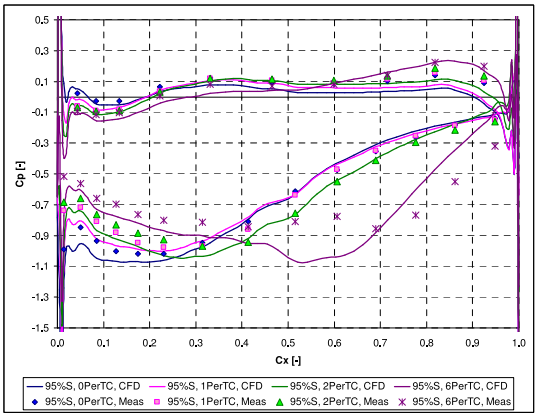

Figure 11, Blade Pressure Coefficient (Cp) at 95% Span

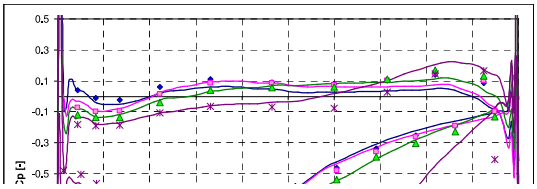

Figure 12, Blade Pressure Coefficient (Cp) at 98% Span

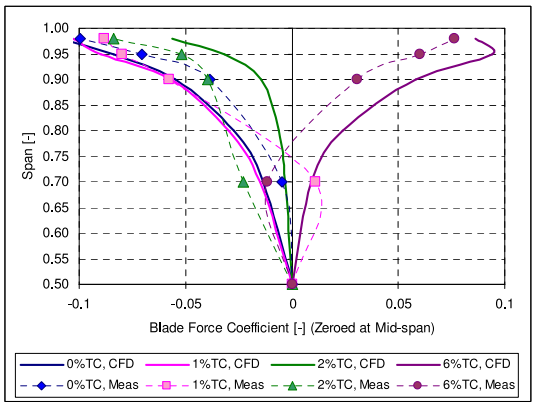

Figure 13, Blade Force Coefficient

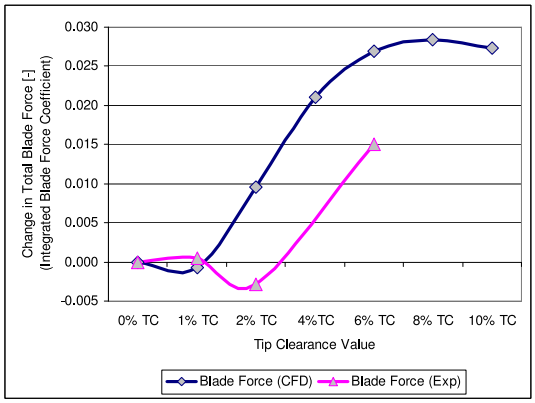

Figure 14, Total Blade Force vs. TC, CFD and Exp. Data

COMPUTATION FLUID DYNAMICS

CFD Code

This paper uses a code developed by He at Durham University; the same code was used by Williams [2] and Walker [3] and a good description of the code's features can be found by He [17]. The code iteratively solves the Reynolds averaged 3D unsteady compressible Navier-Stokes equations and turbulence closure is achieved by using the Spalart-Allmaras model. The governing equations are discretized in space using the cell centred finite volume scheme which are integrated in time using the explicit four stage Runge-Kutta method. To accelerate convergence the multi-grid technique and local time stepping is used.

The code was run to 5000 time steps, this ensured good convergence with a maximum axial velocity change between time steps <0.001 and the difference between inlet and outlet Mass flow <0.05%. Boundary layer trips are located on

the blade SS and the casing to ensure a turbulent boundary layer and convergence.

Grid

A structured H mesh is used for this study and the tip clearance is modelled using the pinch tip method. Several methods for modelling the tip clearance have been proposed throughout literature and these have varying levels of complexity and success. This work uses a simple pinch tip model as used by Williams [2] and also reported in various open literature e.g. Van Zante [12] and Gupta [18]. Although this method is not as accurate as what can be achieved, it has been shown to give a reasonable result without adding complexity and increasing computational time. To ensure the pinch tip does not create numerical instabilities, good practice is to ensure that the tip angle is no larger than sixty degrees from the radial direction (as shown in Figure 15). The tip clearance is defined as the distance between the tip of the pinch and the casing.

Understanding the grid dependency of the solution is crucial to obtain a good quality result. For this reason a mesh dependency study was undertaken to develop a mesh capable of picking up all the physical flows while ensuring convergence and a good quality result using the experimental data as a reference. In general it was found that the grid dependency diminishes with increased tip clearance i.e. the interaction between the flow on the tip and the casing diminishes. The pitch-wise grid was found to have little effect at mid-span as long as the blade boundary layer mesh size was reasonable. However to prevent diffusion of the tip clearance vortex the mesh needs to be as fine as possible close to the casing, and therefore a balance needs to be obtained. Within the tip clearance it was found that if the pitch-wise grid is too fine then convergence is poor due to instabilities. Therefore the pitch mesh was made uniform at the casing and then linearly distributed until the start of the pinch, as seen in Figure 16. The grid dependency study found that there was a 15% change in Cpo loss at 1.2Cx between the grids investigated.

The radial spacing of the mesh has a large effect on the qualitative result. Thus while ensuring that the y+ values were reasonable on the casing the best result was used from that obtained from the grid dependency study. The mesh in general is fine and uniform within the outer 12 % span and then expands until the cells are approximately 2.5% span at the hub.

As shown in Figure 16 in the k plane (constant radius) the inlet mesh follows the inlet flow angle 0.5Cx upstream and downstream the mesh extends 2.0Cx after the trailing edge approximately at the flow angle, so this allows for any potential boundary effects to be minimised.

The hub was defined as an inviscid wall thus ensuring that only the outer part of the cascade has an effect on the result. To approximate a linear cascade the hub radius is set to 100m. Therefore there are 6981 blades to ensure the correct pitch of 90mm although only 3 passages are solved.

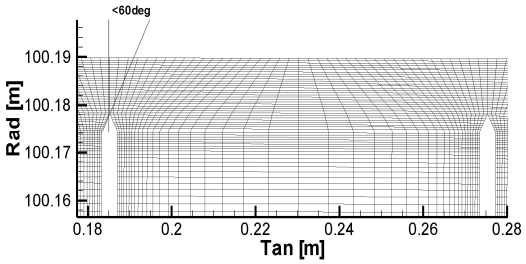

Figure 15, Example of Mesh for 6%TC at 0.9Cx

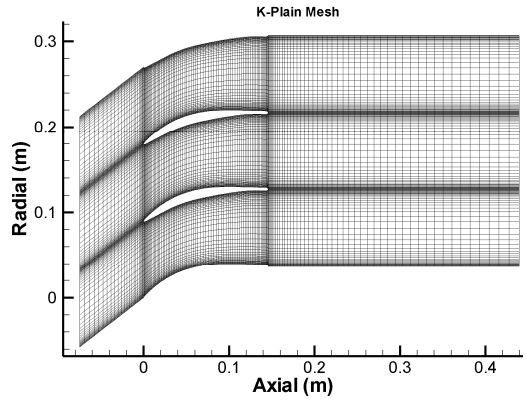

Figure 16, Example Mesh for K-Plain

Boundary Conditions

At inlet the yaw angle and total pressure are set to be the same as for the experimental inlet conditions for the outer 50%. Closer to the hub the inlet conditions are set the same as at mid-span.

At outlet the static pressure is set at the hub and the span-wise variation is determined by radial equilibrium. The back pressure is set to ensure the velocity is approximately 3 times higher than for the experimental rig to ensure convergence. However the Reynolds number is set to be the same as for the experimental cascade (Re = 1.91×10^5).

CFD STUDY, EXPERIMENTAL VS. COMPUTATIONAL

Seven different TC values have been computationally assessed 0%, 1%, 2%, 4%, 6%, 8% and 10%. Often it is more useful to consider the TC in terms of blade chord so for this case with an aspect ratio of 1.27 the clearances assessed are 0%, 1.27%, 2.53%, 5.07%, 7.6%, 10.13% and 12.67% of chord.

Firstly it is important to assess CFD against experimentation. Figure 8 and Figure 9 show the pitch mass average yaw and Cpo for the 0%, 1%, 2% and 6% tip

clearances; 20% axial chord downstream of the trailing edge. Yaw angle is defined relative to the axial direction. Quantitatively the results are reasonable and show a good comparison, especially with the yaw angle although the loss is slightly over predicted. The 0% and 6% cases show the best comparison with the smaller tip clearances (1% & 2%) showing poorer comparisons. Figure 17 to Figure 20 show the loss (Cpo) contours of the CFD on the 1.2Cx plain. These can be compared with the previously presented experimental data (Figure 4 to Figure 7). The agreement is reasonable but in general the CFD is more dissipative so that the extent of the loss cores of the tip clearance and profile loss is larger although the peak values are lower for the CFD; this explains the loss over-prediction in the CFD solution.

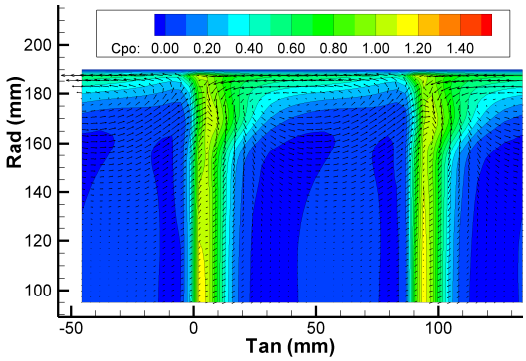

Figure 17, 0%TC 1.2Cx, CFD Loss (Cpo)

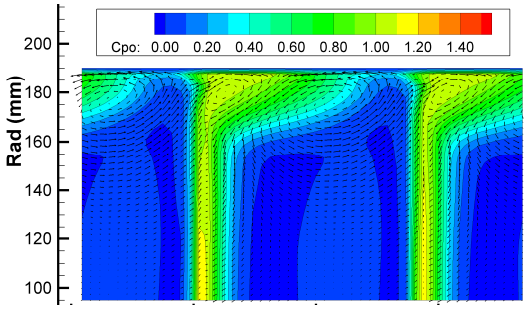

Figure 18, 1%TC 1.2Cx, CFD Loss (Cpo)

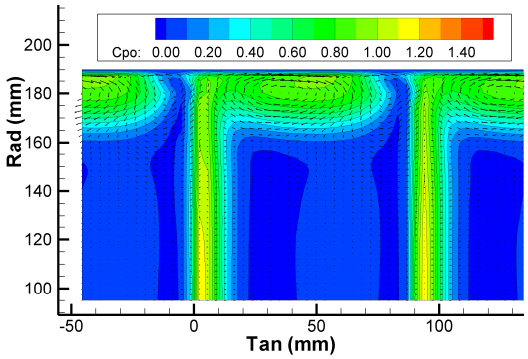

Figure 19, 2%TC 1.2Cx, CFD Loss (Cpo)

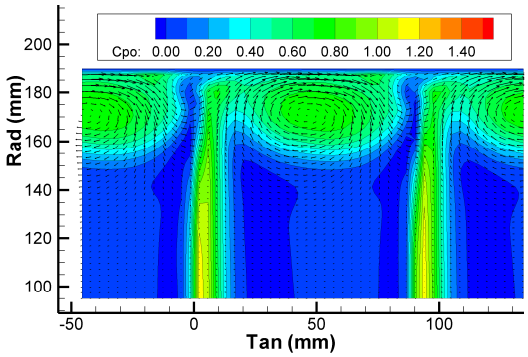

Figure 20, 6%TC 1.2Cx, CFD Loss (Cpo)

The blade loading as shown in Figure 10 to Figure 12 at mid span shows a good agreement with the experimental data. Closer to the tip the computational result varies slightly from the experimental; this is most noticeable for the 6%TC case where two bumps can clearly be seen on the suction surface (Figure 12). However as stated above, this is almost certainly attributable to the experimental rig's blade support bar.

The blade force shown in Figure 13 shows good agreement with the 0% and 6% TC cases. Noticeably for both the computational and experimental data there is an increase in blade loading for the larger tip clearance of 6%.

COMPUTATIONAL STUDY

Having examined the difference between experimental and computational results it is clear that there is an over prediction in loss, but the yaw is reasonable and qualitatively the results are similar. Therefore the following section shows results with varying tip clearance from 0% to 10% percent span.

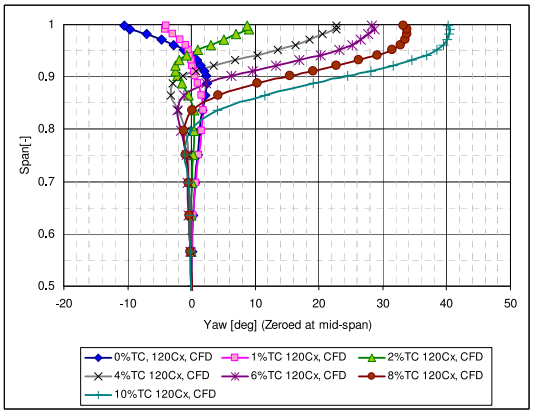

Figure 21, CFD Study, 1.2Cx CFD Yaw Angle with Varying TC

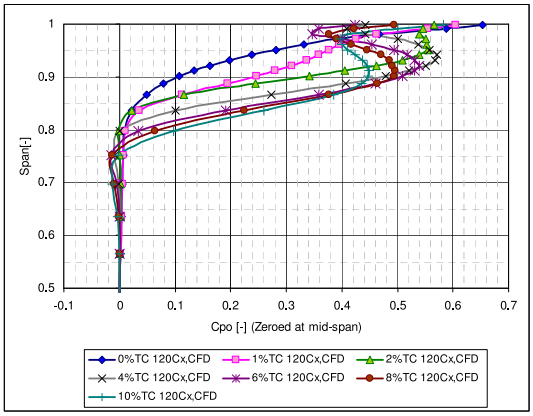

Figure 22, CFD Study, 1.2Cx CFD Total Pressure Loss with Varying TC

Pitch averaged plots of yaw and loss are presented for the various tip clearance values at 0.12Cx (Figure 21 and Figure 22). As shown by Williams [2] the yaw angle for the 0 percent case shows the classic under turning overturning and the loss is increased towards the casing due to the secondary flow and corner stall; in fact the loss on the casing for the zero percent case shows the highest loss peak. The 1% case has less overturning on the casing because the TC flow suppresses the corner stall. For the large tip clearances, 2-10%, the flow undergoes a significant overturning and then under turning caused by the tip clearance vortex. The loss peak at the TC vortex core decreases in magnitude with increased TC but the area of loss moves away from the casing, and so it is important to examine the overall loss at 1.2Cx. Figure 23 shows the increase in loss from inlet to exit for the outer 50% span, and it can be seen that the overall loss increases until 4%TC and then it falls slightly. A decline in mass flow occurs through the cascade with increased TC and so to eliminate this discrepancy the overall loss between tip clearance values is shown for 2 different definitions. These use different reference values of dynamic pressure; upstream dynamic pressure and the dynamic pressure across the cascade, i.e. the exit isentropic dynamic pressure. This is important because the mass flow rate is reduced with increased TC (Figure 24).

Removing the profile loss from the overall loss for the outer 50% span gives the loss attributed to the endwall secondary flows including the tip clearance this is shown in Figure 23. The Tip region loss accounts for approximately 45% of the total loss for the smaller TC values (including 0%) and increases to approximately 62% of the total loss for the 10% TC case. The tip clearance flow has mostly mixed out by 1.2Cx, although not shown if a plot is made of the loss at 3.0Cx then the same pattern is observed as in Figure 23.

The experimental Mass Weighted Averaged Cpo loss is shown in Figure 23 and follows the same pattern as the CFD results. Experimentally the overall loss is slightly higher than the CFD loss even though the pitch averaged results would not suggest this; this is because the values are mass weighted averaged therefore the velocity profile has an effect on the values.

These results are very similar to Williams [2], even through in this case has a skewed inlet boundary layer, suggesting that the inlet angle within the TC region has limited effect on the loss and exit angle.

The blade loading integrated becomes the tangential blade force (Figure 25) and then the blade force integrated along the blade gives the overall tangential blade force (Figure 14); these are all referenced to mid-span. The overall blade force is referenced to the zero percent TC case.

It can be seen that the blade loading increases for the larger tip clearances towards the tip of the blade. This is an unexpected result as it shows that the blade force in the outer half of the cascade increases with TC value above 1%TC. This increase in blade loading carries on until 8% TC where the total blade force levels off and appears to start to diminish. Also shown in Figure 14 is the experimental data, although the loading increase is lower it does show an increase with 6%TC, thus it can be assumed that this is a valid result. Unfortunately no experimental data was taken above 6%TC so the decline in blade force above 6%TC is not experimentally investigated. The differences between the CFD and experimental blade force can be seen by examining the Cp loading plots (Figure 10 to Figure 12) in general on the suction surface, CFD results are overloaded especially at the leading edge, therefore the calculated blade force is higher than the experimental force.

Figure 24 shows the mass flow rate per passage vs. tip clearance. A linear relationship exists between blockage and tip clearance values above 2%TC. There is a 4.8% reduction in mass flow from 0% to 10%. Therefore for the computational results the mass flow reduction is approximately 0.5% per 1% increase in tip clearance.

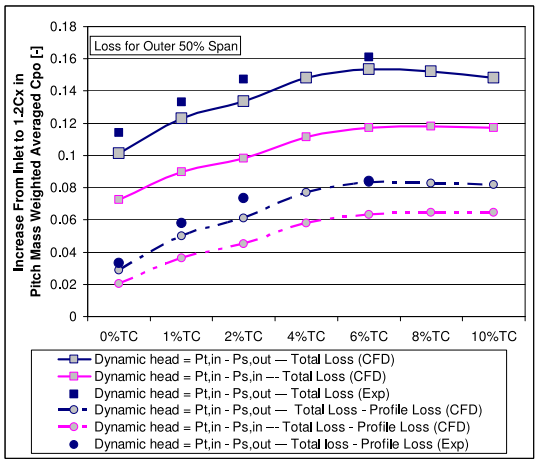

Figure 23, CFD Study, Increase in Loss through Cascade

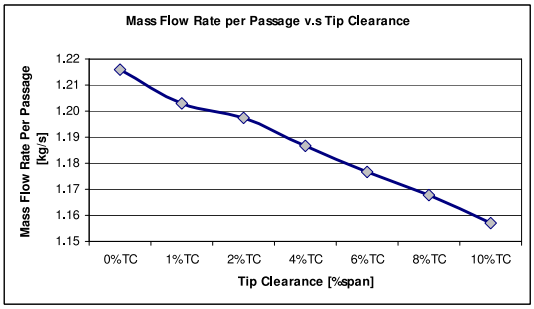

Figure 24, Mass Flow Rate per Passage

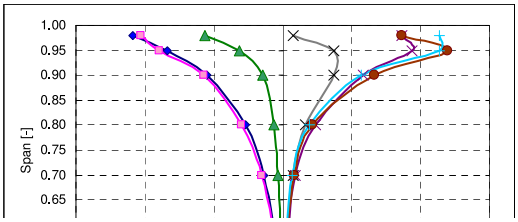

Figure 25, CFD Study, Blade Force Coefficient 6% tip clearance

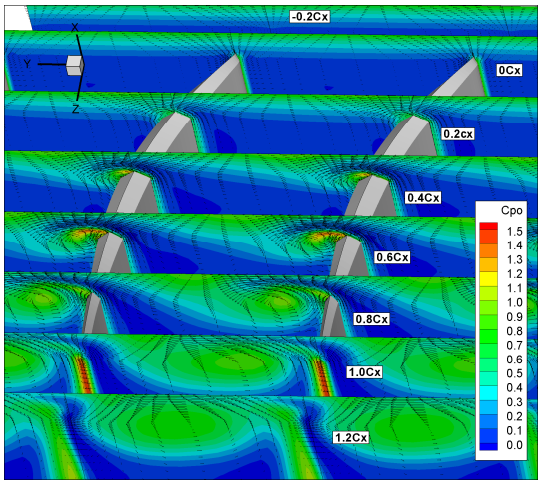

Figure 26, CFD Study, 6% TC Cpo loss Contour plots

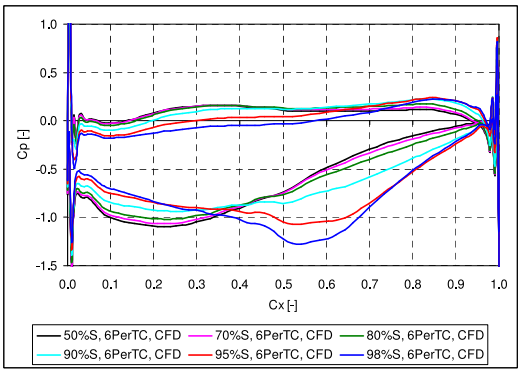

Figure 27, CFD, 6%TC, Blade Pressure Profile

In order to investigate the cause of the increase in loading it is useful to look at one TC value in detail, and 6% is examined. Loss contours and velocity vectors through the cascade are shown in Figure 26, and the blade surface pressure profiles are shown in Figure 27. The flow features are described through the cascade:

0.0Cx: At inlet to the blade row the inlet boundary layer is skewed and there is already some loss due to the friction on the casing.

0.20Cx: now the blade loading is developing and the TC flow accelerates through the clearance. A small separation bubble is present on the tip. Although this is almost certainly due to the pinch tip, a vena contractor over a square blade end would also create such a feature. The blade loading close to the tip has decreased due to the TC flow increasing the pressure on the suction surface and lowering it on the pressure surface.

0.4Cx: the blade loading now approaches its maximum and the TC flow has significantly accelerated approximately in the tangential direction. The start of a tip clearance vortex can be seen although it is small and positioned close to the suction surface.

0.6Cx: the TC flow has further increased and the vortex starts to move away from the suction surface. Unlike smaller TC values no counter rotating vortex is seen, although a lower momentum region does exist at mid-passage. The incoming flow is now pushed against the pressure surface and down into the cascade due to the significant blockage created by the TC flows.

0.8Cx: the TC vortex continues to move away from the suction surface of the blade. The TC vortex induces lower pressure fluid up the blade towards the tip thus lowering the SS pressure creating a higher blade force. Lower loss fluid is also pulled through the tip clearance reducing the loss on the casing.

1.0Cx: the TC vortex has moved away from the SS and now fills the majority of the passage in the outer 20% span. A counter rotating vortex is just apparent. This is due to the incoming flow interacting with the low momentum fluid in the boundary layer. As found by Williams [2] a relatively rotating casing would suppress the counter rotating vortex.

DISCUSSION

This work shows that there is an unexpected increase in blade loading towards the tip of the blade for the higher values of tip clearance, and that although the loss of the cascade increases with increased tip clearance up to approximately 4%TC, above this the loss levels off and there is no further increase in loss. This section aims to relate these phenomena to the flow physics to further the understanding of large tip clearance flows.

A simple pinch tip model for the tip clearance has been used which has allowed an investigation of several tip clearances without use of extensive computer or manpower resources. Experimental measurements have been used to assess the computational work's reliability. It has been found that at 0% and 6% tip clearance, the computation gave good agreement with experiment, particularly for yaw angle (Figure 8). The 1% and 2% results are not so good, and this is to be expected with the pinch tip model. However as the thrust of this work is to the larger clearances, the choice of the pinch tip appears justified. As the tip clearance increases the solution becomes less grid dependent; this is because the end-wall has a smaller effect on the Tip clearance flow. The detailed blade tip modelling and meshing also becomes less influential at a large tip gap. For this reason it can be assumed that the 8 and 10 percent solutions are valid. The observation from the numerical work so far suggests that if an improved solution to the smaller tip clearance value is required then the use of another tip clearance modelling method would be essential.

The detailed study for 6% TC shows that from the static pressure values on the blade (Figure 27), at entry to the blade row the blade loading is significantly reduced for the first 35% chord within 20% span of the casing. This is because the high pressure flow moves from the PS to the SS across the tip, increasing the pressure on the SS and reducing the pressure on the PS pressure. At mid chord the TC vortex starts to roll up close to the SS of the blade. This flow feature creates a blockage reducing the row mass flow rate and forcing the incoming flow towards mid span. The TC vortex induces low pressure fluid up the SS of the blade for 20% span reducing the SS pressure and so increasing the blade force. At approximately 60% chord the TC vortex leaves the suction surface of the blade and moves across the passage, and this coincides with the blade's peak force for the outer 5% blade span. The TC vortex continues to induce fluid along the blade SS into the tip clearance region. Low loss fluid is also pulled through the TC gap from the PS and this serves to reduce the loss on the casing.

An important feature here is that the TC vortex stays relatively close to the suction surface, moving to about mid passage by blade exit. This means that with the high tip clearance, the very strong vortex not so far from the suction side is able to induce the high velocities on the suction surface as noted above. Also the pressure on the pressure surface is raised by the jet stagnating near the tip of the blade.

This lack of movement is in contrast to the movement right across the passage to near the pressure surface usually observed in most of the studies in the literature. It does not appear that the high tip clearance is the reason for the lack of movement of the TC vortex, as the lower TC values studied here (Figure 18 and Figure 19) show that the vortex is also at about mid passage at exit. The significant feature of this blading is probably the low stagger so that the tip jet is nearly perpendicular to the axial direction.

After 6% TC there is no significant change in blade loading and this suggests that the casing has a decreasing effect on the blade loading and that as the TC value is increased further, the flow around the blade starts to behave independently of the casing. This may help to explain the levelling off of loss with tip clearance, since as the flow crosses the tip as a pressure driven jet there is little further increase in the loss producing mechanisms on the end wall or tip. In effect the flow becomes more like that of a wing tip trailing vortex.

It should be noted that the blade force values shown here (Figure 14) are dimensionless values based on the span of the actual blade. As the TC increases, of course the blade gets shorter. If the 'annulus height' of this linear cascade were used, then an inspection of Figure 14 shows that the actual force is reducing. For instance at 6% TC the dimensionless blade force is increased by about 2.7% so that the actual force will reduce by approximately 3.3%, and this is reflected in the large amount of underturning seen in Figure 21 at higher TC values. Thus the work done by the blade (if it were a rotor) is reduced, but not by as much as might be expected. This coupled with the overall loss becoming independent of the TC value, means that the penalties associated with TC values around 4% and above are not as great as might be expected with typical LP blading of high stagger. Unfortunately there is still an increase in

blockage so that the mass flow reduces by 0.5% per 1% increase in tip clearance.

With the significant blockage effect, the axial velocity will not be constant at blade inlet, even though the upstream boundary is the same for the different tip clearances. To try and separate the tip clearance flow effects from the blockage effect, the results for angle, loss and blade force distributions along the span have been referenced to the mid-span value. This is perhaps debatable, but it was felt to be most helpful for this study.

It is important to remember that this study is for a linear cascade and that in a rotating machine there will be a number of differences. For instance in a multi-row environment the inlet boundary layer is skewed and there is relative motion of the end wall. However the results of Williams [2] showed that the moving end wall did not have much effect for large tip clearances. Thus these cascade results have relevance for HP industrial compressor design.

The aerodynamic designer may find these results interesting; if a design with similar HP blades requires a large tip clearance then the designer who has always strived to reduce the tip clearance value may find that in fact the aerodynamic penalty is not as large as previously thought. Therefore cost savings may be made in the mechanical design of the HP stages. The overall blade loading also increases for the larger clearances allowing for slightly higher stage loading.

CONCLUSION

The physics of tip clearance flow for a low stagger cascade of compressor blades has been studied experimentally and computationally. Tip clearances of up to 10% span (12.67% chord) have been studied with application to the HP compressor of an industrial gas turbine. A pinch tip clearance model for the computation was used, and this was found to give satisfactory results for the larger tip clearances. The following conclusions may be drawn:

- Increasing the tip clearance above 4% incurs no further increase in loss and at the same time there is an unexpected increase in blade force towards the tip due to the tip clearance flows.
- The increase in blade force is due to the effect of the strong tip clearance vortex which does not move across the blade passage to the pressure surface, as is often observed for high stagger blading.
- The levelling off of loss may be attributed to the lack of increasing loss production mechanisms of the pressure driven tip clearance jet as the clearance is increased to large values.
- In general it was found that the CFD over-predicted the loss in the casing region although at midspan there was a very good agreement. The flow angle prediction is very good for the higher tip clearance values although it was not accurate for the smaller clearances.
- These results are significant for the design of HP compressors for industrial gas turbines.

REFERENCES

[1] Denton, J. D., 1993, “Loss Mechanisms in Turbomachines,” ASME Paper No. 93-GT-435,

[2] Williams, R.J., Gregory-Smith, D., and He, L., “A Study of Large Tip Clearance Flows in an Axial Compressor Blade Row,” ASME Paper No. GT2006-90463,

[3] Walker M., Gregory-Smith D., and He L., 2005. “A Study of Large Tip Clearance in a Row of Low Speed Compressor Blades,” Proc. 6th. European Conference on Turbomachinery, Lille, **1**, pp. 122-134.

[4] Peacock, R.E., 1982a, “A Review of Turbomachinery Tip Gap Effects: Part 1 Cascades,” International Journal of Heat and Fluid Flow., **3**, pp. 185-193

[5] Storer, J. A. and N. A. Cumpsty., 1991, "Tip Leakage Flow in Axial Compressors." J. Turbomachinery., **113**(2), pp. 252-259.

[6] Hunter, I. H. and N. A. Cumpsty., 1982, "Casing Wall Boundary-Layer Development through an Isolated Compressor Rotor," Journal of Engineering for Gas Turbines and Power **104**(4): 805-818.

[7] Gbadebo, S.A., 2006, “Interaction of Tip Clearance Flow and Three-Dimensional Separations in Axial Compressors,” ASME Paper No. GT2006-90071.

[8] Tang, G., Simpson, R.L., 2006, “Experimental study of Tip-Gap Turbulent Flow Features,” ASME Paper No. GT2006-90359.

[9] Sjolander, S.A., 1997, “Physics of Tip Clearance Flows - 1,” von Karman Institute for Fluid Dynamics, Lecture Series 1997-01, Secondary and Tip-Clearance Flows In Axial Machines.

[10] Saathoff, H., and Stark, U., 2001, “Tip Clearance Flow in a Low-Speed Compressor and Cascade,” Proc. 4th. European Conference on Turbomachinery – Fluid Dynamics and Thermodynamics, Firenze, Italy, pp. 81-91.

[11] De Cecco, S., Yaras, M.I., and Sjolander, S.A., 1995, “Measurements of the Tip-Leakage Flow in a Turbine Cascade with Large Clearances,” ASME Paper 95-GT-77, June 1995.

[12] Van Zante, D.E., Strazisar, A.J., et al., 2000, "Recommendations for Achieving Accurate Numerical Simulation of Tip Clearance Flows in Transonic Compressor Rotors." J. Turbomachinery **122**(4): 733-742.

[13] Yang, H., 2004, “3D Unsteady Flow in Oscillating Compressor Cascade,” Ph.D. thesis, Durham University, UK.

[14] Sanger, N. L., 1983, “The Use of Optimization Techniques to Design-Controlled Diffusion Compressor Blading,” ASME Journal of Gas Turbines and Engineering for Power, **105**, pp.256-264.

[15] Sanger, N. L., and Shreeve, R.P., 1986, “Comparison of Calculated and Experimental Cascade Performance for Controlled-Diffusion Compressor Stator Blading,” ASME Journal of Gas Turbines and Engineering for Power, **108**, pp.42-50.

[16] Ingram, G., Gregory-Smith, D., 2005, “An Automated Instrumentation System for Flow and Loss Measurement in a Cascade,” Flow Measurement and Instrumentation 17(2006) 23-28, Elsevier, www.sciencedirect.com.

[17] He, L., 2000, "Three-Dimensional unsteady Navier-Stokes analysis of stator-rotor interaction in axial-flow turbines." Proc. I. Mech. E., Part A, Journal of Power and Energy, **214**, pp.13-22.

[18] Gupta, A., Arif Khalid, S., McNulty, G.S., and Dailey, L., 2003, “Prediction of Low Speed Compressor Rotor Flowfields with Large Tip Clearances,” ASME Paper No. GT2003-38637.

B.3 Paper 3. Williams et al. [2009])

LARGE TIP CLEARANCES AND HIGHLY SKEWED INLET CONDITIONS

Richard Williams[1], David Gregory-Smith[2], Grant Ingram[3]

[1]University of Durham, South Road, Durham, DH1 3LE, UK, r.j.williams5@durham.ac.uk
[2]University of Durham, South Road, Durham, DH1 3LE, UK, d.g.gregory-smith@durham.ac.uk
[3]University of Durham, South Road, Durham, DH1 3LE, UK, g.l.ingram@durham.ac.uk

ABSTRACT

Multi stage and end-wall effects result in a highly skewed inlet boundary layer to high pressure axial compressor rotor rows, this paper investigates the influence of these skewed boundary layers on tip clearance flows. The particular focus is on compressor stages where the tip clearance values are relatively large and the tip clearance flow accounts for a large proportion of the row loss. Experimental measurements have been undertaken upon a linear cascade of a typical high pressure compressor geometry with upstream tangential injection implemented to create a realistic inlet boundary layer skew. Results are presented for two inlet boundary conditions: large skew (realistic inlet conditions) and low skew (less realistic inlet conditions) with tip clearances from 0 to 12%. This paper reports that although the loss is reduced with increased tip clearance a penalty is paid in terms of reduced flow turning, for example a tip clearance of 12% of span halves the turning through the cascade. This paper shows that the results are consistent whether or not inlet skew is applied.

NOMENCLATURE

C	Chord	m	SS	Suction Surface	-
Cx	Axial Chord	m	$\mathrm{Re} = \frac{VC}{\nu}$	Reynolds Number	-
$Cpo = \frac{Po_1 - Po}{Po_1 - Ps_2}$	Total Pressure Loss Coefficient	-	TC	Tip Clearance % Duct Height	-
HP	High Pressures Stages	-	V	Velocity	ms^{-1}
Po	Total Pressure	Pa	X	Axial	-
Po_1	Inlet Total Pressure	Pa	Y	Tangential	-
Ps	Static Pressure	Pa	Z	Radial	-
Ps_2	Exit Static Pressure	Pa	B	Yaw angle Rel. Axial	-
PS	Pressure Surface	-			

INTRODUCTION

Stage matching is fundamental to axial compressor design. Close to the casing the inlet flow to a rotor is highly skewed due to a combination of the upstream stator root secondary flows and casing motion. This means that within the casing region stage matching is difficult and historically not accounted for in 2D design. Large axial compressors consist of low pressure, intermediate pressure and high pressure (HP) stages. In the HP stages the skewed inlet at casing occupies a significant percentage of the annulus height (typically 20% Span) therefore a significant proportion of the blade undergoes increased loading. This also occurs at the stator hub clearance resulting in a blockage that can extend up to 40% of the annulus height. For compressors which operate at large pressure ratios the short annulus height or blade length within the high pressure compressor (HPC) results in a relatively large rotor tip clearance, typically 6% span. This means that the tip clearance flows are a significant source of loss within the HPC.

The purpose of this work is to increase understanding on HPC flow fields, particularly how the skew on the casing influences stage performance at high tip clearance. A new cascade has been

constructed with typical HPC geometry and upstream tangential injection to control the inlet casing skew. Previous work undertaken by the authors (Williams et.al (2006 & 2008)) found that increasing tip clearance has a smaller penalty than previously thought. This paper shows that this is still the case with engine representative boundary conditions and geometry.

TIP CLEARANCE FLOW PHYSICS

The tip clearance (TC) flow consists of a pressure driven jet which passes from the pressure surface to the suction surface across the tip of a blade through the gap between the blade tip and casing. The strength of the jet depends on the blade pressure field close to the tip of the blade (as found by Peacock (1982)). The tip clearance flow rolls up in to a vortex close to the suction surface which then moves across the passage. The axial location at which this happens is usually close to the maximum blade loading on the tip (as found by Storer and Cumpsty (1991)). Cited in Sjolander (1997), De Cecco (1995) found that with large TC the blade loading is not entirely responsible for the over tip flow. This is because the large clearances allow flow to pass through the gap creating large under turning in the casing region. Storer and Cumpsty (1991) found that increasing the tip clearance gap moved the maximum loading downstream and therefore moved the point of TC vortex detachment downstream. Williams et al. (2006 & 2008) also found that this occurs with high pressure blading with much higher relative tip clearances and that the TC vortex remained closer to the blade suction surface. Further across the passage a counter rotating vortex occurs. This vortex hinders the movement of the tip clearance vortex across the passage.

Saathoff and Stark (2001) investigated the trajectory of the TC vortex with varying inlet angle. They showed that increasing the inlet angle pushes the tip clearance vortex across the passage creating a larger blockage. This eventually creates stall when the TC vortex moves around the leading edge (LE) of the next blade. This work suggested that increasing the skew raises the blade loading at tip magnifying the TC flow and pushing the vortex further across the passage creating a large blockage.

EXPERIMENTAL APPARATUS

This work uses a linear cascade, detailed large scale measurements are possible within and without the blade row but not all flow features are modelled. Real (rotating) machines have skewed inlets, twisted blades, radial effects, moving end-walls and multiple stages. Cascade work provides insight into the fundamental flow patterns but application to real machines must take into account the differences between the model and machine.

Williams (2006) studied the effect of a moving end wall and showed that there is a significant but predictable difference to the tip clearance flow. He found that with end wall motion the flow undergoes increased skew, increasing the loading on the tip of the blade. The motion pulls fluid through the gap increasing the TC vortex strength and moving the TC vortex further across the passage creating a large blockage. In the relative frame the end wall motion does work on the flow reducing the losses in the casing region; therefore the loss measured in a linear cascade is higher than in the real case.

The blade geometry used in this paper is that of Build II of the Dresden 4-Stage Low Speed Research Compressor (LSRC), this geometry is representative of a HPC. Details of the LSRC are given by Boos et al. (1998), and Muller and Vogeler (2007). The blade geometry is that of the casing section scaled by 1.75 in the circumferential plane and 1.5 radially (See Table 1). A requirement of the cascade design was to provide realistic inlet conditions; these are chosen to match those at inlet to rotor 3 of the LSRC build II. The aim for the natural inlet condition of the cascade is to have an inlet angle of 55º at mid-span and a natural boundary layer on the casing. With the increased skew (realistic inlet boundary condition) the aim was to have an increase of 10º on the casing with a linear distribution up to the nominal inlet angle at 80% span.

A schematic of the cascade is shown in Figure 1 and in picture form (Figure 2). The linear cascade was designed to mate with an existing open flow wind tunnel as used by Williams et al.

(2008). This consists of a fan, diffuser, settling chamber, gauze screen, 7.5:1 contraction and honey comb section providing uniform flow to the linear cascade.

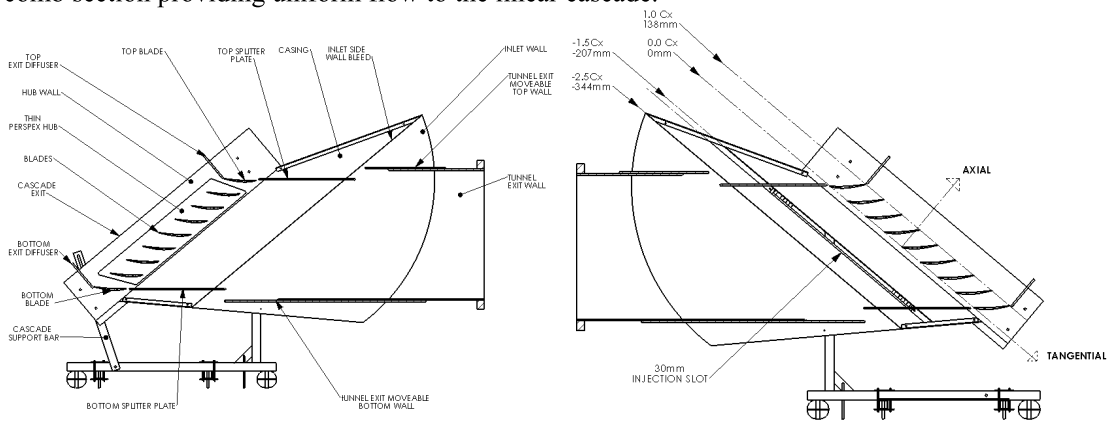

Figure 1: Cascade Schematic

The following table shows some of the cascade and blade dimensions.

Number of Aerofoils	7
Number of Passages	8
Aerofoil Pitch	131.25 mm
Cascade Annulus Height	180 mm
Side Wall Bleed Location	-2.5Cx from LE
Injection Location	-1.5Cx from LE
Pitot-Probe Location	-1.0Cx from LE
Cascade Exit	2.0Cx from LE
Inlet Flow Angle (Mid-Span)	55º
Cascade Reynolds Number	3.622×10^5
Aerofoil Chord (C)	204 mm
Aerofoil Axial Chord (Cx)	140 mm
Stager Angle	46.5º
Aspect Ratio (Span/C)	0.88
Solidity (Chord/Pitch)	1.55
Inlet Velocity	23 m/s

Table 1: Cascade Properties

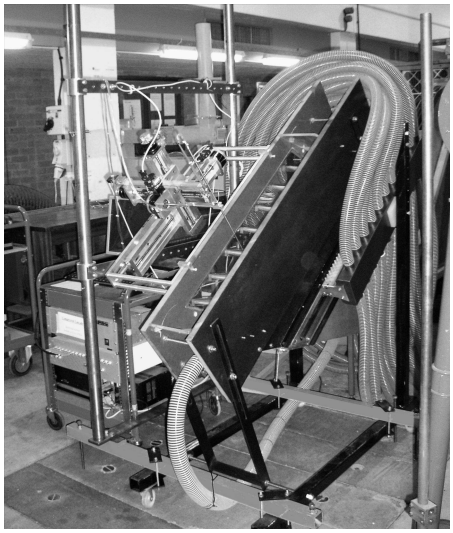

Figure 2: Picture of Cascade

Removal of the tunnel hub and casing boundary layer is accomplished by bleeding 2.5 axial chord lengths upstream of the blade leading edge. The cascade is hinged around the leading edge of the top blade to allow for change in incidence and was set to a blade inlet angle of 58º. Top and bottom inlet horizontal splitter plates allow for changes to the inlet angle and removal of the top and bottom tunnel boundary layers. The splitter plates extend 3 chord lengths upstream.

The cascade has 7 moveable blades which pass through the hub and are cantilevered from a plate to vary tip clearance. Two fixed blades form the top and bottom passages of the cascade giving 8 passages. Variable exit diffusers are located at the trailing edge of the top and bottom blades to allow control of the cascade periodicity.

Control of the inlet boundary layer flow angle is implemented by injected air through a slot located at 1.5Cx, that is 150% of axial chord upstream of the blade leading edge. The slot is nominally 30mm wide. For the first configuration without injection this slot is blanked to create a

smooth casing. Injection takes place over 95% of the cascade starting from the top. The inlet traverse is located at 0.5Cx upstream of the blade row so is **after** the injection slot.

This work uses two inlet flow configurations to examine the effect of a skewed boundary. The first uses the natural inlet boundary layer of the cascade (2º skew, 10% Span thickness, labelled "natural inlet") and the second has a more engine representative inlet boundary layer (10º skew, 20% Span thickness, labelled "high skew inlet").

Instrumentation

All measurements were conducted with a five-hole probe equipped with a three axis traverse allowing movement of the probe in the axial, tangential and radial direction. The probe was positioned through the blades for the upstream (-0.5Cx or 50% axial chord upstream of the LE) traverse; which is downstream of the injection slot. Downstream traversing was undertaken at 1.2Cx and 1.5Cx (20 and 50% axial chord after the trailing edge (TE)). Measurement of the internal flows was undertaken at constant axial planes between 0.3Cx and 1.0Cx for the central blade. The traverse plane definitions are shown in Figure 4.

Traversing was undertaken up to 5mm from the wall or 2.8% span. Exit pitch averaging was carried out across three passages as shown in Figure 4. Area averaging then extended from mid-span to 97.2% span. All pressures were measured relative to a Pitot probe located at 1.0Cx upstream. The reference dynamic pressure was calculated from the upstream total pressure and the atmospheric static pressure.

Inlet Injection

To achieve the casing inlet skew, upstream tangential injection was implemented. Within the injection slot forty nine injection guide vanes (IGV's) could be altered to give a geometrical exit angle between 5° and 40° to the casing wall. Twenty two pipes supplied air to the slot, which were attached to a fan via a settling chamber. The fan speed was altered to vary the injection mass flow rate. At either end of the injection slot the flow is affected by the slot end plates, however because this occurs away from the measured passages it was considered to have a negligible effect on the results. In order to obtain the desired inlet flow the slot width, IGV angle and injection mass flow were systematically varied. In the end the IGV angle was altered along the length of the injection slot to improve the inlet periodicity. Figure 5 shows the yaw angle at inlet to 6 passages of the cascade with the chosen set up. The IGV angle is set to 10º at the top of the cascade and 5º at the bottom. A fan speed of 30 Hz was chosen which approximates to a mass flow of 7.5% of the tunnel mass flow rate and the slot width was set to 30mm. With the final injection set up the mid-span variation was approximately 1º. The variation on the casing was around 6º across the length of the cascade but only 4° for the passages used for pitch averaging.

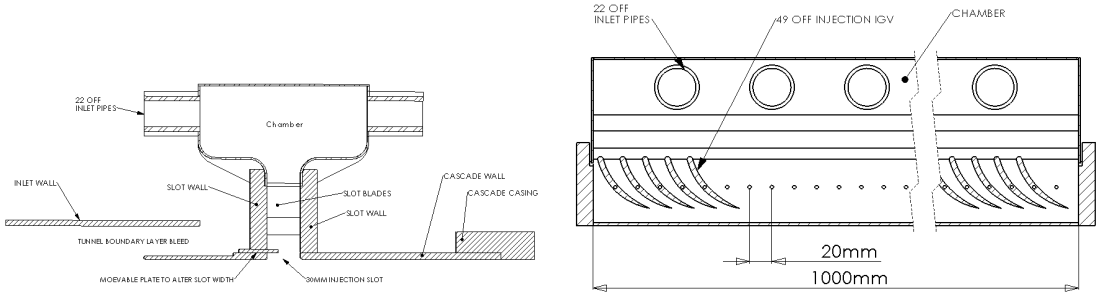

Figure 3: Injection System Schematic

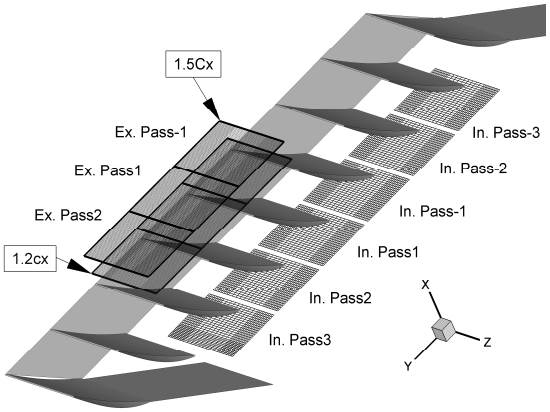

Figure 4: Measurement Plane

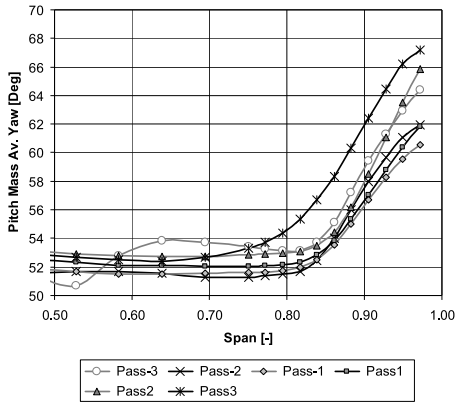

Figure 5: Inlet Yaw Angle along Cascade

EXPERIMENTAL RESULTS

Results for the cascade with the two different inlet skew configurations; natural inlet and the realistic boundary layer (high skew inlet) are presented. Seven tip clearance values between 0 and 12 % cascade span were used; these are shown below in Table 2 along with conversions to absolute and percent chord values.

% Cascade Span	0	1	2	4	6	8	10	12
Tip Clearance (mm)	0.0	1.8	3.6	7.2	10.8	14.4	18	21.6
% Blade Chord	0.00	0.88	1.76	3.51	5.27	7.02	8.78	10.54

Table 2: Tip Clearance Value Definition

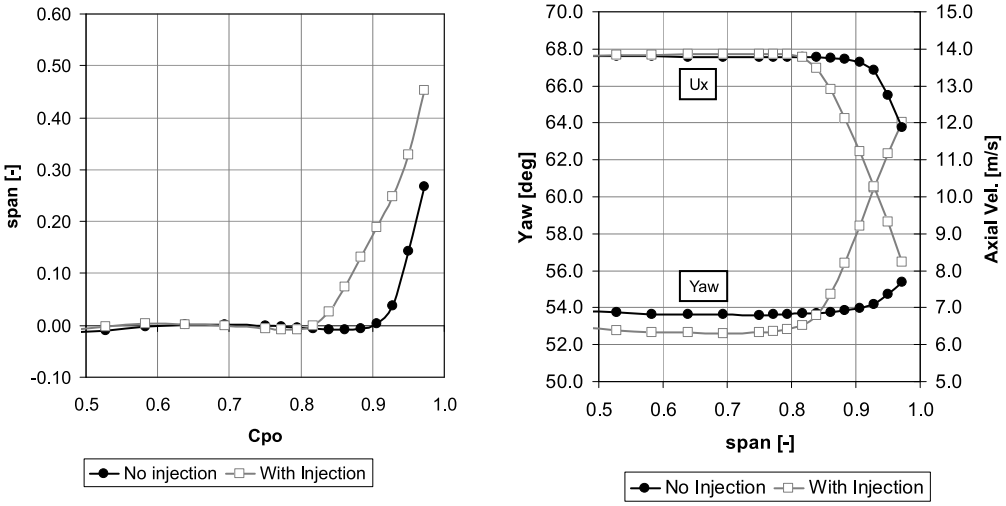

Figure 6: Cascade Inlet Conditions

Inlet Traverse

A significant effort was undertaken to ensure quality uniform periodic flow at inlet to the cascade. At mid-span with the natural inlet the cascade had a 2º variation in yaw angle, 0.2 variation in loss coefficient and 1 m/s variation in axial velocity for both cascade conditions. Figure 6 presents the pitch averaged axial velocity, yaw angle and loss across the inlet to the central 4 passages with 0%TC. At mid-span (0.5Span) there is little difference between the axial velocity and

Cpo for the different inlet boundary conditions. However the yaw angle with increased skew is approximately 1º higher than without, this is due to a redistribution of the mass flow brought about by the increased boundary layer blockage. The tunnel fan settings were kept the same throughout the measurement campaign.

Exit Traverse, Pitch Averaged Results

Traversing at the exit of the cascade has been undertaken at 1.2Cx and 1.5Cx across the exit of 3 passages. There was little difference between the results at both downstream axial locations therefore only 1.2Cx results are shown in this section.

Exit pitch averaged results of yaw angle, axial velocity and stagnation pressure loss are shown with the natural and high skew inlet conditions at 1.2Cx in Figure 7 and Figure 8 respectively for different tip clearance values. The inlet value is included for comparison.

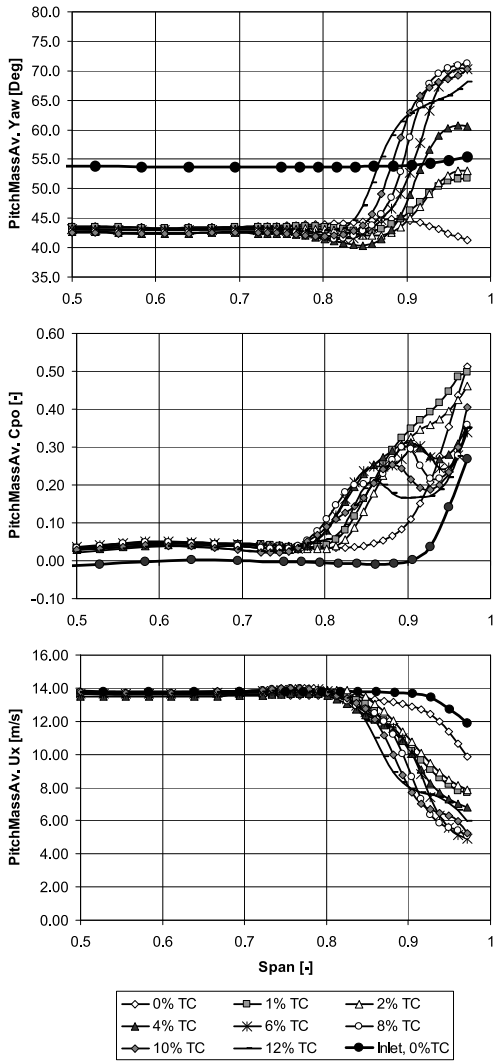

Figure 7: Pitch Averaged Exit Traverse, Natural Inlet

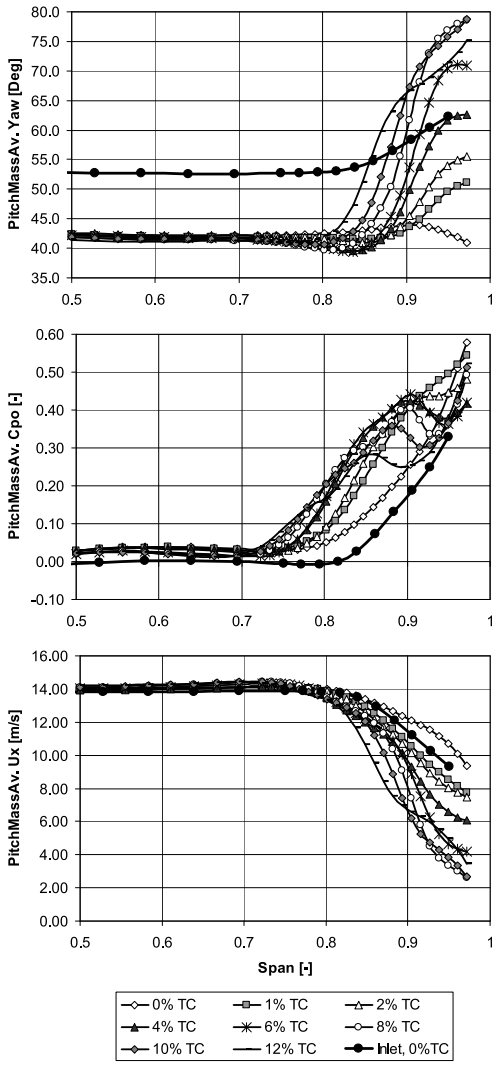

Figure 8: Pitch Averaged Exit Traverse, High Skew Inlet

With the natural skew (Figure 7) the yaw angle without tip clearance follows a classic over-turning (0.85Span) under-turning (>0.9Span) pattern towards the casing this is caused by the passage vortex and possible corner stall. Increasing the TC value increases the over-turning but then significantly increases the under-turning close to the casing. 6%TC to 10%TC values have the

same outlet flow angle at the casing of approximately 70 º and an under-turning of 26º. This is 14º higher than the inlet angle on the casing. In general (except for the extreme 12% TC case) an increase in tip clearance pushes the under-turning further from the casing.

Figure 7 also shows the pitch averaged loss. With 0%TC there is a significant increase in loss towards the casing where there is the highest peak in loss (Cpo). Increasing the TC to 2% pushes the loss away from the casing creating a much larger loss area; with a slightly lower peak loss on the casing. Above 2%TC a bump in loss resembles the TC vortex core which moves away from the casing and reduces in magnitude with increasing TC. Above 2%TC towards the casing the loss at first reduces from the vortex core and then increases in magnitude as the casing is approached. Williams (2006) showed computationally that the loss increase on the casing is reduced with relative casing motion. Therefore in a real machine this effect may not occur.

The axial velocity at mid-span is slightly higher than at inlet, this is caused by a redistribution of mass flow to the centre of the cascade because of TC flow blockage. Towards the casing there is a reduction in axial velocity of approximately $2ms^{-1}$ which increases to $5ms^{-1}$ for the higher tip clearances. Increasing the TC reduces the axial velocity away from the casing. As with yaw angle and loss coefficient the 12%TC result shows a different pattern.

With the increased skew at inlet the exit flow follows a similar pattern to that with the natural inlet boundary layer of the cascade (Figure 8). The area of under-turning moves slightly away from the casing and the flow angle on the casing is increased from 70º to 80º which is similar to the 10º increase in inlet angle. With 6%TC, the yaw angle reaches a similar under-turning to that of natural inlet (approximately 70º) but the larger tip clearances carry on increasing in under-turning. With 0%TC there is a slight increase in axial velocity compared to inlet. Above 2%TC there is an increase in blockage compared to the natural inlet boundary condition.

Increasing the inlet boundary layer thickness in general increases the blockage and under-turning of the cascade within the casing region. Figure 9 shows the total mass averaged Cpo at 1.2Cx, as expected from the pitch averaged plots (Figure 7 & Figure 8) the total loss at 1.2Cx is higher with increased skew. However when the inlet loss at -0.5Cx is subtracted from the exit loss to give net loss there is an overall reduction. This reduction in loss at higher tip clearances attracts a severe penalty with a large reduction in turning (Figure 10). At 12%TC the turning is halved for the outer 50% Span and both inlet conditions have the same turning.

Figure 11 (natural inlet) and Figure 12 (high skew inlet) are contour plots of Cpo at 1.2Cx for the TC values measured. This is the area data used for the previous pitch averaged results (Figure 7 & Figure 8). The 0%TC plots indicate the quality of the cascade periodicity. Although at the hub there is increased loss compared to the casing, this is not of interest as it does not affect the TC flow.

Several features are observed with the natural inlet. There is a small variation in the TC vortex core location in the radial direction between TC values as seen in the Pitch averaged plots. However in the tangential direction there is a significant change; up until 6%TC the vortex moves across the passage away from the SS towards the PS of the adjacent blade. Above 6%TC the TC vortex core moves back closer to the suction surface of the blade.

The same trend is observed with the increased inlet skew. With injection the vortex core is approximately 3% span further from the casing and moves further across the passage. The movement across the passage varies with TC; approximately 9% pitch for the small tip clearances down to 2% pitch at 12% TC.

These results suggest that the TC vortex has less interaction with the casing for the higher TC values. At 12%TC there is very little interaction of the vortex core with the casing - this can be seen by the low loss area between the two. The large tip clearances pull lower loss fluid through the tip gap reenergising the end-wall flow. This however results in a counter-rotating vortex due to the shear on the end-wall. Therefore in a real machine (as seen in previous studies (Williams et al., 2006)) with relative end-wall motion this shear will be reduced suppressing the counter-rotating vortex, reducing the loss in the end-wall region.

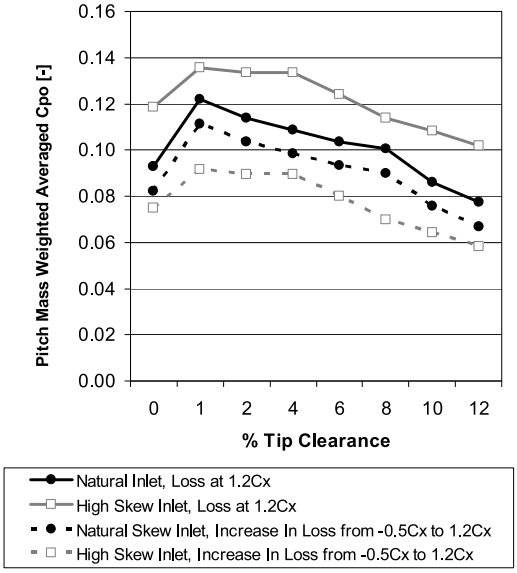

Figure 9: Pitch Mass Weighted Averaged Cpo

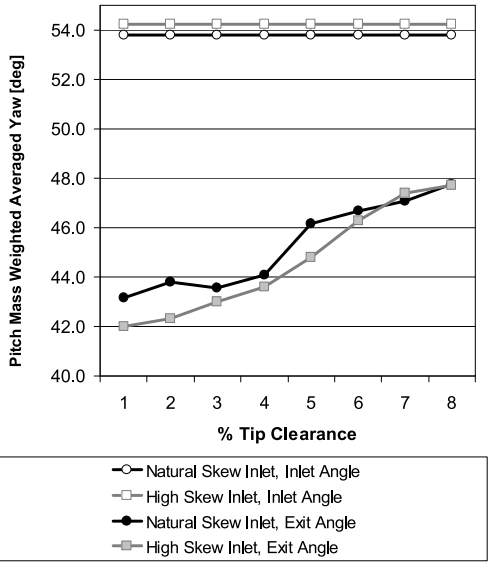

Figure 10: Pitch Mass Weighted Averaged Yaw

Stagnation Pressure Loss Contour Plots

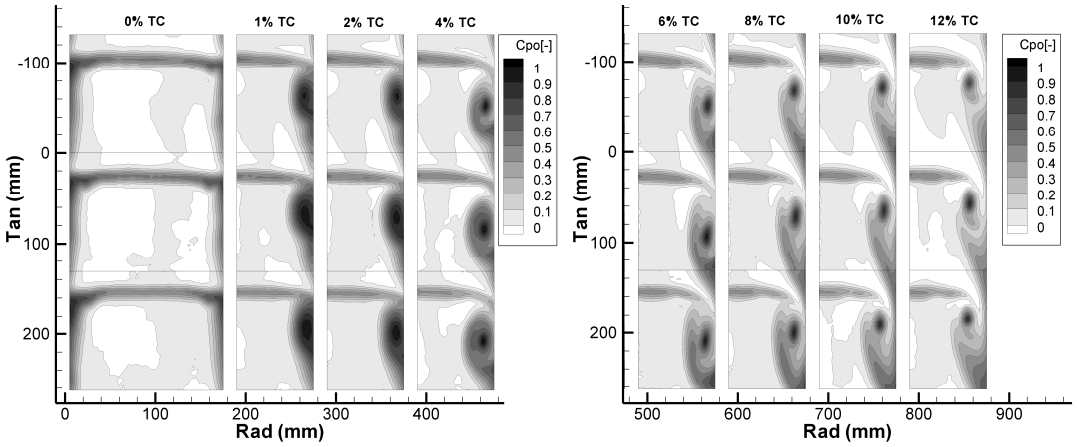

Figure 11: 1.2Cx Cpo Contour Plots, Natural Inlet

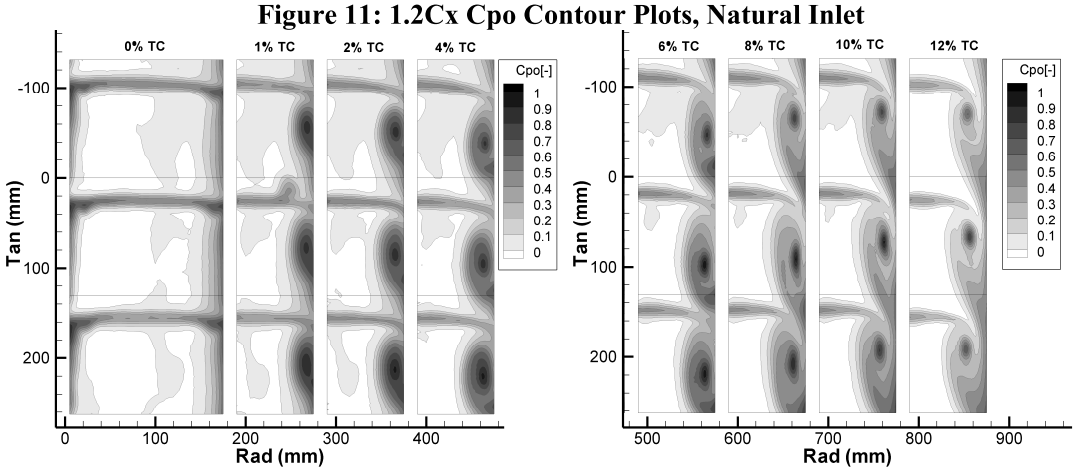

Figure 12: 1.2Cx Cpo Contour Plots, High Skew Inlet

Internal Traverses

Traversing within the passage is shown in Figure 13, Figure 14 and Figure 15 for 2, 6 and 10%TC values for both natural and high skew boundary layer configurations.

At 2 % TC with the natural boundary layer there is a much stronger loss core than with the increased inlet skew. However with injection the vortex is more elongated in the pitch-wise direction and fills much more of the passage. The counter rotating vortex loss is however much larger with increased skew. As with the downstream plots it can be seen that the TC vortex pushes across the passage with increased TC up to 6%TC and then moves back towards the SS. The axial location at which the TC vortex moves away from the suction surface of the blade moves downstream with increased TC. This occurs at a slightly lower axial location with the increased inlet skew than with the natural skew.

DISCUSSION

The new cascade used for this work has the capability to study large tip clearances with relevant geometry and inlet conditions. The geometry has a much higher stagger angle and lower turning than previously investigated (Williams et al. (2008)). Previously it was observed that the tip clearance vortex behaves differently from low or intermediate pressure stages. It was shown that the tip clearance vortex remains within the SS side of the passage at nominal operating conditions. This has the effect of reducing the pressure on the SS increasing the blade loading towards the tip of the blade. It was also shown that the loss increase through the cascade was reduced with increased tip clearance.

Measurements from the new cascade have shown the same results with more realistic HPC inlet conditions and geometry and a more comprehensive data set. Traversing within the cascade passage has given a clear insight in to the progression of the tip clearance vortex and counter rotating vortex. In this paper the TC vortex appears to have a much higher elongation in the pitch-wise direction, however the traverse plane was at a higher angle to the vortex trajectory than with the previous low stagger aerofoil.

Effect of Tip Clearance Size

The effect of the tip clearance size is very similar to previously reported results. The patterns of the variations due to the tip clearance size are the same for both inlet conditions with slightly different magnitudes. Compared to the previous cascade the pitch averaged exit yaw angle is higher than at inlet close to the casing. This is most likely the result of the over tip leakage flow direction which although not measured is expected to have a negative axial velocity. The axial velocity within the casing region is very low creating a large blockage.

The TC flow effects are evident in the pitch averaged loss much closer to mid-span than in the yaw angle or axial velocity plots. The trajectory of the tip clearance vortex moves away from the casing with increased tip clearance value which is to be expected because the blade tip moves from the casing; interestingly the trajectory across the passage differs significantly with tip clearance as seen in the internal plots (Figure 13 to Figure 15).

At the lower tip clearance value of 2% (Figure 13) the tip clearance vortex core moves away from the suction surface at approximately 0.4Cx and then proceeds to move across the passage to approximately 0.3Pitch at the TE. With a 6% gap the vortex core moves from the SS much later at approximately 0.6Cx and then moves across the passage exiting at approximately 0.28Pitch from the SS. The vortex core is weaker and smaller in size than for 2%TC. Increasing the gap further to 10% prolongs the detachment of the tip clearance vortex from the SS further to 0.8Cx. At the TE with 10%TC the vortex core is approximately 15%Pitch from the SS and therefore only fills approximately 30% of the pitch-wise passage. The magnitude of the tip clearance vortex core is reduced with increased tip clearance.

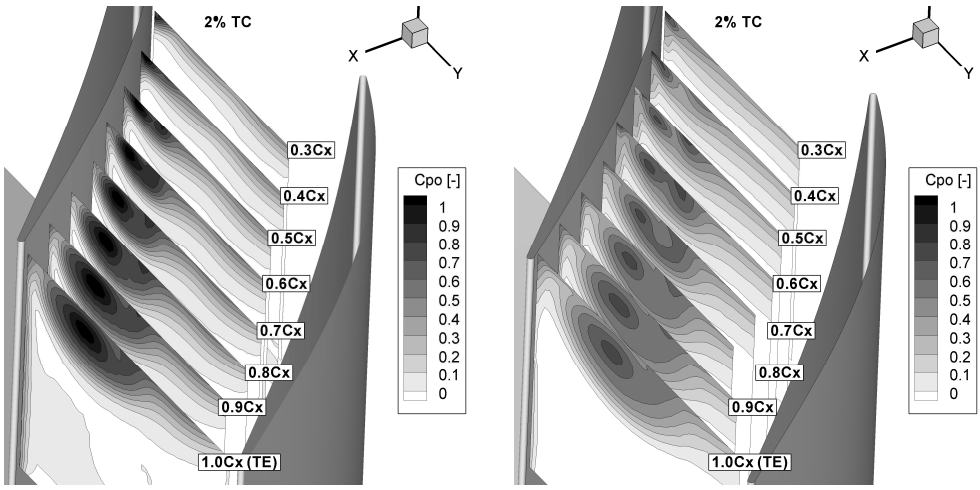

Figure 13: 2%TC, Cpo Contour Plots Through Passage (Left: Natural Inlet, Right: High Skew Inlet)

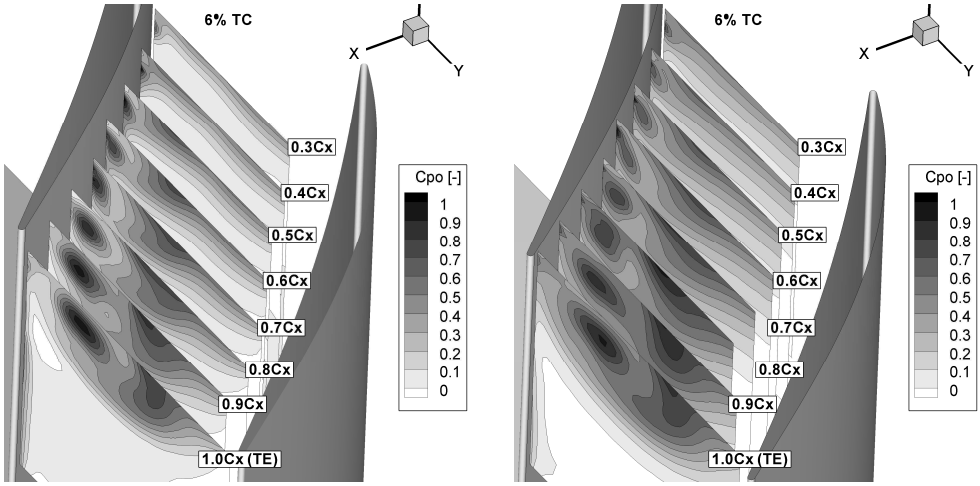

Figure 14: 6%TC, Cpo Contour Plots Through Passage (Left: Natural Inlet, Right: High Skew Inlet)

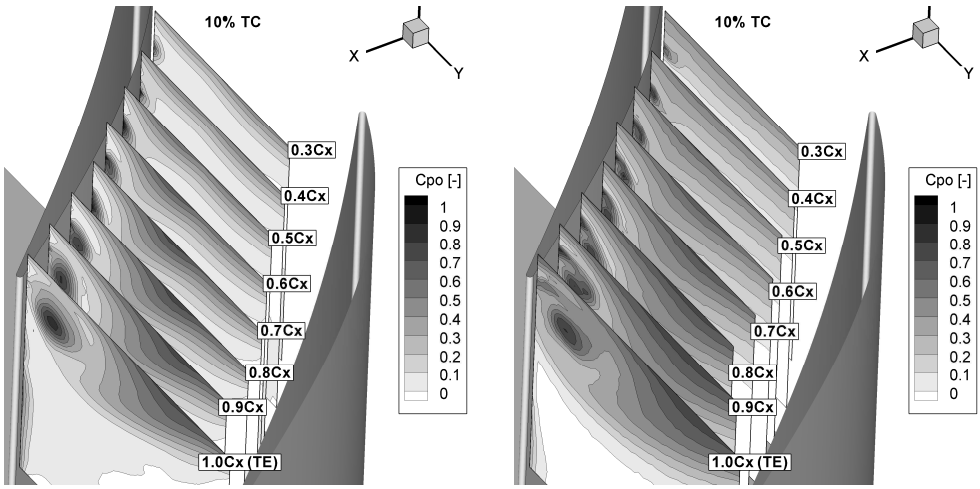

Figure 15: 10%TC, Cpo Contour Plots Through Passage (Left: Natural Inlet, Right: High Skew Inlet)

As previously found (Williams et al., 2008) a secondary counter rotating vortex is evident on the casing wall adjacent to the tip clearance vortex; this is a result of the incoming casing flow which passes over the blade and tip clearance vortex separating from the wall due to the adverse pressure gradient (deceleration of the flow) and the casing shear separating the flow. This in turn creates a counter rotating vortex which creates a large blockage with the larger tip clearances as a result of the increased flow passing over the tip clearance vortex.

An area average of loss coefficient in the outer 50% of blade span shows that increasing the tip clearance from 1 to 8%TC incurs an increase in loss though the cascade compared to the 0% case, however above this there is a reduction in loss with increased TC. This is different to the previous cascade (Williams et al. 2008) where it was shown that there was a levelling of increased loss above 6%TC. However area averaging the yaw shows a significant reduction in turning through the cascade with increased TC.

Effect of Inlet Boundary Layer

The previous cascade (Williams et al., 2008) reported results with a realistically skewed inlet of 10º relative to mid-span; however the boundary layer was unrealistically thin (within 10% span of the casing). The new cascade has allowed for a realistic inlet boundary layer to be implemented and to be compared to the cascade with a small natural boundary layer.

The pitch averaged exit plots at 1.2Cx (Figure 7 and Figure 8) show the difference at exit between the two inlet conditions. With a tip clearance of 6% or less there is only a small change in yaw angle with the injection; an increase less than 2º close to the casing and no significant radial shift. Above 6%TC an increase in exit angle of 10º close to the casing and a radial shift (although small) away from the casing is apparent. Figure 10 showing the total yaw at exit of the cascade for the measured area (0.5 to 0.977Span) indicates that for the smaller tip clearance values there is a decrease in exit angle. This however is a result of a mid-span reduction in inlet angle reducing the exit angle, which can be seen in the pitch averaged plots. Note however that the total inlet angle with injection is higher than without as a result of the increased inlet skew.

The inlet flow has a significant impact on the stagnation pressure loss at exit. The pitch averaged plots show a significant thickening of the exit loss regions and increase in the loss attributed to the TC vortex. However this increase in loss is not a result of an increased TC vortex core loss as the contour plots (Figure 11 to Figure 15) clearly show that the loss core is lower in magnitude with the increased skew. The origin is an overall thickening of the loss area in the casing region including the counter rotating vortex loss increase. Pitch mass averaging the loss at exit shows that there is an overall increase in loss at exit with increased inlet skew. Subtracting the inlet loss profile from the exit profile results in a reduction in loss with the highly skewed inlet compared to the natural inlet. Therefore the loss increase through the cascade has been reduced by the increased inlet skew.

It is not yet clear from this work whether this reduction in loss increase is due to the increase in thickness of the inlet boundary layer or its skew. The effect of the skew is seen in the exit yaw angle for the higher tip clearances, but not for 6% or less. This may be explained by the lessening effect of the blade on the tip clearance flow as the clearance is increased. It may be that a CFD investigation might help clarify these issues further provided the loss generating mechanisms are correctly modelled.

CONCLUSIONS

A new cascade has been built at the University of Durham, UK. The cascade has realistic high pressure compressor geometry and the ability to alter the inlet boundary layer using upstream tangential injection to realistically skew the inlet flow. The cascade turning at mid-span is in the region of 10º and the stagger angle is 46.5º. The cascade therefore has a much higher stagger angle and lower turning than the cascade previously reported which had turning of 30º and stagger angle of 14.2º. Tip clearance values between 0 and 12%Span have been measured experimentally with

both a natural low skew inlet and a highly skewed thick inlet boundary layer to represent a real machine. The key findings are:

- Compared to previous work (Williams et al., 2008) similar conclusions are drawn with a more realistic cascade geometry
- Increasing the tip clearance above 1%TC incurs no further increase in loss through the cascade. The loss reduces with increased tip clearance until 10%TC where the loss is similar to the 0%TC case.
- A reduction in mass averaged turning occurs with increased TC gap. With 12%TC the turning is halved compared to 0%TC.
- Increasing the inlet boundary layer skew and thickness increases the exit gross loss. However the net loss increase through the cascade is reduced.
- The tip clearance vortex remains close to the suction surface of the blade and does not propagate across the passage.
- Overall remarkably similar results are obtained with and without large values of inlet skew.

These conclusions are derived from results at the design condition and may change at off-design conditions.

ACKNOWLEDGEMENTS

The authors would like to thank Alstom Power, Switzerland and in particular Michael Loetzerich for their help during this project. Thanks are also due to Prof. Le Hi of Oxford University, Dept of Engineering Science, for his help with this work.

REFERENCES

Williams, R.J., Gregory-Smith, D., and He, L., "*A Study of Large Tip Clearance Flows in an Axial Compressor Blade Row*," ASME Paper No. GT2006-90463

Williams, Richard Gregory-Smith, David, He, Li & Ingram, Grant 2008, Experiments And Computations On Large Tip Clearance Effects In A Linear Cascade, GT2008-50557

Peacock, R.E., 1982a, "A *Review of Turbomachinery Tip Gap Effects: Part 1 Cascades*," International Journal of Heat and Fluid Flow., **3**, pp. 185-193

Storer, J. A. and N. A. Cumpsty., (1991), "*Tip Leakage Flow in Axial Compressors*," J. Turbomachinery., **113**(2), pp. 252-259.

Sjolander, S.A., 1997, "*Physics of Tip Clearance Flows - 1*," von Karman Institute for Fluid Dynamics, Lecture Series 1997-01, Secondary and Tip-Clearance Flows In Axial Machines.

De Cecco, S., Yaras, M.I., and Sjolander, S.A., 1995, "*Measurements of the Tip-Leakage Flow in a Turbine Cascade with Large Clearances*," ASME Paper 95-GT-77, June 1995.

Saathoff, H., and Stark, U., 2001, "*Tip Clearance Flow in a Low-Speed Compressor and Cascade*," Proc. 4th. European Conference on Turbomachinery – Fluid Dynamics and Thermodynamics, Firenze, Italy, pp. 81-91.

Muller, R., and Vogeler, K., 2007 "*Effects of 3D Aerofoil Tip Clearance Variation on a 4-Stage Low Speed Compressor*," Proc. of the 8th International Symposium on Experimental and Computational Aerothermodynamics of Internal Flows, Lyon, July 2007. Paper Reference : ISAIF8-00112.

Boos, P., Mocker, H., Henne, J.M., Selemeier, R. "*Flow measurement in a Multistage Large Scale Low Speed Axial Flow Research Compressor*,", ASME 98-GT-432